Dissertation

EXTRACELLULAR VESICLES FROM HUMAN CARDIAC CELLS AS FUTURE ALLOGENIC THERAPEUTIC TOOL FOR HEART DISEASES.

zur Erlangung des akademischen Grades

Doctor rerum naturalium

(Dr. rer. nat.)

im Fach Biologie

eingereicht an der Lebenswissenschaftlichen Fakultät
der Humboldt-Universität zu Berlin

von

Dipl. Biochemikerin Christien M. Beez

Präsidentin der Humboldt-Universität zu Berlin
Prof. Dr.-Ing. Dr. Sabine Kunst

Dekan der Lebenswissenschaftlichen Fakultät
Prof. Dr. Bernhard Grimm

GutachterInnen:

1. Prof. Dr. Martina Seifert
2. Prof. Dr. Hans-Dieter Volk
3. PD Dr. Irina Nazarenko

Tag der mündlichen Verteidigung: 23.Februar.2021

The thesis was performed during July 2015 till December 2019 under the supervision of Prof. Dr. Martina Seifert at the Institute of Medical Immunology and the Berlin Institute of Health (BIH) Centre for Regenerative Therapies (BCRT), Charité-Universitätsmedizin Berlin, as graduate student of the Berlin-Brandenburg School for Regenerative Therapies (BSRT, DFG-Graduiertenschule 203). The work was funded by the Friede-Springer-Herz-Stiftung and the Einstein Foundation.

„Ein Ei ist ein Ei", sagte jener und nahm das größere.

K. Tucholsky

Abstract

Extracellular vesicles (EVs) facilitate intercellular communication by transferring molecules from a donor to a recipient cell. It is proposed that EVs from regenerative cells as a therapeutic tool can help to overcome the leading role of cardiovascular diseases as cause of death. Accordingly, this thesis aimed to evaluate the suitability of EVs from regenerative human cardiac-derived adherent proliferating (CardAP) cells as an allogenic cell-free approach to treat heart diseases. For that purpose, we isolated EVs by differential centrifugation from the conditioned medium that was derived either in the presence or absence of a pro-inflammatory cytokine cocktail (IFNγ, TNFα, and IL-1β). Afterwards, isolated EVs were analysed *in vitro* for their phenotypical characteristics, therapeutic effects, and immunological compatibility.

Isolated EVs from CardAP cells exhibited vesicular structures with diameters mostly of exosomes (d < 100 nm), known EV-associated proteins (e.g. tetraspanins) as well as miRNAs (e.g. miRNA 146-5p). Interestingly, cytokine stimulated EVs were observed to have significantly smaller diameters and a greater repertoire of transported miRNAs than their unstimulated counterpart. Nevertheless, both unstimulated as well as cytokine stimulated EVs were equally internalized by murine cardiac cells, namely HL-1 and MHEC5-T cells, and protected murine cardiomyocytes from reactive oxygen species or starvation induced apoptosis. Virus induced apoptosis was, however, only reduced by treatment with unstimu-lated EVs. Deviations between both EVs were also determined for their pro-angiogenic effect. Human umbilical vein endothelial cells (HUVECs) increased the release of different pro-angiogenic factors when treated with unstimulated EVs (e.g. VEGF) or cytokine stimulated EVs (e.g. IL-8). Nonetheless, both EVs were capable to amplify the tube formation capabilities of treated HUVECs. The exposure of both EVs to unstimulated peripheral blood mono-nuclear cells (PBMCs) did neither induce T cell activation, T cell proliferation nor the release of IFNγ. Additionally, isolated EVs demonstrated immune modulating features in induced immune responses of stimulated PBMCs as observed by diminished T cell proliferation, higher frequencies of regulatory T cells, and a weakened inflammatory milieu (e.g. decreased IFNγ concentrations). Moreover, it was shown that $CD14^+$ cells are essential for this desired immune modulating effect of isolated EVs. In particular, isolated EVs interacted predominantly with $CD14^+$ cells, which consequently acquired a regulatory immune phenotype (e.g. reduced expression of HLA-DR, increased expression of PD-L1). Moreover, EVs solely modulated induced immune responses of isolated T cells when EV-primed $CD14^+$ cells were present.

Overall, EVs derived from CardAP cells appear to convey beneficial characteristics that could contribute to an enhanced regeneration in damaged cardiac tissue by limiting unwanted inflammatory processes, enhancing angiogenesis, decreasing apoptosis and their immune-logical compatibility. Future *in vivo* studies are necessary to validate this indicated suitability of EVs as cell-free allogenic therapeutic approach. In addition, some molecules transported by EVs (e.g. galectin-1 or miRNA 302d-5p) are hypothesized to contribute to the observed beneficial features. In future, these molecules could be used to achieve a more efficient therapeutic approach by further selection of isolated EVs.

Keywords: cardiac EVs, regenerative therapies, immunomodulation, angiogenesis

Zusammenfassung

Von einer Spenderzelle freigesetzten extrazellulären Vesikel (EVs) können wichtige Prozesse in einer Empfängerzelle beeinflussen. Es wird angenommen, dass durch die Behandlung mit EVs regenerativer Zellen die führende Stellung von Herz-Kreislauf-Erkrankungen als Todesursache reduziert werden könnte. In diesem Zusammenhang untersuchte die vorliegende Dissertation, ob EVs von regenerativen humanen kardialen adhärenten proliferierenden (CardAP) Zellen geeignet wären Herzerkrankungen in einem allogenen zellfreien Ansatz zu behandeln. Dazu wurden EVs aus dem konditionierten Medium von CardAP Zellen, die mit oder ohne pro-inflammatorischen Zytokin-Cocktail (IFNγ, TNFα und IL-1β) kultiviert wurden, durch Differentialzentrifugation gewonnen. Im Anschluss wurden die isolierten EVs *in vitro* bezüglich ihrer phänotypischen Eigenschaften, therapeutischen Wirkungen und immunologischen Verträglichkeit charakterisiert.

Generell besaßen die isolierten EVs vesikuläre Strukturen, hauptsächlich mit Durchmessern von Exosomen (d <100 nm), bekannte EV-assoziierte Proteine (z.B. Tetraspanine) und miRNAs (z.B. miRNA 146-5p). Interessanterweise wiesen stimulierte EVs kleinere Durchmesser sowie ein größeres Repertoire an transportierten miRNAs gegenüber unstimulierten EVs auf. Dennoch wurden EVs beider Biogenesebedingungen gleichermaßen von kardialen Mauszellen internalisiert und sie reduzierten sowohl die durch reaktive Sauerstoffspezies als auch durch Nährstoffmangel induzierte Apoptose von murinen Kardiomyozyten. Im Gegensatz dazu konnten ausschließlich unstimulierte EVs die Virus-induzierte Apoptose verringern. Ebenso zeigten humane Endothelzellen der Nabelschnurvene (HUVECs) Unterschiede in der Freisetzung proangiogener Faktoren nach Kontakt mit unstimulierten EVs (z.B. vaskuläre endotheliale Wachstumsfaktor) oder stimulierten EVs (z.B. IL-8). Allerdings konnten EVs beider Biogenesebedingungen die Netzwerkausbildung von HUVECs *in vitro* deutlich erhöhen. Immunzellen, die mononuklearen Zellen des peripheren Blutes (PBMCs), reagierten auf isolierte EVs weder mit einer Aktivierung noch einer Proliferation von T Zellen oder der Freisetzung von pro-inflammatorischem IFNγ. Allerdings, konnte die induzierte Immunantwort von PBMCs durch beide EVs moduliert werden, was sowohl die verminderte Proliferation von T Zellen, den erhöhten Anteil regulatorischer T Zellen und ein gemindertes entzündliches Milieu umfasste. Es wurde zudem gezeigt, dass die untersuchten EVs vor allem mit $CD14^+$ Zellen in PBMC Kulturen interagierten und diese Zellen infolgedessen einen regulatorischen Immunphänotyp annahmen (z.B. verringerte Expression von HLA-DR, erhöhte Expression von PD-L1). Darüberhinaus konnte die induzierte Immunreaktion von isolierten T Zellen nur in Anwesenheit von EV-behandelten $CD14^+$ Zellen moduliert werden.

EVs von CardAP Zellen erscheinen durch ihre immunmodulativen, pro-angiogenen und anti-apoptotischen Effekte bei gleichzeitiger immunologischer Kompatibilität durchaus geeignet, geschädigtes Herzgewebe zu regenerieren, was in künftigen *in vivo* Studien zu validieren ist. Darüber hinaus wurden Moleküle (z.B. Galectin-1 oder miRNA 302d-5p) identifiziert, die vermutlich diese gewünschten Eigeneschaften vermitteln. Dies bietet die Möglichkeit EVs mit potentiell erhöhter Funktionalität spezifisch aufzureinigen.

Schlagwörter: kardiale EVs, Regenerative Therapie, Immunmodulation, Angiogenese

TABLE OF CONTENT

List of abbreviations

Abbreviation	Full name
7AAD	7-amino-actinomycin D
APCs	Antigen presenting cells
CardAP cells	Human cardiac-derived adherent proliferating cells
CD	Cluster of differentiation
CDCs	Cardiosphere derived cells
CFSE	Carboxyfluorescinsuccinimidylester
CPCs	Cardiac progenitor cells
CVDs	Cardiovascular diseases
d	Diameter
DAPI	4´,6-diaminidin-2-phenylindol
DiD	1,1'-dioctadecyl-3,3,3',3'-tetramethylindodi-carbo-cyanine perchlorate
DMEM	Dulbecco´s Modified Eagle´s Medium
ECM	Extracellular matrix
EDTA	Ethylendiamintetraacetat
ELISA	Enzyme-linked immunosorbent assay
EVs	Extracellular vesicles
FCS	Foetal calf serum
FoxP3	Forkhead Box protein 3
FSC	Forward scatter
Gal-1	Galectin-1
GM130	Golgin subfamily A member 2
h	Hour
HUVECs	Human umbilical vein endothelial cells
IFNγ	Interferon gamma
IL	Interleukin
IMDM	Iscove's Modified Dulbecco's Medium
LC/ESI-MS	Liquid chromatography electron spray mass spectrometry
L-Glut	L-Glutamine
MACS	Magnetic activated cell sorting
MFI	Geometrical mean fluorescence intensity
min	Minute
miRNA	Micro ribonucleic acid
MSCs	Mesenchymal stromal cells
P/S	Penicillin streptomycin solution
PBMCs	Peripheral blood mononuclear cells
PBS	Phosphate buffered saline
PD-L1	Programmed death 1 ligand 1
PFA	Paraformaldehyde
PKH26	Derivate of 3-n-propyl-3'-n-docosanyloxacarbocyonine iodide
ROS	Reactive oxygen species
RPMI	Roswell Park Memorial Institute 1640 Medium
RT	Room temperature (~24°C)
SSC	Sideward scatter
TDG	Thiodigalactoside
TEM	Transmission electron microscopy
TGFβ	Transforming growth factor beta
T_{reg}	Regulatory T cells
VEGF	Vascular endothelial growth factor
versus	*vs.*

List of figures

List of tables

1. Introduction

1.1 Cardiovascular diseases

Disorders of the heart and blood vessels, such as arrhythmia, stroke, thrombosis, or heart failure, are summarized as cardiovascular diseases (CVDs). Although some CVDs appear as an acute event, their underlying cause can be of chronic nature. A pre-existing atherosclerosis, for example, can eventually lead to the acute blockage of blood vessels in the heart (= myocardial infarction), brain (= stroke) or other parts of the body (= thrombosis, acute kidney disease, etc.). In contrast, bacteria or virus induced myocarditis are examples of actual acute CVDs. Accordingly, therapies range from antibiotic treatment to address bacterial causes to anti-coagulating drugs, bypass surgeries, application of stents to support the interrupted flow of the blood, as well as long term behavioural changes of the patient itself [1,2]. One disadvantage of the current therapies for CVDs is that they can solely limit or halt disease progression [3,4]. Thus, final options for severely damaged cardiovascular tissue are narrowed down to remove non-essential parts, replace it by artificial devices, or by donor organs. Although the number of donors increased in Germany in the last two years, the demand outnumbers available donor organs [5]. For that reason, the life of these patients is not only considerably deteriorated but also comes along with a poor prognosis. Indeed, CVDs are the worldwide leading cause of death, which is illustrated by the fact that in 2016 more than 40,800 people died daily due to a CVD and estimates even predict to surpass 53,000 daily deceased in 2030 [6,7]. Moreover, the economic burden caused by CVDs weighs heavy on society. Health costs, productivity losses of patients and relatives as informal care takers are predicted to exceed the mark of US$ 1,000 billion of worldwide annual CVD related expenses already in 2025 [8]. What this all amounts to is that there is an urgent need to overcome these multiple harms caused by CVDs.

1.2 Ways to minimize damages of CVDs

In general, the impact of CVDs on communities and indiduals is intended to be reduced via two general strategies. On the one hand, an approach concentrates on the prevention of CVDs, for example by highlighting and educating people about the impact of risk factors, such as obesity or smoking [6]. On the other hand, the focus is put on improving existing or developing novel therapies. As such, pre-clinical and clinical trials are investigating how damaged tissue can be replaced with 3D printed grafts, decellularized or biologically inactive tissue that was, for example, obtained by improved cryopreservation techniques [9–13]. Additionally, the application of regenerative cells is a widley studied therapeutic approach that is hypothesized to represent an treatment option with disease reverting properties [4,11,14–16]. Herein, different traits were identified to influence the regenerative process in damaged cardiovasculatere tissue, which are in the following exemplarily discussed for heart tissue affected by an acute myocardial infarction and the subsequent following resolution phases. This particular disease was chosen as a representative, because it is not only one of the most frequent CVDs but also has a high incidence to manifest heart failure as subsequent illness [17].

1.2.1 Myocardial infarction and its untreated resolution

The acute event of a myocardial infarction describes the clogging of the coronary artery or arteries by atherosclerotic plaques. It abruptly obstructs the blood flow and consequently disrupts the supply with oxygen and nutrients [2]. This ischemic condition causes oxygen-sensitive cells to perish immediately. For example Cheng *et al.* showed that up to three million cardiomyocytes had died in the infarcted cardiac tissue of rats during the first two hours [18]. Consequently, the heart function is impaired due to the death or apoptotsis of cardiomyocytes in animal models as well as humans [2,18]. Other cells, like cardiac fibroblasts, survive this ischemic environment by adapting their metabolism respectively [19]. In order to resolve the caused injury in the affected cardiac tissue, different processes will take place that can roughly be summarized as three phases: the inflammatory, the proliferative, and the remodelling phase (**Figure 1**).

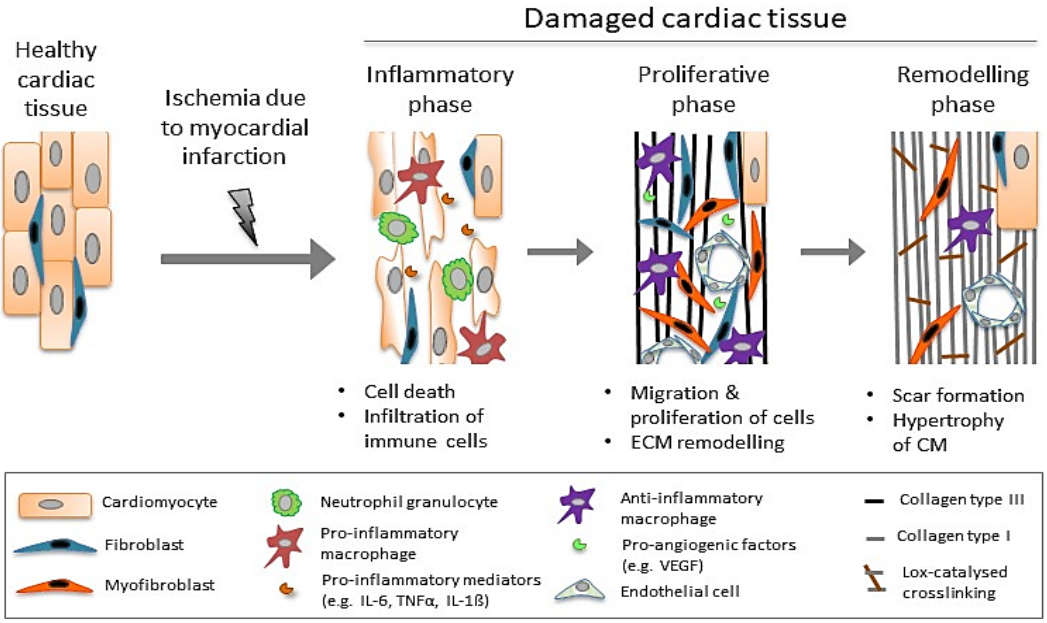

Figure 1: Schematic illustration how scar tissue is formed after an acute myocardial infarction. Myocardial infarction leads to the interruption of oxygen and nutrient supply (= ischemia) of the affected cardiac area. For the resolution of the caused damage, three phases lead to a scar formation. At first, a pro-inflammatory phase takes place, which includes impaired heart function due to dead cardiomyocytes and the establishment of a pro-inflammatory immune response (e.g. infiltration of immune cells, polarization of pro-inflammatory immune cells, and release of pro-inflammatory cytokines/chemokines). Then, the proliferative phase leads to the exchange of immune cells by endothelial cells, fibroblasts and myofibroblasts. Accordingly, angiogenesis, migration, proliferation, and extracellular matrix (ECM) remodelling are major processes during that phase. Finally, a scar tissue will be formed in the remodelling phase. Here, myofibroblasts will vanish nearly completely, whereas the ECM will be strengthen via exchange of collagen type II with collagen type I and crosslinking. Surviving cardiomyocytes (mostly in the neighboring boarder zone) will enlarge.

The **inflammatory phase** is characterized by the infiltration of neutrophils, monocytes and other immune cells that contribute to the clearance of apoptotic cells and extracellular matrix debris [20]. As a matter of fact, immune cells are attracted by released mediators of apoptotic cells, such as danger signals, the so-called danger/damage-associated molecular patterns, or chemokines and cytokines, like interferon γ (IFNγ) or the stromal cell-derived factor 1 α (SDF-1α) [21,22]. At the same time, cardiac fibroblasts express matrix metalloproteinases to

enable an enhanced accessibility of the damaged area for infiltrating immune cells [23]. It was shown that during this phase an increased number of pro-inflammatory M1-type macrophages were observed in the affected cardiac tissue [20]. Furthermore, concentrations of pro-inflammatory cytokines, such as interleukin 1ß (IL-1ß), tumour necrosis factor alpha (TNFα) and IL-6, were elevated in the respective tissue and its periphery [20,24–26]. For the **proliferative phase**, it is vital that the inflammatory immune response is dampened, which consequently results in fewer infiltrated immune cells in the tissue [20,27,28]. In order to avoid a rapture of the ventricular wall due to the missing biomass of immune cells and the pressure of the still contracting heart, newly migrated or already present fibroblasts and myofibroblasts proliferate and additionally strengthen the affected cardiac wall by expressing extracellular matrix (ECM) proteins, such as collagen III [19]. Fibroblasts and myofibroblasts are supplied with oxygen and nutrients by newly formed vascularized networks that were formed by migrated and proliferated endothelial cells (Jaffer et al. 2006; Deb and Ubil 2014; Frangogiannis 2014). These endothelial cells are attracted and supported in their network formation by the still prevailing hypoxic condition that results in the release of pro-angiogenic factors, like vascular endothelial growth factor (VEGF) [21]. Additionally, anti-inflammatory M2-type macrophages are recruited or polarized towards this immune cell subset in the damaged cardiac tissue [20,29]. These immune cells contribute by releasing mediators, including growth factors and chemokines, to an environment that favours proliferation, migration, and enhanced angiogenesis [28,30,31]. Finally, the **remodelling phase** leads to the formation of a scar that allows for a higher stability to elevate the contraction capacity and strength, however, to a lower extent than before the acute myocardial infarction. Herein, a deposition of the ECM takes place, like the replacement of collagen type III with collagen type I or the LOX-catalysed crosslinking of ECM proteins [19]. On the cellular level, surviving cardiomyocytes will enlarge, while the number of myofibroblasts will significantely decrease [25].

1.2.2 Desired regenerative effects

Different complementing strategies can be chosen for a regenerative approach within the whole process of resolving the damage caused by myocardial infarction. Despite which approach is selected, cardiomyocytes are a crucial component for the overall therapeutic success. Although, it was shown that new cardiomyocytes are formed at an annual rate of approximately 0.3 - 1% by hypoxic conditioned cardiomyocytes, this turnover of cardiomyocytes is, however, not sufficient enough to replace the dead cardiomyocytes in the damaged cardiac tissue [32]. Thus, the heart has, in contrast to the liver, only a very limited regenerative potential and vanished cardiomyocytes crucially contribute to the decreased heart function during and after myocardial infarction [2,18,33]. For that reason, it appears attractive for therapeutic approaches to either prevent apoptosis of cardiomyocytes, reduce already induced apoptosis of cardiomyocytes, or even to replace dead cardiomyocytes with viable ones. It was for example shown in a rodent myocardial infarction model by Wang and colleauges that the cardiac function improved significantely when patches of decellularized porcrine matrix with seeded embryonic cardiac progenitor cells were transplanted onto the outer surface of the myocardial affected tissue [34]. But in general, all three options are capable to diminish the level of impaired heart function, which would subsequently enhance the prognosis of myocardial infarction patients.

In order to influence the apoptosis of cardiomyocytes, treatments can increase the expression of survival signals, block the cascaded activation of caspases, or target other components of the intrinsic or extrinsic apoptotic pathway, for example via the delivery of micro ribonucelic acids (miRNAs) [35–37]. Such an apoptotic influencing feature also appears attractive to possibly enhance current therapies, like bypass surgeries or the application of stents. Although both treatment options help to resolve the shortage of nourishment in the infarcted area by reperfusion, they come along with a sudden oxygen increase and a subsequent formation of so-called reactive oxygen species (ROS). These charged radicals can cause cells, especially cardiomyocytes, to undergo apoptosis in beforehand not severely damaged areas, so-called boarder zones, which can lead to a myocardial reperfusion injury [38,39]. Notably, apoptosis is not only induced via ROS but also by the ischemic condition in the infarcted cardiac area [21,40]. For that reason, the abolishment of ischemia by supporting angiogenesis, neovascularization, or endothelial repair would have beneficial therapeutic effects. This is also emphasized by studies showing that the later a treatment for a better oxygen and nutrient supply was initiated, the severer was the damage caused by CVDs [41,42].

As previously mentioned, the immune system plays a key role in the resolution of the damage caused by myocardial infarction. The pro-inflammatory response is essential for the initiation of the processes, however, a persisting inflammation opposes the proliferative phase and consequently lead to a greater impairment of heart functions [27]. Regenerative therapies could therefore facilitate immunomodulation, which describes the capability to modify ongoing immune responses, mainly pro-inflammatory ones, towards a lesser inflammatory state or even to convert it towards an anti-inflammatory response. Herein, it would be possible that the therapeutic tool enhances the polarization or the infiltration of immune responses regulating immune cells, such as M2-type macrophages, tolerogenic DCs, or regulatory T cells, that were shown to contribute to enhanced regeneration of damaged tissue [20,29,30,43,44]. Lastly, the ECM plays a crucial role in strengthening the damaged cardiac tissue to resist rupturing due to the applied force by the steady contraction of the heart. However, the ECM remodelling can also develop very stiff tissue as a consequence of accelerated fibrosis that is susceptible towards increased heart pressure. Different approaches are working on the replacement of scar tissue with synthetically produced ECM, decellularized tissue, or regenerative tools that own anti-fibrotic effects to avoid the unwanted stiffness of the tissue [19,45,46].

1.3 Cell therapy as a regenerative approach

Researchers are trying to incorporate at least one of the above listed features for a therapeutic approach to diminish the caused cardiac damage. The administration of regenerative cells is one example of an approach that combines several principles of action.

1.3.1 Autologous and allogenic cell therapy

Human regenerative cells can be either obtained from the same person receiving the treatment (= autologous cell therapeutic approach) or from a donor (= allogenic cell therapeutic approach). Both options have advantages and disadvantages [47–50]. As such, autologous cells do vary across donors in their yield, purity and potency to influence regenerative effects, which is related to the fact that the biological starting material, like bone marrow, of each individual

patient comes in different qualities, quantities and with different donor-specific confounding factors, such as gender, disease status, or age. Additionally, the isolation of this starting material can bear risks for the patient itself due to invasive procedures. Instead, allogenic cells can be obtained without any invasive procedure, too, like from post-natal tissue of the placenta, the amniotic fluid or the umbilical cord blood. Furthermore, in contrast to autologous cells, allogenic ones appear relatively robust in their desired characteristics, purities and potencies. Additionally, allogenic cells are storable by cryopreservation. Thus, their immediate availability, also in acute situations, contrasts the time-consuming process of isolating and expanding autologous cells until their administration to the patient. However, the autologous cell therapeutic approach prevents the risks of pathogen transmission from donor to recipient as well as undesired immune rejections. Indeed, one of the major worries of an allogenic therapeutic cell approach is that the immune competent recipient will develop an immune response towards the applied allogenic cells, which could lead to severe complications [16].

In general, the immune system is capable to distinguish between foreign antigens that could originate from bacteria or viruses, and antigens from the host itself. While auto-antigens shall not induce a reaction, foreign material will trigger a cascade of responses involving processes and cells of the naïve as well as of the adaptive immune system to eliminate the pathogen. In the case of an immune rejection, the administrated allogenic cells are recognized as foreign and danger material, which consequentely leads to a comparable processes as against pathogen invasions. Crucial for the induction of the immune response or rejection is the presentation of the foreign antigens by major histocompatibility complex (MHC) molecules, which are called human leukocyte antigen (HLA) in humans. All nucleated cells constitutively express MHC class I molecules (e.g. HLA-ABC), whereas immune cells, like professional antigen presenting cells (APCs), additionally express MHC class II molecules (e.g. HLA-DR). Non-professional APCs, like endothelial cells, were also shown to induce expression of HLA-DR in the presence of pro-inflammatory cytokines [51].

Three different proposed mechanisms about how foreign cells are recognized exist (**Figure 2A**): i) donor antigens (e.g. processed proteins) are presented either directly by HLA molecules of the donor APCs, ii) indirectly by MHC molecules of the recipient APCs, or iii) in a semi direct manner when recipient APCs present the antigen via HLA molecules that were transferred from donor APCs [52,53]. Importantly, antigens presented on HLA-ABC molecules will be specifically recognized by $CD8^+$ T cells, whereas $CD4^+$ T cell responses are triggered by the presentation via HLA-DR molecules. For a sufficient activation, not only the HLA molecule presenting the antigen will bind to the T cell receptor and to the CD4 or CD8 molecule, respectively, but also co-stimulating molecules from the APC side, such as CD80 or CD86, will interact with the co-receptor CD28 on the T cell side (**Figure 2B**) [54].

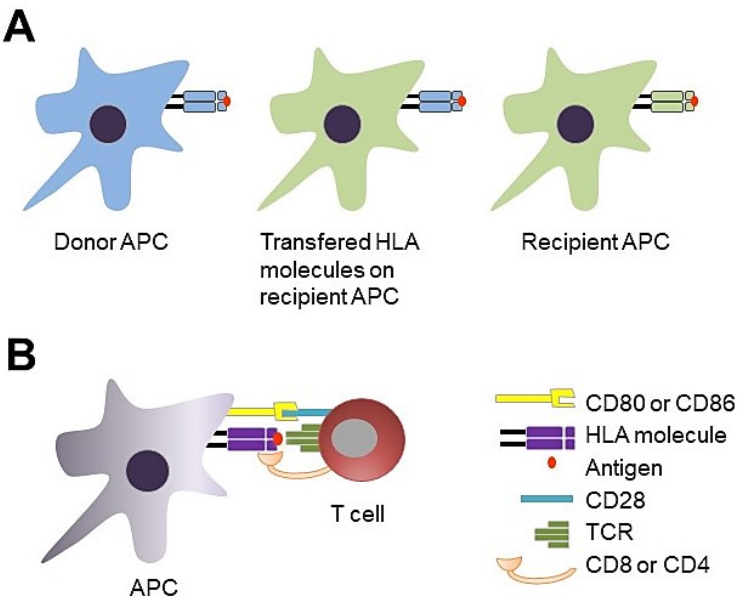

Figure 2: Schematic overview of ways immune reactions towards applied allogenic donors cells are initiated.
Allogenic cells can be recognized as foreign cells by donor's immune system. **(A):** Antigens (red) are presented via HLA molecules either directly (left) via antigen presenting cells (APCs) of the donor, in a semi direct manner (middle) via HLA molecules of the donor that were transferred to recipient APCs, or in-directly by the recipient APCs itself. **(B):** T cells are activated by the binding of different receptors to their ligands, including the T cell receptor (TCR) with the HLA molecule that presents the antigen, CD8 or CD4 with the HLA molecule, and co-stimulatory molecules (like CD80, CD86) with the co-receptor CD28.

Thereafter, a pro-inflammatory T cell response against the administrated allogenic cells is induced. It includes the elevated release of pro-inflammatory cytokines, such as IFNy or TNFα, the activation and expansion of antigen specific T helper cells, and induced cytotoxicity of $CD8^+$ T cells, while the activation state of T cells can be traced by the expression of certain surface molecules, namely CD69, CD25 and HLA-DR as early, intermediate, or late activation marker, respectively [55]. Also other immune cells, such as B cells and natural killer cells, are involved in the rejection response towards the applied allogenic cells. Overall, the immune rejection will not only lead to the clearence of donor cells but also impairs or even abolishes the desired therapy.

1.3.2 Chronology of regenerative cell therapy

Crucial for autologous and allogenic cell therapy was the discovery of mesenchymal stromal cells (MSCs). These cells, which were originally extracted from the bone marrow and later on from other sources, such as adipose tissue or umbilical cord blood, are adherent non-hematopoietic cells that were shown to own capacity to differentiate in the presence of specific growth factors into osteoblasts, chondrocytes, or adipocytes [50,56,57]. Soon after, investigators examined the heart for such a regenerative cell type with the rationale to derive with these cells a therapeutic tool that could replace vanished cardiomyocytes in damaged cardiac tissue. This step was necessary, since it was long thought that MSCs are not capable to differentiate into cardiomyocytes. As a matter of fact, it needed nearly 30 years until the discovery of MSCs to discover the exact supplements and conditions to derive cardiomyocytes from embryonic stem cells or MSCs [58]. Several different cardiac cells were isolated from human or rodent cardiac tissue, including cardiosphere-derived cells (CDCs), cardiac progenitor cells (CPCs), or human cardiac-derived adherent proliferating (CardAP) cells [59–62]. In contrast to MSCs, these cardiac cells have the advantage to be already primed by this particular tissue, the heart. Wang and colleagues could, for example, show that histone modifications of cardiac-specific genes differed between murine cardiac-derived cells and bone marrow derived

MSCs. Moreover, these changes correlated with a greater propability to induce cardiomyogenesis by cardiac derived cells than MSCs [63].

Preclinical studies of CardAP cells, which were outgrown from endomyocardial biopsies, demonstrated that these cells supress apoptosis, support angiogenesis, and modulate induced immune responses *in vitro* [13,64,65]. Furthermore, their administration in rodent CVD disease models impaired immune responses and improved the cardiac function significantly [13,60]. Beside these beneficial effects, CardAP cells have an additional advantage in comparison to the other regenerative cardiac cell types. A retrospective analysis of a clinical study showed that the therapeutic benefit of administrated CDCs was negatively influenced by the expression of their membrane glycoprotein Cluster of Differentiation 90 (CD90) [66]. In contrast to other mesenchymal and cardiac mesenchymal-like cells, CardAP cells were found to be predominantly negative for CD90 [67]. But not only CardAP cells were shown to have cardio protective features. Also CPCs, CDCs, and other cardiac cell types exhibited desired features for the treatment of CVDs, including anti-fibrotic, pro-angiogenic, anti-apoptotic and immune modulating effects, in preclinical studies [3,11,14,61,62,68–70]. However, clinical trials showed solely limited to moderate effects of applied bone marrow cells, MSCs or CPCs [61,69,71,72]. For a better understanding, why results from clinical trials did not meet the expectations built by the encouraging results from previous preclinical studies, comprehensive mechanistic studies were conducted.

In the beginning, it was mechanistically suggested that the applied regenerative cells differentiate into the desired cell type and integrate into the appropriate damaged tissue, like their differentiation into cardiomyocytes and integration into the damaged heart [73–75]. However, studies failed to show a sufficient retention of therapeutically applied cells in the myocardium [73,76] and no evidence could be provided for this theory. Moreover, it was shown that intravenous injected MSCs were rather trapped in lungs than at the site of the desired damaged organ [77]. Nowadays, it is considered that regenerative cells facilitate their beneficial effects in a paracrine manner. Initial investigations compared cells with their conditioned medium. In fact, it was observed that already the conditioned medium contained the information for enhanced regeneration in animal myocardial infarction models [78–80]. Later on, the different components of the conditioned medium, including cytokines, chemokines, growth factors, and extracellular vesicles (EVs), were investigated for their therapeutic potential of regenerative cells.

1.4 Extracellular vesicles as regenerative cell-free approach

In 1946, Cargaff and West observed pro-coagulated particles in platelet isolations, which Wolf referred to as "platelet dust" according to their appearance in electron microscopic images [81,82]. Today, these vesicular structures with a lipid bilayer are called EVs.

In total, three types of EVs can be distinguished according to their biogenesis and size: apoptotic bodies, microvesicles, and exosomes (**Figure 3**) [83–89]. The largest EVs are **apoptotic bodies** (diameter (d) > 1000 nm), which occur as consequence of the programmed cell death in which the plasma membrane dissembles. **Microvesicles** range in their size between 100 to 1000 nm and therefore occupy the middle position in terms of diameter. This subset is budded directly from the plasma membrane into the extracellular space. The smallest EVs are the **exosomes**

with diameters less than 100 nm. They are generated intracellularly in the endosomal compartment, where exosomes are called intraluminal bodies contained in multivesicular bodies (MVBs). When MVBs eventually fuse with the plasma membrane, exosomes are released into the extracellular space. Although major progress was achieved in the research field of EVs, distinct proteins are still missing to distinguish between exosomes and microvesicles. Nevertheless, a number of EV-associated proteins were identified [85]. It includes next to transmembrane or plasma membrane anchored proteins, such as integrins or representatives from the tetraspanin family (e.g. CD9), also cytosolic proteins, like heat shock proteins (HSPs), syntenin, or annexins to name just a few. Apoptotic bodies additionally contain typical cell organelle proteins, such as calnexin, cytochrome C, or cytokeratin 18. Moreover, recent studies showed that the isolation by differential centrifugation purifies EVs together with a non-EV compartment, which includes next to apo-lipoproteins A1/2, also fibronectin or the RNA binding protein Argonaute-2 [90–92].

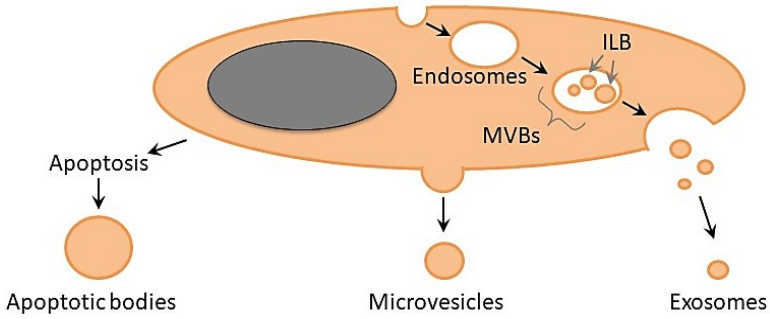

Figure 3: Schematic illustration of the biogenesis of the three EV types.
EVs can be differentiated by their biogenesis and size into apoptotic bodies, microvesicles and exosomes. During apoptosis, the plasma membrane dissembles, which leads to the formation of apoptotic bodies (> 1,000 nm). A viable cell buddes microvesicles (100-1,000 nm) directly from the plasma membrane, whereas exosomes (<100 nm) are formed in endosomes as intraluminal bodies (ILB) contained in multivesicular bodies (MVBs). Fusion of MVBs finally release exosomes into the extracellular space.

Interestingly, not only the most investigated mammalian cells but also parasites, gram-negative bacteria and fungi were observed to release these vesicular structures into the extracellular space [93,94]. The reason for such an omnipresent behaviour lies in the capability of EVs to function as intercellular communicator. Multiple processes, such as differentiation, angiogenesis, or migration, were shown to be influenced in recipient cells upon interaction with EVs and their transported molecules [95–97]. It has to be highlighted that EVs do not only carry lipids and proteins but also RNA molecules, such as messenger (mRNA) or micro RNA (miRNA), as well as small signalling molecules [88,89,98–102].

At present, EVs are evaluated for their potential as medical tool, including as biomarkers for diseases or as therapeutic option. In context of CVDs, several studies could already prove that EVs from MSCs, CPCs, and cardiac fibroblasts are capable to improve cardiac function in rodent MI disease models [37,40,100–103]. In these studies, mechanistic studies were included that demonstrated that the cardio protection could be attributed to EV-mediated reduction of fibrosis, inhibition of apoptosis, support of angiogenesis, and modulation of immune responses. As such, it was discovered that MSC-EVs diminished T cell proliferation[104–107], the release of pro-inflammatory cytokines, such as IFNy or IL-1ß [104–107], or enhanced the frequency of regulatory T cells [107,108] in induced immune reactions *in vitro*. Also APCs gained a tolerogenic

or anti-inflammatory phenotype when treated with EVs derived from MSCs as observed for dendritic cells, monocytes as well as macrophages [109–111]. Herein, this phenotype included an amplified expression of programmed cell death 1 ligand 1 (PD-L1), the macrophage mannose receptor (CD206) on their cell surface, while, in contrast, other surface proteins, such as the co-stimulatory molecule CD86, HLA-DR or activation markers, like CD83, were significantly reduced.

Yet, no satisfying answer can be given on how EVs from regenerative cells facilitate their beneficial effects. Some studies indicate that their transported RNA molecules have a superior role. The anti-apoptotic or proliferative inducing effect of MSC-EVs could be shown to be abolished when EVs were treated with RNase [112]. Likewise, Zou and colleagues could provide evidence that the RNase treatment of MSC-EVs also eliminated the pro-angiogenic effect [113]. In the last years, several miRNAs transported by EVs were identified as potential candidates to trigger beneficial effects, such as miRNA 126, miRNA 146 or miRNA 149 to name just a few [16]. But also mRNAs can be transferred from an EV to a recipient cell. Herein, it was demonstrated that murine cells expressed human proteins, like the DNA-directed RNA polymerase II 23 kDA polypeptide (POLR2E) or the small ubiquitin-related modifier 1 (SUMO-1), when treated with human MSC-EVs [112]. Additionally, EVs were shown to transport proteins with crucial enzymatic function for immunomodulation. Clayton *et al.* showed that EVs from different human cancer cells (colon, breast and prostate) own ATP hydrolytic activity via their transported ectonucleoside triphosphate diphosphohydrolase-1 (CD39) and CD73 . Moreover, it was revealed that this enzymatic activity of EVs contribute to the modulation of induced immune responses, like the decrease of T cell proliferation or IL-2 production, *in vitro* [114]. Also the pro-angiogenic effect of EVs was shown to be influenced by their transported proteins, such as VEGF or other molecules [95,113]. Up to now, the field of EV transported lipids is scarely studied, but future investigations will elucidate whether lipids have an impact on beneficial therapeutic effects or on the delivery to certain target cells. Additionally, mechanistic analysis becomes increasingly complex when considering that the cell source and especially the milieu during the biogenesis of EVs determines which molecules will be transported. For example, EVs from MSCs cultivated under normoxic versus hypoxic conditions revealed that hypoxia enhances the pro-angiogenic feature of these generated EVs significantly in comparison to their normoxic counterpart [115]. Likewise, a pro-inflammatory stimulation with IL-3 favoured the angiogenesis promoting features of EVs from endothelial cells [116].

Investigations will also elucidate key molecules of these EVs and hopefully provide insight into the underlying mechanism for the various beneficial effects needed for treating CVDs. Most importantly, EVs derived from regenerative cells provide an attractive alternative for cell therapy. One advantage is that EVs do not, in contrast to their originating regenerative cell, bear the risk of teratoma formation. Additionally, it is proposed that EVs could be used as an "emergency" therapeutic tool, since they are storable and thus immediately available for administration to the patient without any time-consuming preparation. Nevertheless, before CVD patients can be treated with EVs from regenerative cells, certain challenges have to be explored. This includes question about dosing, delivery routes, and identity markers of EVs, but also innovations for isolation procedures that allow obtaining large amounts of EVs as well as evaluation of potential off-target effects of administrated EVs.

2. Aim and purpose

Over the last decade, several regenerative mesenchymal cells have been demonstrated to release EVs that play an important role in mediating regenerative effects. Although cardio protective properties have already been shown in preclinical studies for human CardAP cells, it has not yet been clarified whether this specific cell type is able to mediate its regenerative effect through its released EVs. For that reason, the major aim of the present work was to evaluate the suitability of EVs from CardAP cells as a future allogenic cell-free treatment for heart diseases. It additionally included the assessment of two different EV biogenesis conditions, namely the presence or absence of a pro-inflammatory cytokine cocktail consisting of IFNγ, TNFα and IL-1β in otherwise serum free medium. Both conditions were included to gather knowledge under what conditions CardAP cells release the most effective EVs in context of regenerative features.

Therefore, the following aspects were addressed:

- **What are the characteristics of isolated EVs?**

  Obtained EV preparations were studied for their concentration, diameter, transported repertoire of proteins and miRNAs, and subsequently these characteristics were compared between cytokine stimulated and unstimulated EVs.

- **Do EVs influence important processes of tissue regeneration *in vitro*?**

  Obtained EV preparations were firstly assessed for their interaction capability with cells, and their intra- or extracellular location 24 h after an interaction with murine cells. Thereafter, isolated unstimulated and cytokine stimulated EVs were analysed in a comparative manner for their impact on the angiogenic behaviour of human endothelial cells, the induced apoptotic behaviour of murine cardiomyocytes, and on typical characteristics of induced immune responses (e.g. T cell proliferation). Furthermore, immune responses were not only investigated with stimulated human isolated peripheral blood mononuclear cells (PBMCs) but also with respective subpopulations of PBMCs, namely $CD14^+$ and $CD3^+$ cells, to provide further mechanistic insights.

- **Do EVs induce adverse immune reactions and contraindicate an allogenic approach?**

  The exposure of unstimulated and cytokine stimulated EVs to otherwise unstimulated human immune cells was analysed for signs of adverse immune responses, which included next to T cell activation and T cell proliferation also a more detailed investigation of $CD14^+$ cells.

3. Materials and methods

3.1 Material

3.1.1 Cells, cell medium and supplements for cell culture

Table 1: Overview of all cells used during this study.

Cells	Acronym	Supplier
Human cardiac-derived adherent proliferating cells	CardAP cells	Isolated and kindly provided by lab group of Prof. Sittinger (Charité)
Human umbilical vein endothelial cells	HUVECs	Cascade Biologics®, Thermo Fisher Scientific, Rochester, NY, USA and Lonza, Wakersville, MD, USA
Human immune cells:		
• Peripheral blood mononuclear cells	PBMCs	All immune cells are isolated from healthy blood donors either freshly or from Buffy coats
• Monocytes	$CD14^+$ cells	
• T cells	$CD3^+$ cells	
Murine atrial tumour cells	HL-1 cells	Both cell line kindly provided by the lab group of PD Dr. Van Linthout (Charité)
Murine cardiac endothelial cells	MHEC5-T cells	

Table 2: Cell culture medium, supplements, and coating reagents used during this study.

Components for culture culture	Supplier
Animal free human epidermal growth factor (rhEGF)	PeproTech Germany, Hamburg, Germany
Animal free human fibroblast growth factor (rhFGF)	PeproTech Germany, Hamburg, Germany
Claycomb medium	Sigma-Aldrich Chemie GmbH, St. Louis, MO, USA
Corning® Matrigel® Basement Membrane Matrix, LDEV-Free	Discovery Labware Inc., Bedford, MA, USA
Coxsackievirus B3 (CVB3; Nancy strain)	Kindly provided by lab group of Prof. Rauch (Charité)
Dulbecco's Modified Eagle Medium (DMEM)	Biochrom GmbH, Berlin, Germany
EBM2 medium	Lonza, Wakersville, MD, USA
EGM2 BulletKit (e.g. hEGF, VEGF, R3-IGF-1)	Lonza, Wakersville, MD, USA
Fibronectin from bovine plasma	Sigma-Aldrich Chemie GmbH, St. Louis , MO, USA
Gelatin from bovine skin, type B	Sigma-Aldrich Chemie GmbH, St. Louis , MO, USA
Ham's F12 Medium	Biochrom GmbH, Berlin, Germany
Human IFNγ1b; IL-1ß; TNFß; and VEGF	Miltenyi Biotec GmbH, Bergisch Gladbach, Germany
Human Serum	Kindly provided by lab group of Prof. Sittinger, Charité (here supplied from Deutsches Rotes Kreuz, Berlin, Germany)
HyClone™ Foetal Bovine Serum (FCS)	Lonza Group AG, Basel, Switzerland
Iscove's Modified Dulbecco's Medium (IMDM)	Biochrom GmbH, Berlin, Germany
L-Glutamine (L-Glut) 100x Gibco™	Thermo Fisher Scientific, Carlsbad, CA, USA
Norepinephrine	Sigma-Aldrich Chemie GmbH, St. Louis, MO, USA
Penicillin/Streptomycin (P/S) solution, 100x, Gibco™	Thermo Fisher Scientific, Carlsbad, CA, USA
VLE-RPMI-Medium 1640 Medium	Biochrom GmbH, Berlin, Germany

Table 3: Composition of the different cell culture media used during this study

Cell	Culture medium
All cells	Freezing medium: FBS + 10% DMSO
CardAP cells	Stock IDH medium mixture: Equal parts of IMDM, DMEM, and Ham´s F12 + 1% P/S; immediately before use + 0.2 µL/mL EGF (stock c 100 ng/µL) + 0.5 µL/mL FGF (stock c 20 ng/µL) Complete IDH medium (cIDH): IDH medium + 5% human serum Centrifuged IDH medium (cenIDH): IDH medium + 10% centrifuged human serum Isolation IDH medium (isoIDH ± cyt): IDH medium ± 10 ng/mL of each: IFNγ, TNFα, and IL-1β
HL-1 cells	complete Claycomb medium (cClaycomb): Claycomb medium + 1% P/S, + 1% L-Glut, + 1% noradrenalin (stock c 10mM), + 10% FCS DMEM 11966 medium (starvation medium): DMEM11966 medium + 5mM glucose, + 0.1% FCS
HUVECs	EGM2 medium: EBM medium + EGM-2 Bulletkit, + 1% P/S, + 10% centrifuged human serum EBM medium: EBM medium + 1% P/S, + 10% centrifuged human seru
Immune cells	Complete RPMI medium (cRPMI): RPMI medium + 1% P/S, + 1% L-Glut, + 10% centrifuged human serum
MHEC5-T cells	Complete DMEM medium (cDMEM): DMEM medium + 1% P/S, + 1% L-Glut, + 10% FC

3.1.2 Off-the-shelf solutions, buffers and kit-based test systems

Table 4: Kit-based test systems used during this study

Test systems	Supplier
Advanced miRNA Assay, Applied Biosys-tems®, (human miRNAs: 494-3p, 146a-5p, 132-3p, 26b-5p, 199a-3p, 186-5p, ans 302-3p)	Life Technologies Corporation, Pleasanton, CA, USA
Caspase-Glo® 3/7 Assay Kit	Promega, Madison, WI, USA
CFSE Cell Division Tracker Kit	BioLegend, San Diego, CA, USA
ELISA kit, human IFNy, Max™ Deluxe	Biolegend, San Diego, CA, USA
ELISA kit, human IL-6, Max™ Deluxe	Biolegend, San Diego, CA, USA
ELISA kit, human IL-8, Max™ Deluxe	Biolegend, San Diego, CA, USA
FoxP3-Transcription Factor Staining Buffer Set, eBiosciences™	Thermo Fisher Scientifics, Waltham, MS, USA
LEGEND Max™ Total TGF-β1 ELISA Kit with Pre-coated Plates	BioLegend, Fell, Germany
LEGENDplex™ human inflammation panel or human monocytes/macrophages panel	BioLegend, San Diego, Ca, USA
LEGENDplex™ human monocytes and macrophages panel	BioLegend, San Diego, Ca, USA
LIVE/DEAD® Fixable Aqua Dead Cell Stain Kit, Invitrogen®	Thermo Fisher Scientific, Eugene, OR, USA
miRNeasy Micro Kit (50 samples)	Qiagen GmbH, Hilden, Germany
nCounter® Human v2 miRNA expression assay kit	NanoString Technologies, Seattle, WA, USA
Pierce™ BCA Protein Assay Kit	Thermo Fisher Scientific, Rockford, IL, USA
PKH26 Red Fluorescent Cell Linker Kits for General Cell Membrane Labelling	Sigma Aldrich Chemie GmbH, St. Louis, MO, USA
Quantikine® ELISA kit for human VEGF-A	R&D Systems, Biotechne brand, Mineapolis, MN, USA
TaqMan™ Advanced miRNA cDNA Synthesis Kit, Applied Biosystems®	Life Technologies Corporation, Pleasanton, CA, USA

Table 5: Off-the-shelf solutions and buffers used during this study

Reagents	Supplier
7-amino-actinomycin D (7AAD) Viability Staining Solution	BioLegend, San Diego, CA, USA
Accutase® , StemPro®, Gibco™	Thermo Fisher Scientific, Carlsbad, CA, USA
AnnexinV binding buffer	BioLegend, San Diego, CA, USA
Bicoll separation solution	Biochrom GmbH, Berlin, Germany
Descosept AF	Dr. Schumacher GmbH, Malsfeld, Germany
Dulbecco's phosphate buffered saline (PBS), without calcium (Ca^{2+}) and magnesium (Mg^{2+})	Biochrom GmbH, Berlin, Germany
ELISA stop solution (2N sulphuric acid)	Sigma-Aldrich Chemie GmbH, St. Louis, Mo, USA
Fix/Perm buffer, Perm buffer (both from FoxP3-Transcription Factor Staining Buffer Set), eBiosciences™	Thermo Fisher Scientifics, Waltham, MS, USA
Hydrogen peroxide solution 30% (w/w)	Sigma-Aldrich Chemie GmbH, St. Louis , MO, USA
Incidin™ Extra N	Ecolab Deutschland GmbH, Monheim am Rhein, Germany
QIAzol Lysis Reagent	Qiagen GmbH, Hilden, Germany
Softaskin®	B. Braun Melsungen AG, Melsungen, Germany
Sterillium® classic pure	BODE Chemie GmbH, Hamburg (GER)
TaqMan™ Fast Advanced Master Mix, Applied Biosysystems®	Life Technologies Corporation, Pleasanton, CA, USA
Trypsin 0.5% (Trypsin-EDTA solution 10 x) Gibco™	Thermo Fisher Scientific, Carlsbad, CA, USA
Vybrant® DiD cell label solution (DiD = 1,1'-dioctadecyl-3,3,3',3'-tetramethylindodi-carbo-cyanine perchlorate)	Invitrogen™, Molecular Probes, Eugene, OR, USA

3.1.3 Consumables, reagents, prepared buffers and antibodies

Table 6: Reagents used during this study

Reagents	Supplier
AKASOLV Aqua Care (blue indicator)	Carl Roth GmbH & Co. KG, Karlsruhe, Germany
Aldehyde/Sulphate Latex Beads (4% w/v; 4 µm)	Invitrogen™, Thermo Fisher Scientific, Eugene, OR, USA
Ampuva water	Sigma-Aldrich Chemie GmbH, St. Louis , MO, USA
Chloroform	Sigma-Aldrich Chemie GmbH, St. Louis , MO, USA
Crystal violet	Sigma-Aldrich Chemie GmbH, St. Louis , MO, USA
Dimethyl sulfoxide (DMSO)	Sigma-Aldrich Chemie GmbH, St. Louis, MO, USA
Ethanol 96%	Carl Roth GmbH & Co. KG, Karlsruhe, Germany
Ethanol 70%	Carl Roth GmbH & Co. KG, Karlsruhe, Germany
Ethylenediamintetra acetic acid (EDTA)	Sigma-Aldrich Chemie GmbH, St. Louis , MO, USA
Goat serum	Sigma-Aldrich Chemie GmbH, St. Louis , MO, USA
Isopropanol	Carl Roth GmbH & Co. KG, Karlsruhe, Germany
Paraformaldehyde (PFA)	Carl Roth GmbH & Co. KG, Karlsruhe, Germany
SDS	Sigma-Aldrich Chemie GmbH, St. Louis , MO, USA
Trifluoroacetic acid (TFA)	Fluka, St. Louis, MO, USA
Trypsin (in 50 mM ammonium bicarbonate)	Promega, Madison, WI, USA
Tween® 20	Sigma-Aldrich Chemie GmbH, St. Louis, MO, USA

Table 7: Consumables used during this study

Consumable	Supplier
Amico filters (10kDA cut off)	Merck, Darmstadt, Germany
BD Vacutainer® LH 170 I.U. Pluss Blood Collection Tubes	Becton, Dickinson and Company (BD), Belliver Industrial Estate, Plymouth, UK
BD Vacutainer® One Use Holder	BD, Belliver Industrial Estate, Plymouth, UK
BD Vacutainer® Safety-Lok™ Blood Collection Set	BD, Franklin Lakes, NJ, USA
Combi tips advanced® (5, 10, 12.5 mL)	Eppendorf AG, Hamburg, Germany
Corning® clear steril flat-bottom culture plates (96-, 46-, 24-, or 6-well plates)	Corning, Corning, NY, USA
CryoPure tubes (1.6 mL)	Sarstedt AG &Co., Nümbrecht, Germany
Eppendorf tubes® (5 mL)	Eppendorf AG, Hamburg, Germany
Express Plus Stericup® filter systems (0.1 or 0.22 μm)	Merck, Shanghai, China
Falcon® Cell culture flasks (25; 75; 175 cm^2)	Corning, Oneonta, NY, USA
Falcon® FACS tubes (5 mL)	Corning, Reynosa, Mexico
Falcon® Polypropylene tubes (15; 50 mL)	Corning, Tamaulipas, Mexico
Falcon® Serological pipettes (5; 10; 25 mL)	Corning, Corning, NY, USA
Formavor-carbon coated EM grids	Electron Microscopy Sciences, Hatfield, PA, USA
MACS® separation coluums (LS)	Miltenyi Biotec GmbH, Bergisch Gladbach, Germany
MicroAmp® Optical 8-cap strip	Applied Biosystems, Foster City, CA, USA
MicroAmp™ Optical Adhesive Film Kit	Applied Biosystems; Life Technologies Corporation, Carlsbad, CA, USA
Mr. Frosty™	Thermo Scientific Nalgene, Schwerte, Germany
Nunc™ MaxiSorp™ ELISA plates	Thermo Fisher Scientific, Rochester, NY, USA
Parafilm® M	Bemis Company, Inc., Menasha, WI, USA
Pipette tips (10; 200; 1000 μL)	Eppendorf AG (Hamburg)/ Sarstedt AG &Co. (Nümbrecht) /Greiner Bio-One GmbH (Frickenhausen); all three from Germany
Safe Seal Tips Premium steril (2.5; 10; 200; 1000 μL)	Biozym Scientific GmbH, Oldendorf, Germany
Safe-lock tubes (0.5; 2; 1.5 mL)	Eppendorf AG, Hamburg, Germany
SafeSeal low binding micro tubes (1.5 mL)	Sarstedt AG &Co., Nümbrecht, Germany
Steriflip® filter systems (0.22 μm)	Merck, Shanghai, China
Transfer pipettes (6 mL)	Sarstedt AG &Co., Nümbrecht, Germany
Ultra-Clear tubes for centrifugation	Beckman Coulter, Inc., Brea, CA, USA
White flat-bottom 96-well plates	Greiner Bio-One GmbH, Frickenhausen, Germany

Reagents and consumables used either for electron microscopy were kindly provided by the Charité Electron Microscopy Core facility or for liquid/electron ionization mass spectrometry (L/ESI-MS) were kindly provided by the Charité Cardioproteomic Unit, such as trypsin, TFA and others.

Table 8: Buffers that were prepared during this study.

Buffers	Composition of buffers
FACS buffer	PBS + 1% FCS
MACS buffer	PBS + 1% FCS, + 2mM EDTA
4% PFA solution	500 μL H2O + 0.4g PFA, + 25 μL 1N NaOH and 9.5 mL PBS
0.5% PFA fixation solution	Dilution of 4% PFA with FACS buffer, e.g. 100μL + 700μL respectively
Blocking buffer	FACS buffer + 5 % goat serum

Table 9: Antibodies used during this study, while the exact dillutions for cell, EVs, EV-cell interaction is enlisted in the following sections, respectively.

Supplier	Human specific antibodies (if not indicated otherwise)
Biolegend	AnnexinV-FITC, CD105 FITC, CD106 PE, CD120b PE-Cy7, CD127 APC-Cy7, CD144 PE, CD163 FITC, CD206 APC, CD25 PerCP-Cy5.5, CD273 (PD-L2) APC, CD274 (PD-L1) PE-Cy7, CD3 FITC, CD4 APC, CD54 APC, CD54 FITC, CD62L APC-Cy7, CD8a PE-Cy7, CD81 FITC, CD81 PE, CD86 PE, CD9 FITC, CD90 APC, HLA-ABC FITC, HLA-ABC APC-Cy7, HLA-DR APC, HLA-DR PR, HLA-DR APC, (isotype controls: IgG1 FITC, IgG1 PE, IgG2a FITC, IgG1 APC-Cy7)
BD Biosciences	CD14 APC-Cy7, CD19 V450, CD3 PerCPCy5.5, CD44 PE, (isotype control: IgG1 PErCPCy5.5, IgG2a APC)
Miltenyi Biotech	CD69 PE, CD8 PE, (isotype control: IgG1 PE, IgG2a PE, IgG1 APC)
R&D Systems	CD121a APC
Novus	Galectin1 APC, GM130 (without fluorescence)
Molecular Probes	AF488 (anti goat; secondary antibody)

3.1.4 Hardware, software, and databases

Table 10: Software or data bases used during this study

Software	Supplier
Axio Vision Release (Version 4.7.2)	Carl Zeiss, Jena, Germany
Columbus™ Image Data Storage	Perkin Elmer, Waltham, MA, USA
FACS Diva Software	BD Bioscience, San Jose, CA, USA
FlowJo for Windows 7/10 (Version: 10.4.2)	TreeStar Inc., Ashland, OR, USA
Functional Enrichment Analysis Tool (FunRich; version 3.1.3)	Analysis tool developed at La Trobe University, Melbourne, Australia [117,118] (available at http://www.funrich.org)
GraphPad Prism™ (Version: 5.03)	GraphPad Software Inc, La Jolla/San Diego, CA, USA
Harmony® Imaginang and analysis	Perkin Elmer, Waltham, MA, USA
ImageJ1.50i	Wayne Rasband, NIH, USA
ImageSP Viewer (Version:1.2.7.11)	SYS-PROG, Minsk, Belarus
LEGENDplex™ version 7.1	VirgineTech Inc., Carlisle, MA, USA
Mascot software (version number 2.2)	Matrix Sience, Boston, MA, USA
Mendeley Desktop (Version: 1.19.1)	RELX Group, London, UK
MikroWin Version 4.41	Berthold Technologies, Bad Wildbach, Germany
MS® Office System 2016	Microsoft, Unterschleißheim, Germany
nSolver software (version 4.0)	NanoString Technologies, Seattle, WA, USA
String database (version 10.5)	ELIXIR Core Data Recources (available at http://string-db.org)
SwissProt database	For analysis: human 553474 sequences and 198069095 residues, Cambridgeshire, UK

Table 11: Hardware used during this study

Hardware	Supplier
AxioObserver	Zeiss, Jena, Germany
CASY® Cell Counter & Analyzer	OLS OMNI Life Science GmbH & Co KG, Bremen, Germany
Centrifuges: i) Allegra™ X-15R, ii) Allegra™ X-22R, iii) Ultracentrifuge L7-55, and iv) Optima L-80 XP	All from Beckman Coulter, Inc., Brea, CA, USA
ESI-QTOF mass spectrometer	Impact II, bruker daltonics, Billerica, MA, USA
FACS Canto II (flow cytometer)	Becton Dickinson, Heidelberg, Germany
Flow hood Hera Safe and Safe 2020	Thermo Fisher Scientific, Rockford, IL, USA
Freezer (-80°C) UF 756	Dometic WAECO International GmbH, Emsdetten, Germany)
Freezer and fridges (4°C and/or -20°C)	Liebherr-International Deutschland GmbH, Bierbach an der Riß, Germany
Ice machine AF80	Scotsman Ice S.r.L., Milano, Italy
Innova® CO_2-incubator (CO-170)	New Brunswick™, Eppendorf AG, Hamburg, Germany
Liquid nitrogen tanks BIOSAFE® MD with BIOSAFE®-Control β	Cryotherm GmbH & Co. KG, Kirchen/Sieg, Germany
MACS Quant (flow cytometer)	Miltenyi Biotec GmbH, Bergisch Gladbach, germany
Microscope DMIL	Leica Microsystems GmbH, Wetzlar, Germany
Midi MACS Separator	Miltenyi Biotec GmbH, Bergisch Gladbach, Germany
Mithras LB 940 micro-plate reader	Berthold Technologies GmbH & Co.KG, Bad Wildbad, Germany
Multipipette HandyStep®	Eppendorf AG, Hamburg, Germany
NanoDrop 2000 spectrophotometer	Thermo Fisher Scientific, Waltham, MA, USA
nCounter® Digital Analyzer	NanoString Technologies, Seattle, WA, USA
PIPETBOY/PIPETGIRL acu	Integra Biosciences AG, Zizers, Switzerland
Pipettes (2.5/ 10/ 20/ 100/ 200/ 1000 µL)	Eppendorf AG, Hamburg, Germany
QuantStudio 6 Flex Real-Time PCR machine	Applied Biosystems/Thermo Fisher Scientific, Darmstadt, Germany
TissueRuptor	Quiagen, Hilden, Germany
UPLC Dionex Ultimate 3000	ThermoFisher, Waltham, MA, USA
VacuSafe	Integra Biosciences AG, Zizers, Switzerland
Vortex mixers: i) Vortex-Genie 2, ii) neoVortex® and iii) Sunlab® Mini Vortex Mixer (SU1900)	i): Beckman Coulter, Inc., Brea, CA, USA; ii-iii): neoLab Migge GmbH, Heidelberg, Germany
Water bath 1003	Gesellschaft für Labortechnik mbH, Burgwedel, Germany
Zeiss LEO 906 Transmission electron microscope	Carl Zeiss Microscopy GmbH, Jena, Germany
ZETAView®	Particle Metrix, Meerbusch, Germany
Thermocycler	Eppendorf AG, Hamburg, Germany
Cell strainer (40; 70 µm)	BD Biosciences, NJ, USA

3.2 Methods

3.2.1 Cell biological methods

3.2.1.1 Isolation of human cells

Isolation of cardiac-derived adherent proliferating (CardAP) cells: Endomyocardial biopsies from the right or left ventricular side of the interventricular septum were obtained according to the local guidelines of the Charité-Universitätsmedizin Berlin and the study was approved by the ethics committee of the Charité-Universitätsmedizin Berlin (No. EA2/140/16). These biopsies were used to isolate CardAP cells by outgrowth culture conditions as previously published [67]. For this study, cryopreserved CardAP cells were kindly provided by the lab of Prof. Sittinger.

Isolation of human immune cells: Human peripheral blood mononuclear cells (PBMCs) were derived from buffy coats (German Red Cross, Berlin, Germany) or from fresh blood of healthy volunteers with their written informed consent according to approved protocols by the ethics committee of the Charité-Universitätsmedizin Berlin (EA1/226/14, EA2/139/10). At the start, a 1:1 (v/v) mixture of blood and PBS was prepared and then layered on top of 15 mL Biocoll in 50 mL falcon tubes. After a centrifugation at 800 *x* g for 30 min at RT without breaks, erythrocytes and the majority of granulocytes were beneath the Biocoll, while PBMCs were present in an interphase between Biocoll and an upper phase consisting of plasma and thrombocytes. The PBMC interphase was cautiously collected into a 50 mL falcon tube already filled with 10 mL ice-cold PBS and centrifuged at 300 *x* g for 10 min and 4°C. The cell pellet was washed at least four times with ice-cold PBS and isolated PBMCs were either cryopreserved (*see section 3.2.1.1*), separated into different immune cell subtypes (*see section 3.2.3.5*), or experimentally used (*see sections 3.2.1.4/5/6*).

3.2.1.2 Cell culture

All cell culture experiments were performed in a laminar flow hood to enable sterile conditions. Furthermore, unsterile materials were autoclaved at 120°C and one bar before usage. Primary cells and cell lines were cultivated in aseptic incubators at 37°C, 21% O_2, and 5% CO_2 in their appropriate medium as enlisted in **Table 3**. In order to limit the influence of EVs from serum sources, ultracentrifuged human serum was used in the medium for functional assays or for the expansion of CardAP cells.

Preparation of centrifuged human serum: Serum was mixed with the same volume of the appropriate medium needed for cell culture (isoIDH medium for CardAP cells, RPMI medium for PBMCs, EBM medium for HUVECs) and centrifuged for 24 h at 100,000 *x* g and 4 °C. The next day, the supernatant (= centrifuged human serum) was collected and stored at -20°C till further usage.

Cell cryopreservation: Cells were regularly cryopreserved by taking them up in freezing medium (1 - 4 x 10^6 cells/mL). The cell suspension was immediately transferred into cryotubes, which were placed in Mr. Frosty™ freezing containers and stored at -80°C. The next day, samples were transferred to -160°C tanks for long-time storage.

Cell thawing: Cryopreserved cells were defrosted by shortly thawing them in a 37°C heated water bath. Then, the cells were transferred to a 50 mL falcon tube filled with 10 mL of the respective complete medium. The cryotube was rinsed with PBS for three to four times and transferred to the same 50 mL falcon tube. Then, the suspension was centrifuged for 10 min at 300 *x* g and 4°C. The obtained cell pellet was taken up in 10 - 20 mL complete medium, and cell number and viability were accessed with a cell counter, namely Casy® Cell Counter.

Cell passaging: Cultured cells were passaged when a confluence of approximately 80 % was reached, except for HL-1 cells. These cells were passaged at a confluence of 100 % to avoid their dedifferentiation. Suspension cells were collected immediately into a 50 mL falcon tube and centrifuged for 10 min at 300 *x* g and 4°C. Adherent cells needed to be detached from the surface of the culture plastic by treatment with trypsin or accutase. In general, the medium was removed and cells were washed once with PBS. Afterwards, cells were incubated at 37 °C either for three min in a trypsin/EDTA solution or for 30 to 45 min in an accutase containing solution. The proteolytic activity was inhibited by adding the double volume of the respective medium. Detached and floating cells were collected in 50 mL falcon tubes and centrifuged as previously described. Lastly, the obtained cell pellet was suspended in 10 - 20 mL medium and the cell number and viability were determined with a Casy® Cell Counter.

3.2.1.2.1 Human cells

Human cardiac-derived adherent proliferating (CardAP) cells: Cryopreserved CardAP cells from seven donors were thawed and cultured in cIDH medium at a density of 4,000 cells/cm². Afterwards, CardAP cells were cultured and passaged at the same density for up to eight times with cenIDH medium, if not stated otherwise. Some characteristics of all used CardAP donors are displayed in **Table 12**.

Table 12: Characteristics of the seven CardAP donors used during this study.

CardAP donor IDs	Frequency $CD90^+$ cells	Sex	Age [years]
36	14.5 %	Male	49
48	21.7 %	Female	63
52	23.2 %	Female	39
50	15.0 %	Male	24
63	26.4 %	Male	57
64	14.7 %	Male	63
69	15.5 %	Female	52

Human umbilical vein endothelial cells (HUVECs): Cryopreserved or cultured HUVECs were seeded at a density of 1,000 – 2,000 cells/cm² in EGM2 medium, if not stated otherwise. Cells were included into functional assays until passage six.

Human immune cells: Cryopreserved or freshly isolated human immune cells were cultured in cRPMI medium. The exact cell concentrations are highlighted in the description of the T cell proliferation assay (*see section 3.2.1.5*) or regulatory T cell assay (*see section 3.2.1.6*), respectively.

3.2.1.2.2 Murine cells

Murine cardiac endothelial cells (MHEC5-T cells): Cryopreserved or cultured MHEC5-T cells were grown in cDMEM medium and seeded at a density of about 10,000 cells/cm². During this study, MHEC5-T cells were used between passage three and six.

Murine cardiomyocytes (HL-1 cells): Cryopreserved or cultured HL-1 cells were seeded at a density of 40,000 cells/cm² in cClaycomb medium on gelatine (0.2 mg/mL) and fibronectin (0.0125 mg/mL) coated culture dishes. The coating solution was prepared in two steps. Firstly, 0.1 g gelatine was mixed with 50 mL PBS and heated in the microwave to solubilize. Secondly, 44.375 mL PBS was mixed with 625 µL (1mg/mL) fibronectin and 5 mL of the previously prepared gelatine solution. This final coating solution was used to coat culture dishes for 30 min at 37°C. Afterwards, the remaining coating solution was collected and reused at least twice. Reused coating solution was stored at 4°C for up to six weeks, while stock solutions and unused final coating solutions were stored at -20°C. During this study, HL-1 cells were used between passages 24 and 29.

3.2.1.3 Isolation of EVs by differential centrifugation

Unlabelled as well as fluorescence labelled EVs were isolated via differential centrifugation of the conditioned cell culture medium (**Figure 4**) by an adapted protocol from Théry *et al.* [89].

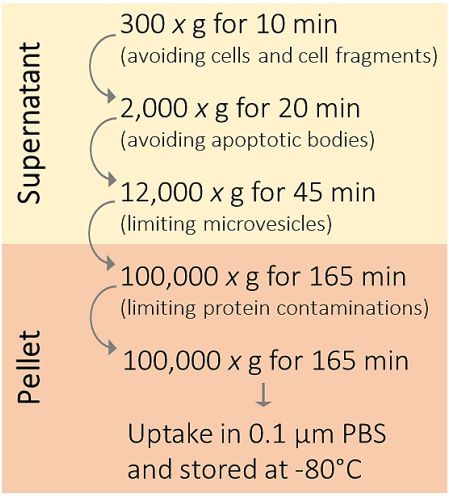

Figure 4: Steps of differential centrifugation to isolate EVs from the conditioned medium of CardAP cells.
CardAP cells were washed twice with PBS after a confluence of 80% was reached. Then, isoIDH medium with or without pro-inflammatory cytokines (10ng/mL of IFNγ, TNFα and IL-1β) was applied for 20 h. The conditioned medium was collected and subjected to a differential centrifugation protocol to isolate small EVs. Therefore, the supernatant was centrifuged at 300 *x* g for 10 min (exclusion of cells and cell debris), at 2,000 *x* g for 20 min (exclusion of small cell debris and apoptotic bodies), at 12,000 *x* g for 45 min (exclusion of most microvesicles) and at 100,000 *x* g for 165 min (small EV pellet). Protein contaminations were limited by washing the obtained small EV pellet with 0.1 µm filtered PBS. Finally, EVs were suspended in 0.1 µm filtered PBS and stored at -80°C until further analysis.

Isolation of unlabelled EVs: CardAP cells were grown in cenIDH medium to a confluence of about 80%. Then, CardAP cells were washed twice with PBS and isoIDH medium with or without a pro-inflammatory cytokine cocktail (10 ng/mL of TNFα, IFNγ as well as IL-1β) was applied for 20 h. The conditioned medium was collected and stepwise centrifuged at 300 *x* g for 10 min, 2,000 *x* g for 20 min, 12,000 *x* g for 45 min and 100,000 *x* g for 165 min. Each step was performed to exclude cells, cell fragments, apoptotic bodies, and the majority of microvesicles (as indicated in **Figure 4**) to obtain mainly exosomes, the smallest EV type. To minimize protein contaminations, a washing step was performed by suspending the received EV pellet in 0.1 µm filtered PBS and repeating the last centrifugation step. Finally, EVs were

stepwise suspended in a total of 500 µL of 0.1 µm filtered PBS, transferred to low-binding tubes, and stored at -80°C till further usage.

Isolation of fluorescence labelled EVs: Lipids of EVs were labelled with lipophilic fluorescent dyes, namely PKH26 or DiD. Therefore, the pellet of EVs after the first 100,000 *x* g centrifugation step was suspended in 6 mL PBS and supplemented with either 6 µL Vybrant® DiD cell label solution or 3 µL PKH26 for 10 min on ice prior to the final centrifugation step. Additionally, a negative control for each of the fluorescence dye was prepared to identify false positive signals by proceeding with unconditioned isoIDH medium. All samples were reconstituted in a total of 500 µL of 0.1 µm filtered PBS, transferred to low-binding tubes and stored at -80 °C till further usage.

Importantly, CardAP cells were harvested by accutase treatment after each EV isolation procedure to determine the cell number by Casy® Cell Counter. Afterwards, cells were used for surface protein analysis by flow cytometry (*see section 3.2.3.1.1*) as well as for reseeding in cenIDH medium for the next EV isolation procedure until passage eight.

3.2.1.4 EV-cell interaction assay

The interaction of EVs with different potential target cells was accessed by using either fluorescence labelled or unlabelled EVs.

EV-cell interaction assay with fluorescence labelled EVs: HUVECs, HL-1, or MHEC5-T cells were seeded according to **Table 13** and allowed to adhere to the culture dish for 24 h. The next day, medium was discarded and fresh medium was added with either 6 µg/mL DiD or PKH26 labelled EVs or the equal volume of the negative control for DiD or PKH26. In contrast, PBMCs were seeded and immediately treated with 12 µg/mL of fluorescence labelled EVs and corresponding controls. After certain incubation times (**Table 13**), cells were either analysed by flow cytometry (*see section 3.2.3.1*) or by microscopy (*see section 3.2.3.2*).

Table 13: Culturing conditions to investigate the interaction of DiD⁺ EVs with target cells and conducted staining for analysis by flow cytometry (FC) or by microscopy (M)

Target cell	Cells cultured	Culture period [h]	Staining
PBMCs	5×10^5 cells/well in 6-well-plate	48 (FC and M)	M: DAPI (1:100) and CD14 APC-Cy7 (1:50) FC: CD14 PE, CD3 FITC, CD19 V450, CD56 PE-Cy7, liefe/dead marker V510
HL-1	2×10^5 cells/well in 48-well-plate	0, 2, 7, 19 and 24 (FC and M)	M: DAPI (1:100) FC: Dead/viable marker
MHEC5-T	2×10^5 cells/well in 48-well-plate	0, 2, 7, 19 and 24 (FC)	FC: Dead/viable marker
HUVECs	2×10^5 cells/well in 24-well-plate	24 (FC) 0, 2, 24 (M)	M: DAPI (1:100) FC: Dead/viable marker

EV-cell interaction assay with unlabelled EVs: HL-1 or MHEC5-T cells were seeded in 48-well plates (2×10^5 cells/well). After 24 h, the medium was changed and cells were treated either with 6 µg/mL of unlabelled unstimulated or cytokine stimulated EVs or they were left untreated. After another 24 h, cells were harvested by accutase treatment and proceeded for

analysis by flow cytometry to assess the occurrence of human EV proteins on the surface of cells by an extracellular staining or within murine cells by an intracellular staining (*see sections 3.2.3.1.1/3*).

3.2.1.5 T cell proliferation assay

The immunogenicity or the immune modulating feature of EVs was determined by their capability to initiate or to alter T cell proliferation, respectively. By flow cytometry, the frequency of proliferated T cells was monitored via the fading fluorescent signal of carboxyfluorescein succinimidyl ester (CFSE). Two different set-ups were conducted for the T cell proliferation assay with either PBMCs (**Figure 5A**) or separated immune cell subtypes (**Figure 5B**).

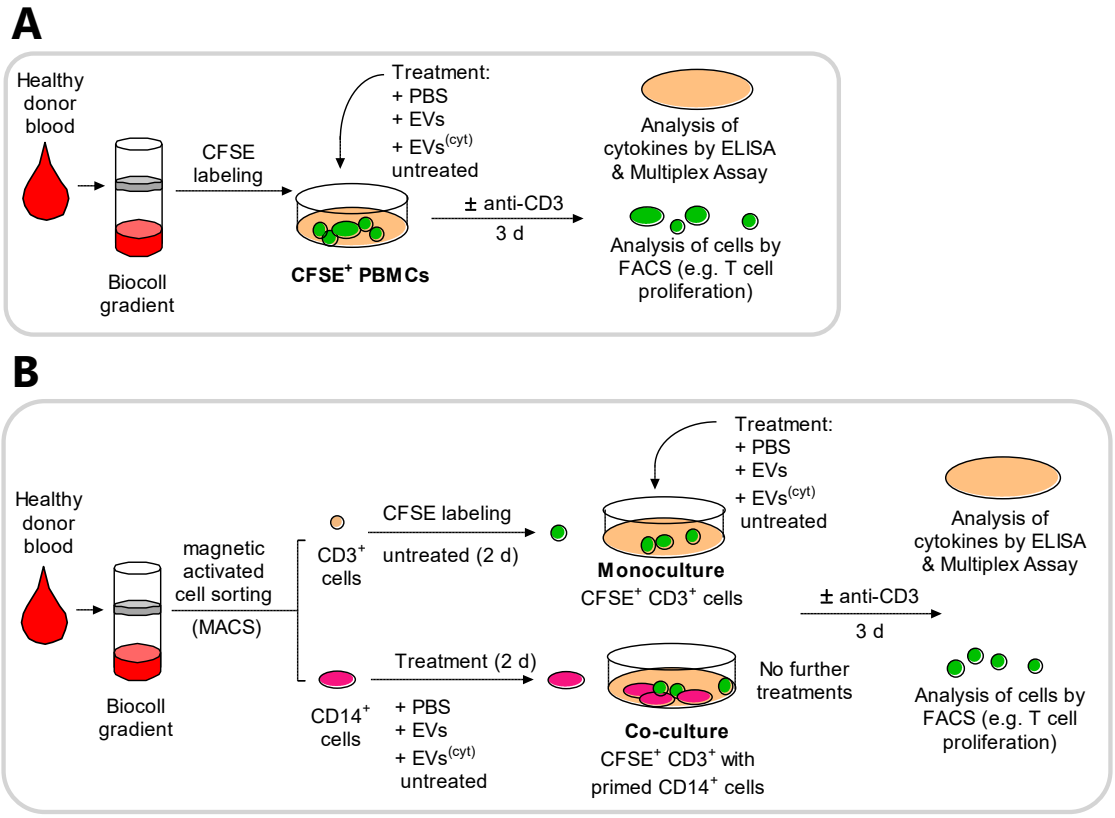

Figure 5: The two configurations of performed T cell proliferation assays.
At the beginning of each assay, PBMCs were isolated from the blood of healthy volunteers by Biocoll gradient. Then T cell proliferation assays were performed either with PBMCs **(A)** or with separated immune cell subpopulations **(B)**, namely $CD14^+$ and $CD3^+$ cells. **(A):** PBMCs were labelled with CFSE, cultured in 96-well plates ($3x10^5$ cells/well), treated with unstimulated or cytokine stimulated EVs, with PBS in equal volumes of EVs or they were left untreated. Furthermore, those cultures were either left unstimulated to examine the immunogenicity or immune responses were provoked with anti-CD3 stimulation to monitor immunomodulation. **(B):** $CD3^+$ and $CD14^+$ cells were isolated from PBMCs by magnetic activated cell sorting (MACS) and kept separately for two days. $CD14^+$ cells were treated with unstimulated or cytokine stimulated EVs, PBS, or were left untreated, whereas $CD3^+$ cells were left untreated after they had been labelled with CFSE. After two days, monocultures of $CD3^+$ cells were treated with unstimulated or cytokine stimulated EVs, PBS or were left untreated. Additionally, a T cell response was induced by applying anti-CD3 as trigger. Besides, $CD3^+$ T cells were co-cultured with beforehand primed $CD14^+$ cells (ratio one to five) and treated with anti-CD3 or left untreated. After each assay, the conditioned medium was collected to determine cytokines and chemokine concentrations, while cells were harvested for analysis by Flow cytometry (e.g. T cell proliferation).

CFSE labelling: Prior to an assay, 1x10^6 PBMCs or $CD3^+$ cells were labelled with 5.0 µM CFDA in 1 mL PBS for three min in the dark at RT. The reaction was inhibited by adding 5 mL cRPMI medium and the suspension was centrifuged at 300 *x* g for 10 min at 4°C. After the cells were washed again in cRPMI medium, the cell number was determined and different assays were conducted as described in the following.

T cell proliferation assay with PBMCs: $CFSE^+$ PBMCs were seeded in 96-well plates (3×10^5 cells/well) and stimulated with 12.5 ng/mL anti-CD3 for immunomodulation assays or left unstimulated to determine the immunogenicity. Additionally, these PBMC cultures were treated with up to 12 µg/mL unstimulated or cytokine stimulated EVs, PBS in equal volumes to EVs or they were left untreated. The needed amount of EV protein were initially investigated in establishment assays and later on solely conducted with one concentration.

T cell proliferation assay with separated immune subsets: PBMCs from fresh blood of healthy donors were used to separate $CD3^+$ and $CD14^+$ cells by magnetic activated cell sorting (MACS, *see section 3.2.3.5*). Afterwards, $CD14^+$ cells were seeded in 6-well plates (1x10^6 cells/well) and additionally treated with 12 µg/mL of either unstimulated or cytokine stimulated EVs, PBS in equal volumes of EVs, or they were left untreated. $CFSE^+$ $CD3^+$ cells were seeded in 6-well plates (2 - 3 x 10^6 cells/well) without any further treatment. Both immune cell subtypes were then cultured for two days. It allowed $CD14^+$ cells to interact with EVs and $CD3^+$ cells to be completely free of contaminations with $CD14^+$ cells, which were observed directly after MACS sort at highest frequencies of about 2 %. After this incubation, supernatants of $CD14^+$ cells were collected and stored at -80°C until further investigation for their released cytokines and chemokines (*see section 3.2.3.4*). Then, $CD14^+$ cells were harvested by accutase treatment, while $CD3^+$ cells were harvested as suspension cells. The different pre-incubated $CD14^+$ cells were co-cultured with $CFSE^+$ $CD3^+$ cells in a 48-well flat-bottom plate in a ratio of one to five (0.1 x 10^6 $CD14^+$ cells with 0.5 x10^6 $CD3^+$ cells/well). Furthermore, pre-incubated $CD14^+$ cells were investigated for surface protein expression analysis of cells by flow cytometry (*see section 3.2.3.1.1*). Additionally, a monoculture of $CD3^+$ cells served as assay control. Therefore, $CFSE^+$ $CD3^+$ cells were seeded in 48-well plates (0.5 x10^6 cells/ well) and treated either with 12.0 µg/mL unstimulated or cytokine stimulated EVs, PBS in equal volumes of EVs or they were left untreated. Monocultures as well as co-cultures were either stimulated with 12.5 ng/mL anti-CD3 or they were left unstimulated for three days.

Analysis: After three days for immunomodulation assays or five days for immunogenicity assays, the supernatants were collected and stored at -80°C until further investigation of the released cytokines and chemokines (*see sections 3.2.3.3/4*). Then after, the cells were harvested by accutase treatment and proceeded for surface protein expression analysis by flow cytometry (*see section 3.2.3.1.1*).

3.2.1.6 Regulatory T cell assay

The immune modulating feature of EVs was furthermore characterized for their ability to affect regulatory T cells. Here, the frequency of viable $CD3^+$ $CD4^+$ $CD127^-$ $CD25^{++}$ $Foxp3^+$ cells was determined by flow cytometry in induced immune responses of immune cell cultures of T cell proliferation assays. The T cell proliferation assay of separated immune subsets was performed

as previously described, while total PBMCs were seeded in 48-well plates (0.6 x 10^6 cells/well), treated with either 12 µg/mL of unstimulated or cytokine stimulated EVs, PBS in equal volumes of EVs or they were left untreated and additionally stimulated with anti-CD3, as previously described. The immune response was allowed to take place for three days at 37°C and 5% CO_2. Afterwards, immune cells were harvested by accutase treatment and proceeded for the investigation of intracellular and extracellular protein expression analysis by flow cytometry (*see section 3.2.3.1.3*).

3.2.1.7 Apoptosis assay

Apoptosis was determined via changes of the cell plasma membrane by flow cytometry or via the activity of caspases by luminescence. CardAP cells were investigated for the different culture conditions, while HL-1 cells were provoked via different triggers to undergo apoptosis.

3.2.1.7.1 7AAD/AnnexinV-FITC detection assay

By flow cytometry, AnnexinV-FITC was used to detect phosphatidylserine present on the extracellular side of early and late apoptotic cells, while 7AAD can solely cross the porous plasma membrane and intercalate with the DNA of late apoptotic or necrotic cells.

Preparation HL-1 cells: Cultured HL-1 cells were passaged and reseeded in 6-well plates (1x10^6 cells/well). Additionally, these cells were treated with 6 µg/mL of either unstimulated or cytokine stimulated EVs, PBS in equal volumes of EVs or they were left untreated. After 24 h, HL-1 cells were washed once with PBS and then 1 mL 0.5 mM H_2O_2 containing cClaycomb medium was applied for 60 min at 37°C. A negative control was incorporated by adding solely cClaycomb medium to untreated HL-1 cells. Afterwards, the media was removed, HL-1 cells were washed twice with PBS and 1 mL cClaycomb medium was applied for 23 h.

Preparation CardAP cells: CenIDH medium was used to seed CardAP cells in 6-well plates (1x10^6 cells/well). After 24 h, CardAP cells were washed once with PBS and then cultured for 20 h in 1 mL of cenIDH, cIDH or iso IDH medium with or without cytokine cocktail.

Procedure: The next day, suspension cells were collected in 5 mL FACS falcon tubes. Adherent cells were harvested by accutase treatment and collected into the respective falcon tube. The cells were centrifuged for 10 min at 300 *x* g and 4°C, followed by an additional washing step with AnnexinV binding buffer. Then, each cell pellet was suspended in 50 µL AnnexinV binding buffer containing 2 µL 7ADD and 2 µL AnnexinV-FITC. The staining was performed for 15 min at RT in the dark and abolished by adding 250 µL ice cold AnnexinV binding buffer. Samples were acquired within 45 min at a flow cytometer (MACSQuant).

Analysis: The frequency of apoptotic cells was determined with the help of FlowJo Software. Accordign to published guidelines, cell debris and solely single cells were incorporated in the analysis (**Figure 6**). In total, four different populations are possible to determine: non-apoptotic cells ($7AAD^-$ AnnexinV-$FITC^-$), early apoptotic cells ($7AAD^-$ AnnexinV-$FITC^+$), late apoptotic cells ($7AAD^+$ AnnexinV-$FITC^+$) and necrotic cells ($7AAD^+$ AnnexinV-$FITC^-$).

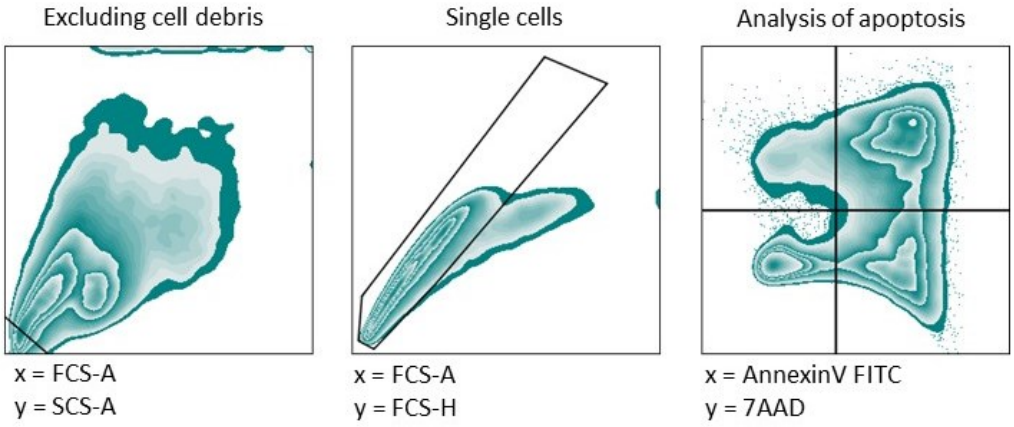

Figure 6: Gating strategy for evaluating cell death by flow cytometry via 7AAD and AnnexinV-FITC staining.
Apoptosis of HL-1 cells or CardAP cells was determined by measuring the signal of AnnexinV-FITC and 7AAD via flow cytometry. For that purpose, harvested cells were stained with AnnexinV-FITC and 7AAD, measured at the MACSQuant and analysed by FlowJo Software. The gating strategy is shown representatively here for HL-1 cell treated with 2 mM H_2O_2. Firstly, cell debris were excluded (left), single cells determined (middle) and then analysed for their fluorescence of AnnexinV-FITC and 7AAD (right). Herein, cells can be distinguished as non-apoptotic cells (AnnexinV-FITC$^-$ 7ADD$^-$), early apoptotic cells (AnnexinV-FITC$^+$ 7ADD$^-$), late apoptotic cells (AnnexinV-FITC$^+$ 7ADD$^+$), and necrotic cells (AnnexinV-FITC$^-$ 7ADD$^+$). FCS = forward scatter, SCA = side scatter, -A = area, -H = height.

3.2.1.7.2 Caspase 3/7 apoptosis assay

Intrinsic and extrinsic apoptotic pathways lead to a cascaded activation of caspases, starting with caspase 8, 9 or 10, which will cleave and thereby activate effector caspases, such as caspase 3, 7 and 6. For that reason, it is possible to determine apoptosis by the activity of caspases. In this study, the Caspase-Glo® 3/7 Assay from Promega was used to determine the activity of caspase 3 and 7 by luminescence through a proluminescent caspase 3/7 DEVD-aminoluciferin substrate.

Preparation: White as well as transparent gelatine and fibronectin coated 96-well plates were seeded with HL-1 cells and treated with either 6 µg/mL unstimulated or cytokine stimulated EVs, PBS in equal volumes of EVs or they were left untreated. Each treatment was at least performed in quadruplicates. Cell concentrations and further details are enlisted in **Table 14** for each apoptotic trigger.

Table 14: Experimental set-up for the different apoptotic triggers.

Apoptotic trigger	Executed by	Seeded HL-1 cells
Starvation	Starvation medium	$2x10^4$ cells/well
Virus infection	Coxsackievirus B3 infection	$2x10^4$ cells/well
Reactive oxygen species	0.5 mM H_2O_2	$1x10^4$ cells/well

After one day, HL-1 cells were washed once with PBS before applying the different apoptotic treatments, which are described in the following:

- **Reactive oxygen species (ROS):** 100 µL 0.5 mM H_2O_2 containing cClaycomb medium was applied for 60 min to HL-1 cells at 37°C. Additionally, a negative control was incorporated by adding solely cClaycomb medium to untreated HL-1 cells. Afterwards, the

media was removed, HL-1 cells were washed twice with PBS and 100 µL cClaycomb medium was applied for 23 h at 37°C.

- **Starvation:** 25 µL starvation medium was applied for 60 min to HL-1 cells at 37°C. Afterwards, the media was removed, HL-1 cells were washed twice with PBS and 100 µL cClaycomb medium was applied for 23 h at 37°C.
- **Viral infection:** Starvation medium was supplemented with coxsackievirus B3 (CVB3) at a 100,000 multiplicity of infection (m.o.i.). Then, 25 µL CVB3 containing starvation medium was applied for 60 min to HL-1 cells at 37°C. Afterwards, the media was removed, HL-1 cells were washed twice with PBS and 100 µL cClaycomb medium was applied for 23 h at 37°C.

Analysis: Caspase 3/7 reagent was freshly prepared by mixing same volumes of caspase-glo buffer with caspase-glo substrate. The equivalent volume of media (~ 100 µL) was added from the caspase 3/7 reagent to each well of the white 96-well flat-bottom plate. The plate was stored at RT and the luminescence was determined after 60, 120, or 180 min at the Mithras LB 940 micro-plate reader. The determined luminescence of 120 min time point was related to the cell concentration, which was determined by crystal violet assays of transparent 96-well plates (*see section 3.2.2.2*).

3.2.1.8 Endothelial cell tube formation assay

Endothelial cells will form capillary-like structures and networks when they were applied to appropriate extracellular matrix, such as matrigel. This tube formation assay recreate the reorganization stage of angiogenesis *in vitro* and can help to identify compounds with enhancing or inhibiting properties. After several establishment assays, the tube formation assay was conducted as described in the following.

Preparation: Thawed HUVECs were cultured in EGM2 medium at relatively low passage number (one till three) for up to five days and several culture medium changes. 24 h prior to an assay, HUVECs were passaged and 1 mL of cells in EGM2 medium were seeded in 6-well plates (1.9×10^5 cells/ well). Before cells were left for 24 h at 37°C in aseptic incubators, they were treated with either 6 µg/mL unstimulated or cytokine stimulated EVs, PBS in equal volumes of EVs or they were left untreated.

Procedure: For the assay itself, a pre-cooled 24-well plate was coated with matrigel (200 µL/well) on ice. The gel was then allowed to solidify for 30 min at 37°C. Pre-incubated HUVECs were harvested by accutase treatment and seeded in 400 µL cEBM medium (0.16×10^5 cells/well) after wells were shortly washed with PBS. Each treatment was performed at least in duplicates. Untreated HUVECs were either left unstimulated or stimulated with 10 ng/mL VEGF during the tube formation assay. The matrigel-coated plates with the different stimulated HUVECs were put in the aseptic incubator for up to 24 h.

Analysis: The formation of tubular structures was documented over the course of time by microscopy (AxioObserver microscope). Images of the 20 h time point were observed to be most suitable for the quantitative analysis by Angiogenesis Analyzer plugin of ImageJ software [119]. Therefore, five to eight random brightfield images were taken of each well, these images were converted into suitable formats (here: RGD) and the tubular network was quantified by

Angiogenesis Analyser with following settings: minimum object size = 10 pixel (px), minimum branch = 25 px, artifactual loop size = 850 px, isolated element threshold = 25 px, master segment size threshold = 30 px, and iteration number = 3. Two parameters, namely the number of junctions and the total branching length, were chosen and displayed in this thesis as quantification of thedetermined tube formation.

3.2.1.9 Pro-angiogenic factor release assay

Endothelial cells release factors that can enhance or reduce their angiogenic behaviour. Whether HUVECs change their secreted pro-angiogenic factors upon EV exposure was elucidated in pro-angiogenic factor release assays.

Cultured HUVECs (passage number three) were seeded in 96-well plates (0.5 x 10^6 cells/ well) and treated in triplicates with either 6 µg/mL unstimulated or cytokine stimulated EVs, PBS in equal volumes of EVs or they were left untreated. After 24 h, the cells were washed once with PBS and fresh cEBM medium was applied for another 24 h. The conditioned medium was collected and stored in low binding tubes at -80°C until determination for IL-6, IL-8 and VEGF concentrations by ELISAs (*see section 3.2.3.3*), while the cells were used for crystal violet assays to determine a cell correction factor (*see section 3.2.2.2*). Relative concentrations of the different factors were obtained by relating determined concentrations to the corresponding cell correction factor.

3.2.2 Molecular biological methods

3.2.2.1 Bicinchoninic acid (BCA) protein assay

The BCA protein assay uses the ability of proteins to reduce copper ions in alkaline solutions. This reduction can be tracked by a colorimetric detection of a purple coloured complex that is formed between bicinchoninic acid and reduced copper ions. Concentrations ranging from 1,000 to 12.5 µg/mL of bovine serum albumin (BSA) were used for a standard curve that helped to determine the protein concentrations of EVs.

Procedure: BSA standard stock solution (2,000 µg/mL) and BCA reagents were provided by the Pierce™ BCA protein Assay Kit. For each assay, a working solution was freshly prepared consisting of 50 parts of BCA reagent A (sodium carbonate, sodium bicarbonate, bicinchoninic acid and sodium tartrate in 0.1 M sodium hydroxide) and one part of BCA reagent B (4 % cupric sulphate). Per well and sample, 200 µL working solution was mixed with 25 µL of standards or EV preparations in transparent 96-well plates. After 30 min at 60°C with short shacking after each 10 min, the absorbance was measured at 570 nm with the Mithras LB 940 microplate reader.

Analysis: The protein concentration of EV samples was calculated with the help of the BSA standard curve. Furthermore, the determined protein concentrations of EVs were normalized to 1x10^6 CardAP cells, since cell number varied within isolations.

3.2.2.2 Crystal violet assay

Ribose type molecules, such as DNA, and proteins can be stained by crystal violet. Since the amount of staining is directly proportional to the amount of cells or the biomass, it is possible to use crystal violet assays in order to derive a cell correction factor.

Procedure: Identical stimulations and treatments were performed in parallel for caspase 3/7 assays (*see section 3.2.1.7.2*) or pro-angiogenic factor release assays (*see section 3.2.1.9*) in transparent 96-well plates. At the end of the incubation time, the cells were fixed with 200 µL 4 % PFA overnight at 4 °C. The next morning, each well was washed twice with 200 µL H_2O and then incubated with 100 µL 10% (w/v) crystal violet in H_2O solution for 30 min at RT in the dark. Afterwards, each well was washed three times with H_2O and then 100 µL 1 % SDS in H_2O solution was applied for 60 min with short shacking after each 10 min at RT.

Analysis: The absorbance was measured at 595 nm with the Mithras LB 940 microplate reader. The mean of at least triple determination (= cell correction factor) was used to calculate the relative luminescent unit (RLU) of caspase activity or the relative released concentrations of pro-angiogenic factors by HUVECs, respectively.

3.2.2.3 Transmission electron microscopy (TEM)

EVs were evaluated for its morphology and diameter by TEM at the electron microscopy facility of the Charité-Universitätsmedizin Berlin. All steps and measurements were performed together with Mrs. Petra Schrade, technician and person in charge of the EM facility at the Virchow Campus of the Charité Universitätsmedizin.

Procedure: Unstimulated and cytokine stimulated EVs from three different CardAP donors (36, 48, and 50) as well as PBS controls were investigated by TEM according to an adapted method for positive-negatively stained EVs [89]. Formavor-carbon coated copper EM grids were incubated for 20 min with 20 µL of sample. Afterwards, following steps were performed: 20 min in 2 % PFA solution, shortly wiping residual drops on a tissue, five min in 1 % glutaraldehyde, followed by six washing steps with H_2O. Then the samples were positive-negatively stained for 10 min in freshly prepared 4 % uranyl acetate 2 % methylcellulose solution in the dark at 4°C. After residual staining solution was wiped off, the samples were dried overnight in the dark at RT.

Analysis: Samples were analysed with the transmission electron microscope Zeiss Leo 906. Up to 21 images of each sample were accessed for diameter of EVs by ImageSP Viewer. Here, vesicular structures exposing a lipid bilayer, visible as two distinct lines, were measured by drawing a line from both outer layers through the centre. These diameters are displayed as individual points as well as diameter distributions for each EV isolation condition in this study.

3.2.2.4 Nanoparticle tracking analysis (NTA)

Nanoparticle tracking analysis (NTA) is a method to determine the concentration and diameter of particles in a solution. The basic principle of this method is the dependency of a particle´s size and its Brownian molecular motion. By tracking the motion of each particle, for example through detecting scattered light, conclusions can be drawn about their diameters as well as concentrations. EVs from four different CardAP donors (36, 48, 50, and 46) were analysed at the ZetaView® with 14 different camera levels and according to the manufacture´s manual.

Water, 0.1 µm filtered PBS and a calibration with 100 nm sized styrolbeads was conducted before EV samples were characterized in at least two different dilutions (1 to 1,000 or 2,000) and in triplicate measurements. Determined particle concentrations of EVs were related to the derived number of CardAP cells after each isolation procedure, accordingly to protein amount determination of EVs.

3.2.2.5 Liquid/electron spray ionization mass spectrometry (LC/ESI-MS)

Liquid chromatography/electron spray ionization-mass spectrometry (LC/ESI-MS) was used to gather a broader overview of proteins transported by isolated EVs. Samples were processed and measured at the Cardioproteomics/Tissue Typing Unit at Charité Universitätsmedizin Berlin under the supervision of Dr. Oliver Klein.

Procedure: EVs from three different CardAP donors (36, 48, and 69) either in unstimulated or cytokine stimulated conditions were transferred to 10 kDA cut off amico filters followed by an overnight digestion with trypsin at 37°C. Peptide samples were extracted with 0.1 % TFA and measured by a mass spectrometer (here: UPLC ESI-QTOF).

Analysis: The obtained mass spectra were analysed by searching the SwissProt database with Mascot software. The following parameters were set for analysis: i) taxonomy = *homo sapiens* (human; 20175 sequences); ii) proteolytic enzyme = trypsin; iii) maximum of accepted missed cleavages = 1; iv) mass value = monoisotopic; v) peptide mass tolerance = 10 ppm; vi) fragment mass tolerance = 0.05 Da; and vii) variable modifications = oxidation. Afterwards, identified proteins were considered for further analysis if scores corresponded to $p < 0.05$ and if at least one detected peptide were determined in at least two from three donors. By String database, networks of interactions between the identified proteins were analysed and visualized as connecting line, when they fulfilled a high confidence interaction (0.77) of active interaction sources by experiments, databases, co-expression and co-occurrences.

3.2.2.6 Micro RNA expression assays

MiRNAs are a post-transcriptional tool of a cell to abolish the translation of mRNAs into proteins, which crucially influence thereby processes such as differentiation, proliferation or apoptosis [120]. Since EVs can also transport miRNAs to recipient cells, it was of interest to gather a broader overview of the transported miRNAs by EVs from CardAP cells. For that reason, total RNA was isolated and analysed by an nCounter miRNA expression assay. Some obtained miRNA results were additionally verified by quantitative real-time polymerase chain reaction (qPCR).

3.2.2.6.1 Isolation of RNA from EVs

Total RNA was isolated from unstimulated and cytokine stimulated EVs from three different CardAP donors (36, 48, and 50) by miRNeasy Mini Kit according to the manufacture´s protocol. EV pellets from the final centrifugation step during EV isolation were suspended in 700 µL QIAzol Lysis Reagent instead of filtered PBS. This suspension was homogenized for 25 sec on ice at highest level. The lysates were transferred to low binding tubes and stored at -80°C. After all samples were collected, the lysates were gently thawed at RT and mixed with 140 µL chloroform. After a centrifugation for 15 min at 12,000 *x* g and 4°C, the aqueous phase (upper

layer) was collected and transferred to RNeasy Mini columns. These columns were washed with different provided washing buffers until the RNA was eluted with 30 µL RNase free water. Absorbance at 260 nm and 280 nm were measured at a NanoDrop 2000 spectrophotometer to evaluate the purity and concentration of isolated RNAs.

3.2.2.6.2 NCounter® Human v2 miRNA expression assay

This method allows to identify the expression of almost 700 different miRNAs in one sample by four different steps at an nCounter® Digital Analyzer. Firstly, unique oligonucleotide tags are ligated to previously isolated miRNAs. Secondly, tagged miRNAs are hybridised to reporter and capture probes. Finally, unbound probes are removed and the expression of miRNAs can be detected through the previous barcoding of tagged miRNAs with bound probes. Those steps were kindly performed by Dr. Maria Schneider according to the manufacturer's protocol.

Analysis: The gathered raw data of detected miRNAs was analysed with the help of nSolver software (version 4.0, NanoString Technologies). Firstly, the data was normalized using the top 100 most abundant miRNAs in all samples as well as the positive controls to normalize for any differences in preparation, hybridization, and processing efficiency. Secondly, the mean plus two standard derivations of the negative control was subtracted from each sample to derive normalized background corrected data. Finally, miRNAs were considered to be present in EVs when a count of ten or more copy numbers was measurable in at least two of the three donors from either unstimulated or cytokine stimulated conditions. Enrichment analysis, such as for biological pathways, was performed by an open-source software called Functional Enrichment Analysis Tool [117,118].

3.2.2.6.3 Quantitative real-time polymerase chain reaction (qPCR)

Some selected miRNAs were additionally quantified for their expression level by a different method, the quantitative real-time PCR. This method allows the detection of specifically amplified target sequences by fluorescence in real-time. Here, the miRNA will be transcribed into complementary DNA (cDNA), which serves as template strands for the annealing and amplification phase of fluorescence labelled probes, binding forward and reverse primers in the PCR process. The annealed probe does not emit its fluorescence on the 5´-end due to a present quencher on the 3´-end. During the amplification, the DNA polymerase will not only synthesize the new strand but also cleave probes that hybridized to the template strand beforehand. Thereby, the fluorescence dye will be separated from its quencher, which can now be detected and monitored over a given time period and cycle numbers (CT). Since the emitted fluorescence is directly proportional to the amount of miRNA product in each PCR cycle, a retrograde quantification of the initial target miRNA expression is allowed.

Preparation: 10 ng of the previously isolated total RNA from EV samples as well as a negative control (solely RNase-free water) was reverse transcribed into cDNA with TaqMan® Advanced miRNA cDNA Synthesis Kit according the manufacture´s protocol. At the start, the miRNA and negative control undergoes a poly(A) tailing reaction followed by an adaptor ligation reaction. Afterwards, the reverse transcription (RT) and the amplification of miRNAs was performed by using a miRNA primer mix. The obtained cDNA samples were stored at -20°C until further analysis or immediately diluted in TE buffer (one to ten) for qPCR.

Procedure: TaqMan™ Fast Advanced Master Mix, seven different TaqMan™Advanced miRNA Assays (human miRNAs for 494-3p, 146a-5p, 132-3p, 26b-5p, 199a-3p, 186-5p, and 302d-3p) and RNase-free water were mixed for each PCR mix (**Table 15)**. Master mixes of each miRNA Assays were distributed to 384-well plates (15 µL/well), while three technical replicates were performed for each sample. Then after, cDNA samples were added (5.0 µL/well), the plate was sealed with an adhesive foil, shortly vortexed and centrifuged at 300 *x* g for 60 sec at 4°C. The plate was cautiously transferred to the QuantStudio 6 Flex Real-Time PCR machine and the PCR run was immediately started with the thermal cycling condition as shown in **Table 16**. After the run was finished, the CT threshold was set at 0.2 and the values were analysed as described in the following.

Table 15: PCR reaction mix.

Component	Mix for one reaction
TaqMan™ Fast Advanced Master Mix (2x)	10 µL
TaqMAn™ Advanced miRNA Assay (20x)	1 µL
RNase-free water	4 µL
PCR Reaction Mix	15 µL

Table 16: PCR thermal cycling conditions for QuantStudio

Step	Temperature [°C]	Time [sec]	Cycles [#]
Enzyme activation	95	20	1
Denature	95	1	40
Anneal/Extension	60	20	
Stop	4	∞	1

Analysis: The delta-delta CT (ΔΔ CT) method was used to analyse the expression data. Firstly, samples, which were always performed as three technical replicates, were normalized (Δ CT) to the expression of the median of miRNA26b-5p and miRNA199a-3p. Both miRNAs were identified to be the most stable in EV preparations according to NormFinder [121]. Then the fold change (ΔΔ CT) of target miRNA expression was calculated for unstimulated EVs in relation to the corresponding cytokine stimulated EV reference sample.

3.2.3 Immunological methods

3.2.3.1 Flow cytometry

Flow cytometry allows the analysis of different features of a cells, including their size, granularity or presence of proteins when stained with fluorescence labelled antibodies. In a flow cell, suspension of cells or EV-bound particles is channelled through a micro-cuvette . It ensures the screening of single events by an optic system consisting of laser and diverse filters. The optical signals are converted into electrical signals, which are amplified and can be analysed with suitable software programs.

3.2.3.1.1 Surface proteins on cells

Detection of surface proteins can help to monitor changed expression upon different stimulations as well as to distinguish between different cell subsets. Although diverse cells were

investigated in this study, an identical procedure was conducted to elucidate the repertoire of surface proteins.

Procedure: Harvested cells were collected in 5 mL FACS tubes (e.g. CardAP cells 2 x 10^4 cells/tube). The cell suspension was topped up with up with 4 mL FACS buffer and centrifuged at 300 *x* g for 10 min at 4°C. Afterwards, the supernatant was discarded and cells were suspended in 50 µL FACS buffer with a mix of human specific fluorescence labelled antibodies. Furthermore, single staining for the incorporated fluorescence as well as an unstained control were conducted in parallel. The composition and dilutions of master mixes are shown in **Table 17** for immune cells of the conducted T cell proliferation assays or in **Table 18** for CardAP cells after the EV isolation process.

Table 17: Fluorescence labelled human specific antibody mixes for immune cells

Assay set-up	Assay	Antibody mix
PBMCs, $CD3^+$ cells, or $CD3^+$ with $CD14^+$ cells (anti-CD3 or unstimulated)	T cell proliferation	CD19 V450 (1:1000), CD14 APCCy7 (1:50), CD8 PECy7 (1:50), CD4 PerCPCy5.5 (1:75), CD56 PacificBlue™ (1:50) and live/dead marker V510 (1:100)
PBMCs (unstimulated)	Expression analysis of $CD14^+$ cell markers	CD86 PE (1:100), PD-L1 PerCPCy5.5 (1:50), HLA-DR PECy7 (1:1000), CD206 APC (1:100), CD14 APCCy7 (1:50) and live/dead marker V510 (1:100); if cells were not CFSE labelled also CD163 FITC (1:50) was included

Table 18: Fluorescence labbeld human specific antibody mixes for CardAP cells

Targeting	Human specific antibody mix
Tetraspanins	CD63 PE (1:1000), CD81 FITC (1:1000), CD81 PE (1:1000), CD9 FITC (1:1000)
Cytokine receptors	CD120c PECy7 (1:50), CD119 PE (1:50) and CD121a APC (1:50)
Immunological markers	PD-L2 APC (1:50), PD-L1 PerCPCy5.5 (1:50), CD54 APC (1:50), HLA-ABC FITC (1:100), HLA-DR APC (1:50), CD86 PE (1:50), CD80 FITC (1:20), CD106 PE (1:100)
Mesenchymal markers	CD90 APC (1:50), CD44 PECy7 (1:100), CD73 APC (1:50), CD29 PE (1:200)

Afterwards, cells were washed with 3 mL FACS buffer, fixed with 200 µL 0.5% PFA-supplemented FACS buffer and stored in the dark at 4°C until measurement at the flow cytometer (Canto II).

Analysis: Acquired flow cytometry data were in general analysed with the help of FlowJo Software by gating on the particular population of interest. As such, the frequency of proliferated $CD4^+$ or $CD8^+$ T cells (= diluted CFSE signal) was obtained by the gating strategy shown in **Figure 7A**. These obtained frequencies were related for each sample and individually for each assay to the respective untreated immune cell control (immunogenicity = unstimulated; immunomodulation = anti-CD3 stimulated). The geometrical mean fluores-cence intensity (MFI) served as value of the expression of surface proteins. Cells were at least gated on living single cells (**Figure 7B**) or when applicable for included subpopulations, like $CD14^+$ cells in PBMC cultures (**Figure 7A**). These obtained MFIs were related to their respective unstained control and displayed as normalized MFIs. Additionally, the freuquency of the expressing

population were valuated (**Figure 7B**), when a clear positive and negative population was detectable.

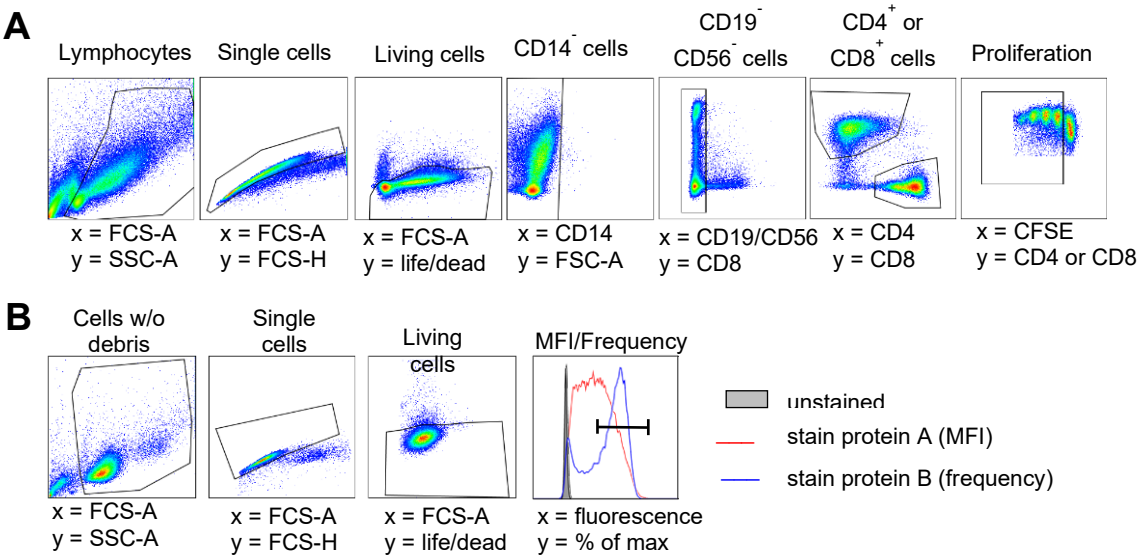

Figure 7: Gating strategies to measure T cell proliferation or expression of surface proteins.
Flow cytometry allows, for example, to identify proliferated T cells as well as the expression of surface proteins in distinct subpopulations. **(A):** The gating strategy is shown here exemplarily for anti-CD3 stimulated PBMC cultures to determine T cell proliferation. Firstly, all detected events were narrowed down towards a lymphocyte gate. Afterwards, cell aggregates and dead cells were avoided by the shown gating for single and living cells. Other cell types than T cells were excluded (NK cells, B cells or monocytes and macrophages). $CD4^+$ as well as $CD8^+$ cells were identified and each subset individually subjected for their CFSE signal. The proliferating cell frequency was determined by using a gate for the fading/dilluted CFSE signal. **(B):** Expression of surface proteins was accessed by gating at least on single viable cells and determining the geometrical mean fluorescence intensity (MFI) of the invesitgated target (red line). The relation between unstained and stained sample gave clue about the expression. In some cases also the frequency of protein expressing cells was determined, when a clear differentiation between expressing and non-expressing cells was detectable (blue line). FCS = forward scatter, SSC = sideward scatter, -A = area, -H = height.

3.2.3.1.2 Surface proteins on EVs

Specialized methods as well as equipment is recommended to measure EVs by flow cytometry. To overcome this issue, we chose an indirect measurement by binding EVs to beads before measurement. Therefore, two drops of aldehyde/sulphate latex beads were given to 4 mL PBS and centrifuged at 300 x g for 10 min. Afterwards, the supernatant was carefully discarded and the bead pellet was suspended in 400 µL PBS. For one staining, 15 µL of beads were incubated with 2 µg of EV protein for 15 min at RT. Afterwards, the solution was topped up with PBS to a total volume of 1 mL and incubated with 50 *x* rpm shaking for 60 min at RT. Afterwards, beads with or without bound EVs were centrifuged at 300 x g for 10 min, washed once in FACS buffer, and then stained with fluorescence labelled human-specific antibodies (**Table 19**) for 30 min at 4 °C in the dark.

Table 19: Fluorescence labelled human specific antibody mixes for EVs from CardAP cells

Targeting	Mix	Human specific antibody mix
Tetraspanins, immunological and mesenchymal proteins	1	CD81 PE (1:50), CD9 FITC (1:50), CD90 APC (1:50), PD-L1 PerCPCy5.5 (1:50)
	2	CD63 PE (1:50), HLA ABC FITC (1:100), CD73 APC (1:50)
	3	CD29 PE (1:100), PD-L2 APC (1:50), CD105 FITC (1:50)
	4	CD144 PE (1:50), CD54 APC (1:50)
	5	HLA-DR APC (1:50), CD44 PE (1:100), CD106 PE (1:100)

Several controls were incorporated: i) stained beads without EVs to elucidate unspecific antibody binding, ii) unstained EV-bound beads to measure auto-fluorescence, and iii) EV-bound beads stained with antibody´s appropriate isotype controls to evaluate unspecific binding/false positive results. Afterwards, all samples were washed, fixed in 0.5% PFA-supplemented FACS buffer and stored at 4°C until measurement at the flow cytometer (MACSQuant). Acquired flow cytometry data were analysed by gating on single beads and extracting the MFI (as shown in **Figure 8**) with the help of FlowJo Software. The obtained MFIs were normalized/related to the respective unstained EV-bound bead control.

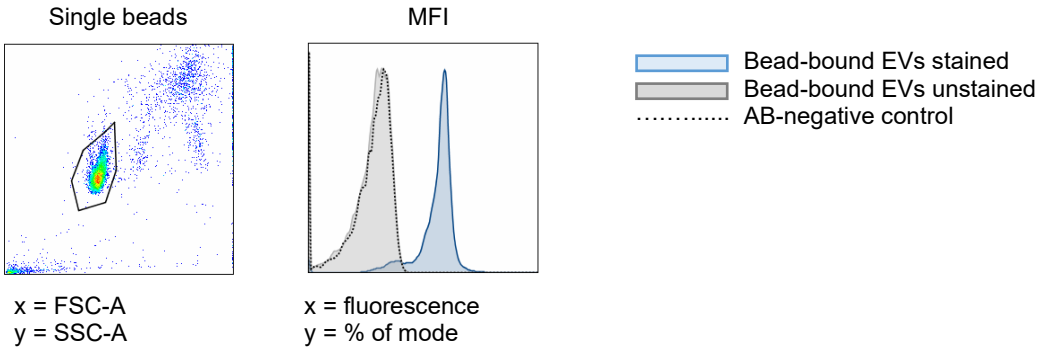

Figure 8: Gating strategy for determining protein expression of EVs bound to beads.
Different surface proteins were detected by flow cytometry on EVs that were previously bound to aldehyde/sulphate latex beads and then stained with human specific fluorescence labelled antibodies. The used gating strategy is shown. The geometrical mean fluorescence intensity (MFI, histogram on the right) were determined from single beads (left). Normalized MFIs were calculated by relating stained towards unstained bead-bound EV samples.

An exception from the general staining procedure was the determination of the presence of GM130 on EVs. Here, a two-step staining protocol was performed. Bead-bound EVs and controls were firstly stained with a polyclonal rabbit GM130 antibody (1:100) for 30 min at 4°C. After a washing step with FACS buffer, the samples were blocked with 5 % (v/v) goat serum supplemented FACS buffer. Secondly, the samples were labelled with a fluorescence labelled anti-rabbit antibody (goat anti-rabbit AF488; 1:100) for another 30 min at 4°C. Afterwards, they were washed, fixed, measured and analysed as previously mentioned. Additional controls served to determine false positive signals by solely performing the second staining step with samples. The general success of the staining for GM130 (**Figure 9**) was verified by performing the previous stated procedure with apoptotic bodies, collected after the 2,000 x g centrifugation step of the conducted EV isolation procedure, instead of EV preparations.

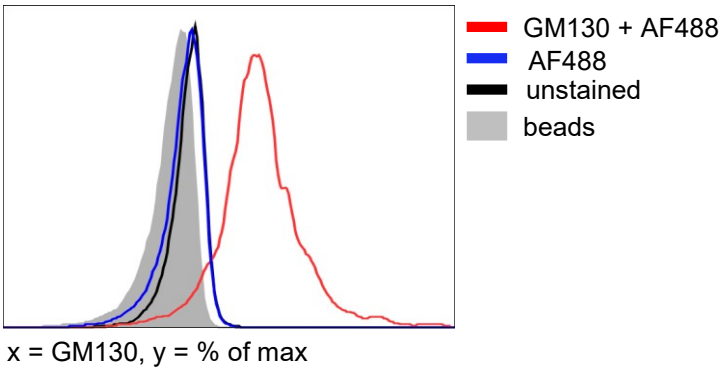

Figure 9: Positive control for GM130 staining protocol.
During the EV isolation process, a pellet of the apoptotic body fraction (2000 *x* g centrifugation step) was collected and stained for GM130 for analysis by flow cytometry. Here, the apoptotic bodies were bound to latex/sulphate beads, stained with the anti-GM130 antibody. Before the secondary antibody anti-rabbit AF488 was applied, a blocking step with goat serum containing FACS buffer was performed. Finally, the samples were washed, fixed in 0.5% PFA-supplemented FACS buffer and measured at MACSQuant. GM130 was detected on apoptotic bodies bound to beads when staining was performed with primary and secondary antibody (red line), while no unspecific binding was detected for the staining with the secondary antibody alone (blue line) as compared to the unstained controls (apoptotic body-bound beads = black line, or beads alone = grey filled area).

3.2.3.1.3 Intracellular proteins in cells and EVs

Intracellularly located proteins, such as transcription factors, were investigated by permeablizing the cell´s plasma membrane in advance to the respective staining via the Foxp3/Transcription Factor Staining Buffer Set according to the manufacture´s manual. It was performed during this study for regulatory T cell assays (*see section 3.2.1.6*) as well as for EV-cell interaction of unlabelled EVs with murine cells (*see section 3.2.1.4*).

Regulatory T cell assays: Immune cells were harvested by accutase treatment, washed with FACS buffer and stained on their surface for 15 min at RT with CD127 APC-Cy7 (1:50). Then, cells were additionally stained with CD3 FITC (1:200; when not CFSE labelled immune cells were used), CD19 V450 (1:50), CD56 Pacific Blue (1:20), CD11b V450 (1:100), CD8 PE-Cy7 (1:100), CD25 PerCP-Cy5.5 (1:100), CD14 APC-Cy7 (1:100), CD69 PE (1:50) and live/dead marker 510 (1:100) for another 15 min at 4°C. After cells were washed in FACS buffer, 500 µL freshly prepared fixation/permeabilzation reagent was applied on the cells for 30 min at 4°C in the dark. Freshly prepared premeabilization buffer was used to wash cells and perform an intracellular staining with FoxP3 Alexa647 (1:400) for 30 min at 4°C in the dark. After two washing steps, the samples were immediately analysed at the flow cytometer (ContoII). The obtained data were analysed for the frequency of regulatory T cells according to the gating strategy shown in **Figure 10** with the help of FlowJo software. Importantly, gates for CD127 and FoxP3 were set with respect to conducted fluorescence minus one (FMO) controls.

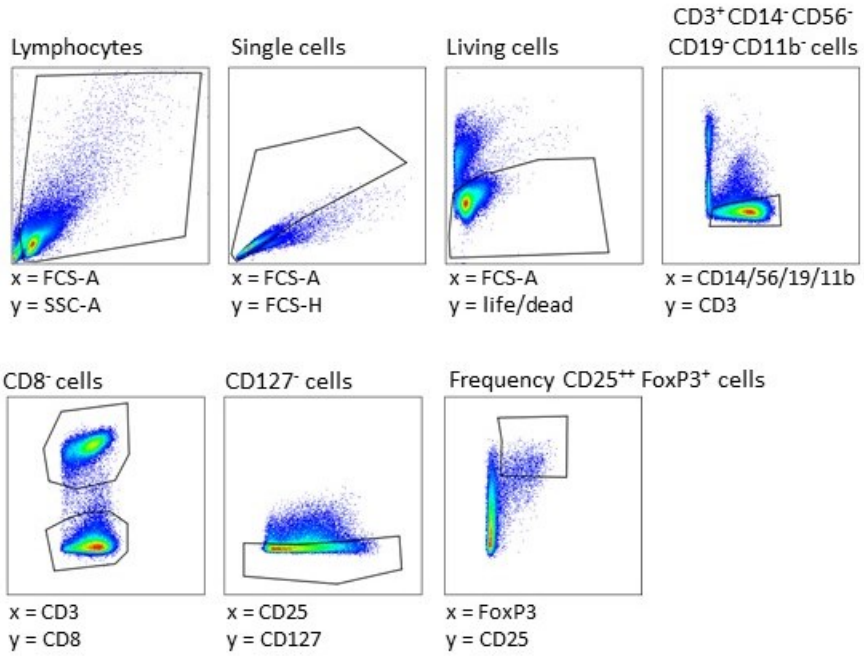

Figure 10: Gating strategy for determining the frequency of regulatory T cells in stimulated immune cell cultures by flow cytometry.
Stimulated PBMCs or co-cultures of EV-primed $CD14^+$ cells with CD3+ T cells were investigated by flow cytometry for the frequency of regulatory T cells. The gating strategy is shown here exemplarily for anti-CD3 stimulated PBMC cultures. Firstly, all detected events were narrowed down towards a lymphocyte gate. Afterwards, cell aggregates and dead cells were avoided by the shown gating for single and living/viable cells. Other cell types than $CD3^+$ T cells were excluded (NK cells, B cells or monocytes and macrophages). $CD8^+$ cells and $CD8^-$ (and therefore respectively $CD4^+$ T cells) were identified. The $CD4^+$ subset was further excluded for expression of CD127 via fluorescence minus one (FMO) controls. Then the frequency of $CD25^{++}$ $FoxP3^+$ cells (= regulatory T cells) was determined as shown in the last flow cytometry dot plot. The signal for FoxP3 was gated with the help of FMO controls. FCS = forward scatter, SSC = sideward scatter, -A = area, -H = height.

EV-cell interaction: Murine cells were harvested by accutase treatment and washed with FACS buffer. Importantly, one sample was distributed in at least four different 5 mL FACS tubes (stained/unstained sample for either the intra- or extracellular protocol). For the extracellular staining, cells were stained with human-specific antibodies for CD73 APC, CD63 PE and CD81 FITC (all 1:50), and a live/dead marker V510 (1:100) for 30 min and 4°C in the dark. For the intracellular staining, cells were firstly stained with the live/dead marker V510 as previously described. Secondly, washed cells were permeabilized as described beforehand. Finally, cells were stained intracellularly with the same antibodies used for the extracellular stain except the live/dead marker V510. Afterwards, stained cells were washed, fixed with 0.5 % PFA containing FACS buffer and immediately acquired at the flow cytometer (CantoII). The obtained data were analysed for the MFIs of human EV proteins on or within murine cells by gating on single viable murine cells with the help of FlowJo software (according to previously shown gating strategy in **Figure 7 B**). The MFIs were normalized to the respective unstained control. Furthermore, EV treated cells were stained by both protocols with isotope control antibodies (mouse IgG1, kappa APC for CD73 APC, mouse IgG1, kappa PE for CD63 PE, mouse IgG1, kappa FITC for CD81 FITC) to exclude false positive signals.

3.2.3.2 Immunofluorescence staining assay

EV-cell interaction assays were not solely determined by flow cytometry but also by microscopy. In order to identify cells or specific cell subsets, an immunofluorescence staining was conducted by washing adherent cells twice with PBS. Then after, the cells were fixed with 4% PFA for 15 min at RT. Afterwards, a staining with 4´, 6-diamidino-2-phenylindole (DAPI) was performed for 20 min at 4°C to visualize the nucleus of cells and human specific antibodies as stated for each individual assay in **Table 13**. Afterwards, the samples were carefully washed with PBS and examined at an AxioObserver microscope or the High Content Screener.

3.2.3.3 Enzyme-linked immunosorbent assay (ELISA)

In this study, concentrations of cytokines and other soluble factors were determined by enzyme-linked immunosorbent assays (ELISAs). The soluble factors are bound by immobilized (monoclonal) capture antibodies and by detection antibodies, which are already enzyme-linked or can be spotted through enzyme-linked fusion proteins. The activity of enzymes can be tracked by a colorimetric approach or luminescence. In this study, commercially available ELISA kits were used according to the manufacturer's protocol for different assays (**Table 20)**. In brief, ELISA microplates were coated overnight with the capture antibody (1:200) and followed by several washing steps with 0.05% Tween 20 in PBS on the next day. Microplates were blocked with the blocking buffer for at least 180 min. Next, samples and freshly prepared standards were added to the wells for an overnight incubation at 4°C. On the next day, the plate was washed several times and the detection antibody (1:200) was applied for additional 120 min. After washing, the avidin-HRP conjugate (1:1000) was added to each well and washed away after 60 min by thorough washing. Fresh TMB substrate was added to the wells and incubated for 15 to 20 minutes. The reaction was stopped with stop solution and the absorbance was measured at 450 nm and 570 nm on a Mithras LB 940 microplate reader. Similar to the BCA protein detection assay, a standard curve for each individual cytokine or factor was used to calculate the concentrations in the collected conditioned medium, respectively.

Table 20: Summary of used ELISAs during this study

Conditioned medium samples from	ELISAs	Notes
T cell proliferation assay	Human IFNγ	Samples were diluted 1:2 or 1:4
	Active human TGFβ	Samples were used undiluted
Pro-angiogenic factor release assay	Human IL-6	Samples were diluted 1:5, 1:10 and 1:20
	Human IL-8	Samples were diluted 1:5, 1:10 and 1:20
	Human VEGF	Samples were diluted 1:5 and 1:10

3.2.3.4 Multiplex bead-based soluble factor determination assay

The principle of ELISAs was transferred towards a flow cytometry approach in so called multiplex bead-based assays. Here, capture and detection antibodies are labelled with fluorescence dyes, while capture antibodies are additionally coupled to beads (partially with different sizes). In this study, LEGENDplex™ bead-based assays were purchased from BioLegend, and partially customized for the purpose to investigate TNFα, IL-1β, IL-17a, and IL-10 concentrations in supernatants from diverse T cell proliferation assays. Supernatants from $CD14^+$ cells incubated for 24 h with EVs from CardAP cells were subjected to a different set

of cytokines and chemokines, namely IL12p70, TNFα, IL-4, MCP1, IL-10, IL1-ß, IL-8, TARC, IL-1RA, IL-6, IL-23, IFNγ, and IP-10. Samples as well as standards are proceeded according to the manufacturer's protocol, and finally measured at a flow cytometer (CantoII). The analysis was conducted according to supplier´s protocol with the help of the provided software (LEGENDplex™ version 7.1).

3.2.3.5 Magnetic activated cell sorting

Magnetic bead-coupled antibodies allow the separation of desired subsets from a heterogenic population. This magnetic activated cell sorting (MACS) was used during this study to derive relatively pure population of $CD14^+$ or $CD3^+$ cells. Therefore, freshly isolated PBMCs were incubated with human specific CD3 or CD14 microbeads in MACS buffer for 15 min at 4°C (buffy coats: 1 mL MACS buffer + 250 µL microbeads). Then, the cells were washed and loaded on magnetically active LS Columns, which enabled a collection of negative and positive fractions. After several washing steps, the cells were counted and either used for T cell proliferation assays, cryopreserved, or stained for flow cytometry to determine the achieved purity. Indeed, purities for $CD3^+$ cell isolation were obtained ≥ 97.5 % and for $CD14^+$ ≥ 96.4 %.

3.2.4 Statistical Analysis

In this study, non-parametric data are shown as median with data range and parametric data are shown as mean with data range. Statistical analysis was performed using GraphPad Prism 6.0 software. A parametric distribution of data was tested with Shapiro-Wilk normality tests for considering appropriate statistical analysis. It was further differentiated for either two or more than two groups with one variable. The performed statistical analysis are shown in **Table 21**. Results were considered significant with * $p < 0.05$, ** $p < 0.01$, *** $p < 0.001$.

Table 21: Statistical analysis performed during this study

Number of groups	Paired or unpaired	Distribution of data	Analysis with following statistical test
More than two	Paired	Non-parametric	Friedma´s test with Dunn´s multiple comparison *post hoc* test
		Parametric	Repeated measures ANOVA with Bonferroni´s *post hoc* test
	Unpaired	Non-parametric	Kruskal-Wallis test with Dunn´s multiple comparison *post hoc* test
Two	Paired	Non-parametric	Wilcoxon matched-signed rank test
		Parametric	Paired T Test
	Unpaired	Non-parametric	Mann-Whitney test
		Parametric	Unpaired T Test

4. Results

Previous data from our and collaborating research groups emphasized the suitability of human CardAP cells as regenerative therapeutic tool to treat CVDs. For other regenerative cell types, such as MSCs, it was recently demonstrated that their released EVs play a major role for their therapeutic potential. It can be speculated that CardAP cells release EVs with beneficial therapeutic effects, which would enable a cell-free therapeutic approach. In order to answer this question, EVs were isolated from the conditioned medium of CardAP cells that were cultured for 20 h in serum free medium with or without a pro-inflammatory cytokine cocktail of IFNγ, TNFα as well as IL-1β (each 10 ng/mL). Both culture conditions were chosen, because a pro-inflammatory milieu was present when CardAP cells exhibited its anti-apoptotic, immune modulating as well as cardio protective feature [13,60,65] but not when CardAP cells demonstrated their pro-angiogenic effect [64]. Furthermore, serum free medium was chosen to avoid contamination of EVs originating from the serum source.

4.1 The influence of both EV biogenesis conditions on CardAP cells

It was not yet known how CardAP cells respond towards the two applied EV biogenesisis conditions. For that reason, unstimulated and cytokine stimulated CardAP cells were characterized in more detail for their apoptotic behaviour, morphology, and expression of surface proteins.

4.1.1 Both EV biogenesis conditions maintain the spindle-shaped morphology, while cytokine stimulation induces a mild apoptosis of CardAP cells

Starvation and cytokines, like TNFα, can initiate a cell to undergo the programmed cell death. It was of interest whether apoptosis of CardAP cells is initiated upon such culture conditions applied to derive the further investigated EVs. In total, four different culture conditions were investigated: IDH medium with human serum (cIDH), centrifuged human serum (cenIDH), serum free isolation IDH medium with or without a pro-inflammatory cytokine cocktail (isoIDH ± cyt). The later two were used to derive conditioned medium for the EV isolation procedure, while both serum supplemented media were used for the thawing and expansion of CardAP cells. The frequencies of neither non-apoptotic ($7AAD^-$ $AnnexinV\text{-}FITC^-$; **Figure 11A**) nor early apoptotic ($7AAD^-$ $AnnexinV\text{-}FITC^{+-}$; **Figure 11B**) CardAP cells were significantly influenced upon either EV biogeneisis condition in comparison to both expansion media. However, cytokine stimulated CardAP cells displayed a trend of a reduced non-apoptotic cell population in comparison to the other three culture conditions, such as cenIDH cultured CardAP cells (median frequency of non-apoptotic cells: isoIDH + cyt = 79.30 %; cenIDH = 86.00 %; **Figure 11A**). In fact, cytokine stimulation caused a significant increase in the frequency of late apoptotic ($7AAD^+$ $AnnexinV\text{-}FITC^+$; **Figure 11C**) cells in comparison to cenIDH cultured CardAP cells but not to cIDH nor isoIDH cultured CardAP cells (median frequency of late apoptotic cells (range): isoIDH + cyt = 5.22 (1.71 - 9.64) %; cenIDH = 1.70 (1.28 - 3.97) %; cIDH = 2.38 (1.62 - 4.14) %; isoIDH = 4.84 (2.28 – 5.40) %). Although apoptosis was mildly induced, the spindle-shaped morphology of CardAP cells was never affected by either of the conditions as determined by microscopy (**Figure 11D**).

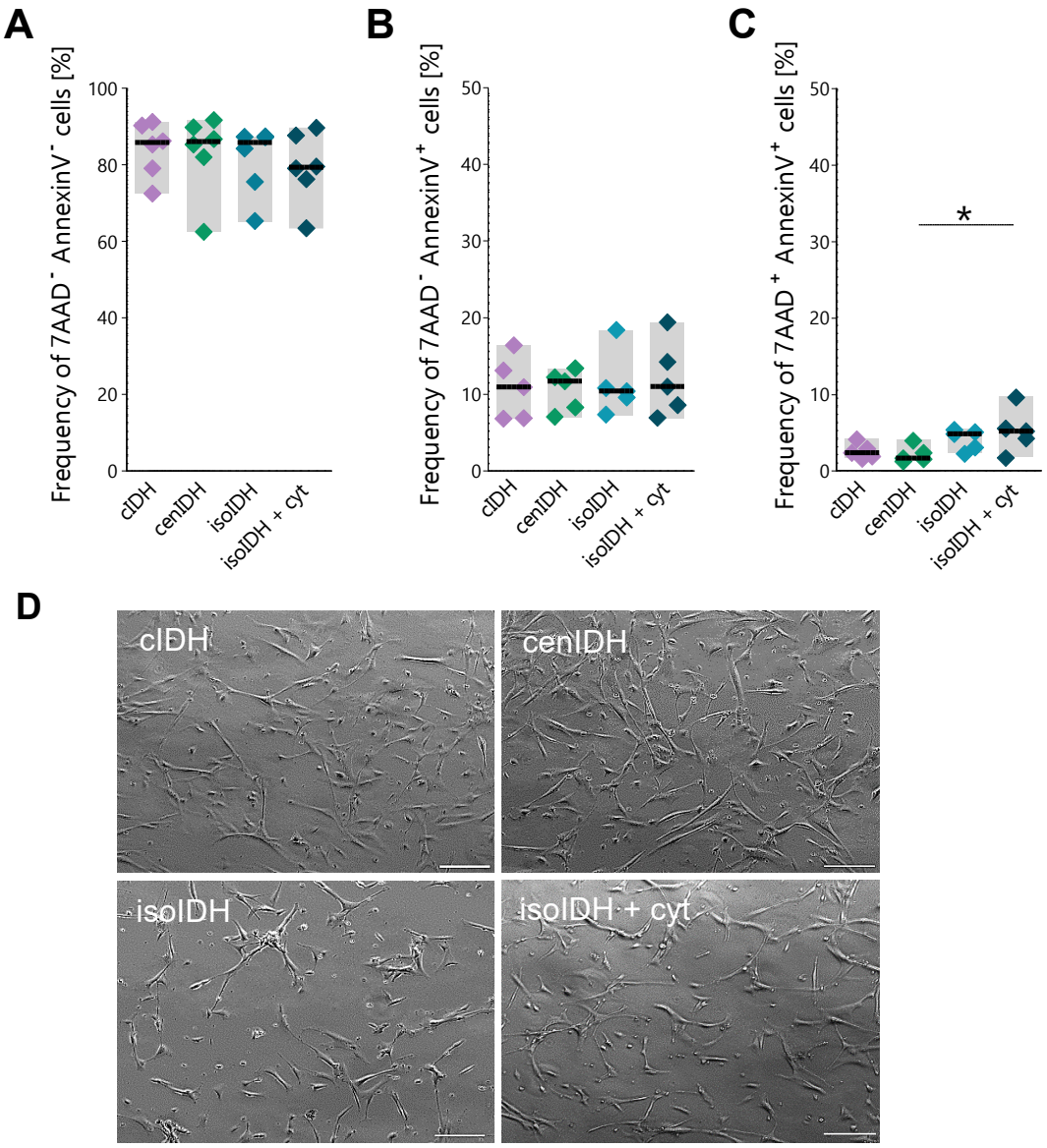

Figure 11: CardAP cells preserved their morphology, while apoptosis was solely mildly induced in the presence but not in the absence of cytokine stimulation during the EV biogenesis.
CardAP cells were cultured in 6-well plates (1x10^6 cells/well) with centrifuged serum IDH (cenIDH) medium. After 24 h, CardAP cells were washed twice with PBS and then cultured either in complete (cIDH), cenIDH, or serum free isolation IDH medium with or without cytokines (isoIDH ± cyt). After 20 h, the morphology of CardAP cells was analysed by light microscopy (AxioObserver). Afterwards, cells and cell debris were harvested, stained with AnnexinV-FITC and 7AAD for 15 min and immediately measured at a flow cytometer (Canto II) to determine the level of apoptosis by flow cytometry. **(A-C):** The individual frequencies of 7AAD$^-$AnnexinV-FITC$^+$ cells **(A)**, 7AAD$^+$AnnexinV-FITC$^+$ cells **(B)** or 7AAD$^-$ AnnexinV-FITC$^-$ cells **(C)** are shown as median with data range for all four conditions (n = 5, four different CardAP donors). **(D):** Representative brightfield images are shown with 100 µm scale bars (n = 4; four different CardAP donors).Statistical analysis was performed by Friedman´s test with Dunn´s multiple comparison *post hoc* test; (*p < .05). Mild apoptosis of CardAP cells is solely induced by the EV biogenesis condition that was supplemented with cytokines (isoIDH +cyt), while the morphology appeared unaffected by the different applied biogenesis conditions.

4.1.2 The expression of surface proteins on CardAP cells differs between both EV biogenesis conditions

Cytokine stimulated and unstimulated CardAP cells were further characterized for a set of surface proteins by flow cytometry after their exposure to both EV biogenesis conditionds. A responsiveness of CardAP cells towards the pro-inflammatory trigger was verified by the expression of IFNγ-receptor type I (IFNγ-RI), TNF-receptor type II (TNF-RII), and by a lower expression level for IL-1 receptor type I (IL-1-RI; **Figure 12A**). From these three receptor subunits solely TNF-RII showed a clear elevated trend in its expression under cytokine stimulation (median normalized MFI unstimulated *versus* (*vs.*) cytokine stimulated: TNF-RII: = 3.01 *vs.* 5.52; IFNγ-RI = 7.93 *vs.* 8.51; IL-1-RI = 1.40 *vs.* 1.44; **Figure 12B**). In contrast, the expression of several immunological relevant surface proteins was significantly enhanced (**Figure 12C**), such as vascular cell adhesion protein-1 (CD106), programmed death ligand 1 and 2 (PD-L1/2), or the intercellular adhesion molecule-1 (CD54;; median normalized MFI unstimulated *vs.* cytokine stimulated: CD106= 1.13 *vs.* 6.57; PD-L1 = 6.50 *vs.* 14.93; PD-L2 = 5.67 *vs.* 22.21 ; CD54 = 31.07 *vs.* 72.69). HLA-ABC solely showed an increased trend in its expression (median normalized MFI unstimulated *vs.* cytokine stimulated = 15.07 *vs.* 20.80). Moreover, CardAP cells from both conditions displayed an absence or very low expression for HLA-DR as well as for the co-stimulatory molecules CD80 and CD86 (highest normalized MFI: HLA-DR = 1.40; CD80 = 1.71; CD86 = 1.17). Typical mesenchymal surface proteins, such as ecto-5'-nucleotidase (CD73), integrin ß1 (CD29), and an adhesion molecule CD44 were detected on the surface of CardAP cells (**Figure 12D**). Upon cytokine stimulation the expression was just by trend increased for CD44 or decreased for CD73, whereas CD29 exhibited comparable expression levels under both EV biogenesis conditions (median normalized MFI unstimulated *vs.* cytokine stimulated: CD44 = 56.15 *vs.* 98.23; CD73 = 262.90 *vs.* 166.30; CD29 = 192.2 *vs.* 198.6). In contrast to other mesenchymal cells, CardAP cells exhibited very low CD90 expression independent of the culture condition (highest normalized MFI = 7.58; **Figure 12D**), which is also reflected by low $CD90^+$ cell frequencies of maximal 26.4 % (**Table 12**). Within the analysed set of molecules of the tetraspanin family, solely CD9 was significantly lower expressed on cytokine stimulated CardAP cells in comparison to their unstimulated counterpart (median normalized MFI unstimulated *vs.* cytokine stimulated = 24.60 *vs.* 10.70; **Figure 12D**). Two other tetraspanins, namely CD63 and CD81, showed solely a comparable trend for reduced expression upon cytokine stimulation (median normalized MFI unstimulated *vs.* cytokine stimulated: CD63 = 73.29 *vs.* 34.95; CD81 = 50.26 *vs.* 32.53; **Figure 12D**).

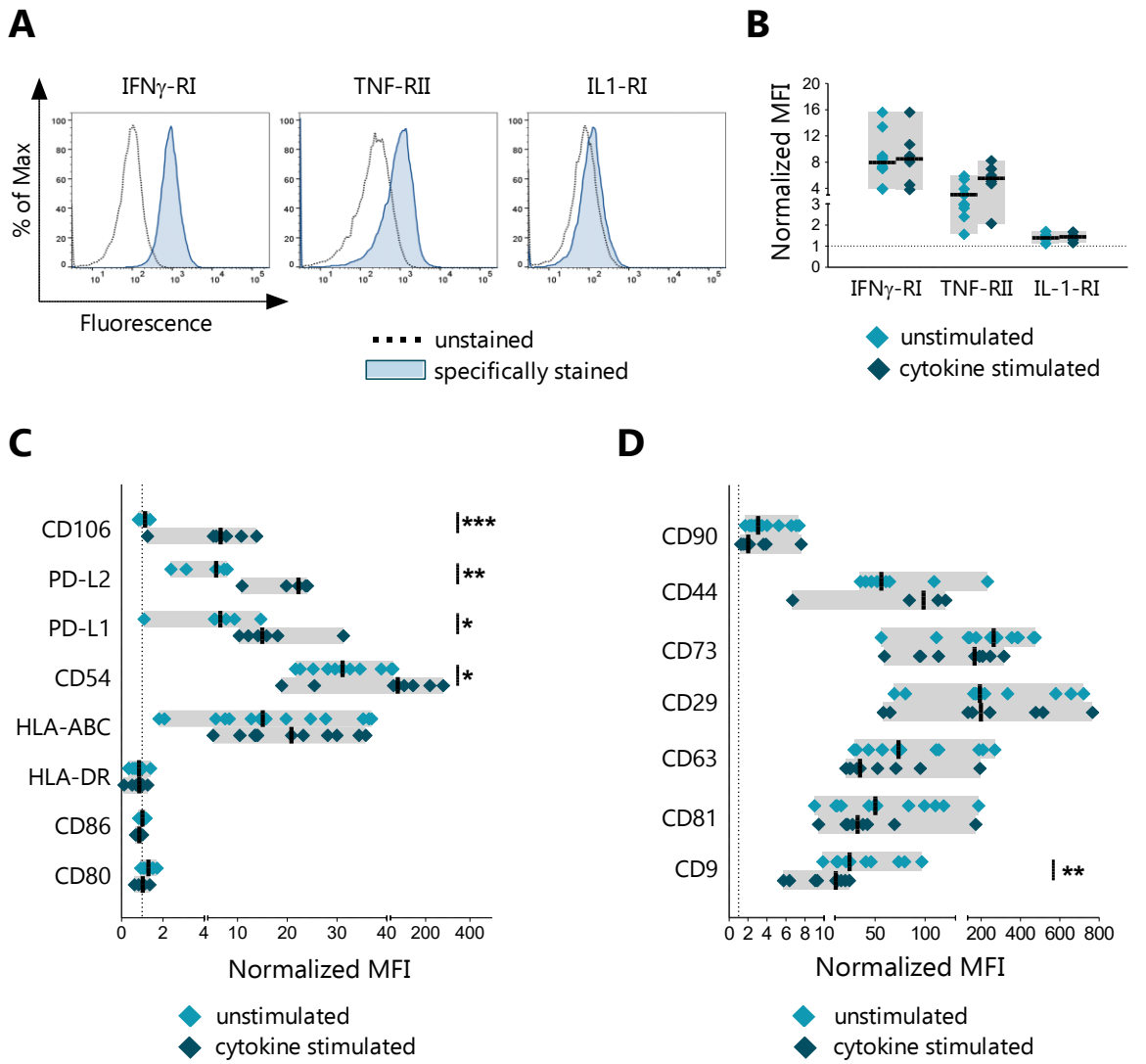

Figure 12: The expression of several surface proteins differed between unstimulated and cytokine stimulated CardAP cells after applying both EV biogenesis conditions.
Cultured CardAP cells were exposed for 20 h to isoIDH medium with cytokines (cytokine stimulated) or without cytokines (unstimulated). EVs were isolated from the conditioned medium, while CardAP cells were harvested by accutase treatment and analysed by flow cytometry. Therefore, $2x10^4$ harvested CardAP cells were stained with human specific fluorescence labelled antibodies. After a washing step, cells were fixed with 0.5% PFA and measured at a flow cytometer (CantoII). Detected geometrical mean fluorescence intensities (MFI) of surface proteins were normalized to the unstained control by calculating the ratio between stained and unstained sample. The normalized MFI for the unstained control (MFI = 1) is indicated as dotted line in the graph. **(A):** Representative histograms are shown for stained and unstained CardAP cells cultured under unstimulated condition for the cytokine receptor subunits IFNy-RI, TNF-RII and IL-1-RI. **(B-D):** Individual normalized MFIs are shown as median with data range for the cytokine receptor subunits (n = 6 - 10; four different CardAP donors; **(B)**), for the immunological relevant proteins CD106, PD-L1/2, CD54, HLA-ABC/DR, CD86, and CD80 (n = 6 - 10, four different CardAP donors; **(C)**), for the mesenchymal proteins CD90, CD44, CD73, and CD29, as well as proteins of the tetraspanin family, namely CD63, CD81, and CD9 (n = 6 - 10; four different CardAP donors; **(D)**). Statistical analysis was performed with Mann-Whitney U test (*p<.05; **p<.01; ***p<.005). CardAP cells replied upon cytokine stimulation by enhancing or inducing the expression of immunological relevant proteins, whereas mesenchymal proteins exhibited equal expression levels.

4.2 The Phenotype of EVs

4.2.1 Cytokine stimulation causes the release of smaller but not more EVs from CardAP cells

Isolated EVs from both EV biogenesis conditions were examined for their diameter (d) by TEM and NTA to obtain information whether they belong to the exosome (d < 100 nm), microvesicle (d = 100 - 1000 nm) or apoptotic body (d > 1000 nm) compartment. Morphological analysis by TEM revealed sphere-like shapes of dehydrated unstimulated as well as cytokine stimulated EVs, while no structures nor shapes were detectable in corresponding PBS controls (**Figure 13A**). The diameters of EVs were assessed for both EV biogenesis conditions from three different CardAP donors for a quantitative analysis. Here, an asymmetrical distribution of EV diameters demonstrated that most unstimulated EVs (77.9 %) as well as cytokine stimulated EVs (90.9 %) are smaller than 100 nm (**Figure 13B**). Strikingly, unstimulated EVs presented significantly larger diameters overall in comparison to their cytokine stimulated counterpart (median diameter (range): EVs = 64.4 (6.3 - 875.8) nm; $EVs^{(cyt)}$ = 39.5 (6.2 - 853.2) nm; **Figure 13C**). This difference between both conditions was able to be verified by NTA for different EV sample preparations. Unstimulated EVs peaked at an larger particle diameter than cytokine stimulated EVs, although the correlation between diameter and amount of particles contrasted previous TEM results by displaying a normal distribution with less than one third of unstimulated EVs (28.9 %) or cytokine stimulated EVs (31.4 %) smaller than 100 nm in their particle diameters (**Figure 13D**). Nevertheless, unstimulated EVs were significantly larger than cytokine stimulated EVs in the measurements of their mean particle diameter (mean particle diameter (± SD): EVs = 125.2 (± 12.2) nm, $EVs^{(cyt)}$ = 118.8 (± 10.5) nm; **Figure 13E**).

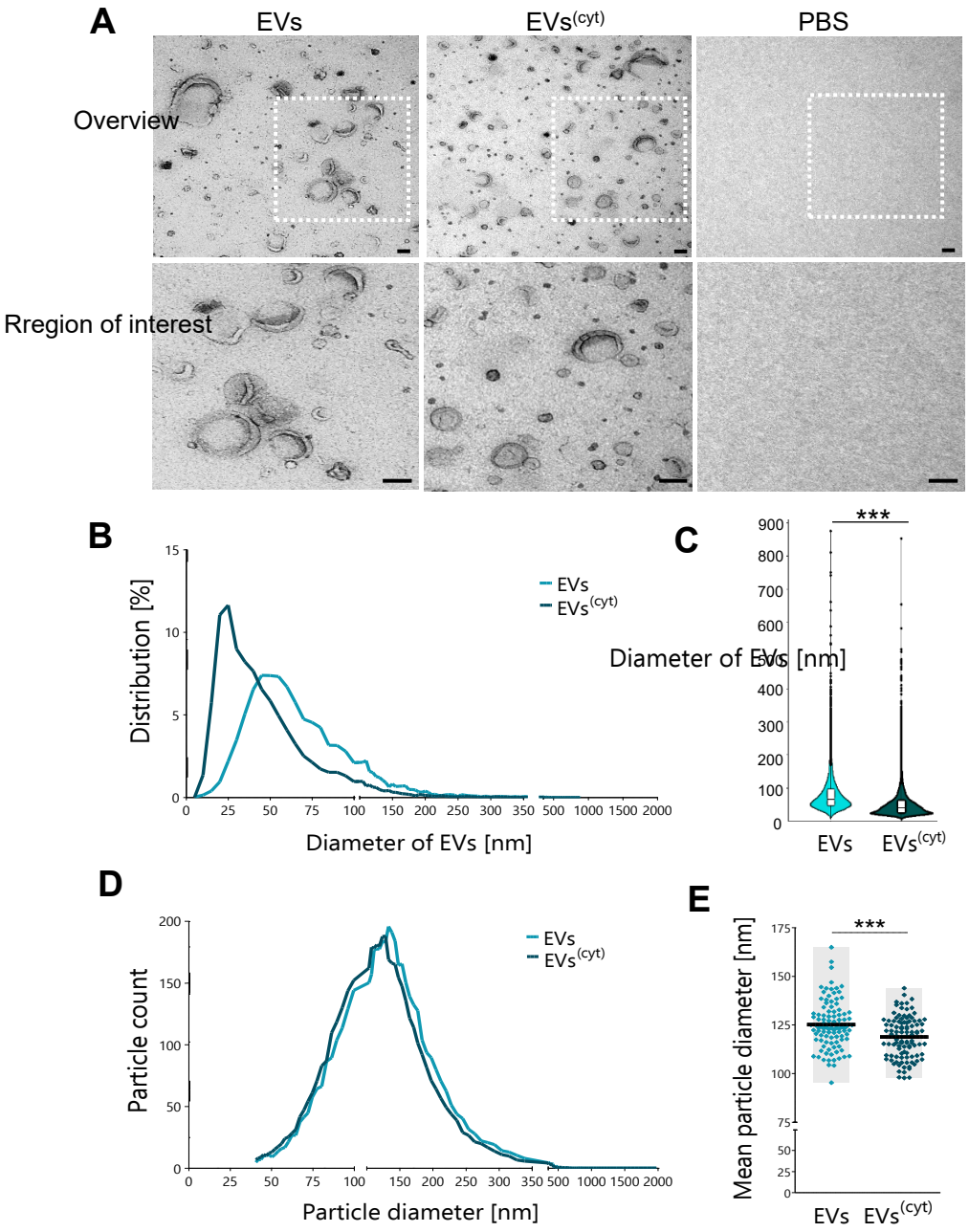

Figure 13: Smaller EVs are released by CardAP cells under cytokine stimulation, while dehydrated EVs of both EV biogenesis condition displayed sphere-like shapes in TEM.
Unstimulated (EVs) and cytokine stimulated (EVs$^{(cyt)}$) EVs were fixed on cupper formavor grids, stained positive-negatively and analysed by TEM at the Zeiss Leo electron microscope. **(A):** Representative images are shown for EVs (left), EVs$^{(cyt)}$ (middle) and PBS (right) as an overview and enlarged region of interest (white square) with scale bars of 100 nm. **(B-C):** The diameters of EVs determined by ImageSPViewer Software from at least 18 individual images per sample are shown for its distribution **(B)** as histograms for EVs (light blue) and EVs$^{(cyt)}$ (dark blue) or as individual data points **(C)** summarized as median with data range (n = 7770, three different Card-AP donors). Additionally, the diameter of particles was measured by NTA. Here, EV samples were diluted 1000-fold and analysed on up to 12 different camera levels at the ZetaView. **(D-E):** The mean of diameter of particles is plotted as histograms **(D)** in correlation to the number (#) of particles for EVs (light blue) and EVs$^{(cyt)}$ (dark blue; n = 8, four different CardAP donors). From each camera level a mean particle diameter was recorded after each measurement. These individual results **(E)** are summarized for both EV types as mean with data range (n = 100; four different CardAP donors). The statistical analysis was performed for parametric data by unpaired T test, or for non-parametric by Mann Whitney U Test (***p < 0.001). TEM and NTA results emphasize the higher

proportion of smaller diameters of vesicles in cytokine stimulated EV preparations than in comparison to the unstimulated counterpart.

NTA not only allowed to characterize EV preparations for their particle diameters but also for their particle concentration. Since the number of CardAP cells varied after each isolation procedure, the examined concentrations were correlated to $1x10^6$ CardAP cells. This was also conducted for an additional mean of concentration by accessing the protein content of EV preparations with the help of BCA protein assays. Neither the EV protein amount (**Figure 14A**) nor the particle concentration (**Figure 14B**) released by $1x10^6$ CardAP cells was statistically different between unstimulated and cytokine stimulated EV preparations (median protein amount: EVs = 2.16 µg; EVs(cyt) = 2.16 µg; median particle concentration: EVs = 8,875 particles*cm^{-3}; EVs$^{(cyt)}$ = 6,953 particles*cm^{-3}).

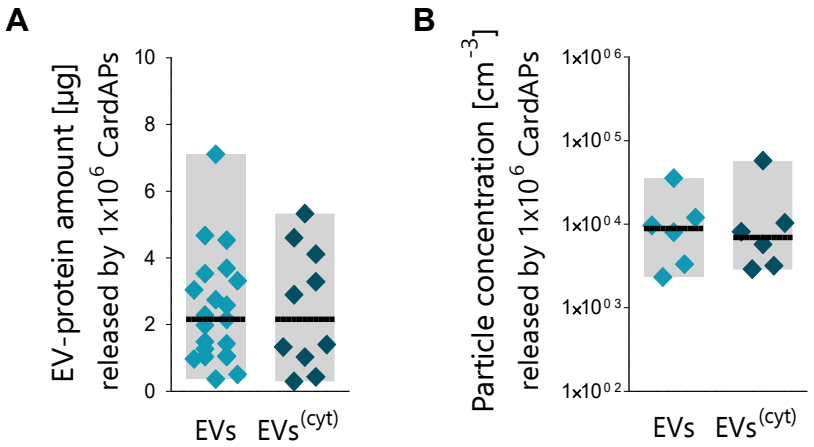

Figure 14: The amount of released EVs was comparable between both biogenesis conditions.
Unstimulated (EVs) and cytokine stimulated EVs (EVs$^{(cyt)}$) were investigated for their protein content by BCA assay as well as for their particle concentration by NTA. **(A):** The individual EV protein amounts that were released from $1x10^6$ CardAP cells under either of both conditions are shown as median with data range (n = 10-21, six different CardAP donors). **(B):** Individual particle concentrations released by $1x10^6$ CardAP cells under either of both conditions are presented as median with data range (n = 6, four different CardAP donors). Statistical analysis was performed with Mann-Whitney U test. Neither of both EV biogenesis condition influenced the amount of released EVs.

4.2.2 The majority of transported proteins are identical between unstimulated and cytokine stimulated EVs

CardAP cells were already shown to alter their protein expression upon cytokine stimulation. In order to elucidate if similar changes occur on their released EVs, this set of surface proteins was analysed on EVs bound to latex/sulphate beads by flow cytometry. Likewise to their originating cell, surface proteins, such as CD73, CD29, CD44, and all three tetraspanins, but not HLA-DR were possible to detect on EVs released from CardAP cells (**Figure 16**). Although all the above mentioned proteins were not significantly altered between both EV biogenesis conditions, a reduced trend for their protein levels were recognizable for CD9, CD81, CD29, and CD73 on cytokine stimulated EVs in comparison to unstimulated EVs (median normalized MFI EVs *vs.* EVs$^{(cyt)}$: CD9 = 6.13 *vs.* 4.32; CD81= 6.20 *vs.* 2.86; CD29 = 75.1 *vs.* 44.9; CD73 = 7.86 *vs.* 4.82). Notably, CD63 showed not only one of the highest determined normilized MFIs but also no difference between both applied conditions (median normalized MFI EVs *vs.* EVs$^{(cyt)}$ = 64.5 *vs.* 61.8). In contrast to their originating cells, other immunological proteins, namely HLA-ABC,

CD106, and PD-L1, were not or only at very low levels detectable on EVs and did not show any difference between both EV biogenesis conditions (**Figure 15**). A significant change was solely observed for CD54, which was significantly decreased on unstimulated EVs in comparison to cytokine stimulated EVs (median normalized MFI EVs *vs.* EVs$^{(cyt)}$ = 1.21 *vs.* 3.53). Three additional surface proteins were included for a more thorough analysis of isolated EV preparations. A potential contamination with cell organelles was investigated by staining for a Golgi matrix protein, namely golgin subfamily A member 2 (GM130). In fact, GM130 was not detectable on neither unstimulated nor cytokine stimulated EVs (**Figure 15**) but on apoptotic body preparations, which served as positive control (**Figure 9**). Furthermore, two proteins with potential beneficial therapeutic effects, namely galectin 1 (Gal-1) and CXC-motive chemokine receptor 4 (CXCR4, CD184), were observed at comparable levels on unstimulated and cytokine stimulated EVs from CardAP cells (median normalized MFI EVs *vs.* EVs$^{(cyt)}$: CD184 = 3.12 *vs.* 2.22; Gal-1 = 1.81 *vs.* 1.62; **Figure 15**).

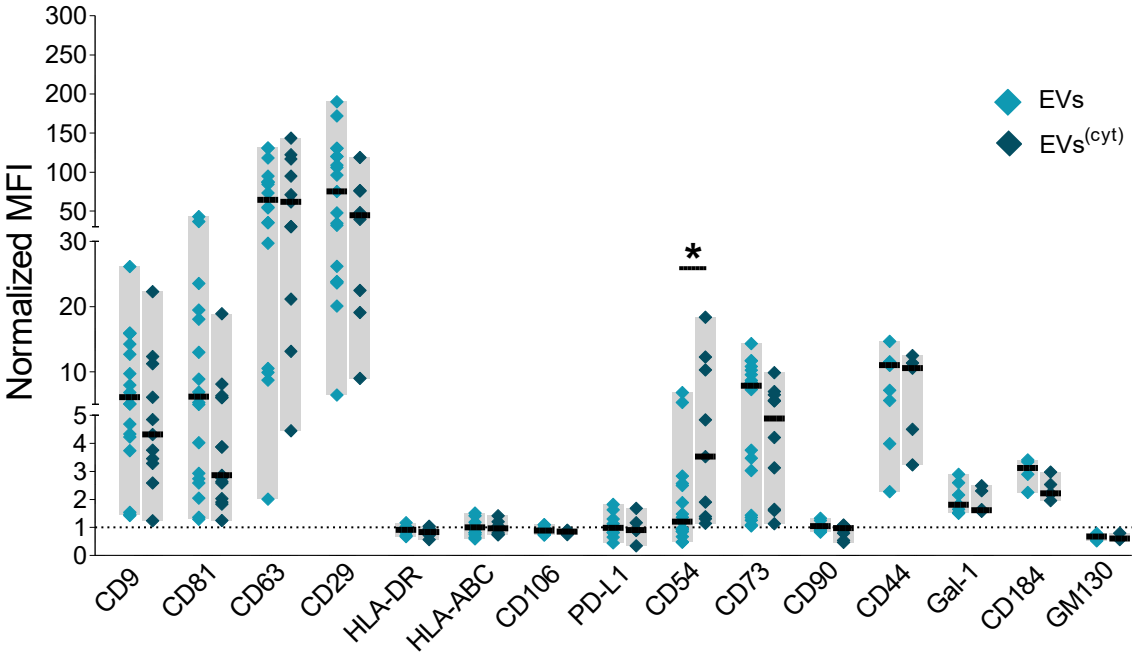

Figure 15: Solely CD54 was significantly increased on cytokine stimulated EVs in comparison to unstimulated EVs from a total of 15 investigated surface proteins.
Unstimulated (EVs) and cytokine stimulated EVs (EVs$^{(cyt)}$) were analysed by flow cytometry for a set of surface proteins. EVs were bound to aldehyde/sulphate beads, stained with human specific fluorescence labelled antibodies and then measured at a flow cytometer (MACSQuant). Normalized geometrical mean fluorescence intensities (normalized MFI) for each fluorochrome/surface protein were calculated as ratio of stained to the corresponding unstained bead-bound EV sample. The dotted line (y = 1) indicates the normalized MFI of the unstained control itself. The results are presented for individual data points summarized as median with data range for proteins of the tetraspanin family (CD9, CD63, and CD81), immunological relevant proteins (CD54, PD-L1, CD106, Gal-1, CD184, HLA-ABC, and HLA-DR), mesenchymal proteins (CD29, CD73, CD44, and CD90), and the Golgi matrix protein GM-130 (n = 3 - 21; three up till six different CardAP donors). Statistical significance was tested by Mann Whitney U-test (*$p < 0.05$). Typical EV-associated proteins were detected on both unstimulated and cytokine stimulated EVs, while just CD54 was determined at significant higher levels on cytokine stimulated EVs.

A liquid chromatograph/electron spray ionisation mass spectrometry (LC/ESI-MS) approach for unstimulated and cytokine stimulated EVs from three different CardAP donors revealed a

broader overview of the transported proteins. The majority of proteins (164 out of total identified 186 proteins) were identical for both EV biogenesis condition, while only 15 or seven proteins were exclusive for unstimulated or cytokine stimulated EVs, respectively (**Figure 16A**). 35 proteins were selected for a comparative illustration via their determined exponentially modified protein abundance index (emPAI). Indeed, some proteins, such as CD73 or integrins, were omnipresent despite donor variabilities and some proteins were exclusive for each EV biogenesis condition (**Figure 16B**). TNFα inducible protein 3 was for example only detectable in cytokine stimulated EVs, while tyrosine-protein kinase Yes was observed exclusively in unstimulated EV preparations. All identified proteins were further explored via a String network database analysis, which not only allowed one to visualize the interaction between each protein as grey connecting lines but also allowed suggestions about the localization and involvement in biological processes of each protein (**Figure 17;** all listed in ***Appendix Table 1***). As anticipated, the majority of proteins (156 out of 186 proteins) could be assigned to the extracellular exosome compartment, of which some were connected to therapeutic beneficial effects, such as angiogenesis (e.g. heparan sulphate proteoglycan 2, neuropillin), wound healing (e.g. endoglin, annexin-5), or the regulation of immune system processes (e.g. annexin-1 or Gal-1; **Figure 17**).

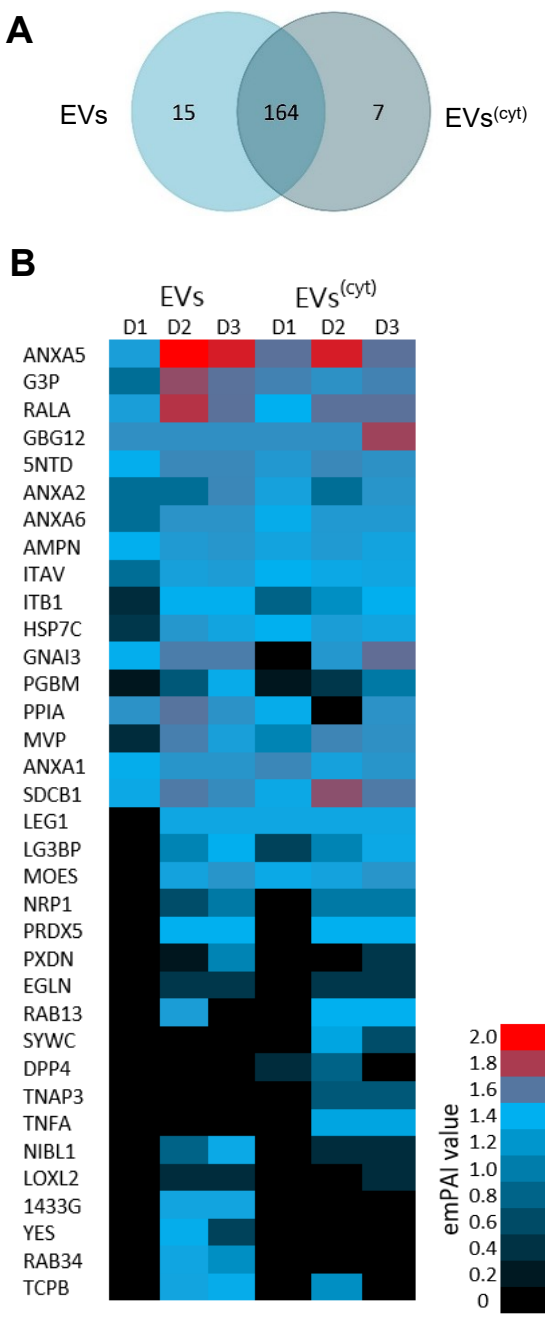

Figure 16: Most transported proteins were shared by both EV biogenesis conditions.
Unstimulated EVs (EVs) and cytokine stimulated EVs (EVs$^{(cyt)}$) from three different CardAP donors were prepared for liquid chromatograph/electron spray ionisation mass spectrometry (LC/ESI-MS). EVs were loaded on amicon filters and digested by trypsin in an overnight step. The derived peptides were then analysed by LC/ESI-MS. The obtained mass spectra were evaluated by MASCOT software searching for protein matches in the SwissProt 51.9 database. A protein was considered to be present in unstimulated (EVs) or cytokine stimulated EVs (EVs$^{(cyt)}$), when at least two of three CardAP donors exhibited a signal. **(A):** All identified proteins (n = 187) are illustrated in a Venn diagram to display shared as well as exclusively identified proteins in EVs and EVs$^{(cyt)}$. **(B):** The obtained exponentially modified protein abundance index (emPai) values of 35 selected proteins are shown as heatmap for the individual three CardAP donors (D1, D2, and D3). Undetected proteins correspond to an emPAI value of 0 (black).. ANAXA1/2/5/6 = annexin I/II/V/VI; G3P = glyceraldehyde-3-phosphate dehydro-genase; RALA = Ras-related protein Ral-A; 5NTD = CD73; AMPN = aminopeptidase N; ITAV = integrin α-V; ITB1 = integrin β-1; HSP7C = heat shock cognate 71 kDA protein; GNAI3 = guanine nucleotide-binding protein G(i) subunit α; PGBM = basement membrane-specific heparin sulfate proteoglycan core protein; PPIA = peptidyl-prolyl cis-trans isomerase A; MVP = major vault protein; SDCB1 = syntenin-1; LEG1 = galectin-1; LG3BP = galectin-3-binding protein; MOES = moesin; NRP1 = neuropilim-1a; PRDX5 = peroxiredoxin-5; PXDN = peroxidasin homolog; EGLN = endoglin; RAB13 = Ras-related protein Rab-13; SYWC = tryptophan-tRNA ligase; DPP4 = Dipeptidyl peptidase 4; TNAP3 = TNFα induced protein 3; TNFA = TNFα; NIBL1 = niban-like protein 1; LOXL2 = lysyl oxidase homolog 2; 1433G = 14-3-3 protein γ; YES = tyrosine-protein kinase Yes; RAB34 = ras-related protein Rab-34; TCPB = T-complex protein 1 subunit β. In general, most identified proteins are identical between unstimulated and cytokine stimulated EVs

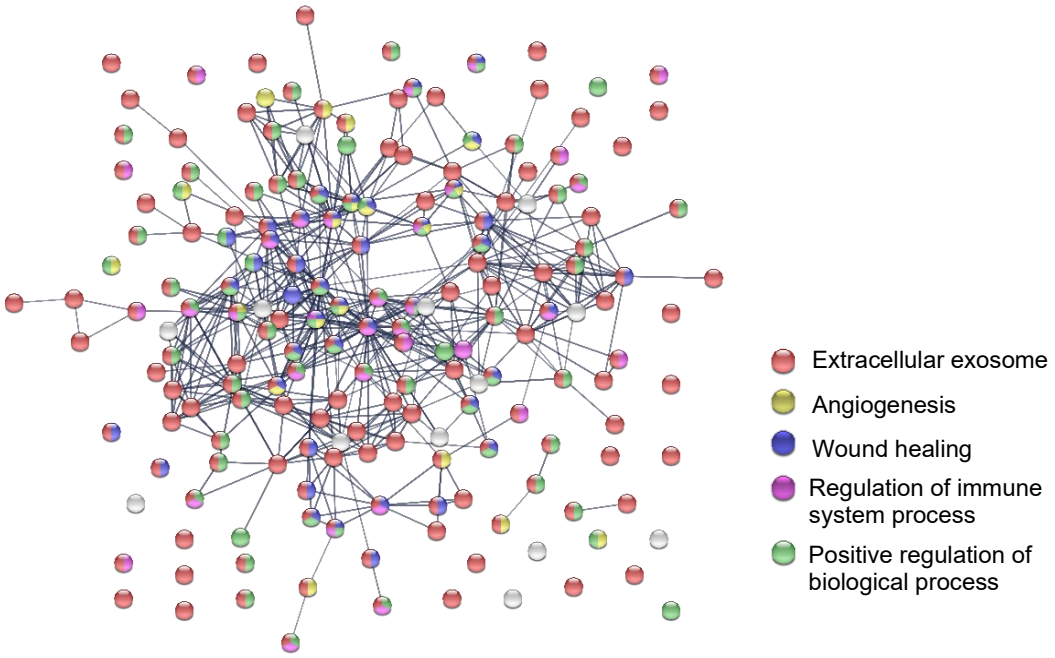

Figure 17: By LC/ESI-MS identified proteins of EVs can be mainly assigned to the extracellular exosome compartment with diverse predicted biological function.
Unstimulated and cytokine stimulated EVs from three different CardAP donors were analysed by LC/ESI-MS. The interaction of all identified proteins (186) was visualized with the help of String network database analysis, where proteins are shown as nodes and known protein interactions are shown as grey connecting lines. The colour of the node represents biological processes or the localisation as following: extracellular exosome = red, positive regulation of cellular process = green, angiogenesis = yellow, wound healing = blue, regulation of immune system process = magenta. Isolated EVs of CardAP cells transport proteins belonging to extracellular exosome compartment and possibly mediate desired biological functions for treating CVDs.

4.2.3 More miRNAs are transported by cytokine stimulated EVs

An overview of transported miRNAs by unstimulated and cytokine stimulated EVs was achieved by nCounter® Human miRNA expression assay. In total 205 human miRNAs were identified in EVs (all listed in ***Appendix Table 2***) from an assay that allows the detection of nearly 800 human miRNAs. Interestingly, cytokine stimulated EVs showed more miRNAs (n = 89) than unstimulated EVs (n = 14) that were exclusive to the respective EV biogenesis condition (**Figure 18A**). The comparative illustration of 40 selected miRNAs for their obtained copy number revealed that several miRNAs, such as miRNA 125b-5p or miRNA 146a-5p, were omnipresent in unstimulated as well as cytokine stimulated EVs at comparable high copy numbers despite of donor variabilities. Other miRNAs were solely observed in unstimulated EVs, such as miRNA 148b-3p, or observed at higher expression levels than in cytokine stimulated EVs, such as miRNA 302d-3p. *Vice versa*, miRNA 494-3p was solely determined in cytokine stimulated EVs. Seven selected miRNAs were validated by real-time qPCR (**Figure 18C**). In accordance to previous results of the nCounter miRNA expression assay, the miRNA 302d-3p could also be shown by qPCR to be significantly enhanced in unstimulated EVs related to the cytokine stimulated counterpart (median relative expression of EVs to $EVs^{(cyt)}$ (range) = 2.48 (1.12 – 5.59)). Although miRNA 494-3p was detectable in unstimulated EVs by qPCR but not by nCounter® miRNA expression assay, cytokine stimulated EVs exhibited a significantly enhanced relative expression level for this particular miRNA (median relative expression of EVs

to EVs$^{(cyt)}$ (range) = 0.61 (0.14 – 1.04)). Other miRNAs were determined at similar levels in unstimulated and cytokine stimulated EVs, including miRNA 186-5p, 146-5p, and 132-3p (median relative expression of EVs to EVs$^{(cyt)}$: miRNA 186-5p = 1.19; miRNA 146-5p = 1.06; miRNA 132-3p = 0.85).

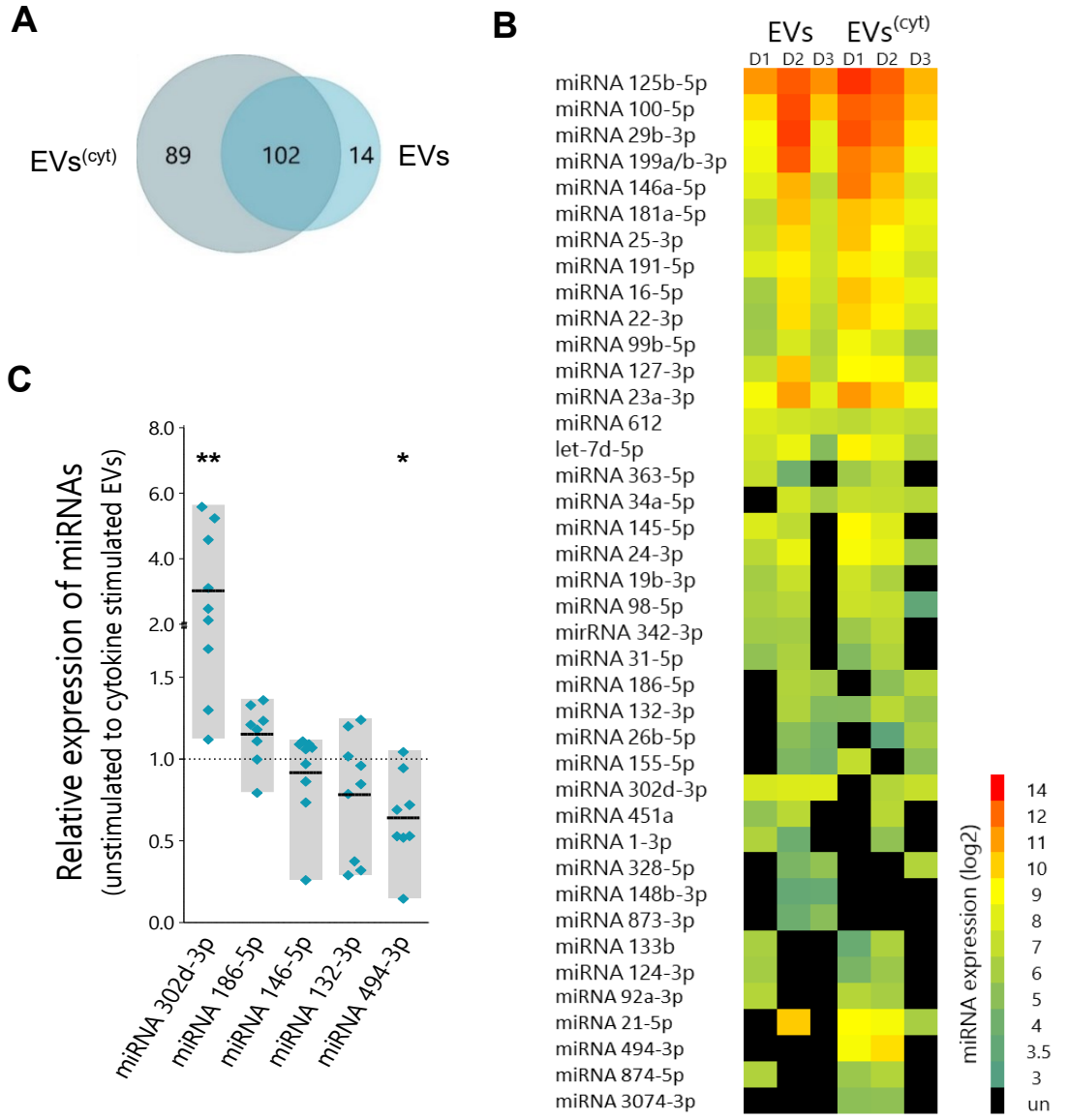

Figure 18: Cytokine stimulation increased the repertoire of miRNAs transported by EVs, while the expression of individual miRNAs, like miRNA 302d-3p, varied significantely between both EV biogenesis conditions.

Unstimulated EVs (EVs) and cytokine stimulated EVs (EVs$^{(cyt)}$) were analysed for their miRNA content by nCounter® Human miRNA expression assay according to the manual. The obtained data of miRNA copies was analysed with the help of nSolver software (version 4.0, NanoString Technologies) by firstly normalizing it to the top 100 most abundant miRNAs in all samples as well as the positive controls, followed by a background correction via subtracting the mean plus two standard derivations of the negative control from each sample. Finally, a miRNA was considered to be present in either EV biogenesis condition, when at least two from three CardAP donors exhibited more than 10 copies. **(A):** All identified miRNAs (n = 205) are illustrated in a Venn diagram to display shared and exclusively identified miRNAs in EVs and EVs$^{(cyt)}$. **(B):** 40 selected miRNAs are displayed for their expression (as log2 data) as heatmap for the individual three CardAP donors (D1, D2, and D3), including undetected miRNAs (un, black). **(C):** Additionally, seven miRNAs were validated by qPCR. By NormFinder analysis two miRNAs, miRNA26b-5p and miRNA199a-3p, were identified to be most suitable for normalization.

The relative expression of miRNAs, as determined by ΔΔCt analysis for unstimulated EVs in correlation to EVs$^{(cyt)}$ (black dotted line), is shown as median with interquartile range (n = 8–9, three different CardAP donors). Statistical analysis was performed with a Wilcoxon signed rank test (** $p < 0.01$, * $p < 0.05$). More individual miRNAs were identified in cytokine stimulated EV preparations, whereas the expression level of individual miRNAs could differ between both EV biogenesis conditions.

By a comparative analysis with FUNRICH software, differences in potential biological pathways were revealed between the miRNA sets of cytokine stimulated *versus* unstimulated EVs. Indeed, cytokine stimulated EVs were highly enriched in biological pathways of signal regulatory protein (SIRP) family interactions and tumour necrosis factor related apoptosis inducing ligand (TRAIL) signalling, whereas being depleted in diverse other biological pathways to unstimulated EVs, such as cytosolic sulfonation of small molecules, AKT-mediated inactivation of forkhead box protein O1 (FOXO1A), cyclic AMP-reponsive element binding protein (CREB) phosphorylation or epidermal growth factor receptor (EGFR) interaction with phospholipase C-γ (PLC-γ; **Figure 19A**). Furthermore, FUNRICH analysis allowed to identify genes that could be potentially affected by the determined miRNAs of either unstimulated or cytokine stimulated EVs. Both sets of genes could be assigned to different entities in processes and pathways of the immune system, including the adaptive and innate immune system as well as the cytokine signalling in the immune system, but also of the ECM organization and apoptosis by performing an overrepresentation analysis with the reactome.org platform (**Figure 19B**). Interestingly, more than 40% of total registered entities were influenced in the processes of apoptosis and ECM organization. Additionally, comparable levels of overrepresentation in the individual processes were observed for both unstimulated and cytokine stimulated EVs.

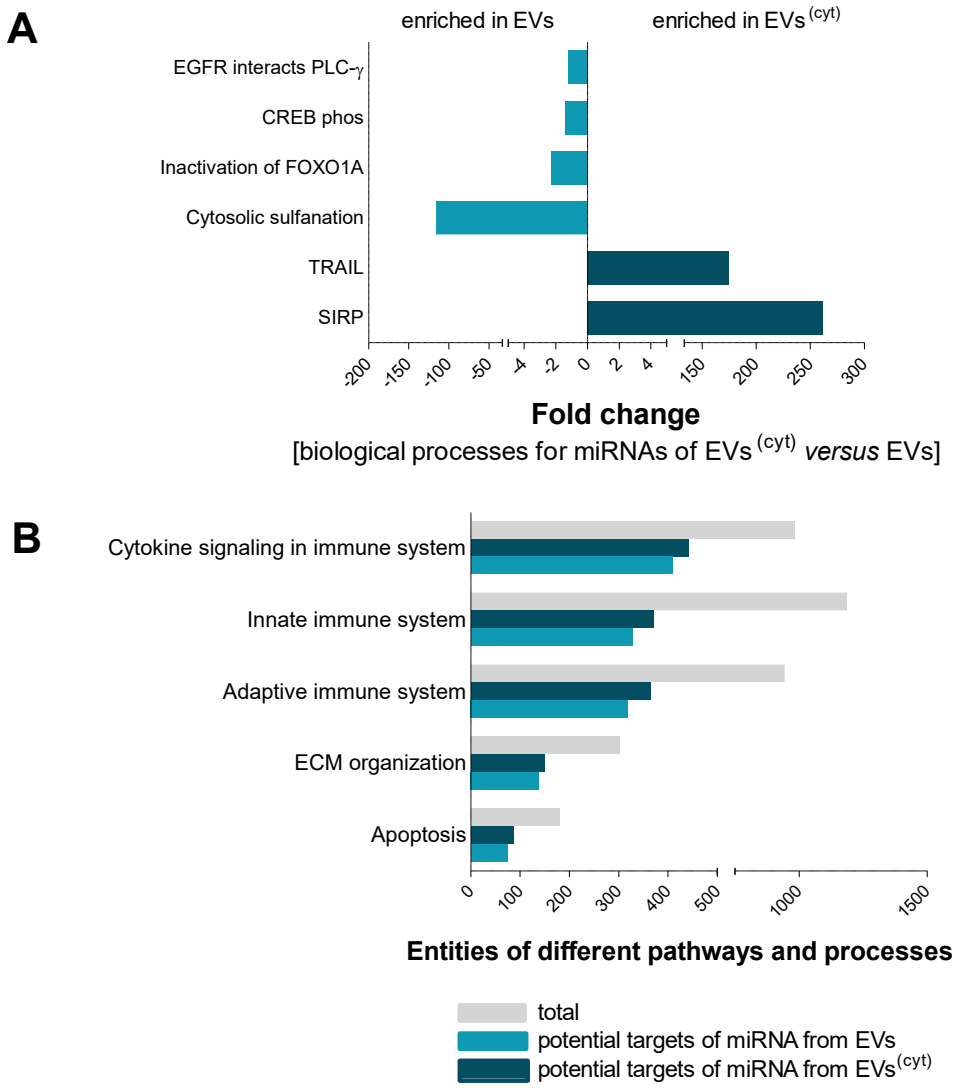

Figure 19: Identified miRNAs of both EVs from CardAP cells seem to influence important processes for regeneration.
Unstimulated (EVs) and cytokine stimulated EVs (EVs(cyt)) from three different CardAP donors were ana-lysed for its transported miRNA content by nCounter® Human miRNA ex-pression assay according to the manual. These identified miRNAs were then analysed for their plausible impli-cation in biological processes. **(A):** The miRNA repertoire of EVs(cyt) was analysed *versus* the repertoire of EVs by FUNRICH analysis for their impact on specific biological pathways. The fold change is presented for the most affected pathways to show enriched processes for EVs (light blue) or EVs(cyt) (dark blue). **(B):** Target genes of both miRNA sets were identified by FUNRICH analysis and further used for an overrepresentation analy-sis via the reactome.org plat-form. Here, entities in different pathways were identified that could be influenced by EVs (light blue) or by EVs(cyt) (dark blue) in comparison to all registered entities (grey). Both unstimulated and cytokine stimulated EVs from CardAP cells seem to influence therapeutic relevant pathways in recipient cells via their transported miRNAs.

4.3 EV-cell interaction

The capability of an EV to interact with a recipient cell marks an essential step for its paracrine action. As the focus of this study lay on the evaluation of a therapeutic approach for CVDs, well-characterized murine cardiac cell lines, representing cardiac endothelial cells (MHEC5-T cells) or cardiomyocytes (HL-1 cells), were used to investigate the interaction with fluorescence labelled or unlabelled EVs.

4.3.1 Fluorescence labelled EVs get in contact with different murine cardiac cell types

For the conduction of a time series analysis of EV-cell interaction, DiD labelled EVs (DiD^+ EVs) were applied to cultured murine cells for various time points and subsequently analysed by flow cytometry. In fact, the frequency of DiD^+ HL-1 cells as well as DiD^+ MHEC5-T cells constantly increased in the course of time (**Figure 20A**). After one day, nearly all HL-1 cells as well as MHEC5-T cells displayed a DiD^+ signal (median frequency (range): DiD^+ HL-1 cells = 93.5 (73.7 - 95.6) %; DiD^+ MHEC5-T cells = 93.7 (90.4 - 97.7) %; **Figure 20B**). Additionally, cells were treated with a DiD negative control, which was derived by labelling differential centrifuged unconditioned medium with DiD in the same manner as EVs. No or very low levels of DiD (highest determined frequency of DiD^+ cells = 0.024 %) were recorded for the DiD negative control at the different time points (**Figure 20B**).

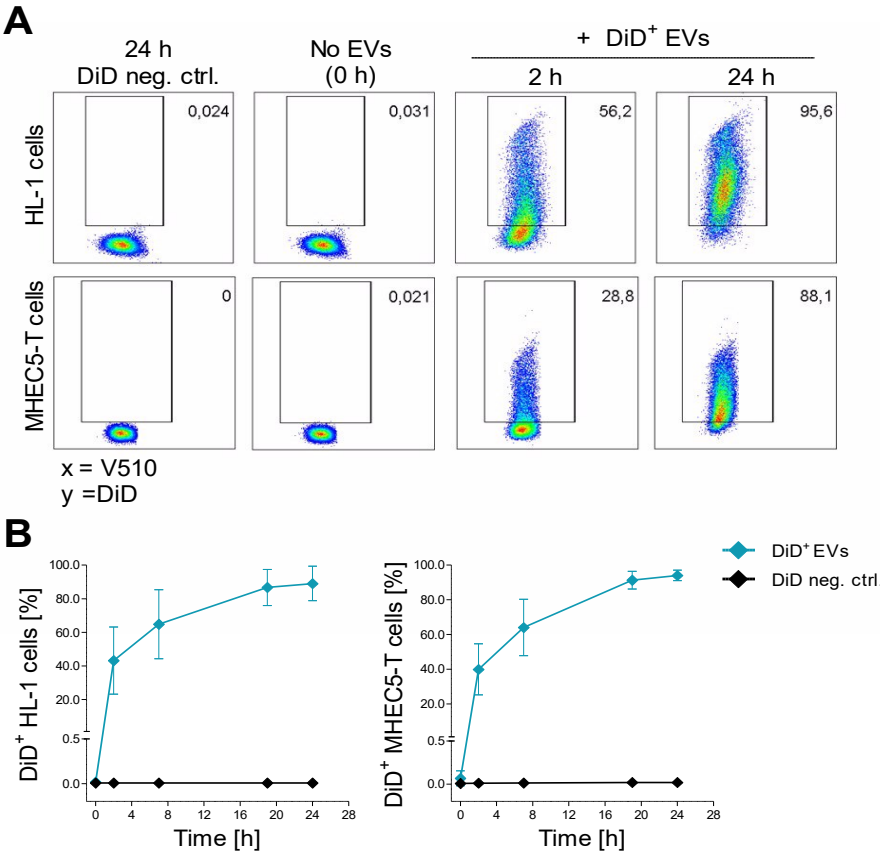

Figure 20: EVs interacted equally with murine cardiomyocytes and cardiac endothelial cells.
DiD labelled EVs (DiD^+ EVs) as well as DiD negative con-trols (DiD neg. ctrl.) were applied to cultured HL-1 or MHEC5-T cells in 48-well plates (2×10^5 cells/well). At different time points (0, 2, 7, 19, and 24 h) cells were washed, harvested by accutase treatment, labelled with a dead/viable marker, and analysed by flow cytometry at the Canto II. **(A):** Representative dot plots are shown for HL-1 cells (upper raw) and MHEC5-T cells (lower raw) treated either with DiD^+ EVs or DiD neg. ctrl. for different time points. **(B):** The frequency of DiD^+ HL-1 cells (right, $n = 4$, four different CardAP donors) and DiD^+ MHEC5-T cells (left, $n = 6$, three different CardAP donors) is shown in relation to the time (h) as median with interquartile range for treatment with either DiD^+ EVs (blue) or DiD neg. ctl. (black). Murine cardiac cells were shown to accumulate the signal of fluorescence labelled EVs after one day.

For an equivalent approach by fluorescence microscopy, lipids of EVs were labelled with PKH26 instead of DiD to optimize sensitivity towards EV detection. Likewise to flow cytometry, an increase of PKH26$^+$ EVs but not for the fluorescence negative control (PKH26 neg. ctrl.) was detectable over the time period of one day (**Figure 21**). Interestingly, some HL-1 cells showed an accumulation of separate single PKH26$^+$ signals for EVs in the proximity of their nucleus at the end point, while other cells displayed no signal (ROI in **Figure 21**).

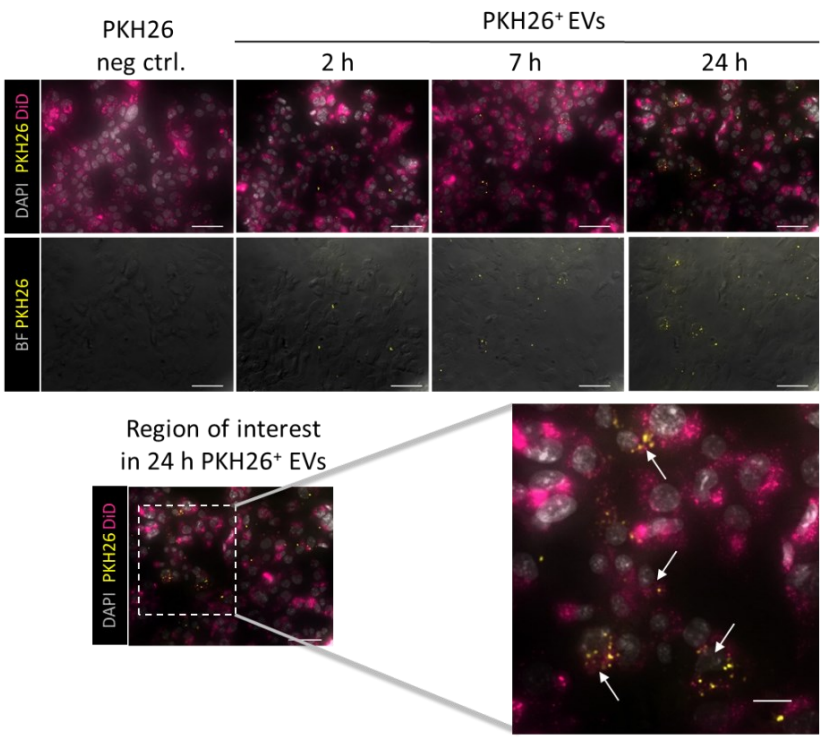

Figure 21: EVs seemed to accumulate in some murine cardiomyocytes after one day.
HL-1 cells were labelled with DiD and seeded in 48-well plates (2 × 10^5 cells/well). After 24 h, DiD$^+$ HL-1 cells were treated with PKH26 labelled EVs (PKH26$^+$ EVs) and PKH26 negative controls (PKH26 neg. ctrl.). At different time points (2, 7, and 24 h) cells were washed with PBS, fixed with 4% PFA and stained with DAPI. The EV-cell interaction was analysed by fluorescence microscopy. Representative images are shown for each time point with scale bars of 50 µm as overlay of HL-1 cells (DiD$^+$, pink), nucleus (DAPI, grey pseudo-coloured) and EVs (PKH26$^+$, yellow) or as overlay of the brightfield (BF) images with EVs (PKH26$^+$, yellow). Additionally, a region of interest (dotted rectangle in 24 h PKH26$^+$ EVs) is shown for detected EV signals (white arrows) with a 20 µm scale bar (n = 3, two different CardAP donors). Isolated EVs from CardAP cells seem to accumulate in some but not all murine cardiomyocytes after one day.

4.3.2 EVs are taken up by murine cells

A more thorough insight of the observed EV-cell interaction was achieved by integrating a novel flow cytometry method in EV research. Key component of this method is to use recipient cell and EV releasing donor cells of different species. Thus, it is possible to discriminate the location of EVs whitin or on recipient cells by appropriate staining methods that use fluorescence labelled antibodies species specific for proteins of the donor cell and consequently their released EVs.

In this study, murine HL-1 and MHEC5-T cells were treated with EVs from human CardAP cells for one day. Afterwards, they were stained with human specific fluorescence labelled antibodies, which were already shown in the phenotypical characterization to be present on isolated EVs. Indeed, human proteins, such as human CD63, were solely detected when HL-1 or MHEC5-T cells have been treated with EVs (**Figure 22A**). Strikingly, the signal of human

CD63, CD73, and CD81 was observed rather intracellularly than on the surface of EV treated HL-1 cells (median normalized MFI intracellular *vs.* extracellular: CD63 EVs = 19.05 *vs.* 1.38; CD63 EVs$^{(cyt)}$ = 8.68 *vs.* 1.24; CD73 EVs = 1.67 *vs.* 1.12; CD73 EVs$^{(cyt)}$ = 1.28 *vs.* 1.09; CD81 EVs = 1.53 *vs.* 1.10; CD81 EVs$^{(cyt)}$ = 1.40 *vs.* 1.05; **Figure 22B**). Likewise, the treatment of MHEC5-T cells with EVs resulted in an enhanced detection of all three human proteins within than on the surface of these murine cardiac endothelial cells (median normalized MFI intracellular *vs.* extracellular: CD63 EVs = 3.01 *vs.* 1.05; CD63 EVs$^{(cyt)}$ = 2.80 *vs.* 1.05; CD73 EVs = 2.56 *vs.* 0.87; CD73 EVs$^{(cyt)}$ = 2.56 *vs.* 0.97; CD81 EVs = 1.41 *vs.* 1.05; CD81 EVs$^{(cyt)}$ = 1.43 *vs.* 1.04; **Figure 22C**). The intracellular detection of these human proteins did not differ significantly between unstimulated and cytokine stimulated EVs, although a tendency for lower normalized MFI values for cytokine stimulated EVs in HL-1 cells were detected in comparison to the unstimulated EV treated counterpart. Additionally, higher normalized MFIs for CD63 were detected within HL-1 cells for both treatments with EVs than the respective samples of MHEC5-T cells (**Figure 22B and C**).

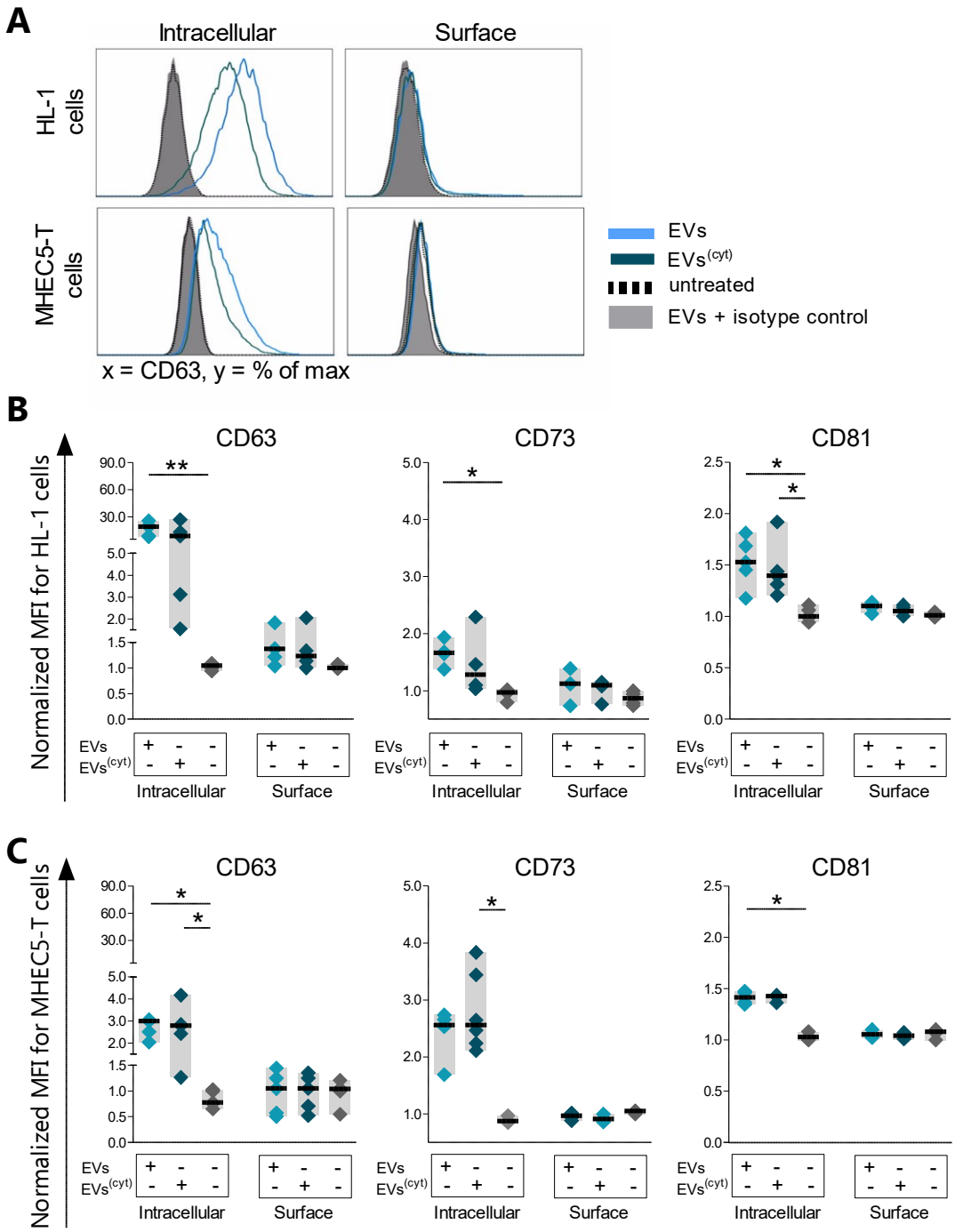

Figure 22: EVs were internalized by cardiac murine cells after an exposure of one day.
HL-1 or MHEC5-T cells were seeded in a 48-well plate (2 × 10^5 cells/well). After 24 h, cells were treated with unstimulated (EVs), cytokine stimulated ($EVs^{(cyt)}$) EVs, or left untreated. After 24 h, harvested cells from each condition were distributed to at least four different FACS tubes. They served either as unstained/stained sample for the intracellular or a cell surface staining with human specific fluorescence labelled antibodies. After samples were measured at a flow cytometer (Canto II), the mean fluorescence intensity (MFI) of each investigated protein was normalized to the respective unstained control. **(A):** Representative histograms of HL-1 (upper row) or MHEC5-T cells (lower row) treated with EVs (blue line), $EVs^{(cyt)}$ (dark blue line) or they were untreated (dotted black line) are displayed for human CD63 via intracellular (left) or surface (right) staining in comparison to the isotype control (EVs + isotype control, grey filled area). **(B-C):** Individual normalized MFIs are shown for human CD63 (left), CD73 (middle) and CD81 (right) on or within HL-1 **(B)** or MHEC5-T cells **(C)** for the three different treatments as median with interquartile range (n = 4 -5, three different CardAP donors). Statistical analysis was

performed by Kruskal-Wallis test with Dunn's *post hoc* test (* $p < 0.05$; **$p < 0.01$). After one day, EVs from human cardiac cells are found rather in murine cardiac cells than on their surface.

4.4 The influence of EVs on apoptotic cell behaviour

The reduction of the programmed cell death in damaged cardiac tissue would be one of the desired effects for a therapeutic approach to treat CVDs. For that reason, isolated EVs were investigated for their capability to influence the *in vitro* apoptotic behaviour of murine cardiomyocytes. For that purpose, HL-1 cells were allowed to sufficiently take up the isolated EVs or its vehicle control (here: PBS) for one day prior to an assay. Then, the apoptosis was provoked by three different apoptotic triggers and the apoptosis was monitored after an additional cultivation day.

4.4.1 EVs exhibit a general anti-apoptotic effect although cytokine stimulated EVs failed to reduce virus induced apoptosis

One scenario in the heart that leads to apoptosis of cells, is the formation of radical oxygen species. It was recreated in *in vitro* experiments through the timely limited supplementation of the culture medium with hydrogen peroxide (H_2O_2). The ROS induced apoptosis was characterized by changes of the cell´s plasma membrane as detected by flow cytometry, which allowed to determine the frequency of apoptotic (AnnexinV-FITC$^+$ cells) and non-apoptotic cells, respectively (7AAD$^-$ AnnexinV-FITC$^-$ cells; **Figure 23A**). The treatment with unstimulated EVs led to a significant reduction of apoptotic cells as well as to a significant increase of non-apoptotic cells in comparison to the PBS control, while the treatment with cytokine stimulated EVs displayed a likewise trend of diminished or enhanced cell population, respectively (median frequency of apoptotic cells (range): PBS = 33.1 (14.1 - 38.6) %; EVs = 24.7 (8.3 - 32.2) %; EVs$^{(cyt)}$ = 28.8 (9.8 - 35.9) %; median frequency of anti-apoptotic cells (range): PBS = 61.1 (55.3 - 70.9) %; EVs = 68.7 (60.0 - 77.35) %; EVs$^{(cyt)}$ = 63.6 (55.0 - 70.2) %; **Figure 23B**). Nevertheless, cytokine stimulated EVs demonstrated an anti-apoptotic effect when apoptosis was determined by a different method. The measurement of the caspase3/7 activity showed significantly reduced levels in HL-1 cells treated with cytokine stimulated EVs as well as unstimulated EVs in comparison to the PBS controls (median caspase 3/7 activity (range): PBS = 1.15 (0.88 - 1.90) RLU; EVs = 0.85 (0.71 - 1.35) RLU; EVs$^{(cyt)}$ = 0.83 (0.42 - 0.96) RLU; **Figure 23C**).

Another investigated apoptotic trigger was the lack of nutrients, which was mimicked *in vitro* by applying starvation medium for one hour. Likewise to ROS-induced apoptosis, the treatment of HL-1 cells with unstimulated as well as cytokine stimulated EVs reduced significantly their caspase 3/7 activity in comparison to PBS treated controls (median enzyme activity (range): PBS = 1.08 (1.00 - 1.54) RLU, EVs = 0.84 (0.38 - 1.15) RLU, EVs$^{(cyt)}$ = 0.76 (0.56 - 0.96) RLU; **Figure 23C**). The third investigated apoptotic trigger was the infection of HL-1 cells with the Coxsackievirus B3 (CVB3). This apoptotic trigger was chosen, because CVB3 are the major viral cause of sever myocarditis in humans [122]. Moreover, a previous study already demonstrated that CardAP cells themselfes limited CVB3 induced apoptosis *in vitro* and *in vivo* [13]. Interestingly, this anti-apoptotic effect was solely reproducible for EVs from CardAP cells derived under the absence of cytokine stimulation. In fact, the caspase activity was significantly

reduced in HL-1 cells treated with unstimulated EVs but not with cytokine stimulated EVs in comparison to the PBS treated controls (median enzyme activity (range): PBS = 1.08 (0.50 - 2.4) RLU; EVs = 0.74 (0.17 - 1.4) RLU; EVs$^{(cyt)}$ = 1.09 (0.48 - 2.29) RLU; **Figure 23C**).

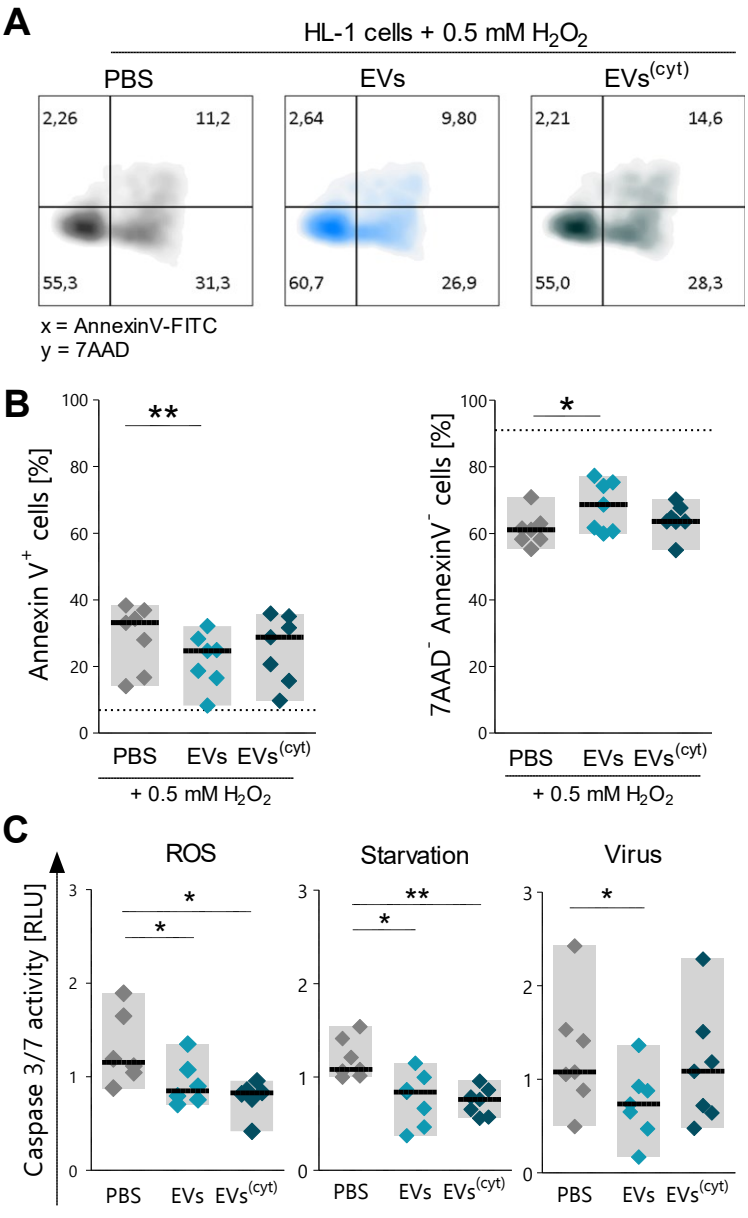

Figure 23: EVs reduced apoptosis in murine cardiomyocytes.
HL-1 cells were seeded in 6-well plates (1x10^6 cells/well) for flow cytometry analysis or in 96-well plates (1-2x10^5 cells/well) for caspase 3/7 activity determination, treated with 6 µg/mL of unstimulated EVs (EVs), cytokine stimulated EVs (EVs$^{(cyt)}$), PBS in corresponding volumes of EVs (PBS), or they were left untreated. The next day, apoptosis was induced by ROS (0.5 mM H_2O_2), starvation (starvation medium), or virus (CVB3; at a 100,000 m.o.i.) for 60 min. Then after, washed cells recieved cClaycomb medium for another 23 h. For flow cytometry analysis ROS induced HL-1 cells were stained with AnnexinV-FITC and 7AAD and analysed at a flow cytometer (MACSQuant). **(A):** Representative AnnexinV-FITC/7AAD dot plots are shown of ROS induced apoptotic HL-1 cells treated with either PBS (left), EVs (middle) or EVs$^{(cyt)}$ (right). **(B):** The individual frequencies of apoptotic cells (AnnexinV$^+$ cells) as well as non-apoptotic cells (7AAD$^-$ AnnexinV$^-$ cells) are shown as median with data range for ROS induced apoptotic HL-1 cells, while the median of the untreated con-trols is indicated as dotted line (n = 7, five different CardAP donors). For analysis of caspase 3/7 activity, HL-1 cells of all three apoptotic triggers received proluminate caspase3/7 sub-strate (100 µL/well) and the luminescence was measured after 120 min at a microplate reader (Mithras). The luminescence was related to the cell concentration factor (absorbance of crystal violet stained cell lysates) as relative luminesce unit (RLU). **(C):** The individual caspase 3/7 activity as RLU is shown as median with data range for ROS induced apoptotic HL-1 cells (n = 6, five different CardAP donors), starved HL-1 cells (n = 7, four different CardAP donors), and virus infected HL-1 cells (n = 7, four different CardAP donors). Statistical analysis was performed by Friedman´s test with Dunn´s multiple comparison *post hoc* test (*p < 0.05; **p < 0.01). ROS, starvation and virus induced apoptosis of HL-1 cells was lessened by treatment with unstimulated EVs, while cytokine stimulated EVs solely reduced starvation, ROS but not virus induced apoptosis of HL-1 cells.

4.5 Influence of EVs on angiogenesis

Another desired beneficial therapeutic effect for the treatment of CVDs would be the support of angiogenesis in the damaged cardiac tissue. Interestingly, the conditioned medium of CardAP cells was already shown to support angiogenesis *in vitro*, thus, first evidence is provided for a paracrine mechanism [64]. In order to clarify whether their released EVs convey a pro-angiogenic feature, tube formation assays were conducted with human endothelial cells (here: HUVECs).

4.5.1 EVs enhance tube formation capabilities of HUVECs

In order to allow time for a sufficient EV-cell interaction, HUVECs were treated with either unstimulated EVs, cytokine stimulated EVs, or PBS, which served as EV vehicle control, one day prior to an assay. Indeed, the success of this EV-cell interaction could be verified when DiD labelled EVs (DiD^+ EVs) were applied for the same time to HUVECs (**Figure 25A**). The DiD signal of HUVECs significantly enhanced in EV treated speciments in comparison to the DiD negative control (median frequency of DiD^+ HUVECs (range): DiD^+ EVs = 97.3 (62.1 – 99.4) %; DiD^+ $EVs^{(cyt)}$ = 96.5 (87.7 – 99.7) %; DiD negative control = 0.7 (0.04 – 5.8) %; **Figure 25B**).

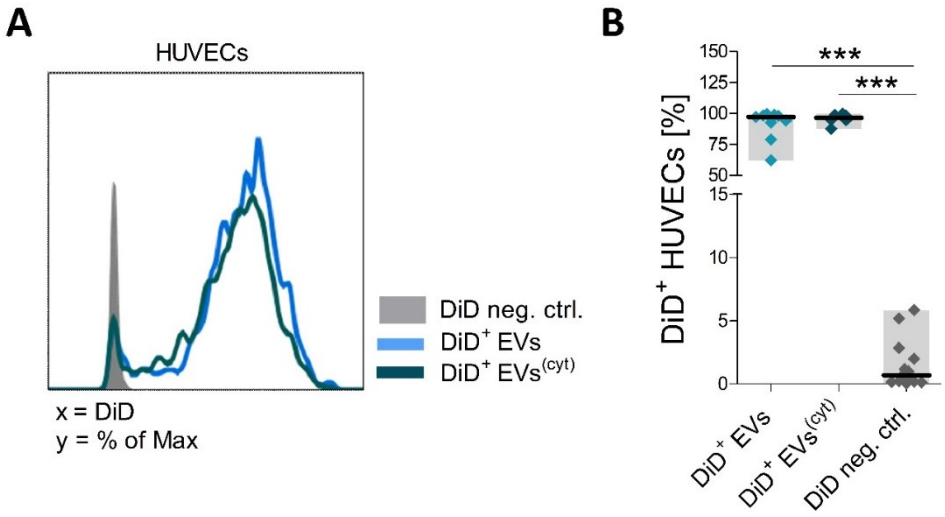

Figure 24: DiD labelled EVs were capable to interact with HUVECs.
HUVECs were seeded in 6-well plates (1.9×10^5 cells/well) and treated with DiD labelled EVs derived from unstimulated (DiD^+ EVs) or cytokine stimulated conditions (DiD^+ $EVs^{(cyt)}$) or with a DiD negative control (DiD neg. ctrl.). After 24 h, HUVECs were washed twice with PBS, harvested, and labelled with a dead/viable marker (V510) for 20 min and fixed with 0.5% PFA after a washing step. All samples were measured at a flow cytometer (CantoII) and analysed by flow cytometry. **(A):** Representative histograms are shown for HUVECs of all three different treatments. **(B):** The individual frequencies of DiD^+ HUVECs are shown as median with interquartile range for the three different treatments (n = 6 - 13, four different CardAP donors). Statistical analysis was performed by Kruskal-Wallis test with Dunn´s multiple comparison *post hoc* test (*** $p < 0.001$). After one day, nearly all HUVECs showed an interaction with fluorescence labelled EVs from CardAP cells despite of their EV biogenesis condition.

For the tube formation assay itself, treated HUVECs were harvested, seeded on Matrigel-coated wells, and their tube formation was documented for the next 20 hours by light microscopy. As shown in representative images, HUVECs formed more networks when treated with unstimulated or cytokine stimulated EVs in comparison to the PBS control (**Figure 25A**).

Quantitative analysis revealed that the total branching length as well as the number (#) of junctions was significantly increased for HUVECs treated with unstimulated or cytokine stimulated EVs in comparison to the PBS control (mean number of junctions (± SD): PBS = 38 (± 19); EVs = 58 (± 21); $EVs^{(cyt)}$ = 51 (± 13); mean total branching length (± SD): PBS = 6,416 (± 3,158) px; EVs = 9,302 (± 2,757) px; $EVs^{(cyt)}$ = 8,232 (± 1,907) px; **Figure 25B**). Interestingly, unstimulated EVs showed a trend towards a greater pro-angiogenic effect than their cytokine stimulated counterpart.

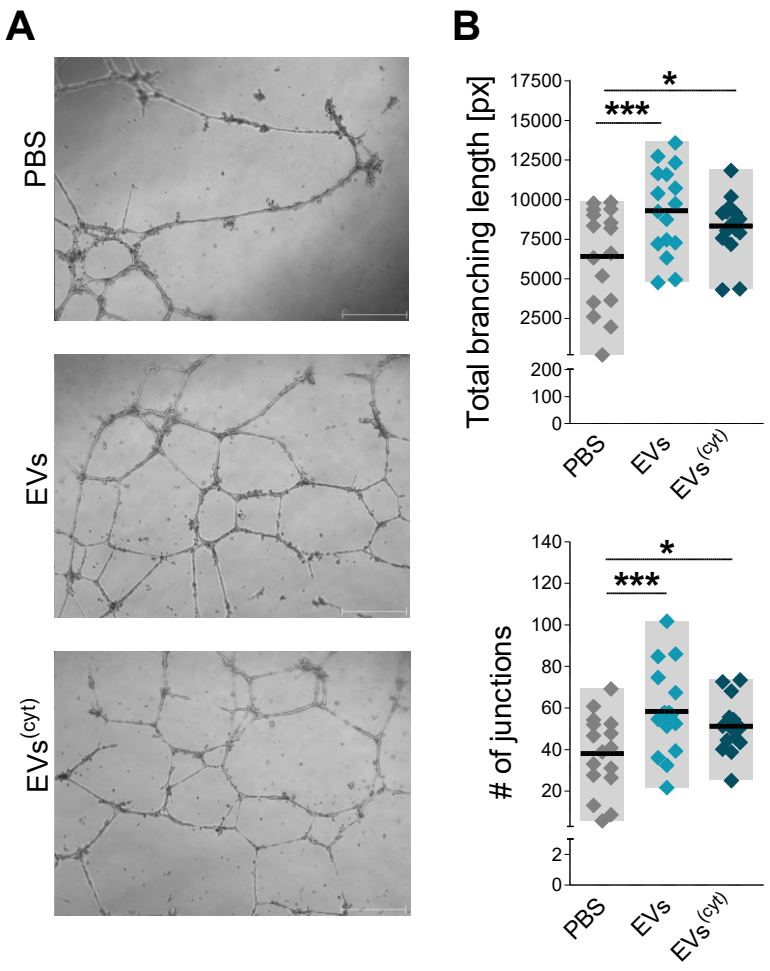

Figure 25: EVs enhanced the tube formation capability of HUVECs. HUVECs were seeded in 6-well plates (1.9×10^5 cells/well) and then treated with 6 µg/mL of unstimulated (EVs), cytokine stimulated EVs ($EVs^{(cyt)}$), or PBS in corresponding volumes of EVs (PBS). After 24h, harvested HUVECs were applied to Matri-gel coated 48-well plates (0.16×10^5 cells/well). The tube forma-tion was documented after 20 h by light microscopy and images were analysed quantitatively with the help of the ImageJ Angiogen-esis Plugin. **(A):** Representative images are shown for HUVECs of the three different treatments with scale bars representing 500 µm. (**B**): The quantitative analysis of the tube formation is repre-sented for the individual total branching length and number (#) of junctions as median with data range (n = 16, six different Card-AP donors). Statistical analysis was performed by repeated mea-sures ANOVA with Bonferroni *post hoc* test (*** $p < 0.001$, * $p < 0.05$). HUVECs treated with unstimulated or cytokine stimulated EVs showed elevated tube formation capabilities.

4.5.2 HUVECs release different pro-angiogenic factors upon treatment with either unstimulated or cytokine stimulated EVs

In a next step, it was investigated whether and how the EV treatment influences the release of typical pro-angiogenic factors by HUVECs. In order to reflect a similar experimental set-up as in the performed tube formation assays, HUVECs were treated with PBS, unstimulated or cytokine stimulated EVs for one day. Then after, cells were washed and fresh medium was applied for another 20 hours. This derived conditioned medium was investigated for the concentrations of VEGF, IL-6, and IL-8, while HUVECs were used to determine the cell correction factor by crystal violet staining.

Remarkably, the conditioned media from HUVECs treated with unstimulated EVs contained significantly more VEGF (increase by 1.7-fold) than the PBS control, while the respective sample for cytokine stimulated EVs solely exhibited a trend of higher VEGF concentrations (median VEGF concentration (range): PBS = 60.6 (53.3 – 66.28) pg/mL; EVs = 103.1 (75.0 – 153.8) pg/mL; EVs$^{(cyt)}$ = 68.3 (59.5 – 74.5) pg/mL; **Figure 26**). However, cytokine stimulated EVs directed to a nearly 4-fold significant increase of released IL-8 by HUVECs in comparison to PBS controls, whereas unstimulated EVs induced merely a moderate but not significant increase of IL-8 concentrations in the respective sample (median IL-8 concentration (range): EVs = 493.4 (394.0 – 1,279.0) pg/mL; EVs$^{(cyt)}$ = 1,564.0 (350.7 – 2,348.0) pg/mL; PBS = 399.0 (163.4 – 476.0) pg/mL; **Figure 26**). Although both EV treatments significantly increased the IL-6 secretion by HUVECs in comparison to PBS treated HUVECs, cytokine stimulated EVs appeared to have a greater impact than their unstimulated counterpart (median IL-6 concentration (range): EVs = 250.3 (138.1 - 929.3) pg/mL; EVs$^{(cyt)}$ = 669.5 (79.0 - 1074) pg/mL; PBS =97.5 (80.7 - 120.9) pg/mL; **Figure 26**).

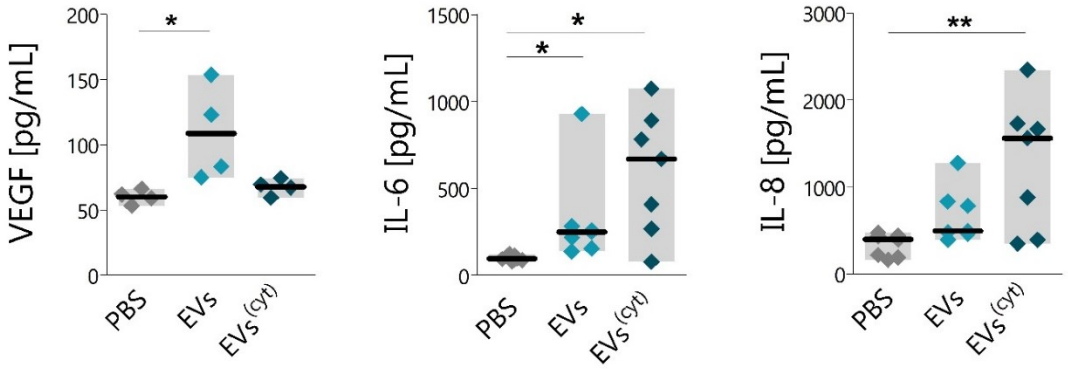

Figure 26: The interaction of HUVECs with unstimulated or cytokine stimulated EVs triggered the release of different pro-angiogenic factors.
HUVECs were seeded in 6-well plates (1.9 × 10^5 cells/well) and treated with 6 µg/mL of either unstimulated (EVs), cytokine stimulated EVs (EVs$^{(cyt)}$) or PBS in volumes corresponding to that of the EVs. The next day, HUVECs were washed twice and fresh medium was applied for 20 h. Then, the medium was collected for detecting IL-6, IL-8, and VEGF by ELISA. The cell correction factor was determined by crystal violet staining. The individual cytokine concentrations in relation to the cell correction factor are shown for VEGF (left; n = 4, four different CardAP donors), IL-6 (middle; n = 7, four different CardAP donors), and IL-8 (right; n = 7, four different CardAP donors) as median with interquartile range. Statistical analysis was performed by Friedman´s test with Dunn´s multiple comparison *post hoc* test (*** $p < 0.001$, ** $p < 0.01$, * $p < 0.05$). HUVECs enhance their release of different pro-angiogenic factors upon treatment with unstimulated EVs (VEGF and IL-6) or cytokine stimulated EVs (IL-6 and IL-8) from CardAP cells.

In order to illustrate the potential of one of the investigated factors, tube formation assays were performed with untreated HUVECs that were stimulated with 10 ng/mL human recombinant VEGF (+VEGF) or HUVECs were left unstimulated (un). As anticipated, the addition of VEGF supported the tube formation capabilities of HUVECs, as shown in representative images (**Figure 27A**). In fact, the total tube length as well as number (#) of junctions was significantely increased in VEGF stimulated HUVECs in comparison to the unstimulated counterpart (mean of total tube length (± SD): + VEGF = 8,138 (± 3,573) px; un = 6,108 (± 3,725); mean of junctions (± SD): + VEGF = 53.3 (± 24.6); un = 37.2 (± 22.9); **Figure 27B**).

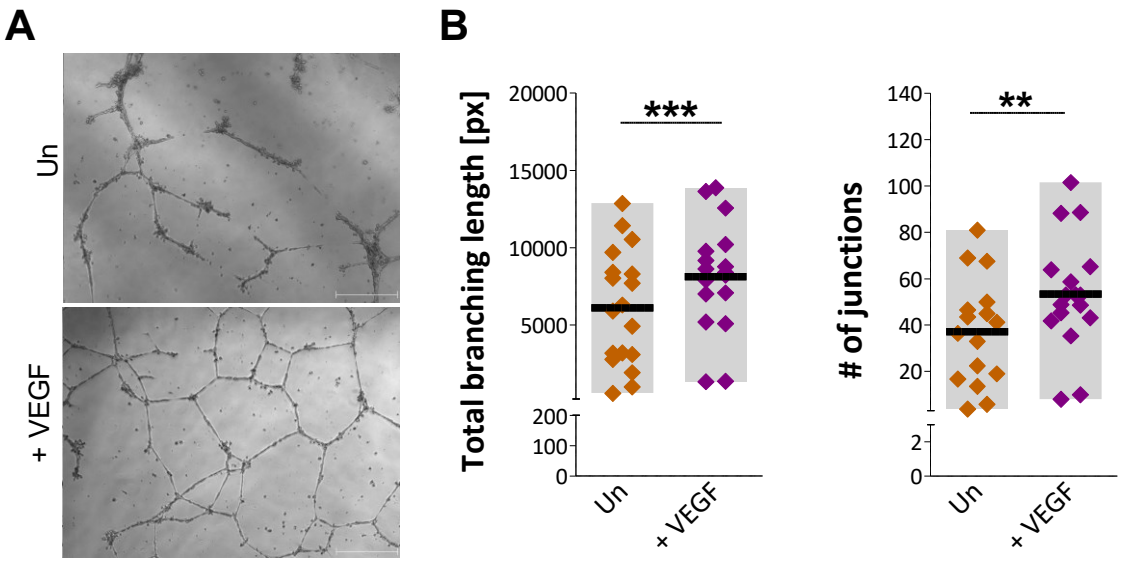

Figure 27: Treatment with VEGF enhanced the tube formation capabilities of HUVECs.
HUVECs were seeded in 6-well plates (1.9×10^5 cells/well) and harvested the next day to be reseeded on Matrigel-coated 48-well plates (0.16×10^5 cells/well). HUVECs were either left unstimulated (un) or treated with 10 ng/mL VEGF (+ VEGF). After 20 h, images were taken by light microscopy to document the tube formation and images were analysed quantitatively with the help of the ImageJ Angiogenesis Plugin. **(A):** Representative pictures are shown for unstimulated or VEGF stimulated HUVECs with scale bars representing 500 µm. **(B):** Individual data points are shown for the total branching length (left) and for the number (#) of junctions (right) as median with interquartile range ($n = 17$). Statistical analysis was performed by paired T test (*** $p < 0.001$, ** $p < 0.01$). The addition of VEGF during a tube formation assay resulted in increased network formation of HUVECs.

4.6 Influence of EVs on human immune cells and immune responses

Two features in the context with the immune system are very important for a future allogenic therapeutic application of EVs from CardAP cells. On the one hand, the therapy shall not induce any adverse immune reactions in the recipient and thus avoid unwanted side effects. On the other hand, the modulation of immune responses aid to vanquish the inhibiting effect of chronic inflammation for the regenerative process in damaged tissue. In order to estimate the immunogenicity and the immune modulating capabilities of isolated EVs, appropriate human immune cell assays were conducted., which were already described as a useful instruments in regenerative medicine [123,124].

4.6.1 EVs display a low immunogenicity

From healthy donors isolated human PBMCs were exposed for up to five days to either unstimulated EVs, cytokine stimulated EVs, PBS in equal volumes to EVs, or immune cells were left untreated. Thereafter, the immunogenicity of isolated EVs was valuated by determining possible induced immune cell reactions of PBMCs towards the isolated EVs. Herein, neither $CD4^+$ nor $CD8^+$ T cell proliferation was induced in these immune cell cultures due to the exposure with unstimulated EVs nor cytokine stimulated EVs in comparison to the PBS or untreated control (median frequency of proliferated $CD8^+$ T cells: un = 1.40 %; PBS = 1.35 %; EVs = 1.16 %; $EVs^{(cyt)}$ = 1.41 %; median frequency of proliferated $CD4^+$ T cells: un = 1.12 %; PBS = 0.83 %, EVs =0.82 %, $EVs^{(cyt)}$ = 1.10 %; **Figure 28A**). While pro-inflammatory IFNγ was not detectable in neither of these immune cell cultures (data not shown), significant

enhanced concentrations of IL-10 were determined in PBMC cultures treated with unstimulated as well as cytokine stimulated EVs in comparison to controls (median IL-10 concentration (range): un = 40.26 (8.24 - 47.57) pg/mL; PBS = 38.86 (6.74 - 120.6) pg/mL; EVs = 210.5 (61.80 - 537.80) pg/mL; $EVs^{(cyt)}$ = 547.80 (172.3 - 768.2) pg/mL; **Figure 28B**).

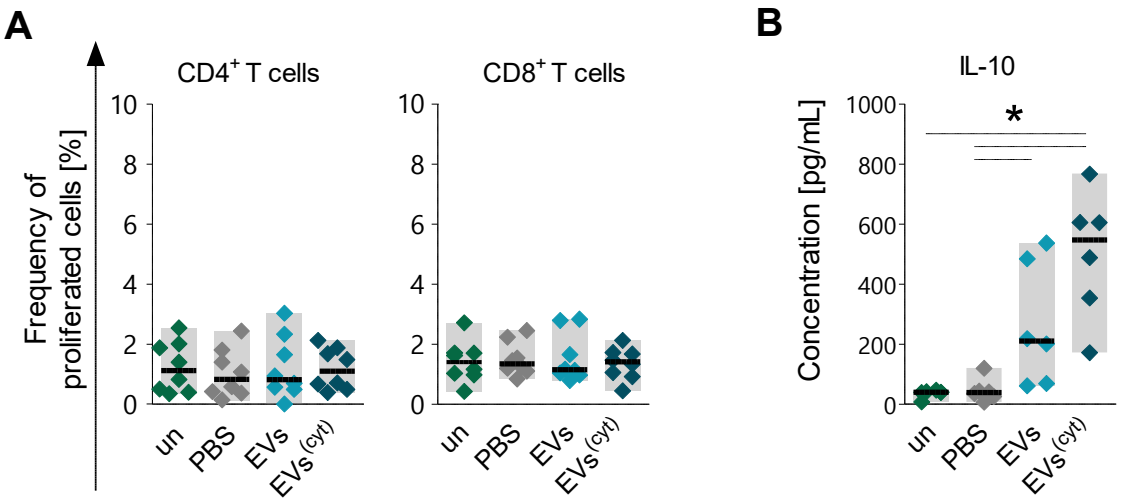

Figure 28: Isolated EVs did not induce T cell proliferation but elevated concentrations of IL-10 in otherwise unstimulated PBMC cultures after five days.
PBMCs were seeded in 96-well plates ($3x10^5$ cells/well) and treated with 12 µg/mL unstimulated (EVs), cytokine stimulated EVs ($EVs^{(cyt)}$), PBS in equal volumes as EVs (PBS), or they were left untreated (un). After five days, cells were harvested, stained with human specific fluorescence labelled antibodies and measured at a flow cytometer (Canto II) to obtain frequencies of proliferated T cells by flow cytometry. **(A):** Individual data are shown as median with data range for $CD4^+$ T cells (left) as well as for $CD8^+$ T cells (right; n = 8, five different CardAP donors). **(B):** Supernatants from unstimulated PBMCs were determined for the concentration of IL-10 by ELISA. Individual data points are shown as median with data range (n = 6; four different CardAP donors). Statistical analysis was performed by Friedman´s test with Dunn´s multiple comparison *post hoc* test (* $p < 0.05$). Neither unstimulated nor cytokine stimulated EVs induced T cell proliferation but enhanced significantly the concentration of IL-10 in otherwise unstimulated PBMC cultures.

Furthermore, control and EV treated PBMC cultures were examined for the expression level of surface proteins on $CD4^+$ T cells that are associated with the activation status of T cells (**Figure 29**). These proteins included the early T-cell activation antigen p60 (CD69), the IL-2 receptor subunit α (CD25) as intermediate activation marker, as well as an late activation marker, namely HLA-DR. Notably, neither of these markers were increased in response towards the exposure of unstimulated or cytokine stimulated EVs in comparison to PBS and untreated controls (median normalized MFI HLADR: un = 1.35; PBS = 1.32; EVs = 1.43; $EVs^{(cyt)}$ = 1.46; median MFI CD25: un = 5.50; PBS = 5.22; EVs = 5.70; $EVs^{(cyt)}$ = 5.32; median MFI CD69: un = 1.74; PBS = 1.63; EVs = 2.22; $EVs^{(cyt)}$ = 1.58). Nevertheless, the frequency of $CD25^+$ $CD4^+$ T cells was significantly enhanced in PBMC cultures treated with unstimulated EVs in comparison to PBS treated controls, while treatment with cytokine stimulated EVs solely displayed a likewise trend (median frequency of $CD25^+$ $CD4^+$ T cells (range): un = 4.05 (1.76 - 6.05) %; PBS = 4.07 (1.44 - 5.17) %); EVs = 5.11 (2.33 - 7.91) %; $EVs^{(cyt)}$ = 5.82 (2.86 - 7.86) %; **Figure 29**). In contrast, the frequencies of $HLA\text{-}DR^+$ or $CD69^+$ $CD4^+$ T cells were comparable between EV treated PBMCs and the respective controls (frequency of $HLA\text{-}DR^+$ $CD4^+$ T cells: un = 6.75

%; PBS = 6.47 %; EVs = 8.19 %; EVs$^{(cyt)}$ = 6.86 %; frequency of CD69$^+$ CD4$^+$ T cells: un = 1.49 %; PBS = 1.69 %; EVs = 1.87 %; EVs$^{(cyt)}$ = 1.74 %).

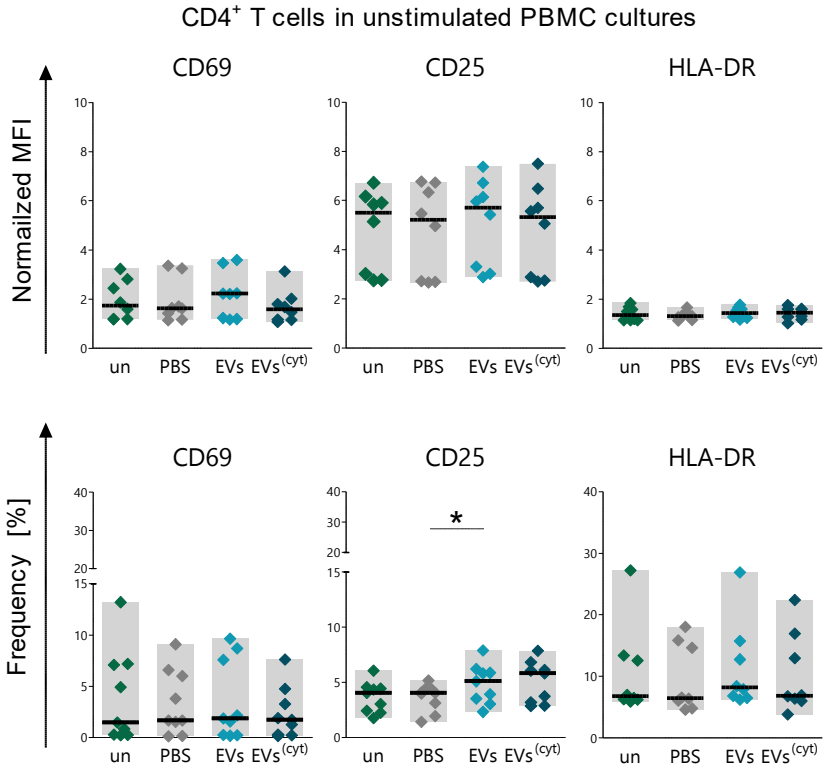

Figure 29: CD4$^+$ T cells were unchanged in their surface expression of activation markers when exposed to isolated EVs in unstimulated PBMC cultures. PBMCs were seeded in 96-well plates (3x10^5 cells/well), treated with 12 µg/mL unstimulated (EVs), cytokine stimulated EVs (EVs$^{(cyt)}$), PBS in equal volumes as EVs (PBS), or they were left untreated (un). After five days, cells were harvested and analysed by flow cytometry. The expression as geometrical mean fluorescence intensity (MFI) and frequency of CD69, CD25, and HLA-DR were determined for the CD4$^+$ T cell population in these unstimulated PBMC cultures. The obtained MFIs were additionally normalized to the respective unstained control. Individual data point of the normalized MFI (upper row) or frequencies (lower row) are shown as median with data range for CD69 (left), CD25 (middle) and HLA-DR (right; n = 8, five different CardAP donors). Statistical analysis was performed by Friedman´s test with Dunn´s multiple comparison *post hoc* test (* $p < 0.05$). Exposure of unstimulated and cytokine stimulated EVs did not induce the expression of typical activation molecules on CD4$^+$ T cells.

Further analysis revealed that the increase of CD25$^+$ CD4$^+$ T cells correlated with a co-expression of L-selectin (CD62L) in this particular immune subset (**Figure 30A**). The treatment with unstimulated EVs as well as cytokine stimulated EVs significantly enhanced the frequency of the CD62L$^+$ CD25$^+$ CD4$^+$ T cell compartment in comparison to the PBS and untreated control (median frequency of CD62L$^+$ CD25$^+$ CD4$^+$ T cells (range): un = 3.73 (3.01 – 4.68) %; PBS = 3.70 (3.29 – 3.07) %; EVs = 5.42 (4.91 – 6.83) %; EVs$^{(cyt)}$= 5.54 (5.06 – 7.57) %; **Figure 30B**). Coherently, significantly enhanced CD62L$^+$ frequencies were obtained for CD4$^+$ T cells in PBMC cultures treated with unstimulated or cytokine stimulated EVs in comparison to the PBS control (median frequency of CD62L$^+$ CD25$^+$ CD4$^+$ T cells (range): un = 78.29 (75.63 – 78.37)%; PBS = 77.71 (77.21 – 78.22) %; EVs = 79.66 (77.81 – 80.61) %; EVs$^{(cyt)}$ = 79.78 (78.67 – 83.20) %; **Figure 30B**).

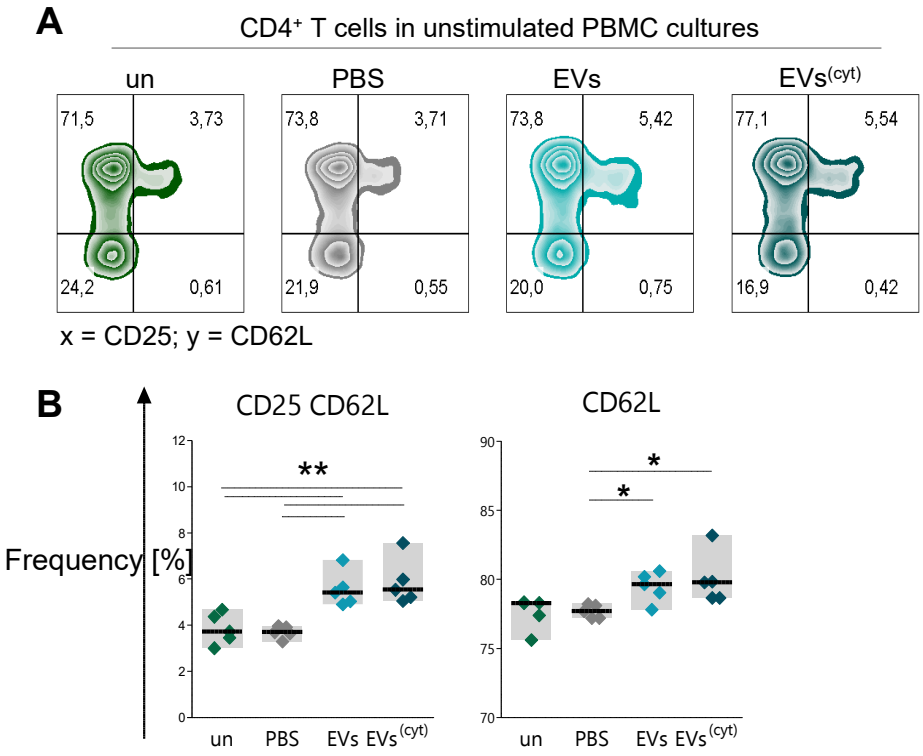

Figure 30: Unstimulated and cytokine stimulated EVs significantly enhanced the frequency of CD25$^+$ CD62L$^+$ CD4$^+$ T cells in otherwise unstimulated PBMC cultures.
PBMCs were seeded in 96-well plates (3x10^{5}cells/well) and treated with 12 µg/mL unstimulated (EVs), cytokine stimulated EVs (EVs$^{(cyt)}$), PBS in equal volumes as EVs (PBS), or they were left untreated (un). After five days, cells were harvested and analysed by flow cytometry. **(A):** Representative dot plots of all four different groups are shown for the expression of CD62L and CD25 on single living CD3$^+$ CD4$^+$ T cells. **(B):** The summarized individual frequencies of CD62L$^+$ or CD62L$^+$ CD25$^+$ CD4$^+$ T cells are shown as median with data range (n = 5, four different CardAP donors). Statistical analysis was performed by Friedman´s test with Dunn´s multiple comparison *post hoc* test (** $p < 0.01$, * $p < 0.05$). The frequency of CD62L$^+$ CD25$^+$ CD4$^+$ T cells was significantly enhanced in PBMC cultures that were exposed to either unstimulated or cytokine stimulated EVs.

4.6.2 EVs modulate induced immune responses

The immune modulating capacity of isolated EVs were accessed in pro-inflammatory immune responses that were induced by stimulation with anti-CD3. A comparative analysis and the determination of affected parameters, such as T cell proliferation, was enabled by treating these PBMC cultures simultaneously with either unstimulated EVs, cytokine stimulated EVs, PBS in equal volumes to EVs, or these stimulated PBMC cultures were left untreated. The frequencies of proliferated CD4$^+$ as well as CD8$^+$ T cells were significantly reduced in anti-CD3 stimulated PBMC cultures treated with both unstimulated or cytokine stimulated EVs from CardAP cells in comparison to the PBS control (**Figure 31A**). Interestingly, cytokine stimulated EVs diminished normalized CD4$^+$ and CD8$^+$ T cell proliferation even greater than their unstimulated counterpart, although both EV treatments exhibited significant diminishing effects in comparison to the PBS control (median normalized CD4$^+$ T cell proliferation (range): PBS = 0.983 (0.764 – 1.23), EVs = 0.928 (0.524 – 1.00), EVs$^{(cyt)}$ = 0.855 (0.548 – 0.983), ; median normalized CD8$^+$ T cell proliferation (range): PBS = 1.00 (0.711 – 1.16); EVs = 0.903 (0.472 – 0.993); EVs$^{(cyt)}$ = 0.929 (0.544 – 1.06); **Figure 31B**).

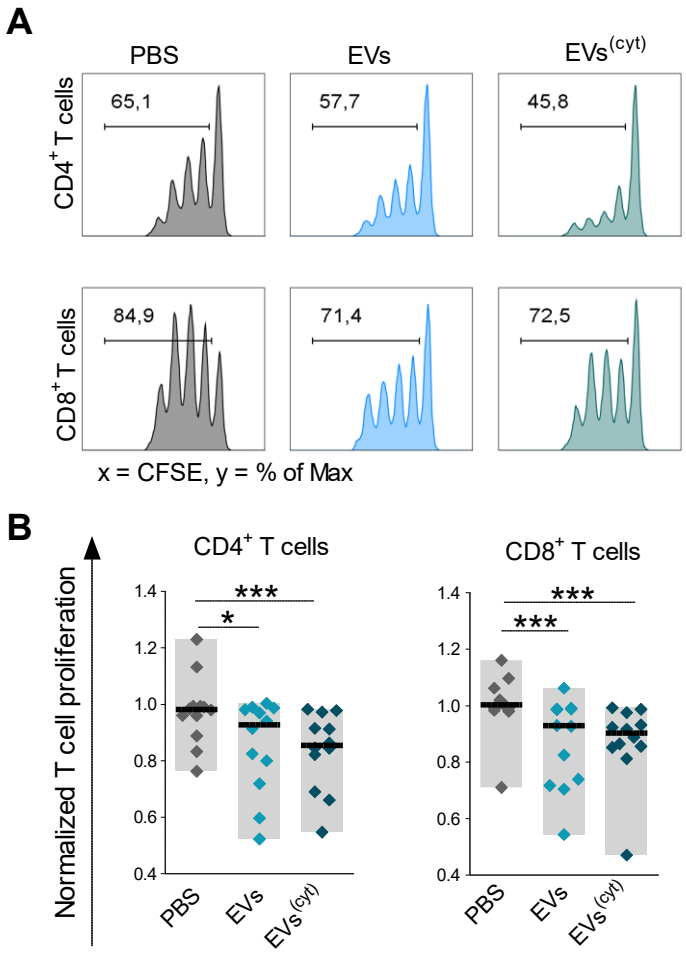

Figure 31: EVs diminished anti-CD3 induced T cell pro-liferation in PBMC cultures.
CFSE labelled PBMCs ($3x10^5$ cells/well) were stimulated with anti-CD3, and treated with 12 µg/mL unstimulated (EVs), cytokine stimulated EVs ($EVs^{(cyt)}$), PBS in equal volumes as EVs (PBS), or they were left untreated. After five days, harvested cells were analysed by flow cytometry. Obtained T cell proliferation frequencies were normalized to the untreated control. **(A):** Representative flow cytometry plots display the frequencies of proliferated $CD4^+$ and $CD8^+$ T cells in anti-CD3 stimulated PBMCs. **(B):** The normalized $CD4^+$ or $CD8^+$ T cell proliferation in anti-CD3 stimulated PBMC cultures is presented as median with data range (n = 9; four different CardAP donors; five different PBMC donors). Statistical analysis was performed by Friedman´s test with Dunn´s multiple comparison *post hoc* test (*** $p < 0.001$, * $p < 0.05$). Unstimulated and cytokine stimulated EVs reduce the T cell proliferation in anti-CD3 provoced immune responses of human isolated PBMCs.

$CD4^+$ T cells of anti-CD3 stimulated PBMC cultures were analysed in more detail for some activation markers. As anticipated, the expression of CD25 as well as CD69 was enhanced on $CD4^+$ T cell in anti-CD3 stimulated PBMC cultures (**Figure 32A**) in comparison to previous results in unstimulated PBMC cultures (**Figure 29**). Notably, treatments with unstimulated or cytokine stimulated EVs did not changed neither the expression level nor the frequency of these activation markers in comparison to PBS treated or untreated controls (median normalized MFI CD69: un = 2.61; PBS = 2.76; EVs = 2.74; $EVs^{(cyt)}$ = 2.49; median normalized MFI CD25: un = 14.78; PBS = 14.33; EVs = 16.82; $EVs^{(cyt)}$ = 14.96; median normalized frequency CD69: un = 18.25; PBS = 25.74; EVs = 18.59; $EVs^{(cyt)}$ = 20.70; median normalized frequency CD25: un = 91.40; PBS = 88.20; EVs = 90.70; $EVs^{(cyt)}$ = 90.70; **Figure 32A**). Since the activation of $CD4^+$ T cells was obtained at comparable levels between all treatments, it was of further interest whether the subset of regulatory T cells were affected by the treatment with isolated EVs. This is alo reasoned by the fact that this specific subset of T helper cells would be beneficial for the treatment of damaged cardiac tissue with prolonged or chronic inflammation. Indeed, PBS treated PBMC cultures exhibited lower frequencies of Tregs (viable, single $CD3^+$ $CD4^+$ $CD127^-$ $CD25^+$ $Foxp3^+$) in comparison to both EV treatments (**Figure 32B**). Although both EVs significantely enhanced the frequency of Tregs, unstimulated EVs exhibited a greater trend to enhance frequency of regulatory T cells than cytokine stimulated EVs (median frequency of

Tregs (range): PBS = 1.68 (1.05 – 2.68) %; EVs = 2.55 (1.96 – 3.38) %; EVs(cyt) =2.40 (1.75 – 2.81) %; **Figure 32B**).

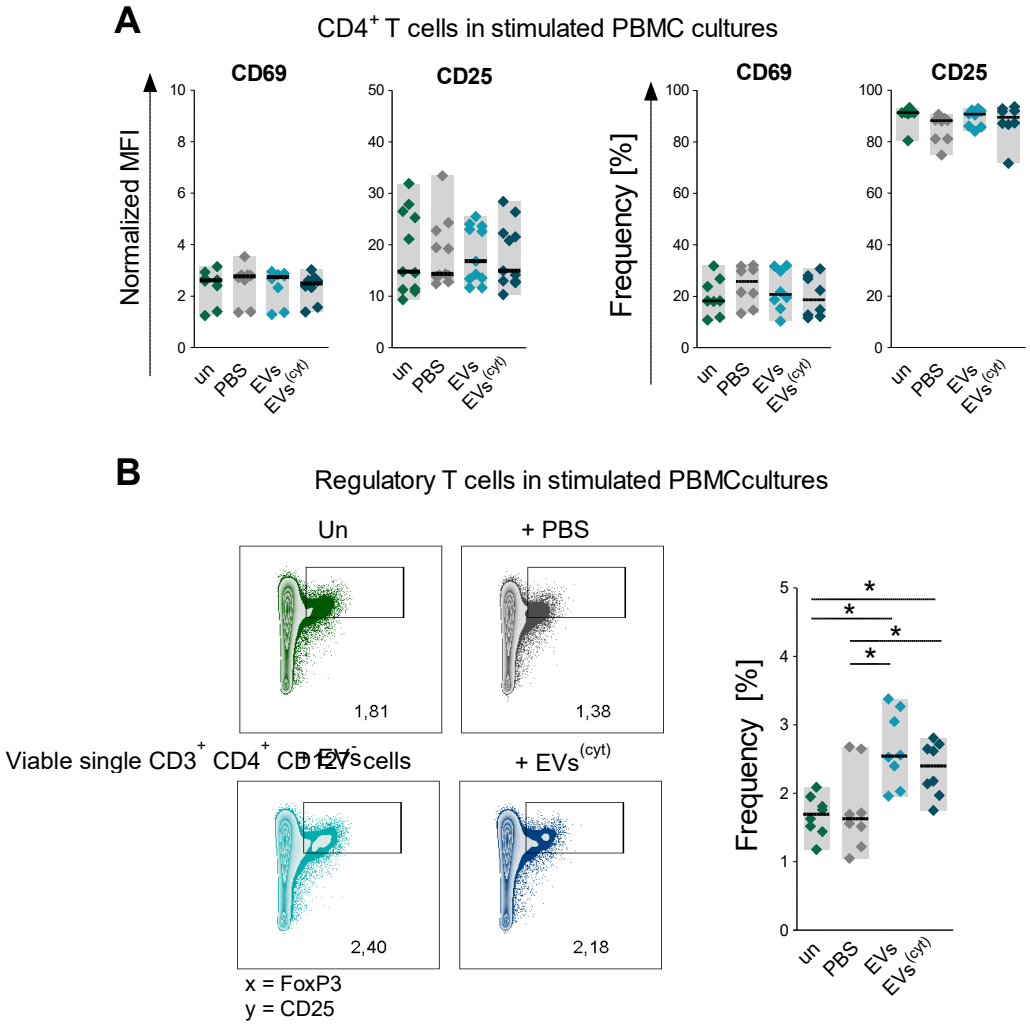

Figure 32: EVs increased the frequency of regulatory T cells, while CD4⁺ T cells showed comparable expression of activation markers in anti-CD3 induced PBMC cultures.
CFSE labelled PBMCs (6x10^5 cells/well) were stimulated with anti-CD3 treated with 12 µg/mL unstimulated (EVs), cytokine stimulated EVs (EVs$^{(cyt)}$), PBS in equal volumes as EVs (PBS), or they were left untreated (un). After three days, cells were harvested and analysed by flow cytometry. **(A):** The frequency and expression as geometrical mean fluorescence (MFI) were determined for CD25 and CD69 in the CD4⁺ T cell population in these anti-CD3 stimulated PBMC cultures. The obtained MFIs were additionally normalized to the respective unstained control. Individual data point of the normalized MFI (upper graphs) or frequencies (lower graphs) are shown as median with data range for CD69 (left), CD25 (middle) and HLA-DR Obtained individual geometrical mean fluorescence intensities (MFI) are displayed as median with data range for an early activation (CD69), mediate activation (CD25). **(B):** Representative flow cytometry plots (left) show the frequencies of regulatory T cells (CD25⁺ Foxp3⁺ T cells with previous gating on viable single CD3⁺ CD4⁺ CD127$^-$) in anti-CD3 stimulated PBMCs. The individual frequencies of regulatory T cells (viable single CD3⁺ CD4⁺ CD127$^-$ CD25⁺ Foxp3⁺ T cells) as median with data range (n = 8; five different CardAP donors; five different PBMC donors). Statistical analysis was performed by Friedman´s test with Dunn´s multiple comparison post hoc test (* $p < 0.05$). Unstimulated and cytocine stimulated EVs enhanced the frequency of regulatory T cells without affecting the general activation level of total CD4⁺ T cells in anti-CD3 stimulated PBMC cultures.

Moreover, the treatment with isolated EVs contributed towards a reduced pro-inflammatory cytokine profile in anti-CD3 stimulated PBMC cultures (**Figure 33**). Two pro-inflammatory

cytokines, namely IFNγ and TNFα, were significantly lowered up to 30% in its concentration in anti-CD3 stimulated PBMCs treated with unstimulated EVs or cytokine stimulated EVs in comparison to the PBS treated control (median IFNγ concentration (range): PBS = 28.82 (9.17 - 77.93) µg/mL; EVs = 18.49 (5.78 - 80.24) µg/mL; $EVs^{(cyt)}$ = 21.86 (5.08 - 44.56) µg/mL; median TNFα concentration (range): PBS = 1.36 (0.32 - 2.92) µg/mL; EVs = 0.76 (0.20 - 1.66) µg/mL; $EVs^{(cyt)}$ = 0.49 (0.12 - 1.98) µg/mL). Not only concentrations of pro-inflammatory but also anti-inflammatory cytokines were affected in these stimulated immune responses. Anti-CD3 stimulated PBMC cultures exhibited significantly more active TGFβ in cultures treated with unstimulated EVs or cytokine stimulated EVs in comparison to the PBS control (median TGFβ concentrations (range): PBS = 15.06 (2.2 - 20.57) pg/mL; EVs = 22.57 (3.56 - 26.29) pg/mL; $EVs^{(cyt)}$ = 22.84 (7.38 - 26.47) pg/mL). Interestingly, significantly more IL-10 was measured upon treatment with cytokine stimulated EVs in anti-CD3 stimulated PBMC cultures in comparison to the respective PBS control, while unstimulated EVs enhanced solely by trend the IL-10 concentration in the respective samples (median IL-10 concentrations (range): PBS = 159.10 (23.76 - 369.10) pg/mL; EVs = 204.70 (23.66 - 369.10) pg/mL; $EVs^{(cyt)}$ = 232.40 (37.90 - 379.90) pg/mL; **Figure 33**). In addition IL-17a and IL-1ß were also investigated for the respective concentrations. While comparable results were determined for IL-17a, a reduced tendency of IL-1ß concentrations were detected in anti-CD3 stimulated PBMC cultures treated with unstimulated or cytokine stimulated EVs (median IL-1ß concentrations: PBS = 660.80 pg/mL; EVs = 496.40 pg/mL; $EVs^{(cyt)}$ = 469.30 pg/mL; median IL-1ß concentrations: PBS = 164.10 pg/mL; EVs = 188.10 pg/mL; $EVs^{(cyt)}$ = 197.4 pg/mL; **Figure 33**).

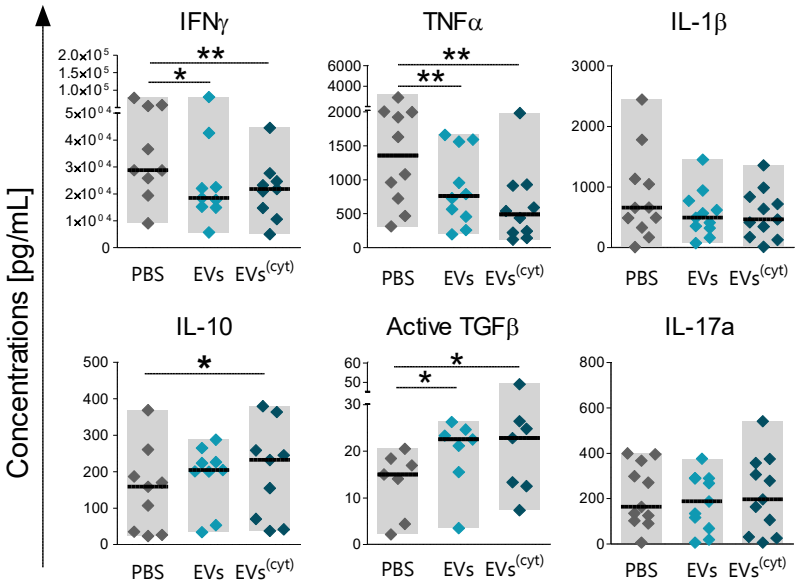

Figure 33: EVs attenuated the in-flammatory milieu in anti-CD3 stimulated PBMC cultures.
PBMCs (3x10^5/well) were stimulated with anti-CD3, treated with 12 µg/mL unstimulated (EVs), cytokine stimulated EVs ($EVs^{(cyt)}$), PBS in equal volumes as EVs (PBS), or they were left untreated. After three days, the conditioned medium was collected and the concentrations of released cytokines investigated by ELISAs (IFNγ, active TGFβ) or bead-based Multiplex assay (IL-10, TNFα, IL-17a, IL-1β). The obtained individual cytokine concentrations are displayed as median with data range (n = 8, four different CardAP donor, four different PBMC donors). Statistical analysis was performed by Friedman´s test with Dunn´s multiple comparison *post hoc* test (** $p < 0.01$, * $p < 0.05$).

Treatment with unstimulated and cytokine stimulated EVs resulted in a reduced pro-inflammatory cytokine milieu of anti-CD3 stimulated PBMC cultures.

4.6.3 EVs modulate induced immune responses in a CD14$^+$ cell dependent manner

As an initial step to understand how EVs facilitate the immune modulating feature, it was investigated with which immune cells EVs are interacting in PBMC cultures. For that reason, EV-cell interaction assays were performed with DiD labelled EVs (DiD$^+$EVs), DiD negative control (DiD neg. ctrl.) and unstimulated PBMCs. The interaction was allowed for one day, as previous results from murine and human cells emphasized a sufficient interaction. The included DiD negative control exhibited solely neglectable signals of PBMC cultures as analysed by flow cytometry (highest determined frequency of DiD$^+$ cells = 0.22 %; **Figure 34A**). Interestingly, the same analysis by flow cytometry revealed that DiD$^+$EVs were predominantly interacting with CD14$^+$ cells rather than with CD14$^-$ cells in these unstimulated PBMC cultures (median frequency of DiD$^+$ cells (range): CD14$^+$ cells = 90.9 (86.0 – 96.9) %; CD14$^-$ cells = 1.9 (1.5 – 3.4) %; **Figure 34A**). Additionally, this observation could be verified by a co-localization of CD14 and EV signal in a fluorescence microscopic approach (**Figure 34B**).

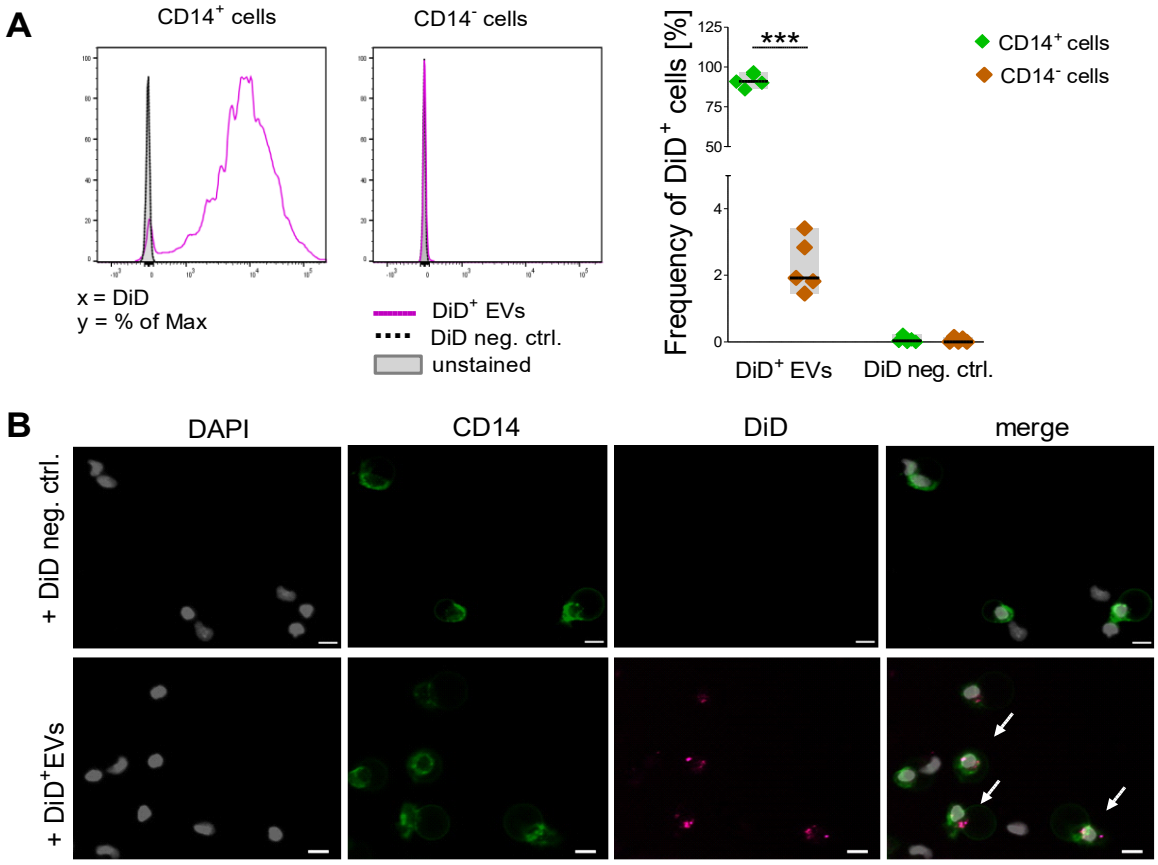

Figure 34: EVs interacted predominantly with CD14$^+$ cells in PBMC cultures.
PBMCs were seeded in 6-well plates (1x10^6 cells/well) and treated with 20 µg/mL DiD labelled EVs (DiD$^+$ EVs) or DiD negative control (DiD neg. ctrl.). After 24 h, this EV-cell interaction was analysed by microscopy or flow cytometry. **(A):** Representative histograms and summarized individual frequency of DiD$^+$ cells are shown for CD14$^+$ and CD14$^-$ immune cells as determined by flow cytometry (n = 5; four different CardAP donors; three different PBMC donors). **(B):** Representative images are illustrating the co-localization (white arrows) of DiD$^+$EVs (magenta) with CD14$^+$ PBMCs (green) in total PBMCs (pseudo coloured white for DAPI) with scale bars

representing 10 µm (n = 3; three different CardAP donors, two different PBMC donors). Statistical analysis was performed with Mann Whitney U test (*** p <0.001). $CD14^+$ cells are the major interaction partner of isolated EVs.

As a next step, the effect of isolated EVs on their predominant recipient cell was analysed in detail. Firstly, it was observed that the frequency of $CD14^+$ cells was significantly increased in unstimulated PBMC cultures treated with unstimulated EVs as well as with cytokine stimulated EVs in comparison to the PBS control (median frequency of $CD14^+$ cells (range): PBS = 3.35 (1.83 – 9.22) %, EVs = 7.39 (3.18 – 20.30) %, $EVs^{(cyt)}$ = 11.10 (3.56 – 29.20) %; **Figure 35A**). Secondly and foremost, these EV-primed $CD14^+$ cells exhibited an intensely changed surface protein expression pattern in PBMC cultures. Antigen presenting proteins, namely HLA-DR and CD86, were significantly reduced on $CD14^+$ cells upon EV treatment, (**Figure 35B**). The expression of HLA-DR was more than halved under treatment with unstimulated EVs or with cytokine stimulated EVs in comparison to the PBS control, while the expression of CD86 was halved by cytokine stimulated EVs and reduced by one third upon treatment with unstimulated EV in comparison to the PBS control (median normalized MFI HLA-DR (range): PBS = 1.08 (0.74 – 1.23), EVs = 0.38 (0.13 – 0.78), $EVs^{(cyt)}$ = 0.25 (0.10 – 0.97); median normalized MFI CD86 (range): PBS = 1.03 (0.72 – 1.34); EVs = 0.67 (0.29 – 1.35); $EVs^{(cyt)}$ = 0.50 (0.29 – 1.02)). Unstimulated EVs also caused a significantly reduced surface expression of the scavenger receptor cysteine-rich type 1 protein M130 (CD163) on $CD14^+$ cells as compared to the PBS treated $CD14^+$ cells. The treatment with cytokine stimulated EVs, however, caused just by trend a reduced surface expression of CD163 (median normalized MFI CD163 (range): PBS = 1.05 (0.74 – 1.20); EVs = 0.45 (0.27 – 0.98); $EVs^{(cyt)}$ = 0.46 (0.23 – 1.43)). Moreover, the treatment with either unstimulated as well as cytokine stimulated EVs significantly enhanced the expression of PD-L1, CD14 and the macrophage mannose receptor 1 (CD206) in comparison to the PBS treated control (median normalized MFI PD-L1 (range): PBS = 1.08 (0.85 – 1.31); EVs = 1.77 (0.84 – 3.6); $EVs^{(cyt)}$ = 2.07 (1.29 – 7.51); median normalized MFI CD14 (range): PBS = 0.91 (0.55 – 1.12); EVs = 1.40 (0.38 – 2.00); $EVs^{(cyt)}$ = 1.52 (0.51 – 1.93); median normalized MFI CD206 (range): PBS = 0.94 (0.64 – 2.24); EVs = 1.96 (0.95 – 5.22); $EVs^{(cyt)}$ = 3.82 (1.37 – 6.95); **Figure 35B**).

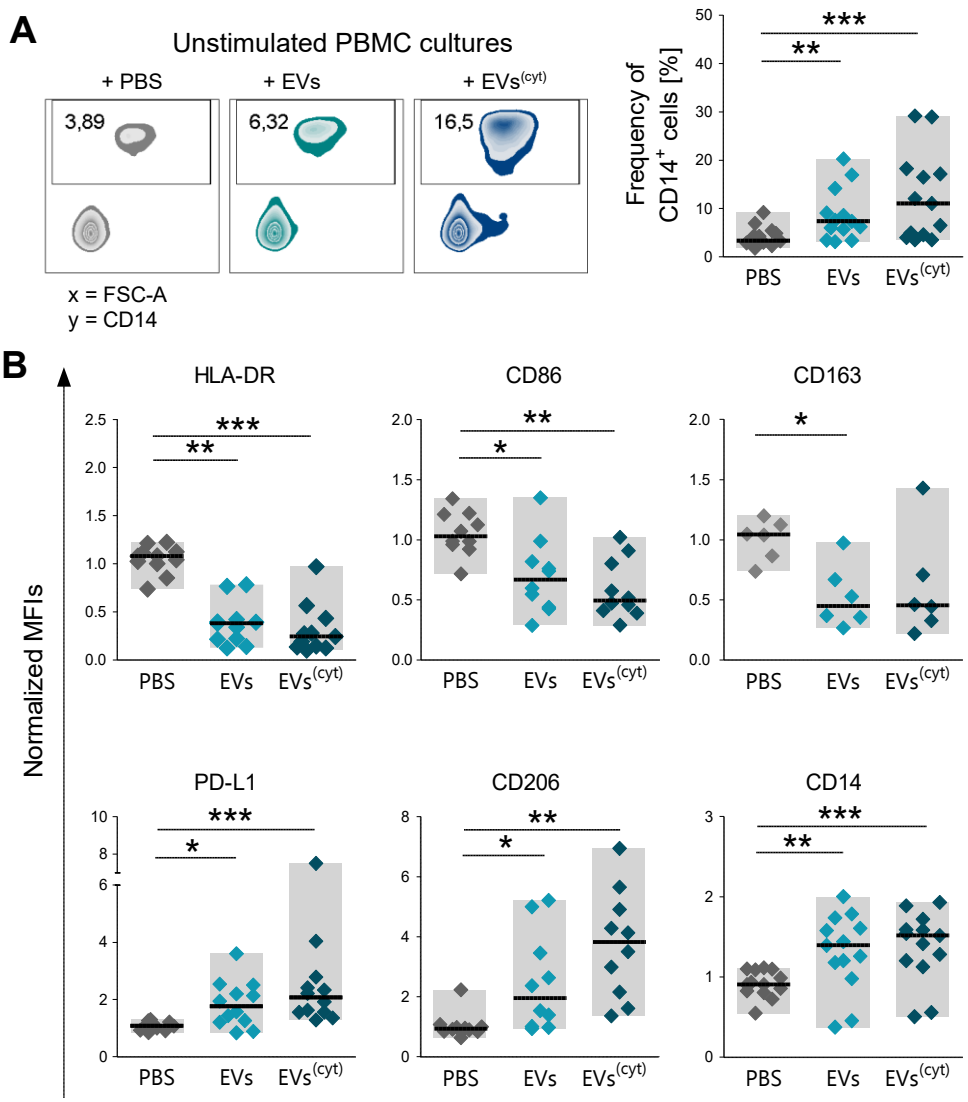

Figure 35: CD14⁺ cells changed significantly their phenotype after interaction with EVs.
PBMCs were seeded in 96-well plates (3x10^5 cells/well) and treated with 12 µg/mL unstimulated (EVs), cytokine stimulated EVs (EVs$^{(cyt)}$), PBS in equal volumes as EVs (PBS), or they were left untreated (un). After three days, cells were harvested and analysed by flow cytometry. **(A):** The frequency of CD14⁺ cells in unstimulated PBMC cultures is shown as representative flow cytometry plots (left) and as summarized individual data as median with range (right; *n* = 13; six different CardAP donors; 9 different PBMC donors). **(B):** The expression as geometrical mean fluorescence (MFI) was determined on CD14⁺ cells in unstimulated PBMC cultures for HLA-DR, CD86, CD163, PD-L1, CD206, and CD14. The obtained MFI values were normalized to the respective unstained sample. The individual normalized MFIs are displayed as median with range (*n* = 10 – 13; at least five different CardAP donors; seven different PBMC donors). Statistical analysis was performed by Friedman´s test with Dunn´s multiple comparison *post hoc* test (* $p < 0.05$; ** $p < 0.01$; *** $p < 0.001$). Unstimulated and cytokine stimulated EVs do not only enhance the frequency of CD14⁺ cells but also change the expression profile of different surface molecules on CD14⁺ cells.

In order to unravel whether EV-primed CD14⁺ cells contribute to the previously observed immunomodulation, the immune modulation assay was adjusted. For that purpose, immune responses of purified CD3⁺ T cells were provoked with anti-CD3 either in a monoculture set-up or as co-culture set-up together with CD14⁺ cells that interacted with isolated EVs two days prior to an assay. Additionally, purified CD3⁺ T cell monocultures treated with isolated EVs simultaneously with the stimulating agent served as control. Monocultures of CD3⁺ T cells treated with either unstimulated or cytokine stimulated EVs exhibited comparable normalized

$CD4^+$ or $CD8^+$ T cell proliferation levels compared with the PBS control (median normalized $CD4^+$ T cell proliferation: PBS = 0.957; EVs = 0.960; $EVs^{(cyt)}$= 0.988; median normalized $CD4^+$ T cell proliferation: PBS = 0.975; EVs = 0.936; $EVs^{(cyt)}$ = 0.939; **Figure 36A**). On the contrary, co-cultures of $CD3^+$ T cells together with EV-primed $CD14^+$ cells resulted in a significant reduction of normalized $CD4^+$ as well as $CD8^+$ T cell proliferation, while cytokine stimulated EVs showed a greater influence than their unstimulated counterpart (median normalized $CD4^+$ T cell proliferation (range): PBS =1.029 (0.951 – 1.056); EVs = 0.946 (0.835 – 1.005); $EVs^{(cyt)}$ = 0.923 (0.839 – 0.987); median normalized $CD4^+$ T cell proliferation (range): PBS = 1.017 (0.941 – 1.035); EVs = 0.945 (0.916 – 1.008); $EVs^{(cyt)}$ = 0.932 (0.835 – 0.986); **Figure 36B**).

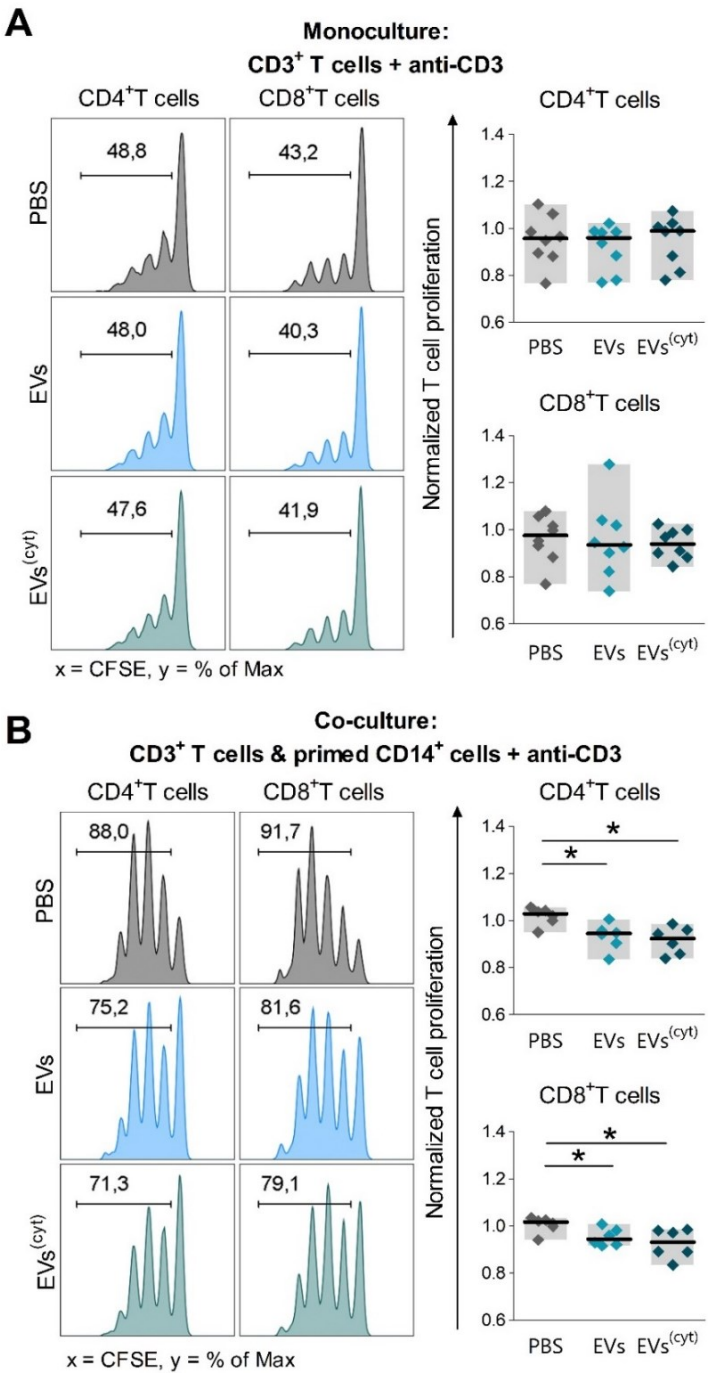

Figure 36: EVs diminished T cell proliferation of purified $CD3^+$ T cells solely in the presence of $CD14^+$ cells. By MACS purified $CD14^+$ and $CD3^+$ cells from isolated PBMCs were cultured in 6-well plates for two days. $CD14^+$ cells ($1x10^6$ cells/well) were additionally treated with 12 µg/mL unstimulated (EVs) or cytokine stimulated ($EVs^{(cyt)}$), PBS in equal volume of the EVs (PBS), or they were left untreated, while $CD3^+$ cells were labelled with CFSE and left untreated ($1x10^6$ cells/well). Afterwards, $CD14^+$ cells were co-cultured one to five with $CD3^+$ T cells and stimulated with anti-CD3. As control, monocultures of $CD3^+$ T cells were stimulated with anti-CD3 and additionally treated with 12 µg/mL EVs, $EVs^{(cyt)}$, PBS in equal volume of the EVs, or left untreated. After three days, the cells were harvested and analysed by flow cytometry. **(A-B):** Representative flow cytometry plots display the frequencies of proliferated $CD4^+$ and $CD8^+$ T cells in anti-CD3 stimulated monocultures of $CD3^+$ cells **(A)** or co-cultures of $CD3^+$ and EV-primed $CD14^+$ cells **(B)**. The T cell proliferation frequencies were normalized to the untreated control. These obtained normalized proliferation of $CD4^+$ and $CD8^+$ T cells in anti-CD3 stimulated monocultures of $CD3^+$ cells **(A)** or in co-culture $CD3^+$ and EV-primed $CD14^+$ cells **(B)** is presented for the three treatments as median with data range (n = 8 - 6; five differ-rent CardAP donors; five differ-rent PBMC donors). Statistical analysis was performed by Friedman´s test with Dunn´s multiple comparison *post hoc* test (*$p < 0.05$; **$p < 0.01$; ***$p < 0.001$). Unstimulated and cytokine stimulated EVs diminished T cell proliferation in a $CD14^+$ cell dependent manner.

Coherently, the concentrations of released pro-inflammatory cytokines, namely IFNγ as well as TNFα, were diminished in co-cultures of $CD3^+$ T cells with EV-primed $CD14^+$ cells but not in the monoculture setting of $CD3^+$ T cells (**Figure 37A, B**). Treatment with cytokine stimulated EVs significantly reduced the level of both cytokines in co-cultures, while unstimulated EVs exhibited solely a trend for reduced concentrations in comparison to the PBS control (median IFNγ concentration (range): PBS = 11.74 (3.62 – 17.62) μg/mL; EVs = 10.28 (0.24 – 10.74) μg/mL; $EVs^{(cyt)}$ = 3.87 (2.06 – 6.36) μg/mL; median TNFα concentration (range): PBS = 2.56 (1.73 – 4.30) μg/mL, EVs = 2.21 (0.58 – 4.35) μg/mL, $EVs^{(cyt)}$ = 1.41 (0.74 – 2.95) μg/mL; **Figure 37B**). Interestingly, the IL-10 level was found to be significantly reduced in co-cultures with $CD14^+$ cells that were primed by cytokine-stimulated EVs, whereas active TGFß was detectable on very low levels (median IL-10 concentrations (range): PBS = 322 (246 – 370) pg/mL; EVs = 286 (77 – 339) pg/mL; $EVs^{(cyt)}$ = 152 (97 – 279) pg/mL; **Figure 37B**). In anti-CD3 stimulated $CD3^+$ T cell monoculture neither pro-inflammatory nor anti-inflammatory cytokines were altered upon treatment with isolated EVs (median active TGFβ concentrations: PBS = 3.93 pg/mL, EVs =5.38 pg/mL, $EVs^{(cyt)}$ = 7.20 pg/mL; median TNFα concentrations: PBS =142.50 pg/mL; EVs = 90.89 pg/mL; $EVs^{(cyt)}$ = 116.00 pg/mL; median IL-10 concentrations: PBS = 15.81 pg/mL; EVs = 9.89 pg/mL; $EVs^{(cyt)}$ = 11.93 pg/mL; median IFNγ concentration: PBS = 3.27 μg/mL, EVs = 2.89 μg/mL, $EVs^{(cyt)}$ = 4.09 μg/mL; **Figure 37A**).

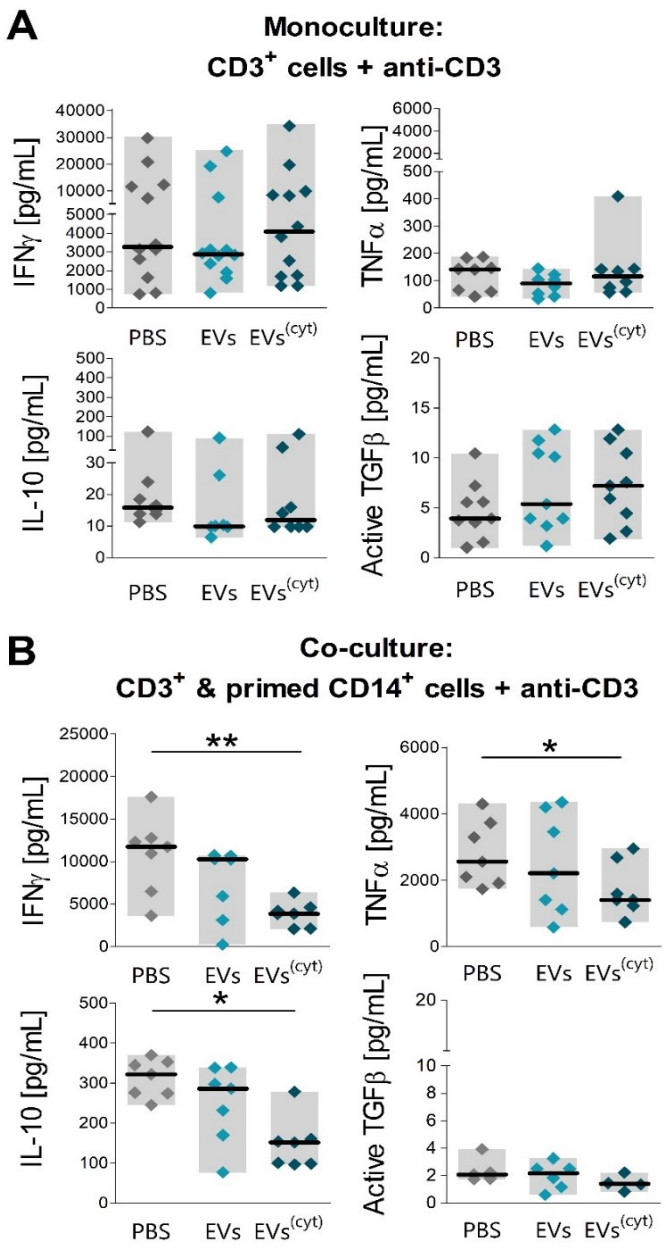

Figure 37: EVs attenuate anti-CD3 induced pro-inflammatory cyto-kine release only in co-cultures of CD14⁺ cells with CD3⁺ T cells but not in monocultures of CD3⁺ T cells.
By MACS purified CD14⁺ and CD3⁺ cells from isolated PBMCs were cultured in 6-well plates for two days. CD14⁺ cells ($1x10^6$ cells/well) were additionally treated with 12 µg/mL unstimulated (EVs) or cytokine stimulated ($EVs^{(cyt)}$), PBS in equal volume of the EVs (PBS), or they were left untreated, while CD3⁺ cells were labelled with CFSE and left untreated ($1x10^6$ cells/well). Afterwards, CD14⁺ cells were co-cultured one to five with CD3⁺ T cells and stimulated with anti-CD3. As control, monocultures of CD3⁺ T cells were stimulated with anti-CD3 and additionally treated with 12 µg/mL EVs, $EVs^{(cyt)}$, PBS in equal volume of the EVs, or left untreated. After three days, the supernatants were collected and cytokine concentrations were analysed by ELISA (IFNγ, active TGFβ) or by Multiplex bead-based assays (IL-10, TNFα). **(A-B):** Concentrations for all tested cytokines are presented for anti-CD3 stimulated monoculture of CD3⁺ T cells **(A)** or co-cultures of CD3⁺ T cells with CD14⁺ T cells **(B)** as median with data range (co-culture: n = 6 - 7, five different CardAP donors, five different PBMC donors; monoculture: n = 7 - 11; four different CardAP donors, four different PBMC donors). Statistical analysis was performed by Friedman´s test with Dunn´s multiple comparison *post hoc* test (* $p < 0.05$; ** $p < 0.01$). Pro-inflammatory cytokines were solely significantly reduced in anti-CD3 stimulated co-cultures of CD3⁺ T cells and CD14⁺ cells that were primed by cytokine stimulated EVs, while the corresponding culture with unstimulated EVs showed a likewise tendency.

Additionally it was observed that the frequency of regulatory T cells was significantly enhanced in co-cultures with EV-primed CD14⁺ cells in comparison to the control setting of PBS-treated CD14⁺ cells (median frequency of Tregs (range): PBS = 3.39 (2.19 – 5.63) %; EVs = 4.65 (2.87 – 8.42) %; EVs(cyt) = 4.43 (3.10 – 7.44) %; **Figure 38A, B**). Analysis of supernatants of the primed CD14⁺ cells showed that interleukin 1 receptor antagonist (IL-1RA) was significantly enhanced, while IL-1β, IFNγ and IL-10 were not detectable in those supernatants (median IL-1RA concentrations (range): PBS = 236.7 (35.4 – 331.9) pg/mL; EVs = 330.5 (56.91 – 384.3) pg/mL; EVs(cyt) = 331.1 (39.6 – 397.1) pg/mL; **Figure 38C**).

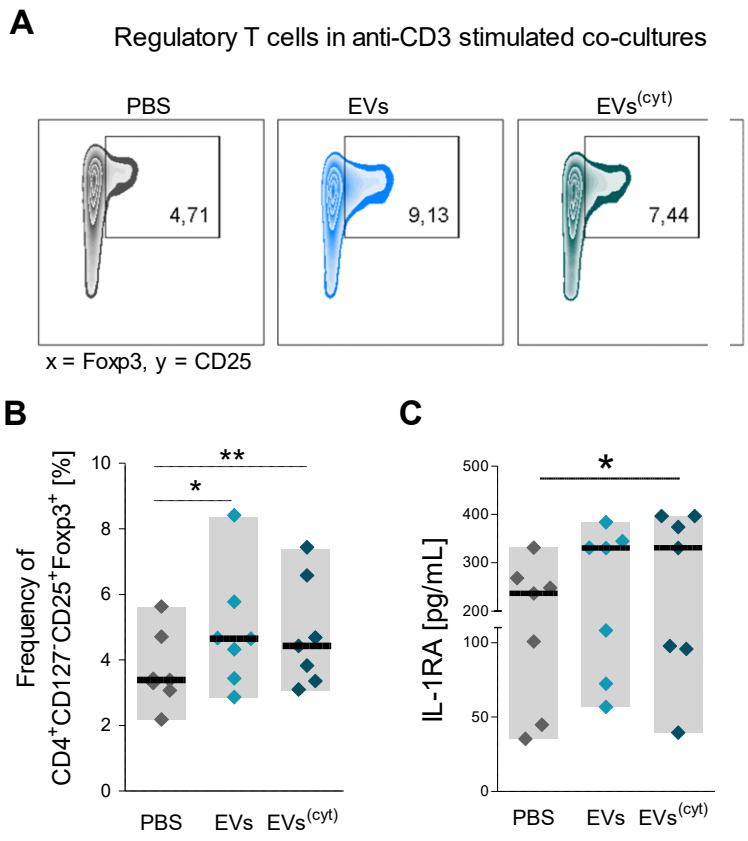

Figure 38: The frequency of regulatory T cells is enhanced in anti-CD3 stimulated co-cultures of CD3⁺ cells with EV-primed CD14⁺ cells.
By MACS purified CD14⁺ and CD3⁺ cells from isolated PBMCs were cultured in 6-well plates for two days. CD14⁺ cells ($1x10^6$ cells/well) were additionally treated with 12 µg/mL unstimulated (EVs) or cytokine stimulated ($EVs^{(cyt)}$), PBS in equal volume of the EVs (PBS), or they were left untreated, while CD3⁺ cells were labelled with CFSE and left untreated ($1x10^6$ cells/well). Afterwards, CD14⁺ cells were co-cultured one to five with CD3⁺ T cells and stimulated with anti-CD3. As control, monocultures of CD3⁺ T cells were stimulated with anti-CD3 and additionally treated with 12 µg/mL EVs, $EVs^{(cyt)}$, PBS in equal volume of the EVs, or left untreated. After three days, cells were analysed by flow cytometry. **(A)** Representative flow cytometry plots display the frequencies of regulatory T cells (single viable $CD4^+CD127^-CD25^+Foxp3^+$ cells) in anti-CD3 stimulated co-cultures of CD3⁺ cells and CD14⁺ cells primed with PBS (left), EVs (middle) or $EVs^{(cyt)}$ (right). **(B):** Quantification of regulatory T cell frequency is shown for the individual frequencies as median with data range for the three different treatments ($n = 6$; four different CardAP donors; four different PBMC donors). **(C):** The supernatants of EV-primed CD14⁺ cells were investigated for the concentration of released IL-1RA, which is shown for the individual concentrations as median with data range ($n = 7$, four different CardAP donors, four different PBMC donors). Statistical analysis was performed by Friedman´s test with Dunn´s multiple comparison *post hoc* test (***$p < 0.001$, **$p < 0.01$, *$p < 0.05$). Unstimulated and cytokine stimulated EVs enhanced the release of IL-1RA by CD14⁺ cells and the frequency of regulatory T cells in co-cultures of CD3⁺ cells and EV-primed CD14⁺ cells.

5. Discussion

New therapeutic approaches with disease reverting properties are desperately needed to limit and evade the health-related but also sociological and economical burdens of CVDs. Different pre-clinical trials demonstrated that the application of diverse regenerative cells exhibited desirable effects including the inhibition of apoptosis, the modulation of pro-inflammatory immune responses, and the significant improvement of cardiac function [11,14,16,34,62,70]. However, clinical trials failed to reproduce the promised therapeutic potential or solely just demonstrated limited therapeutic success of some already tested regenerative cells, namely, bone marrow mononuclear cells, MSCs, and CPCs, in patients suffering from ischemic heart diseases [61,69,71,72]. Mechanistic analysis revealed that not the previously hypothesized integration of the cell itself into the damaged tissue contributed to the beneficial effects but rather paracrine mediators released by the applied cell source [78–80]. Thorough analysis of the conditioned medium disclosed that the contained EVs were the major driving force to diminish symptoms in animals suffering from myocardial infarction or other ischemic diseases [37,101,103,125–127]. Since a pro-angiogenic feature was observed for the conditioned medium of CardAP cells [64], it seems likely that this regenerative cell type uses also a paracrine mechanism.

In this thesis we assessed whether CardAP cells release EVs suitable for an allogenic cell-free approach to treat CVDs by performing a series of *in vitro* studies. For that purpose, EVs were isolated by differential centrifugation from the conditioned medium of CardAP cells cultivated either in the presence or absence of a pro-inflammatory cytokine cocktail. It was not clear yet under which condition CardAP cells release regenerative EVs. For that reason we chose these two EV biogenesis conditions, because CardAP cells exhibited immune modulating, anti-apoptotic and *in vivo* cardio protective capacity [13,60,65] but not their pro-angiogenic effect [13,64] in an inflammation driven milieu. Furthermore, the immune modulating capacity of MSCs, cardiac derived cells and especially EVs from MSCs was boosted by pro-inflammatory stimulation [104,128–131]. It has to be highlighted that in order to avoid contaminations of EVs from the serum source, expansion of CardAP cells as well as all functional assays were consequently performed with centrifuged human serum. Additionally, any serum source was omitted during their EV biogenesis. For that reason, it can be excluded that further discussed experimental data are influenced by contaminations of EVs from a serum source.

5.1 Does the biogenesis condition affect CardAP cells to release EVs with different characteristics?

The general success of the performed EV isolation procedure could be confirmed by different observations, such as the visualization of small vesicular lipid bilayer structure by TEM or the detection of typical transported molecules, such as proteins and miRNAs, in generated and tested EV preparations. It was also observed that one million CardAP cells released comparable quantities of EVs despite of the applied biogenesis condition as neither protein amount nor particle concentrations differed between unstimulated and cytokine stimulated EV preparations (**Figure 14**). Studies from MSC EVs emphasize that the efficacy always needs an individual examination and do not follow a general pattern upon cytokine stimulation, as results range

from similar [107] or higher [132] protein content of EVs from IFNγ stimulated MSCs to a lower particle concentrations upon IFNγ/TNFα stimulation of MSCs [130].

In accordance with the guidelines from the international society of extracellular vesicles (ISEV) [83,85,89,133], it was indeed possible to detect anticipated EV proteins from different cellular locations in unstimulated as well as cytokine stimulated EVs from CardAP cells by flow cytometry or LC/ESI-MS. Three tetraspanins, namely CD9, CD63, and CD81, as well as different integrin proteins, such as CD29 or ITAV, are just some representatives from detected transmembrane proteins, while syntenin and proteins of the annexin family exemplify cytosolic proteins (**Figure 15 and 16**). Also, non-EV categorized proteins were co-isolated in our EV preparations as observed by the detection of fibronectin by LC/ESI-MS. Importantly, an intracellular protein, namely GM-130, was not detectable in unstimulated and cytokine stimulated EVs neither by flow cytometry nor LC/ESI-MS. The lack of GM-130 is especially vital when taking into consideration that CardAP cells displayed an increase of about 4% late apoptotic cells upon cytokine stimulation in comparison to its expansion medium. Although this mild apoptosis was induced, it seems doubtful that isolated EV preparations are containing apoptotic bodies. Firstly, GM-130 was solely detectable in apoptotic body fractions (**Figure 9**) but not in further investigated EV preparations (**Figure 15**). Secondly, diameters of EV preparations never grasped the size of an apoptotic body (d > 1,000 nm) as 875.8 nm was the biggest determined diameter of isolated EVs.

A study by Jeppsesen *et al.* in 2019 achieved a better understanding about proteins transported by small EVs and their co-contaminations as a non-exosomal compartment from EV preparations derived from glioblastoma or colon cell lines [90]. Proteins of EVs from CardAP cells identified by LC/ESI-MS were composed of both the small EV (e.g. annexinA2/V, syntenin-1, ALIX, HSC70, aldolase A, enolase 1, CD73, ITGB1, or ITAV) and the non-exosomal compartment (e.g. GAPDH, MVP, calthrin, histone h2a, or fibronectin; see **Figure 16** and ***Appendix Table 1***). This observation can be accredited as a consequence of our applied isolation procedure, which did not include a gradient or affinity step to separate both components exclusively. Furthermore, studies of manufactured liposomes or nanovesicles showed that they are surrounded by a shell of proteins, also referred to as corona, after being exposed to protein containing liquid, such as plasma/serum [134–136]. Yet, it is not clear whether the proteins of the non-exosomal compartment reflect corona proteins of EVs, since this subject just gained attention in the last years of EV research [137]. In context of the current study, it seems likely that isolated EVs from CardAP cells are also surrounded by a protein corona. Firstly, EVs are released into a protein containing solution, since CardAP cells release next to EVs also soluble proteins into their conditioned medium. Secondly, the applied differential centrifugation allowed the reduction of protein contaminations but not its separation from small EVs, as indicated by the detection of the previously mentioned fibronectin.

Nevertheless, it was possible to allocate the majority of LC/ESI-MS identified proteins (n = 156/186) of EVs from CardAP cells by String Database analysis to the extracellular exosome compartment, while some proteins, such as TNFα induced protein 3 or Rab-34, were exclusively observed for cytokine stimulated or unstimulated EVs, respectively. The pro-inflammatory cytokine cocktail already caused CardAP cells to enhance or even induce the expression of

immunological relevant proteins on its surface, such as PD-L1, PD-L2, CD54 or CD106 (**Figure 12**). In contrast, their released EVs solely exhibited a significant upregulation of CD54 on cytokine stimulated EVs as measured by flow cytometry, while other markers, such as PD-L1, remained underneath the detection limit or exhibited minor alterations upon cytokine stimulation. Interestingly, CD54 was also shown to be enriched on EVs from IFNγ/TNFα stimulated MSCs in comparison to their unstimulated counterpart [130]. In a different study, it was revealed that a blockage of CD54 or its receptor impaired interaction of EVs from bone marrow derived dendritic cells with dendritic cells of a different mice strain [138]. However, the importance of the upregulation of CD54 on EVs from regenerative cell sources is still elusive and needs further investigations.

Striking differences between unstimulated and cytokine stimulated EVs from CardAP cells were determined with respect to their transported miRNAs by nCounter® miRNA expression assay, which was used to study nearly 800 different human miRNAs. Half of the identified miRNAs (102 out of 205 miRNAs) were observed to be present in both unstimulated and cytokine stimulated EVs. Unstimulated EVs solely exhibited 14 uniquely detected miRNAs, while 89 miRNAs were exclusively observed in cytokine stimulated EVs (**Figure 18**). Though, results by qRT PCR elucidated that a previously exclusive cytokine stimulated miRNA, miRNA 494-3p, was also to a lower extent detectable in unstimulated EVs. For that reason, it cannot be ruled out that the high number of 89 exclusively transported miRNAs by cytokine stimulated EVs will be corrected after additional experiments, such as including more CardAP donors or verifying all results by qRT-PCR. Recent studies showed that the separation of small EVs from its co-isolated proteins correlated with the identification of RNA binding proteins in the non-EV compartment [90,91]. Thus, additional changes in the isolation procedure of our CardAP EVs will enable the differentiation whether miRNAs belong to the small EV or non-EV compartment. Nonetheless, it can be excluded that artefacts of miRNA from the serum source or available serum free supplements as previously reported were determined in the current miRNA assays due to the fact that EVs from CardAP cells were released in serum free IDH medium [139,140]. Interestingly, the pro-inflammatory cytokine stimulation, most likely the TNFα stimulation, can be retraced in affected genes by miRNAs from cytokine stimulated EVs, as they were significantly enriched in tumour necrosis factor related apoptosis inducing ligand (TRAIL) signalling than genes from detected miRNAs of unstimulated EVs (**Figure 19**).

Corroborating evidence for CardAP cells altering their released EVs upon cytokine stimulation was obtained by measuring diameters of isolated EVs. Although the majority of EVs from both biogenesis conditions exhibited diameters of exosomes ($d < 100$ nm) as measured by TEM, cytokine stimulated EVs were found to have a significantly smaller mean diameter than their unstimulated counterpart (**Figure 13**). NTA results likewise showed that the majority of cytokine stimulated EVs were smaller than unstimulated EVs (**Figure 13**). However, solely a minority of EVs of both biogenesis conditions appeared in NTA to be smaller than 100 nm in their particle diameter. The discrepancy between determined diameters of NTA and TEM are reasoned by several factors. Firstly, our TEM protocol included a dehydration step, which causes the dehydration of naïve EVs that consequently appeared as sphere-like shapes. Secondly, NTA allows the measurement of all contained particles in the solution that are bigger

than 40 nm, which includes next to isolated EVs also aggregates of EVs with each other or with proteins, protein aggregates and dust particles. Thirdly and most importantly, isolated EVs from CardAP cells were not separated from their protein corona. While TEM allows the measurement of the vesicle itself through its lipid bilayer, NTA does not distinguish between EVs and their surrounding protein corona [141]. Most likely, NTA measurements are even greater influenced, as the diameter of particles are determined in an aqueous solution (here PBS), which additionally adds a hydrate shape. In contrast to our observation, IFNγ stimulated MSCs were observed to release EVs with larger mean diameters than unstimulated MSCs as determined by TEM [132]. But, the diameter distribution illustrates that stimulated EVs conveyed two unequally distributed peaks instead of a single peak as observed for their unstimulated counterpart. Comparing the main peak (≥ 75% of determined EVs), it also seems that stimulated EVs would be smaller than unstimulated EVs, similar to our result, even if a different cell source and different settings for the acquisition of EVs were chosen. In another study from 2020, EVs were generated from umbilical cord mesenchymal stromal cells cultured in the presence or absence of the same cytokine cocktail as CardAP cells and additionally under hypoxia or normoxia [142]. Further analysis did not display differences between diameters obtained by NTA, while TEM data were solely shown for hypoxic and normoxic unstimulated EVs without any quantification. Excitingly, this study applied a highly sensitive proximity extension array to elucidate cytokines and chemokines transported by isolated EVs. Here, it was demonstrated that cytokine stimulated MSCs release EVs independent of the oxygen levels with significantly increased protein expression levels for CSF-1, MCP4, IL-13, IFNγ, CXCL5, as well as significantly reduced levels of CXCL10 in comparison to their unstimulated counterpart. It remains to be investigated whether isolated EVs from CardAP cells display similar changes upon cytokine stimulation, since our performed ESI/LC-MS approach did not cover the determination of either cytokines or chemokines.

It can be hypothesized that the determined differences between unstimulated and cytokine stimulated EVs from CardAP cells are a result of a shift in the proportion of different released small EV species. Studies from other groups support this theory. Herein, small EV preparations were subjected to an additional gradient separation (e.g. top to bottom *vs.* bottom to top) or tetraspanin affinity purification. Qualitative and quantitative proteomic analysis revealed that some proteins were exclusively detected in one separated EV subset, while most proteins were omnipresent in all separated EV subsets [88,143,144]. For that reason, it is assumed that the term small EVs or exosomes relates to a rather heterogeneous than homogenous population of EVs. Although we do not know yet how many different populations of small EVs will be necessary to be considered in future, yet the current study clearly underlines that the milieu during EV biogenesis of CardAP cells has significantly influenced the phenotype of the released EVs as well as their composition of transported miRNA molecules.

5.2 Do CardAP cells release EVs under both EV biogenesis conditions that have valuable properties for an allogenic approach to treat CVDs?

In order to use the generated EVs from CardAP cells as a cell-free allogenic therapeutic approach, two requirements are essential for their future clinical application. On the one hand, EVs have to own properties that may contribute to the improvement of the heart cell function. On the other hand, the therapy needs to be safe for the prospective patients. The risk of an allogenic approach would especially be an adverse immune reaction between donor and recipient. In the current study, both issues were in depth analysed via different *in vitro* approaches and are discussed in the following.

5.2.1 Could both isolated CardAP EVs enhance the cardiac function by preventing apoptosis of cardiomyocytes and supporting vascular nutrient supply?

Some characteristics of the used cellular source for the further investigated EVs would already favour them as therapeutic tool for treating CVDs. CardAP cells exhibited low expression levels of CD90 with at least 73% of $CD90^{neg.}$ cells (**Figure 12 and Table 9**). This unique feature of an otherwise mesenchymal-like phenotype might be valuable for their therapeutic usage, since the reduction of scar sizes after myocardial infarction was negatively correlated with CD90 expression of administrated CPCs [66]. In the present study, we showed that released EVs from CardAP cells also presented either no CD90 or just very low levels on their surface as determined by flow cytometry (**Figure 15**). For EVs from MSCs, Di Trapiani *et al.* documented also CD90 on their surface [130]. However, due to methodological differences (e.g. isolation, flow cytometry) it cannot be evaluated whether EVs from CardAP cells show lesser or comparable levels of CD90 than EVs from MSCs.

Also other surface proteins, which indicated beneficial effects for their intended therapeutic use, were assessed on EVs from CardAP cells by flow cytometry. One of them was CXCR4 (CD184), which was equally detected on unstimulated and cytokine stimulated EVs from CardAP cells (**Figure 15**). Interestingly, this chemokine receptor is capable of binding SDF-1α, which is an overexpressed factor in ischemic tissues [22]. Thus, the presence of CXCR4 on isolated EVs might be advantageous for their delivery towards ischemic cardiac tissue *in vivo*. In fact, it was shown by Ciullo *et al.* that the overexpression of CXCR4 by CPCs generated EVs with higher efficiency to interact with damaged cardiomyocytes *in vitro* than EVs from unmodified CPCs [126]. Moreover, these CXCR4 modified EVs reduced ischemia/reperfusion symptoms *in vivo* more sufficiently than their unmodified counterpart. Since apoptotic cells contribute significantly to the impairment of heart function [2], this plausible functional mechanism was also investigated in this study by measuring the impact of EVs derived from unmodified or modified CPCs on staurosporine induced apoptosis of HL-1 cells. In line with their *in vivo* observations, EVs derived from CXCR4-overexressing CPCs exhibited an even greater anti-apoptotic effect than EVs from unmodified CPCs. In the current study, we were also able to demonstrate anti-apoptotic effects of unstimulated and cytokine stimulated EVs from CardAP cells (**Figure 23**). In contrast to Ciullo *et al.*, three different triggers were tested

to induce apoptosis of HL-1 cells. On the one hand, HL-1 cells were starved to mimic the lacking nutrient supply caused by myocardial infarction, or they were treated with hydrogen peroxide to induce ROS formation. This scenario happens as consequence of bypass surgeries, which foster cells to perish in the boarder zones of the myocardial infarction by a sudden increase of oxygen and subsequently an increased formation of ROS [38,39]. Both starvation and ROS induced apoptosis were equally reduced in HL-1 cells treated with either unstimulated or cytokine stimulated EVs from CardAP cells. On the other hand, HL-1 cells were infected with CVB3, which is not only able to cause apoptosis but also severe myocarditis in humans [145]. It was already shown that CardAP cells are able to diminish CVB3 induced apoptosis *in vitro* and *in vivio* [13]. In the present work, we discovered that unstimulated but not cytokine stimulated EVs from CardAP cells are capable to significantly reduce caspase 3/7 activity (**Figure 23**). It seems likely that CXCR4 does not play a major role in reducing CVB3 induced apoptosis, since unstimulated and cytokine stimulated EVs exhibited similar protein levels on their surface and therefore are unlikely the reason for this discrepancy. Nevertheless, future experiments applying overexpression or knockdowns can elucidate whether the anti-apoptotic effect of ROS or starvation stimulated HL-1 cells are CXCR4 dependent. Other proteins identified in EVs from CardAP cells could also contribute to their anti-apoptotic effect. Heat shock proteins (HSP), namely HSP70 and HSP90, were identified in unstimulated as well as cytokine stimulated EVs from CardAP cells by LC/ESI-MS (***Appendix Table 1***). These two proteins have been shown to reduce the extrinsic apoptotic pathway of cells by different means, like promoting NF-κB activity, inhibition of pro-inflammatory cytokines or ROS-mediated apoptosis, including binding of apoptotic protease activating factor 1 (ARAF1) or other pro-apoptotic factors to inhibit the respective signalling function [146]. Additionally, not only proteins but also miRNAs transported by EVs can transmit anti-apoptotic signalling in recipient cells. As such, a recent study revealed that murine MSCs transfected with miR-320d generated EVs that were capable to diminish apoptosis in a STAT3-dependent manner [147]. Interestingly, in this study apoptosis was induced in mice via atrial fibrillation and the isolated murine cardiomyocytes were afterwards treated with EVs. In the present study, this particular miRNA was also found in EV preparations from CardAP cells, while being predominantly detected in cytokine stimulated than in unstimulated EVs (***Appendix Table 2***). But further investigations are needed to elucidate whether this miRNA-320d or other miRNAs play a role in the working mechanism of EVs from CardAP cells to reduce apoptosis. However, it seems unlikely to reduce their anti-apoptotic effect to a single transported molecule after several molecule classes were identified in isolated EVs from CardAP cells.

It could be argued that solely the detection of miRNAs in our isolated EVs is not enough evidence to proof their actual involvement in beneficial effects, since miRNAs need to be transferred into a recipient cell for influencing the transcription of proteins. In order to gather a better insight of EV-cell interaction, we established a novel methodology in EV research to define between uptake and surface interaction of EVs with cells. At first, we performed time series experiments with fluorescently labelled EVs (DiD^+ or $PKH26^+$ EVs). In accordance to previous studies [40,148,149], an interaction with recipient cells was visualized by tracking the fluorescence signal in recipient cells by flow cytometry (**Figure 20**) or microscopy (**Figure 21**). In addition, the signal of labelled EVs amplified in treated cells over time and reached a plateau

after one day. The corresponding dye control did not exhibit a likewise effect, which is very crucial due to the fact that dyes, such as the utilized PKH26, were shown to form vesicle-like compartments and subsequently can cause false positive signals [148]. We also observed that the interaction of EVs took place independently of the species of the recipient cell and with a comparable efficacy. In a second step, we conducted an interaction study of the isolated human EVs with murine cell lines to answer whether EVs have crossed the plasma membrane of the recipient cell. Therefore, common methods for intracellular staining of transcription factors and extracellular staining of surface proteins were used to measure after one day human proteins within or on murine cells, respectively. Due to the initial phenotypic EV characterization it was already known that unstimulated and cytokine stimulated EVs present certain proteins, such as CD63 (**Figure 15**). It was indeed possible to detect these EV-originating proteins rather within than on the surface of murine cells treated with EVs (**Figure 22**). These observations would advocate for an internalization of CardAP EVs, which consequently would allow the delivery of their transported miRNAs to their cellular site of action.

The intracellular uptake of isolated EVs from a human cardiac cell type does not appear to be limited to murine cells. This conclusion can be drawn from another investigated regenerative feature. In fact, unstimulated and cytokine stimulated EVs significantly enhanced *in vitro* tube formation capabilities of HUVECs by enhancing the release of different pro-angiogenic factors (**Figure 25 and 26**). One of the determined factors was VEGF, which was significantly enhanced by HUVECs treated with unstimulated EVs but not with cytokine stimulated EVs. Interestingly, unstimulated EVs were also observed to show significantly enriched miRNA 302d-3p levels compared to cytokine stimulated EVs by miRNA expression assay and qRT PCR (**Figure 18**). A study from Jiang *et al.* demonstrated that this precise miRNA possessed pro-angiogenic features [150]. Here, it was shown that HUVECs increased in response to miRNA 302d-3p their tube formation capabilities and release of VEGF, which could be abolished by siRNA and specific pathway inhibitors. In context of the current study, one could assume that the higher copy number of miRNA302d-3p in unstimulated EVs correlates to their induced amplified VEGF release by HUVECs. Subsequently, this would imply that EVs from CardAP cells and their transported miRNAs were indeed internalized by the influenced human endothelial cells.

Next to VEGF also IL-6 and IL-8 were investigated in the current study to elucidate the pro-angiogenic effect from CardAP EVs, because all three factors were already described to support angiogenesis as well as being involved in EV transmitted pro-angiogenic effects [95,151,152]. Unstimulated EVs from CardAP cells mediated not only a significant increased release of VEGF by HUVECs *in vitro* but also of IL-6 (**Figure 26**). In contrast, cytokine stimulated EVs induced a significantly enhanced release of IL-6, IL-8 and solely a trend of augmented VEGF release by HUVECs (**Figure 26**). The fact that HUVECs also tended to release more VEGF under the treatment with cytokine stimulated EVs would further implicate the involvement of their transported miRNA 302-3p. This miRNA was found to be present in cytokine stimulated EVs, however, to a significantly lower amount than in unstimulated EV preparations (**Figure 18**). It has to be addressed in future experiments whether the induction of different pro-angiogenic factors is related to the tendency of cytokine stimulated EVs to enhance tube formation abilities

of HUVECs to a lesser extent than unstimulated EVs. Up to now, it could only be shown in the current study that the supplementation with VEGF resulted in enhanced tube formation capabilities of HUVECs in comparable manners as EV treatment (**Figure 27**). In addition, it cannot be excluded that HUVECs released other angiogenesis influencing factors after treatment with EVs from CardAP cells. In that case it would be intersting to investigate known supporters of angiogenesis, such as the epidermal growth factor or the platelet-derived growth factor (PDGF) [95,153]. Nonetheless, it has not yet been shown that for differently derived EVs from either cardiac cells or MSCs induce the release of different pro-angiogenic factors by HUVECs or other endothelial cells.

It seems once more unlikely that a single molecule is exclusively accountable for this determined regenerative feature of EVs from CardAP cells. For instance, the miRNA repertoire impacting angiogenesis is not limited to miRNA 302-3p. Also, other candidates were determined in isolated EVs from CardAP cells, which included miRNA 146a-5p, 132-3p, 125a, 214, 126, and miRNA 210 (**Figure 18 and *Appendix Table 2***). These miRNAs were already shown by other groups to impact angiogenesis via different ways, such as increased VEGF release, expression of PDGF receptor, or suppressing GTPase activating proteins RASA1 [36,154–156]. Interestingly, a miRNA with inconsistent roles in angiogenesis, namely miRNA 494-3p, was observed to be enriched in cytokine stimulated EVs as determined by nCounter® miRNA expression assay and qPCR (**Figure 18**). It is not clear under which condition this miRNA enhances or inhibits angiogenesis [157,158]. Neither is clear what function the miRNA executes in isolated EVs from CardAP cells or whether it might be accountable for the inferior pro-angiogenic effect of cytokine stimulated EVs in comparison to unstimulated EVs. Beyond that, the angiogenesis supporting feature of CardAP EVs could also be facilitated by their transported proteins. One example is the tetraspanins CD63, which was detected on equally high levels on unstimulated and cytokine stimulated EVs by flow cytometry (**Figure 15**). Tugues *et al.* showed that the loss of CD63 expression in endothelial cells resulted in disturbed sprouting and tube structure formation during angiogenesis due to the missing promoting activity of CD63 to form complexes between VEGFR2 and Integrin ß1 [159]. It could be hypothesized that the uptake of CardAP EVs and their presented CD63 by HUVECs might be another plausible mechanism how an increased tube structures were induced. Although several other proteins, such as endoglin, neuropilin, Rab-13, or tenascin, to name just a few, in EVs from CardAP cells could be listed as proteins with angiogenesis supportive features as detected by LC/ESI-MS (***Appendix Table 1***), one particular protein attracted attention in the context of a regenerative approach using our isolated EVs. The carbohydrate-binding protein galectin 1 was confirmed to be equally present on unstimulated and cytokine stimulated EVs from CardAP cells as determined by flow cytometry as well as LC/ESI-MS (**Figure 15 and 16**). This protein does not only play a role in enhancing angiogenesis, migration, and growth but also in modulating immune responses [160–164]. An immune modulating feature would be a great benefit for a therapeutic approach, such as the application of allogenic EVs, to treat MI, heart failure or other CVDs involving a chronic inflammation [165]. This is reasoned by the fact that prolonged or chronic inflammation severely opposes the regenerative process in damaged cardiac tissue [27]. Hence, a reduced inflammatory milieu in the damaged cardiac tissue would subsequently increase the regenerative process and eventually also the cardiac function.

5.2.2 Could both isolated CardAP EVs enhance the cardiac function by modulating inflammatory immune responses?

In order to investigate this important feature for the intended allogenic approach, the interaction of EVs from CardAP cells with cells of the immune system and their impact on key immune responses was analysed in detail by different *in vitro* settings.

Indeed, a significantly reduced inflammatory immune response profile was observed for PBMCs treated with either unstimulated or cytokine stimulated EVs from CardAP cells when their T cell was engaged via the simultaneous application of anti-CD3. The main effects included next to reduced $CD4^+$ and $CD8^+$ T cell proliferation (**Figure 31**), increased frequencies of regulatory T cells (**Figure 32**), also reduced concentrations of pro-inflammatory cytokines, and enhanced concentrations of anti-inflammatory cytokines (**Figure 33**). Herein, cytokine stimulated EVs presented by trend a stronger attenuating effect on induced immune responses than their unstimulated counterpart. Furthermore, the immune modulating capability of EVs from CardAP cells does not seem to depend on the immune stimulating agent, since similar effects regarding cytokine profile and T cell proliferation have also been demonstrated in lectin stimulated PBMC cultures (***Appendix Figure 1***).

In general, it is controversially discussed how EVs from regenerative cells influence T cell proliferation in induced immune responses, since they were shown to diminishing or unchanged the induced proliferation [62,105,107,109,110,127,130,166]. Despite heterogeneities within studies, likr different EV isolation procedures, assay settings, or sources of immune cells, all studies documented lowered pro-inflammatory cytokine concentrations of at least one of the following cytokines: IFNγ, TNFα, IL-1β, or IL-17 [108,127,130,167]. In accordance, EVs from CardAP cells were also significantly reducing the concentration of IFNγ, TNFα and by trend also IL-1ß (**Figure 33**). Moreover, EV treatment resulted in significantly enhanced concentrations of active TGFß, while cytokine stimulated EVs also significantly accelerated another anti-inflammatory cytokine, namely IL-10, in those induced immune responses (**Figure 33**). Elevated IL-10 and TGFß concentrations are a well-described phenomenon in studies of stimulated immune cells treated with EVs from MSCs or glioma stem cells [108,110,166]. *In vivo* studies of CardAP cells itself documented that their application already enhanced IL-10 concentrations [60], which in light of the current study seems to be facilitated in a paracrine manner by their released EVs.

Furthermore, galectin 1 may play a crucial role in all these cumulative immune modulating observations. For example, Gieseke *et al.* revealed that otherwise immune modulating MSCs failed to reduce T cell proliferation or pro-inflammatory cytokine release in induced immune responses of PBMCs *in vitro* when their galectin-1 expression was abolished [164]. Moreover, the binding of galectin 1 to an early activation marker on T cells, namely CD69, was shown to initiate a signalling cascade that leads to the promotion of regulatory T cell development and reduced pro-inflammatory Th1/Th17 T cell activation as recently reviewed [168]. A likewise shift in the T helper cell population can be hypothesized for the treatment of stimulated PBMC cultures with EVs from CardAP cells. This is supported on the one hand by reduced pro-inflammatory cytokine concentrations, which may originate from pro-inflammatory Th1/Th17

population. On the other hand, it was possible to show significantly increased frequencies of regulatory T cells ($CD3^+$ $CD4^+$ $CD127^-$ $CD25^{++}$ $Foxp3^+$ cells) upon treatment with CardAP EVs (**Figure 32**). The increased levels of IL-10 and active TGF-ß in anti-CD3 stimulated PBMC cultures upon CardAP EV treatment already hinted towards a possible increase of regulatory T cells, because both cytokines are known to be highly expressed by this certain T cell subset [169,170]. The application of CardAP cells itself in an angiotensin II systolic heart failure model significantly increased the number of regulatory T cells [60]. Taking results from the current study into consideration, it seems plausible that CardAP cells facilitated this effect also in a paracrine manner. Nevertheless, it is not a novel observation that EVs from regenerative cells boost regulatory T cell frequencies in immune cell cultures, as several studies illustrated this feature for EVs from MSCs [108,127,167]. However, our present study demonstrated that $CD14^+$ immune cells are essential for the immune modulating feature of cardiac derived EVs.

$CD14^+$ cells were not only observed to be the major recipient of fluorescently labelled EVs from CardAP cells in unstimulated PBMC cultures (**Figure 34**), but also that their surface expression profile changed significantly after exposure to EVs. Those changes included the significant upregulation of CD14, PD-L1, CD206 as well as the significant downregulation of HLA-DR, CD86, and CD163 (**Figure 35**). Co-cultures of fluorescently labelled MSCs with PBMCs in a trans-well culture system already showed that $CD14^+$ cells are the main immune cell population that exhibited fluorescence signals of paracrine released factors from MSCs [130]. This observation was further corroborated by results from interaction analysis of isolated EVs from MSCs with PBMCs [108]. Moreover, studies from other groups presented similar changes of CD14 expressing monocytes or macrophages on protein or mRNA level of at least one of the above mentioned markers upon treatment with EVs from glioma stem cells [166] or MSCs [109,171]. IT for example includes the significantly increased CD206 expression on isolated macrophages upon treatment with EVs from MSCs [171]. Already the phagocytosis of MSCs shifted the monocyte phenotype towards a similar immune regulatory phenotype with higher mRNA expression levels for PD-L1 and CD206 [172]. Likewise, in a study by Dam *et al.* the co-culturing of human CPCs with monocytes led to a significantly reduced expression of HLA-DR and CD86 [70]. Although the findings on those two proteins match our observations, a contrarily decreased expression for CD206 on the surface of monocytes was determined. Whether this observation is a consequence of a direct cell-cell interaction needs further exploration. However, it seems likely in reflection to our results that CPCs preferentially use a paracrine mechanism to downregulate HLA-DR and CD86. Interestingly, the study from Dam *et al.* also observed that the down-regulation was facilitated independent of a IFNγ pre-treatment of CPCs [70], which is consistent with our results of isolated EVs from a different regenerative cardiac cell type. The so far described *in vitro* effects were also possible to be verified in *in vivo* models by the application of MSC EVs [171]. Here, markers characteristic for anti-inflammatory macrophages, referred to as M2-type macrophages, were increased after the treatment with MSC EVs in a murine cardio-toxin induced injury model. Furthermore, the enhanced regenerative potential of skeletal muscles was associated with the induction of those macrophages by MSC EVs.

In the present study, also the treatment of $CD14^+$ cells with either unstimulated or cytokine stimulated CardAP EVs induced a phenotype similar to anti-inflammatory macrophages. First of all, we did not hindered the differentiation of $CD14^+$ cells within unstimulated PBMC cultures towards macrophages, which was for example prevented by others via blocking the adherence of monocytes to the tissue culture plate [172]. Secondly, the changed expression of surface proteins would support evidence of an M2-type of the $CD14^+$ cells (**Figure 35**). In accordance to our flow cytometry results, other studies showed that M2-type macrophages significantly increased CD14 itself on mRNA level, significantly reduced the surface expression of HLA-DR and CD86, while expressing higher amounts of surface CD206 and PD-L1 [30,31,43,173,174]. In the current study, the scavenger receptor CD163 was found to be significantly reduced in its expression. This observation does not necessarily contradict an induction of M2-type macrophages by CardAP EVs, since this receptor is not restricted to this macrophage subset [175]. Thirdly, PBMC cultures demonstrated significantly elevated IL-10 concentrations when exposed to isolated CardAP EVs (**Figure 33**). This anti-inflammatory cytokine was shown to promote the polarization of M2-type macrophages and fibroblast activation *in vivo* [29]. Moreover, a rather anti-inflammatory environment is illustrated when taking into account that pro-inflammatory cytokines, such as IFNy, were not detectable in these immune cell cultures. Further evidence for a provoked M2-type macrophage type is provided by the treatment of purified $CD14^+$ cells with isolated CardAP EVs. Although IL-10 was not detectable under a shorter treatment period, a significantly enhanced release of IL-1RA (**Figure 38**) and a likewise phenotypical change (***Appendix Figure 2***) was determined for cultures of purified $CD14^+$ cells treated with CardAP EVs. The immunosuppressive molecule IL-1RA is described to be used by M2-type macrophages itself [30] as well as by MSCs to polarize macrophages towards this macrophage type [176]. Overall, it would be advantageous for a potential therapeutic approach of CardAP EVs to facilitate a M2-type polarization, because these macrophages not only secrete anti-inflammatory cytokines and chemokines but also growth factors [177]. Moreover, it was shown that these macrophages and their released factors enhanced the myocardial repair including via resolved inflammation [28,29,178,179]. Despite of all these beneficial effects, further studies must be conducted to clarify the extent to which they have the potential to induce unwanted fibrosis. As such, it was shown for $CD206^+$ macrophages to promote fibrosis [180], which can have detrimental effects on the heart function by enhanced stiffness of the tissue [45].

This raises the question how CardAP EVs facilitated the M2-type macrophage polarization. Again, the identified galectin-1 on CardAP EVs may play a role, as monocytes or macrophages significantly diminished HLA-DR expression, diminished their NO and IL-6 release, and increased arginase release even in the presence of IFNγ stimulation when the medium was supplemented with galectin-1 [181,182]. In order to investigate whether galectin-1 transported by CardAP EVs contribute to the changes of $CD14^+$ cells, competitive binding assays were performed by supplementing the culture medium with thiodigalactoside (TDG). It was already shown that the binding of TDG to galectin-1 supresses its feature in tumor progression or in the fat metabolism of adipocytes in vivo [183,184]. Although the expression of HLA-DR could be restored and even elevated in $CD14^+$ cells treated with CardAP EVs by TDG addition, it cannot be concluded that galectin-1 inhibition was the trigger (***Appendix Figure 2***). This is

reasoned by the fact that already the treatment with TDG and its vehicle solution (here DMSO) increased the expression of HLA-DR on $CD14^+$ cells. Likewise, CD206 was upregulated on $CD14^+$ cells treated with CardAP EVs, however, the supplementation of TDG or DMSO alone showed already on its own an induction of this particular protein. Future experiments hopefully can overcome this issue, for example, by separating galectin-1 positive and negative EVs via affinity purification or by performing similar assays with the recent published DNA aptomere inhibitor for galectin-1 [185] .

It can be speculated that also other transported proteins are involved in priming M2-type macrophages by CardAP EVs, like annexin 1 that was identified by LC/ESI-MS. This particular member of the annexin family has been shown to enable a polarization towards M2-type macrophages [186,187]. The tetraspanins transported by EVs from CardAP cells could own a probable role, since they are involved in antigen-presentation and internalization of HLA-DR [188]. EVs derived from melanoma or glioblastoma stem cells demonstrated an upregulation of PD-L1 on macrophages or immature myeloid cells via phosphorylated STAT3 that was already transported by the EVs or in a TLR4 dependent manner [174]. Once more, next to proteins also different miRNAs were described to contribute to the process of macrophage polarization [43]. Different studies showed that M2-type macrophages upregulate miRNA 146a, miRNA 132, miRNA 342-3p and miRNA 494 [189–191]. Interestingly, these miRNAs were also found in isolated CardAP EVs at comparable or for miRNA 494 at significantly increased levels in cytokine stimulated EVs as determined by miRNA expression assay and qRT-PCR (**Figure 18**). It could be hypothesized that the delivery of those transported miRNAs by CardAP EVs to $CD14^+$ cells affects their polarization. EVs from MSCs and CPCs were also shown to transport diverse miRNAs including miRNA 146a [103,110,154,156,192]. The spectrum of transported miRNAs is not limited to affect monocytes, as such, miRNA 29a/b, which both were identified in CardAP EVs (***Appendix Table 2***), were shown to target T-bet, Eomes and IFNγ in T cells that subsequently suppressed the polarization towards the T cell subset of Th1 cells [193]. Although CardAP EVs were found to interact predominantly with $CD14^+$ cells, an inferior interaction with T cells was detected (***Appendix Figure 4***). Thus, it appears plausible that miRNA could be transferred to T cells and thereby affecting this cell population directly.

The consequences of $CD14^+$ cell priming by CardAP EVs for induced T cell responses was investigated in the current study by an adaptation of the performed *in vitro* immunomodulation assay that used purified $CD14^+$ and $CD3^+$ cells instead of complete PBMCs. Anti-CD3 stimulated monocultures of purified T cells failed to replicate the immune modulating effects under CardAP EV treatment as neither T cell proliferation (**Figure 36**) nor cytokine release (**Figure 37**) were affected. However, the immune modulating features of EVs were restored when anti-CD3 stimulated T cells were co-cultured with CardAP EV primed $CD14^+$ cells. It included reduced $CD4^+$ and $CD8^+$ T cell proliferation (**Figure 36**) as well as reduced pro-inflammatory cytokines (**Figure 37**). Cosenza et al. noted for murine MSC EVs a likewise effect in PBMCand purified T cell cultures [107]. Although no EV-cell interaction assays were conducted in this study, we could hypothesize that the missing T cell proliferation mediation by EVs from MSCs in purified T cell cultures is linked to the absence of $CD14^+$ cells as major immune modulator of EVs. Murine melanoma EVs were recently shown to upregulate PD-L1

on mouse immature myeloid cells [194]. Interestingly, this upregulation was shown to contribute significantly to reduced $CD8^+$ T cell proliferation in anti-CD3/anti-CD28 stimulated co-cultures of purified $CD8^+$ T cells with primed immature myeloid cells. Also we observed a significant increased expression of PD-L1 on the surface of $CD14^+$ cells treated with unstimulated and cytokine stimulated EVs from CardAP cells (**Figure 35**), which might be contributed to the observed reduced T cell proliferation in both PBMC cultures as well as in co-cultures of primed $CD14^+$ cells with purified T cells. It is well-known that the binding of PD-L1 with the corresponding receptor PD-1 on T cells mediates the suppression of T cell proliferation and induction of apoptosis [195]. Although we were not able to detect PD-L1 on isolated CardAP EVs, it was indeed shown that EVs of MSCs present this molecule on their surface with a supposed function in immunomodulation [163]. Furthermore, the downregulation of HLA-DR and CD86 would impair the antigen-presenting features of monocytes/macrophages within co-cultures with T cells or in complete PBMC cultures. Additionally, the suppression of immune responses might be mediated by primed $CD14^+$ cells in a paracrine manner, which includes next to cytokines and chemokines also EVs released by the immune cell itself that interact with the other immune cell subsets [97]. In the current study, we were able to show that primed $CD14^+$ cells elevated the concentrations of IL-1RA (**Figure 38**). Beside several other functions, this receptor antagonist has been also shown to induce regulatory T cell development [196]. Indeed, we were able to observe higher frequencies of regulatory T cells not only in PBMC cultures treated with CardAP EVs but also in cultures with EV primed monocytes cultivated with isolated T cells (**Figure 38**). This enhanced frequency appeared to be independent of accelerated IL-10 concentrations as this cytokine could not be detected in primed monocyte cultures and IL-10 was significantly reduced in co-cultures of T cells with $CD14^+$ cells that were primed with cytokine stimulated EVs from CardAP cells (**Figure 37**). One study already proposed a monocyte-dependent mechanism how MSC EVs induce regulatory T cell proliferation/frequencies [167], which we could verify for EVs from cardiac mesenchymal-like cells.

Overall, it seems like unstimulated as well as cytokine stimulated EVs from CardAP cells are potent immune modulators of inflammatory immune responses by promoting an anti-inflammatory phenotype of $CD14^+$ cells. For that reason it seems plausible that CardAP EVs can contribute to an enhanced regenerative process in damaged and chronic inflamed cardiac tissue.

5.2.3 Would an allogenic approach be feasible for the isolated CardAP EVs?

After several therapeutically valuable features were identified to be facilitated by isolated CardAP EVs, it remained to be answered whether they would be suitable for an allogenic approach. Already, CardAP cells itself indicated their usage as an allogenic therapeutic tool by their low immunogenicity. This was indicated by the absent surface expression of HLA-DR, which persists even after a three-day exposure to the pro-inflammatory cytokine cocktail of IFNγ, TNFα and IL-1β (data not shown). Indeed, this low immunogenic phenotype was preserved for their released EVs. Unstimulated as well as cytokine stimulated EVs showed very low levels of HLA-ABC and a complete absence of HLA-DR and other HLA molecules as

analysed by flow cytometry (**Figure 15**) or LC/ESI-MS (***Appendix Table 1***). Moreover, the *in vitro* exposure of EVs from different CardAP donors to diverse PBMC donors did not cause any pro-inflammatory immune response. Neither unstimulated nor cytokine stimulated CardAP EVs provoked the proliferation of $CD4^+$ or $CD8^+$ T cells in otherwise unstimulated PBMC cultures (**Figure 28**), which would strengthen the proof of a low immunogenicity of CardAP EVs. In accordance to our observation, also no induction of T cell proliferation was observed for EVs from MSCs in mouse spleenocyte cultures [167] nor in human PBMC cultures exposed to EVs from amniotic fluid stem cells [197]. Additionally, we investigated $CD4^+$ T cells for changes of early (CD69), immediate (CD25) and late (HLA-DR) activation markers upon CardAP EV treatment. Indeed, neither unstimulated nor cytokine stimulated EVs from CardAP cells induced $CD4^+$ T cell activation as no marker was altered in its expression level (**Figure 29**). The absence of T cell activation additionally supports the lack of an adverse immune reaction towards allogenic EVs. Interestingly, the treatment of unstimulated PBMCs with CardAP EVs was accompanied by a significant enhanced frequency of $CD4^+$ $CD25^+$ $CD62L^+$ cells (**Figure 30**). Earlier studies termed this subset "regulatory T cells" and demonstrated their immune modulating capacities by enhanced protection from severe graft versus host disease [198–200]. Further evidence for a safe use of CardAP EVs is indicated by the observation that the pro-inflammatory cytokine IFNγ could not be detected in neither unstimulated nor cytokine stimulated EV treated PBMC or purified $CD14^+$ cultures. In contrast, anti-inflammatory molecules, such as IL-10 or IL-1RA, were determined in these cultures (**Figure 29 and 38**). Interestingly, higher frequencies of $CD14^+$ cells were observed in PBMC cultures treated with EVs after five days (**Figure 35**). This is especially surprising when taking into account that IL-10 concentrations were upregulated in those cultures. Normally IL-10 secretion triggers apoptosis of the secreting monocyte [201]. We hypothesize that the galectin 1 transported by EVs from CardAP cells abolishes the IL-10 induced apoptosis, as reports documented the anti-apoptotic feature of galectin-1 in this scenario *in vitro* [202]. So far, no information is available whether allogenic EVs from regenerative cells induce adverse effects *in vivo*. In initial experiments, we have not observed adverse effects in the application of two different concentrations of CardAP EVs to C57black/6 mice. The treated mice did not lose weight nor did their cardiac tissue exhibit elevated mRNA expression levels for pro-inflammatory cytokines or fibrotic markers (***Appendix Figure 3***). Thus, it seems as if CardAP EVs do not provoke an adverse immune reaction *in vitro* and *in vivo,* which would subsequently support an allogenic therapeutic approach.

5.3 Summary & Outlook

In conclusion, we could demonstrate that unstimulated as well as cytokine stimulated EVs from CardAP cells exhibit a low immunogenicity, are *in vitro* capable to modulate inflammatory immune responses, diminish apoptosis and enhance angiogenesis. This combination of features would enable their future safe usage in allogenic therapies for the treatment of cardiac diseases, such as myocardial infarct or heart failure. Moreover, their capability to derive a pro-regenerative phenotype of $CD14^+$ cells as well as to enhance regulatory T cells could be valuable for the treatment of adverse immune processes. However, it needs to be further elucidated when a therapy is contraindicated. For example, do EVs have beneficial or tremendous effect for co-morbidities of CVDs? What happens when the patient is suffering from an infection with

pathogens or cancer? Should it be avoided since the induced anti-inflammatory milieu contributes to the survival of pathogens or tumours due to a reduced immune defence? Only future experiments in different animal disease models will provide the final conclusion on whether clinical trials with CardAP EVs should be advanced and under which circumstances it would be contraindicated. Furthermore, potent targets, such as galectin 1, CXCR4, miRNA 302d-3p, and others, were identified to play a major role in the induced beneficial effects by our current and other studies. A prospect advanced approach could probably enhance efficacy by selecting and enhancing those targets either via modifications of the cellular source or via adapted purification of EVs, e.g. positive negative selection for surface proteins. Moreover, new targets could be identified in isolated EVs from CardAP cells by evaluating other transported molecules, such as lipids, mRNA, growth factors, or chemokines, which were so far neglected in the current study. A methodological change in the isolation procedure would enhance the knowledge whether small EVs or their co-isolated proteins are the driving force for each beneficial effect. It seems likely that at least the immune modulating feature might be caused by the small EVs, since a recent study observed this feature for small EVs but not for their co-isolated proteins [203]. However, the field of corona proteins will also gain more attention in the future of EV research, because the protein corona of synthesized particles has been observed to influence the efficiency as well as the delivery to target cells [135,136]. A targeted and sufficient delivery of EVs to the desired recipient cells might solve different obstacles in EV research. As such, it could help to overcome the need of great amounts of isolated EVs for therapeutic approaches, especially allogenic ones, in humans.

In order to further characterize the functional effects of CardAP EVs, it would be interesting to elucidate whether they can affect tissue resident immune cells or so far neglected immune cell subsets, such as natural killer cells or eosinophils. A side by side comparison with EVs from CardAP cells and MSCs could deliver valuable information whether similar or different pathways are used to achieve the same beneficial effects. These results could probably enrich the repertoire of potent target molecules transported by EVs. Additionally, the application of different conditions during the EV biogenesis would be a promising future experiment. In the current study, we solely investigated the impact of an inflammatory milieu on released cardiac EVs. Other scenarios could for example include the reduction of oxygen. EVs from MSCs showed an even greater pro-angiogenic feature than their normoxic counterpart [115], which we could also demonstrate for EVs from another cardiac cell type (unpulished data). Current and future studies on EVs from regenerative cells will help to uncover their therapeutic potential and thus overcome the consequences of the pandemic of cardiovascular diseases.

6. List of references

1. Haddad, F.; Berry, G.; Doyle, R.L.; Martineau, P.; Leung, T.K.; Racine, N. Active Bacterial Myocarditis: A Case Report and Review of the Literature. *J. Hear. Lung Transplant.* **2007**, *26*, 745–749.
2. Reed, G.W.; Rossi, J.E.; Cannon, C.P. Acute myocardial infarction. *Lancet* 2017, *389*, 197–210.
3. Van Linthout, S.; Stamm, C.; Schultheiss, H.-P.; Tschöpe, C. Mesenchymal stem cells and inflammatory cardiomyopathy: cardiac homing and beyond. *Cardiol. Res. Pract.* **2011**, *2011*, 757154.
4. Leong, Y.Y.; Ng, W.H.; Ellison-Hughes, G.M.; Tan, J.J. Cardiac Stem Cells for Myocardial Regeneration: They Are Not Alone. *Front. Cardiovasc. Med.* **2017**, *4*.
5. Statistiken zur Organspende für Deutschland und Europa Available online: https://www.organspende-info.de/zahlen-und-fakten/statistiken.html (accessed on Aug 23, 2020).
6. World Health Organization *World Health Statistics 2018: Monitoring Health for the SDGs. Sustainable development goals.*; 1st ed.; Geneva, 2018; ISBN 9789241565585.
7. Mathers, C.D.; Loncar, D. Projections of Global Mortality and Burden of Disease from 2002 to 2030. *PLoS Med.* **2006**, *3*, e442.
8. Bloom, D.E.; Cafiero, E.; Jané-Llopis, E.; Abrahams-Gessel, S.; Bloom, L.R.; Fathima, S.; Feigl, A.B.; Gaziano, T.; Hamandi, A.; Mowafi, M.; et al. *The Global Economic Burden of Noncommunicable Diseases*; 2011;
9. Schneider, M.; Stamm, C.; Brockbank, K.G.M.; Stock, U.A.; Seifert, M. The choice of cryopreservation method affects immune compatibility of human cardiovascular matrices. *Sci. Rep.* **2017**, *7*, 1–14.
10. Becker, M.; Maring, J.A.; Schneider, M.; Martin, A.X.H.; Seifert, M.; Klein, O.; Braun, T.; Falk, V.; Stamm, C. Towards a novel patch material for cardiac applications: Tissue-specific extracellular matrix introduces essential key features to decellularized amniotic membrane. *Int. J. Mol. Sci.* **2018**, *19*, 1032.
11. Madonna, R.; Van Laake, L.W.; Botker, H.E.; Davidson, S.M.; De Caterina, R.; Engel, F.B.; Eschenhagen, T.; Fernandez-Aviles, F.; Hausenloy, D.J.; Hulot, J.S.; et al. ESC working group on cellular biology of the heart: Position paper for Cardiovascular Research: Tissue engineering strategies combined with cell therapies for cardiac repair in ischaemic heart disease and heart failure. *Cardiovasc. Res.* 2019, *115*, 488–500.
12. Ke, N.; Pi, L.H.; Liu, Q.; Chen, L. Long noncoding RNA SNHG7 inhibits high glucose-induced human retinal endothelial cells angiogenesis by regulating miR-543/SIRT1 axis. *Biochem. Biophys. Res. Commun.* **2019**, *514*, 503–509.
13. Miteva, K.; Haag, M.; Peng, J.; Savvatis, K.; Becher, P.M.; Seifert, M.; Warstat, K.; Westermann, D.; Ringe, J.; Sittinger, M.; et al. Human cardiac-derived adherent proliferating cells reduce murine acute coxsackievirus B3-induced myocarditis. *PLoS One* **2011**, *6*, (article e28513)1-16.
14. Montanari, S.; Dayan, V.; Yannarelli, G.; Billia, F.; Viswanathan, S.; Connelly, K.A.; Keating, A. Mesenchymal stromal cells improve cardiac function and left ventricular remodeling in a heart transplantation model. *J. Hear. Lung Transplant.* **2015**, *34*, 1481–1488.
15. Martin-Rendon, E.; Gyöngyösi, M. Mesenchymal stromal cell therapy as treatment for ischemic heart failure: the MSC-HF study. *Cardiovasc. Diagn. Ther.* **2017**, *7*, S69–S72.
16. Malliaras, K.; Li, T.S.; Luthringer, D.; Terrovitis, J.; Cheng, K.; Chakravarty, T.; Galang, G.; Zhang, Y.; Schoenhoff, F.; Van Eyk, J.; et al. Safety and efficacy of allogeneic cell therapy in infarcted rats transplanted with mismatched cardiosphere-derived cells. *Circulation* **2012**, *125*, 100–112.
17. Minicucci, M.F.; Azevedo, P.S.; Polegato, B.F.; Paiva, S.A.R.; Zornoff, L.A.M. Heart Failure After Myocardial Infarction: Clinical Implications and Treatment. *Clin. Cardiol.* **2011**, *34*, 410–414.
18. Cheng, W.; Kajstura, J.; Nitahara, J.A.; Li, B.; Reiss, K.; Liu, Y.; Clark, W.A.; Krajewski, S.; Reed, J.C.; Olivetti, G.; et al. Programmed myocyte cell death affects the viable myocardium after infarction in rats. *Exp. Cell Res.* **1996**, *226*, 316–327.

19. Humeres, C.; Frangogiannis, N.G. Fibroblasts in the Infarcted, Remodeling, and Failing Heart. *JACC Basic to Transl. Sci.* 2019, *4*, 449–467.
20. Yan, X.; Anzai, A.; Katsumata, Y.; Matsuhashi, T.; Ito, K.; Endo, J.; Yamamoto, T.; Takeshima, A.; Shinmura, K.; Shen, W.; et al. Temporal dynamics of cardiac immune cell accumulation following acute myocardial infarction. *J. Mol. Cell. Cardiol.* **2013**, *62*, 24–35.
21. Li, X.; Ren, Y.; Sorokin, V.; Poh, K.K.; Ho, H.H.; Lee, C.N.; de Kleijn, D.; Lim, S.K.; Tam, J.P.; Sze, S.K. Quantitative profiling of the rat heart myoblast secretome reveals differential responses to hypoxia and re-oxygenation stress. *J. Proteomics* **2014**, *98*, 138–149.
22. Hu, X.; Dai, S.; Wu, W.J.; Tan, W.; Zhu, X.; Mu, J.; Guo, Y.; Bolli, R.; Rokosh, G. Stromal cell-derived factor-1α confers protection against myocardial ischemia/reperfusion injury: Role of the cardiac stromal cell-derived factor-1α-CXCR4 axis. *Circulation* **2007**, *116*, 654–663.
23. Westermann, D.; Savvatis, K.; Schultheiss, H.P.; Tschöpe, C. Immunomodulation and matrix metalloproteinases in viral myocarditis. *J. Mol. Cell. Cardiol.* 2010, *48*, 468–473.
24. Gwechenberger, M.; Mendoza, L.H.; Youker, K.A.; Frangogiannis, N.G.; Wayne Smith, C.; Michael, L.H.; Entman, M.L. Cardiac myocytes produce interleukin-6 in culture and in viable border zone of reperfused infarctions. *Circulation* **1999**, *99*, 546–551.
25. Ono, K.; Matsumori, A.; Shioi, T.; Furukawa, Y.; Sasayama, S. Cytokine Gene Expression After Myocardial Infarction in Rat Hearts. *Circulation* **1998**, *98*, 149–156.
26. Ong, S.B.; Hernández-Reséndiz, S.; Crespo-Avilan, G.E.; Mukhametshina, R.T.; Kwek, X.Y.; Cabrera-Fuentes, H.A.; Hausenloy, D.J. Inflammation following acute myocardial infarction: Multiple players, dynamic roles, and novel therapeutic opportunities. *Pharmacol. Ther.* 2018, *186*, 73–87.
27. de Lemos, J.A.; Morrow, D.A.; Blazing, M.A.; Jarolim, P.; Wiviott, S.D.; Sabatine, M.S.; Califf, R.M.; Braunwald, E. Serial Measurement of Monocyte Chemoattractant Protein-1 After Acute Coronary Syndromes: Results From the A to Z Trial. *J. Am. Coll. Cardiol.* **2007**, *50*, 2117–2124.
28. ter Horst, E.N.; Hakimzadeh, N.; van der Laan, A.M.; Krijnen, P.A.J.; Niessen, H.W.M.; Piek, J.J. Modulators of Macrophage Polarization Influence Healing of the Infarcted Myocardium. *Int. J. Mol. Sci.* **2015**, *16*, 29583–29591.
29. Jung, M.; Ma, Y.; Iyer, R.P.; DeLeon-Pennell, K.Y.; Yabluchanskiy, A.; Garrett, M.R.; Lindsey, M.L. IL-10 improves cardiac remodeling after myocardial infarction by stimulating M2 macrophage polarization and fibroblast activation. *Basic Res. Cardiol.* **2017**, *112*, 1–14.
30. Shapouri-Moghaddam, A.; Mohammadian, S.; Vazini, H.; Taghadosi, M.; Esmaeili, S.A.; Mardani, F.; Seifi, B.; Mohammadi, A.; Afshari, J.T.; Sahebkar, A. Macrophage plasticity, polarization, and function in health and disease. *J. Cell. Physiol.* 2018, *233*, 6425–6440.
31. Mantovani, A.; Biswas, S.K.; Galdiero, M.R.; Sica, A.; Locati, M. Macrophage plasticity and polarization in tissue repair and remodelling. *J. Pathol.* **2013**, *229*, 176–185.
32. Kimura, W.; Xiao, F.; Canseco, D.C.; Muralidhar, S.; Thet, S.; Zhang, H.M.; Abderrahman, Y.; Chen, R.; Garcia, J.A.; Shelton, J.M.; et al. Hypoxia fate mapping identifies cycling cardiomyocytes in the adult heart. *Nature* **2015**, *523*, 226–230.
33. Bergmann, O.; Bhardwaj, R.D.; Bernard, S.; Zdunek, S.; Barnabé-Heide, F.; Walsh, S.; Zupicich, J.; Alkass, K.; Buchholz, B.A.; Druid, H.; et al. Evidence for cardiomyocyte renewal in humans. *Science (80-.).* **2009**, *324*, 98–102.
34. Wang, L.; Meier, E.M.; Tian, S.; Lei, I.; Liu, L.; Xian, S.; Lam, M.T.; Wang, Z. Transplantation of Isl1+ cardiac progenitor cells in small intestinal submucosa improves infarcted heart function. *Stem Cell Res. Ther.* **2017**, *8*, 230.
35. Hu, G.; Ma, L.; Dong, F.; Hu, X.; Liu, S.; Sun, H. Inhibition of microRNA-124-3p protects against acute myocardial infarction by suppressing the apoptosis of cardiomyocytes. *Mol. Med. Rep.* **2019**, *20*, 3379–3387.
36. Emanueli, C.; Shearn, A.I.U.; Angelini, G.D.; Sahoo, S. Exosomes and exosomal miRNAs in cardiovascular protection and repair. *Vascul. Pharmacol.* 2015, *71*, 24–30.
37. Xiao, J.; Pan, Y.; Li, X.H.; Yang, X.Y.; Feng, Y.L.; Tan, H.H.; Jiang, L.; Feng, J.; Yu, X.Y. Cardiac progenitor cell-derived exosomes prevent cardiomyocytes apoptosis through exosomal miR-21 by targeting PDCD4. *Cell Death Dis.* **2016**, *7*, e2277.
38. Yellon, D.M.; Hausenloy, D.J. Myocardial reperfusion injury. *N. Engl. J. Med.* 2007, *357*, 1121.

39. Bolli, R.; Jeroudi, M.O.; Patel, B.S.; DuBose, C.M.; Lai, E.K.; Roberts, R.; McCay, P.B. Direct evidence that oxygen-derived free radicals contribute to postischemic myocardial dysfunction in the intact dog. *Proc. Natl. Acad. Sci. U. S. A.* **1989**, *86*, 4695–4699.
40. Chen, L.; Wang, Y.; Pan, Y.; Zhang, L.; Shen, C.; Qin, G.; Ashraf, M.; Weintraub, N.; Ma, G.; Tang, Y. Cardiac progenitor-derived exosomes protect ischemic myocardium from acute ischemia/reperfusion injury. *Biochem. Biophys. Res. Commun.* **2013**, *431*, 566–71.
41. Honan, M.B.; Harrell, F.E.; Reimer, K.A.; Califf, R.M.; Mark, D.B.; Pryor, D.B.; Hlatky, M.A. Cardiac rupture, mortality and the timing of thrombolytic therapy: A meta-analysis. *J. Am. Coll. Cardiol.* **1990**, *16*, 359–367.
42. Hanifi, N.; Rezaee, E.; Rohani, M. Time-to-Treatment and Its Association With Complications and Mortality Rate in Patients With Acute Myocardial Infarction: A Prospective Cohort Study. *J. Emerg. Nurs.* **2020**.
43. Wang, N.; Liang, H.; Zen, K. Molecular mechanisms that influence the macrophage M1-M2 polarization balance. *Front. Immunol.* 2014, *5*, 614.
44. Shiraishi, M.; Shintani, Y.; Shintani, Y.; Ishida, H.; Saba, R.; Yamaguchi, A.; Adachi, H.; Yashiro, K.; Suzuki, K. Alternatively activated macrophages determine repair of the infarcted adult murine heart. *J. Clin. Invest.* **2016**, *126*, 2151–2166.
45. Tschöpe, C.; Van Linthout, S. New Insights in (Inter)Cellular Mechanisms by Heart Failure with Preserved Ejection Fraction. *Curr. Heart Fail. Rep.* 2014, *11*, 436–444.
46. Rienks, M.; Papageorgiou, A.P. Novel regulators of cardiac inflammation: Matricellular proteins expand their repertoire. *J. Mol. Cell. Cardiol.* 2016, *91*, 172–178.
47. MM, L.; L, M.; C, P.; D, F.; BW, W.; JC, M.; J, G.; DJ, S. Safety of cell therapy with mesenchymal stromal cells (SafeCell): a systematic review and meta-analysis of clinical trials. *PLoS One* **2012**, *7*.
48. Berglund, A.K.; Fortier, L.A.; Antczak, D.F.; Schnabel, L. V. Immunoprivileged no more: Measuring the immunogenicity of allogeneic adult mesenchymal stem cells. *Stem Cell Res. Ther.* 2017, *8*.
49. Hoogduijn, M.J.; Dor, F.J.M.F. Mesenchymal stem cells: Are we ready for clinical application in transplantation and tissue regeneration? *Front. Immunol.* **2013**, *4*, 1–2.
50. Jin, H.; Bae, Y.; Kim, M.; Kwon, S.-J.; Jeon, H.; Choi, S.; Kim, S.; Yang, Y.; Oh, W.; Chang, J. Comparative Analysis of Human Mesenchymal Stem Cells from Bone Marrow, Adipose Tissue, and Umbilical Cord Blood as Sources of Cell Therapy. *Int. J. Mol. Sci.* **2013**, *14*, 17986–18001.
51. Denton, M.D.; Geehan, C.S.; Alexander, S.I.; Sayegh, M.H.; Briscoe, D.M. Endothelial cells modify the costimulatory capacity of transmigrating leukocytes and promote CD28-mediated CD4+ T cell alloactivation. *J. Exp. Med.* **1999**, *190*, 555–566.
52. Ingulli, E. Mechanism of cellular rejection in transplantation. *Pediatr. Nephrol.* 2010, *25*, 61–74.
53. Auchincloss, H.; Lee, R.; Shea, S.; Markowitz, J.S.; Grusby, M.J.; Glimcher, L.H. The role of "indirect" recognition in initiating rejection of skin grafts from major histocompatibility complex class II-deficient mice. *Proc. Natl. Acad. Sci. U. S. A.* **1993**, *90*, 3373–3377.
54. Wang, P.; Liu, Z.; Wu, C.; Zhu, B.; Wang, Y.; Xu, H. Evaluation of CD86/CD28 and CD40/CD154 Pathways in Regulating Monocyte-Derived CD80 Expression During Their Interaction With Allogeneic Endothelium. *Transplant. Proc.* **2008**, *40*, 2729–2733.
55. Reddy, M.; Eirikis, E.; Davis, C.; Davis, H.M.; Prabhakar, U. Comparative analysis of lymphocyte activation marker expression and cytokine secretion profile in stimulated human peripheral blood mononuclear cell cultures: An in vitro model to monitor cellular immune function. *J. Immunol. Methods* **2004**, *293*, 127–142.
56. Friedenstein, A.J.; Chailakhjan, R.K.; Lalykina, K.S. THE DEVELOPMENT OF FIBROBLAST COLONIES IN MONOLAYER CULTURES OF GUINEA-PIG BONE MARROW AND SPLEEN CELLS. *Cell Prolif.* **1970**, *3*, 393–403.
57. Caplan, A.I. Mesenchymal stem cells: Time to change the name! *Stem Cells Transl. Med.* **2017**, *6*, 1445–1451.
58. Mummery, C.; Ward-van Oostwaard, D.; Doevendans, P.; Spijker, R.; Van den Brink, S.; Hassink, R.; Van der Heyden, M.; Opthof, T.; Pera, M.; Brutel de la Riviere, A.; et al. Differentiation of human embryonic stem cells to cardiomyocytes: Role of coculture with visceral endoderm-like cells. *Circulation* **2003**, *107*, 2733–2740.

59. Detert, S.; Stamm, C.; Beez, C.; Diedrichs, F.; Ringe, J.; Van Linthout, S.; Seifert, M.; Tschöpe, C.; Sittinger, M.; Haag, M. The atrial appendage as a suitable source to generate cardiac-derived adherent proliferating cells for regenerative cell-based therapies. *J. Tissue Eng. Regen. Med.* **2018**, *12*, e1404–e1417.
60. Miteva, K.; Van Linthout, S.; Pappritz, K.; Müller, I.; Spillmann, F.; Haag, M.; Stachelscheid, H.; Ringe, J.; Sittinger, M.; Tschöpe, C. Human Endomyocardial Biopsy Specimen-Derived Stromal Cells Modulate Angiotensin II-Induced Cardiac Remodeling. *Stem Cells Transl. Med.* **2016**, *5*, 1707–1718.
61. Makkar, R.R.; Demaria, A.; Traverse, J.H.; Marbán, L.; Pogoda, J.M.; Henry, T.D.; Lima, J.A.; Smith, R.R.; Schatz, R.; Francis, G.S.; et al. ALLogeneic Heart STem Cells to Achieve Myocardial Regeneration (ALLSTAR) Trial: Rationale and Design. *Cell Transplant.* **2016**, *26*, 205–214.
62. van den Akker, F.; Vrijsen, K.R.; Deddens, J.C.; Buikema, J.W.; Mokry, M.; van Laake, L.W.; Doevendans, P.A.; Sluijter, J.P.G. Suppression of T cells by mesenchymal and cardiac progenitor cells is partly mediated via extracellular vesicles. *Heliyon* **2018**, *4*, e00642.
63. Wang, M.; Yu, Q.; Wang, L.; Gu, H. Distinct patterns of histone modifications at cardiac-specific gene promoters between cardiac stem cells and mesenchymal stem cells. *Am. J. Physiol. Physiol.* **2013**, *304*, C1080–C1090.
64. Haag, M.; Ritterhoff, J.; Dimura, A.; Miteva, K.; Van Linthout, S.; Tschöpe, C.; Ringe, J.; Sittinger, M. Pro-Angiogenic Effect of Endomyocardial Biopsy-Derived Cells for Cardiac Regeneration. *Curr. Tissue Eng.* **2013**, *2*, 154–159.
65. Haag, M.; Stolk, M.; Ringe, J.; Linthout, S. Van; Tschöpe, C.; Sittinger, M.; Seifert, M. Immune attributes of cardiac-derived adherent proliferating (CAP) cells in cardiac therapy. *J. Tissue Eng. Regen. Med.* **2013**, *7*, 362–370.
66. Cheng, K.; Ibrahim, A.; Hensley, M.T.; Shen, D.; Sun, B.; Middleton, R.; Liu, W.; Smith, R.R.; Marban, E. Relative Roles of CD90 and c-Kit to the Regenerative Efficacy of Cardiosphere-Derived Cells in Humans and in a Mouse Model of Myocardial Infarction. *J. Am. Heart Assoc.* **2014**, *3*, e001260–e001260.
67. Haag, M.; Van Linthout, S.; Schröder, S.E.A.; Freymann, U.; Ringe, J.; Tschöpe, C.; Sittinger, M. Endomyocardial biopsy derived adherent proliferating cells - A potential cell source for cardiac tissue engineering. *J. Cell. Biochem.* **2010**, *109*, 564–575.
68. Savvatis, K.; van Linthout, S.; Miteva, K.; Pappritz, K.; Westermann, D.; Schefold, J.C.; Fusch, G.; Weithäuser, A.; Rauch, U.; Becher, P.-M.; et al. Mesenchymal stromal cells but not cardiac fibroblasts exert beneficial systemic immunomodulatory effects in experimental myocarditis. *PLoS One* **2012**, *7*, (article e41047)1-16.
69. Gerstenblith, G.; Johnston, P. V; Marbán, L.; Bonow, R.O.; Marbán, E.; Mendizabal, A.; Lardo, A.C.; Malliaras, K.; Wu, E.; Smith, R.R.; et al. Intracoronary Cardiosphere-Derived Cells After Myocardial Infarction. *J. Am. Coll. Cardiol.* **2013**, *63*, 110–122.
70. Dam, N.; Hocine, H.R.; Palacios, I.; DelaRosa, O.; Menta, R.; Charron, D.; Bensussan, A.; El Costa, H.; Jabrane-Ferrat, N.; Dalemans, W.; et al. Human Cardiac-Derived Stem/Progenitor Cells Fine-Tune Monocyte-Derived Descendants Activities toward Cardiac Repair. *Front. Immunol.* **2017**, *8*, (article 1413)1-16.
71. Marbán, E.; Malliaras, K. Mixed results for bone marrow-derived cell therapy for ischemic heart disease. *JAMA - J. Am. Med. Assoc.* **2012**, *308*, 2405–2406.
72. Fischer-Nielsen, A.; Ekblond, A.; Kofoed, K.F.; Haack-Sørensen, M.; Qayyum, A.A.; Mathiasen, A.B.; Kastrup, J.; Helqvist, S.; Jørgensen, E. Bone marrow-derived mesenchymal stromal cell treatment in patients with severe ischaemic heart failure: a randomized placebo-controlled trial (MSC-HF trial). *Eur. Heart J.* **2015**, *36*, 1744–1753.
73. Toma, C.; Pittenger, M.F.; Cahill, K.S.; Byrne, B.J.; Kessler, P.D.; Toma, C.; Pittenger, M.F.; Cahill, K.S.; Byrne, B.J.; Kessler, P.D. Human Mesenchymal Stem Cells Differentiate to a Cardiomyocyte Phenotype in the Adult Murine Heart. **2002**, 93–98.
74. Wang, T.; Xu, Z.; Jiang, W.; Ma, A. Cell-to-cell contact induces mesenchymal stem cell to differentiate into cardiomyocyte and smooth muscle cell. *Int. J. Cardiol.* **2006**, *109*, 74–81.
75. Antonitsis, P.; Ioannidou-Papagiannaki, E.; Kaidoglou, A.; Papakonstantinou, C. In vitro cardiomyogenic differentiation of adult human bone marrow mesenchymal stem cells. The role

of 5-azacytidine. *Interact. Cardiovasc. Thorac. Surg.* **2007**, *6*, 593–597.
76. Müller-Ehmsen, J.; Krausgrill, B.; Burst, V.; Schenk, K.; Neisen, U.C.; Fries, J.W.U.; Fleischmann, B.K.; Hescheler, J.; Schwinger, R.H.G. Effective engraftment but poor mid-term persistence of mononuclear and mesenchymal bone marrow cells in acute and chronic rat myocardial infarction. *J. Mol. Cell. Cardiol.* **2006**, *41*, 876–884.
77. Eggenhofer, E.; Benseler, V.; Kroemer, A.; Popp, F.C.; Geissler, E.K.; Schlitt, H.J.; Baan, C.C.; Dahlke, M.H.; Hoogduijn, M.J. Mesenchymal stem cells are short-lived and do not migrate beyond the lungs after intravenous infusion. *Front. Immunol.* **2012**, *3*, 297.
78. He, J.; Cai, Y.; Luo, L.-M.; Liu, H.-B. Hypoxic adipose mesenchymal stem cells derived conditioned medium protect myocardial infarct in rat. *Eur. Rev. Med. Pharmacol. Sci.* **2015**, *19*, 4397–4406.
79. Hynes, B.; Kumar, A.H.S.; O'Sullivan, J.; Klein Buneker, C.; Leblond, A.-L.; Weiss, S.; Schmeckpeper, J.; Martin, K.; Caplice, N.M. Potent endothelial progenitor cell-conditioned media-related anti-apoptotic, cardiotrophic, and pro-angiogenic effects post-myocardial infarction are mediated by insulin-like growth factor-1. *Eur. Heart J.* **2013**, *34*, 782–789.
80. Gnecchi, M.O.; He, H.; Liang, O.D.; Melo, L.G.; Morello, F.; Mu, H.; Noiseux, N.; Zhang, L.; Pratt, R.E.; Ingwall, J.S.; et al. Paracrine action accounts for marked protection of ioschemic heart by Akt-modified mesenchymal stem cells. *Nat. Med. Swiss Med Wkly. Transplant. Nat. Neurol. Eur. J. Immunol. Reischl, I.G. al. Immunol. Lett* **2005**, *11*, 367–368.
81. Chargaff, E.; West, R. The biological significance of the thromboplastic protein of blood. *J Biol Chem* **1946**, *166*, 189–97.
82. Wolf, P. The nature and significance of platelet products in human plasma. *Br. J. Haematol.* **1967**, *13*, 269–288.
83. Lötvall, J.; Hill, A.F.; Hochberg, F.; Buzas, E.I.; Vizio, D. Di; Gardiner, C.; Gho, Y.S.; Kurochkin, I. V.; Mathivanan, S.; Quesenberry, P.; et al. *Journal of Extracellular Vesicles*. 2014,.
84. Fleury, A.; Martinez, M.C.; Le Lay, S. Extracellular vesicles as therapeutic tools in cardiovascular diseases. *Front. Immunol.* 2014, *5*.
85. Théry, C.; Witwer, K.W.; Aikawa, E.; Alcaraz, M.J.; Anderson, J.D.; Andriantsitohaina, R.; Antoniou, A.; Arab, T.; Archer, F.; Atkin-Smith, G.K.; et al. Minimal information for studies of extracellular vesicles 2018 (MISEV2018): a position statement of the International Society for Extracellular Vesicles and update of the MISEV2014 guidelines. *J. Extracell. Vesicles* **2018**, *7*.
86. Osteikoetxea, X.; Balogh, A.; Szabó-Taylor, K.; Németh, A.; Szabó, T.G.; Pálóczi, K.; Sódar, B.; Kittel, Á.; György, B.; Pállinger, É.; et al. Improved characterization of EV preparations based on protein to lipid ratio and lipid properties. *PLoS One* **2015**, *10*.
87. Crescitelli, R.; Lässer, C.; Szabó, T.G.; Kittel, A.; Eldh, M.; Dianzani, I.; Buzás, E.I.; Lötvall, J. Distinct RNA profiles in subpopulations of extracellular vesicles: Apoptotic bodies, microvesicles and exosomes. *J. Extracell. Vesicles* **2013**, *2*.
88. Kowal, J.; Arras, G.; Colombo, M.; Jouve, M.; Morath, J.P.; Primdal-Bengtson, B.; Dingli, F.; Loew, D.; Tkach, M.; Théry, C. Proteomic comparison defines novel markers to characterize heterogeneous populations of extracellular vesicle subtypes. *Proc. Natl. Acad. Sci.* **2016**, *113*, E968–E977.
89. Théry, C.; Clayton, A.; Amigorena, S.; Raposo, G. Isolation and Characterization of Exosomes from Cell Culture Supernatants. In *Current protocols in cell biology*; John Wiley &Sons, Inc., 2006; Vol. Chapter 3, pp. 1–29 ISBN 1934-2616 (Electronic)r1934-2616 (Linking).
90. Jeppesen, D.K.; Fenix, A.M.; Franklin, J.L.; Higginbotham, J.N.; Zhang, Q.; Zimmerman, L.J.; Liebler, D.C.; Ping, J.; Liu, Q.; Evans, R.; et al. Reassessment of Exosome Composition. *Cell* **2019**, *177*, 428-445.e18.
91. Van Deun, J.; Mestdagh, P.; Sormunen, R.; Cocquyt, V.; Vermaelen, K.; Vandesompele, J.; Bracke, M.; De Wever, O.; Hendrix, A. The impact of disparate isolation methods for extracellular vesicles on downstream RNA profiling. *J. Extracell. Vesicles* **2014**, *3*.
92. Sódar, B.W.; Kittel, Á.; Pálóczi, K.; Vukman, K. V.; Osteikoetxea, X.; Szabó-Taylor, K.; Németh, A.; Sperlágh, B.; Baranyai, T.; Giricz, Z.; et al. Low-density lipoprotein mimics blood plasma-derived exosomes and microvesicles during isolation and detection. *Sci. Rep.* **2016**, *6*.
93. Liu, Y.; Defourny, K.A.Y.; Smid, E.J.; Abee, T. Gram-positive bacterial extracellular vesicles and

their impact on health and disease. *Front. Microbiol.* **2018**, *9*.
94. Rizzo, J.; Rodrigues, M.L.; Janbon, G. Extracellular Vesicles in Fungi: Past, Present, and Future Perspectives. *Front. Cell. Infect. Microbiol.* 2020, *10*, 346.
95. Todorova, D.; Simoncini, S.; Lacroix, R.; Sabatier, F.; Dignat-George, F. Extracellular vesicles in angiogenesis. *Circ. Res.* 2017, *120*, 1658–1673.
96. Sluijter, J.P.G.; Verhage, V.; Deddens, J.C.; Van Den Akker, F.; Doevendans, P.A. Microvesicles and exosomes for intracardiac communication. *Cardiovasc. Res.* **2014**, *102*, 302–311.
97. Théry, C.; Ostrowski, M.; Segura, E. Membrane vesicles as conveyors of immune responses. *Nat. Rev. Immunol.* 2009, *9*, 581–593.
98. Andreu, Z.; Yáñez-Mó, M. Tetraspanins in extracellular vesicle formation and function. *Front. Immunol.* **2014**, *5*, (article 442)1-12.
99. Kowal, J.; Tkach, M.; Théry, C. Biogenesis and secretion of exosomes. *Curr. Opin. Cell Biol.* 2014, *29*, 116–125.
100. Sluijter, J.P.G.; Van Rooij, E. Exosomal MicroRNA Clusters Are Important for the Therapeutic Effect of Cardiac Progenitor Cells. *Circ. Res.* **2015**, *116*, 219–221.
101. Barile, L.; Milano, G.; Vassalli, G. Beneficial effects of exosomes secreted by cardiac-derived progenitor cells and other cell types in myocardial ischemia. *Stem Cell Investig.* **2017**, *4*, (article 93)1-13.
102. Gray, W.D.; French, K.M.; Ghosh-Choudhary, S.; Maxwell, J.T.; Brown, M.E.; Platt, M.O.; Searles, C.D.; Davis, M.E. Identification of Therapeutic Covariant MicroRNA Clusters in Hypoxia-Treated Cardiac Progenitor CElls Exosomes Using Systems Biology. *Circ. Res.* **2015**, *116*, 255–263.
103. Barile, L.; Lionetti, V.; Cervio, E.; Matteucci, M.; Gherghiceanu, M.; Popescu, L.M.; Torre, T.; Siclari, F.; Moccetti, T.; Vassalli, G. Extracellular vesicles fromhuman cardiac progenitor cells inhibit cardiomyocyte apoptosis and improve cardiac function aftermyocardial infarction. *Cardiovasc. Res.* **2014**, *103*, 530–541.
104. Harting, M.T.; Srivastava, A.K.; Zhaorigetu, S.; Bair, H.; Prabhakara, K.S.; Toledano Furman, N.E.; Vykoukal, J. V.; Ruppert, K.A.; Cox, C.S.; Olson, S.D. Inflammation-Stimulated Mesenchymal Stromal Cell-Derived Extracellular Vesicles Attenuate Inflammation. *Stem Cells* **2018**, *36*, 79–90.
105. Pachler, K.; Ketterl, N.; Desgeorges, A.; Dunai, Z.A.; Laner-Plamberger, S.; Streif, D.; Strunk, D.; Rohde, E.; Gimona, M. An In Vitro Potency Assay for Monitoring the Immunomodulatory Potential of Stromal Cell-Derived Extracellular Vesicles. *Int. J. Mol. Sci.* **2017**, *18*, (article 1413)1-11.
106. Burrello, J.; Monticone, S.; Gai, C.; Gomez, Y.; Kholia, S.; Camussi, G. Stem Cell-Derived Extracellular Vesicles and Immune-Modulation. *Front. Cell Dev. Biol.* **2016**, *4*, (article 83)1-10.
107. Cosenza, S.; Toupet, K.; Maumus, M.; Luz-Crawford, P.; Blanc-Brude, O.; Jorgensen, C.; Noël, D. Mesenchymal stem cells-derived exosomes are more immunosuppressive than microparticles in inflammatory arthritis. *Theranostics* **2018**, *8*, 1399–1410.
108. Giorda, E.; Scapaticci, M.; Luciano, R.; Fierabracci, A.; Del Fattore, A.; Pascucci, L.; Muraca, M.; Goffredo, B.M. Immunoregulatory Effects of Mesenchymal Stem Cell-Derived Extracellular Vesicles on T Lymphocytes. *Cell Transplant.* **2015**, *24*, 2615–2627.
109. Gonçalves, F. da C.; Luk, F.; Korevaar, S.S.; Bouzid, R.; Paz, A.H.; López-Iglesias, C.; Baan, C.C.; Merino, A.; Hoogduijn, M.J. Membrane particles generated from mesenchymal stromal cells modulate immune responses by selective targeting of pro-inflammatory monocytes. *Sci. Rep.* **2017**, *7*, (article 12100)1-13.
110. Reis, M.; Mavin, E.; Nicholson, L.; Green, K.; Dickinson, A.M.; Wang, X.N. Mesenchymal stromal cell-derived extracellular vesicles attenuate dendritic cell maturation and function. *Front. Immunol.* **2018**, *9*, 2538.
111. Sicco, C. Lo; Reverberi, D.; Balbi, C.; Ulivi, V.; Principi, E.; Pascucci, L.; Becherini, P.; Bosco, M.C.; Varesio, L.; Franzin, C.; et al. Mesenchymal stem cell-derived extracellular vesicles as mediators of anti-inflammatory effects: Endorsement of macrophage polarization. *Stem Cells Transl. Med.* **2017**, *6*, 1018–1028.
112. Bruno, S.; Grange, C.; Deregibus, M.C.; Calogero, R.A.; Saviozzi, S.; Collino, F.; Morando, L.;

Busca, A.; Falda, M.; Bussolati, B.; et al. Mesenchymal Stem Cell-Derived Microvesicles Protect Against Acute Tubular Injury. *J. Am. Soc. Nephrol.* **2009**, *20*, 1053–1067.
113. Zou, X.; Gu, D.; Xing, X.; Cheng, Z.; Gong, D.; Zhang, G.; Zhu, Y. Human mesenchymal stromal cell-derived extracellular vesicles alleviate renal ischemic reperfusion injury and enhance angiogenesis in rats. *Am. J. Transl. Res.* **2016**, *8*, 4289–4299.
114. Clayton, A.; Al-Taei, S.; Webber, J.; Mason, M.D.; Tabi, Z. Cancer Exosomes Express CD39 and CD73, Which Suppress T Cells through Adenosine Production. *J. Immunol.* **2011**, *187*, 676–683.
115. Almeria, C.; Weiss, R.; Roy, M.; Tripisciano, C.; Kasper, C.; Weber, V.; Egger, D. Hypoxia Conditioned Mesenchymal Stem Cell-Derived Extracellular Vesicles Induce Increased Vascular Tube Formation in vitro. *Front. Bioeng. Biotechnol.* **2019**, *7*, 292.
116. Lombardo, G.; Dentelli, P.; Togliatto, G.; Rosso, A.; Gili, M.; Gallo, S.; Deregibus, M.C.; Camussi, G.; Brizzi, M.F. Activated Stat5 trafficking Via Endothelial Cell-derived Extracellular Vesicles Controls IL-3 Pro-angiogenic Paracrine Action. *Sci. Rep.* **2016**, *6*, 25689.
117. Pathan, M.; Keerthikumar, S.; Chisanga, D.; Alessandro, R.; Ang, C.S.; Askenase, P.; Batagov, A.O.; Benito-Martin, A.; Camussi, G.; Clayton, A.; et al. A novel community driven software for functional enrichment analysis of extracellular vesicles data. *J. Extracell. Vesicles* **2017**, *6*, 1321455.
118. Pathan, M.; Keerthikumar, S.; Ang, C.-S.; Gangoda, L.; Quek, C.Y.J.; Williamson, N.A.; Mouradov, D.; Sieber, O.M.; Simpson, R.J.; Salim, A.; et al. FunRich: An open access standalone functional enrichment and interaction network analysis tool. *Proteomics* **2015**, *15*, 2597–2601.
119. C. Carpentier, M. Martinelli, J. Courtey, I. Cascone, . Angiogenesis Analyser for ImageJ. In Proceedings of the 4th ImageJ user and developer conference proceedings.; Mondorf-les-Bains, Luxemburg, 2012; p. 198.201.
120. Collino, F.; Bruno, S.; Deregibus, M.C.; Tetta, C.; Camussi, G. MicroRNAs and Mesenchymal Stem Cells. *Vitam. Horm.* **2011**, *87*, 291–320.
121. Andersen, C.L.; Jensen, J.L.; Ørntoft, T.F. Normalization of Real-Time Quantitative Reverse Transcription-PCR Data: A Model-Based Variance Estimation Approach to Identify Genes Suited for Normalization, Applied to Bladder and Colon Cancer Data Sets. *Cancer Res.* **2004**, *64*, 5245–5250.
122. Batra, A.S.; Lewin, A.B. Acute myocarditis. *Curr. Opin. Pediatr.* **2001**, *13*, p 234-239.
123. Lener, T.; Gimona, M.; Aigner, L.; Börger, V.; Buzas, E.; Camussi, G.; Chaput, N.; Chatterjee, D.; Court, F.A.; del Portillo, H.A.; et al. Applying extracellular vesicles based therapeutics in clinical trials - An ISEV position paper. *J. Extracell. Vesicles* **2015**, *4*, (article 30087)1-31.
124. Ketterl, N.; Brachtl, G.; Schuh, C.; Bieback, K.; Schallmoser, K.; Reinisch, A.; Strunk, D. A robust potency assay highlights significant donor variation of human mesenchymal stem/progenitor cell immune modulatory capacity and extended radio-resistance. *Stem Cell Res. Ther.* **2015**, *6*, 236.
125. Zhang, R.; Liu, Y.; Yan, K.; Chen, L.; Chen, X.-R.; Li, P.; Chen, F.-F.; Jiang, X.-D. Anti-inflammatory and immunomodulatory mechanisms of mesenchymal stem cell transplantation in experimental traumatic brain injury. *J. Neuroinflammation* **2013**, *10*, 871–883.
126. Ciullo, A.; Biemmi, V.; Milano, G.; Bolis, S.; Cervio, E.; Fertig, E.T.; Gherghiceanu, M.; Moccetti, T.; Camici, G.G.; Vassalli, G.; et al. Exosomal expression of CXCR4 targets cardioprotective vesicles to myocardial infarction and improves outcome after systemic administration. *Int. J. Mol. Sci.* **2019**, *20*, 1–24.
127. Chen, W.; Huang, Y.; Han, J.; Yu, L.; Li, Y.; Lu, Z.; Li, H.; Liu, Z.; Shi, C.; Duan, F.; et al. Immunomodulatory effects of mesenchymal stromal cells-derived exosome. *Immunol. Res.* **2016**, *64*, 831–840.
128. Sheng, H.; Wang, Y.; Jin, Y.; Zhang, Q.; Zhang, Y.; Wang, L.; Shen, B.; Yin, S.; Liu, W.; Cui, L.; et al. A critical role of IFNγ in priming MSC-mediated suppression of T cell proliferation through up-regulation of B7-H1. *Cell Res.* **2008**, *18*, 846–857.
129. Renner, P.; Eggenhofer, E.; Rosenauer, A.; Popp, F.C.; Steinmann, J.F.; Slowik, P.; Geissler, E.K.; Piso, P.; Schlitt, H.J.; Dahlke, M.H. Mesenchymal Stem Cells Require a Sufficient, Ongoing Immune Response to Exert Their Immunosuppressive Function. *Transplant. Proc.* **2009**, *41*, 2607–2611.
130. Di Trapani, M.; Bassi, G.; Midolo, M.; Gatti, A.; Kamga, P.T.; Cassaro, A.; Carusone, R.; Adamo, A.; Krampera, M.; Takam Kamga, P.; et al. Differential and transferable modulatory effects of

mesenchymal stromal cell-derived extracellular vesicles on T, B and NK cell functions. *Sci. Rep.* **2016**, *6*, 24120.
131. Diedrichs, F.; Stolk, M.; Jürchott, K.; Haag, M.; Sittinger, M.; Seifert, M. Enhanced Immunomodulation in Inflammatory Environments Favors Human Cardiac Mesenchymal Stromal-Like Cells for Allogeneic Cell Therapies. *Front. Immunol.* **2019**, *10*, 1716.
132. Varkouhi, A.K.; Jerkic, M.; Ormesher, L.; Gagnon, S.; Goyal, S.; Rabani, R.; Masterson, C.; Spring, C.; Chen, P.Z.; Gu, F.X.; et al. Extracellular Vesicles from Interferon-γ-primed Human Umbilical Cord Mesenchymal Stromal Cells Reduce Escherichia coli-induced Acute Lung Injury in Rats. *Anesthesiology* **2019**, *130*, 778–790.
133. Witwer, K.W.; Buzás, E.I.; Bemis, L.T.; Bora, A.; Lässer, C.; Lötvall, J.; Nolte-'t Hoen, E.N.; Piper, M.G.; Sivaraman, S.; Skog, J.; et al. Standardization of sample collection, isolation and analysis methods in extracellular vesicle research. *J. Extracell. Vesicles* **2013**, *2*, 1–25.
134. Hadjidemetriou, M.; Al-Ahmady, Z.; Mazza, M.; Collins, R.F.; Dawson, K.; Kostarelos, K. In Vivo Biomolecule Corona around Blood-Circulating, Clinically Used and Antibody-Targeted Lipid Bilayer Nanoscale Vesicles. *ACS Nano* **2015**, *9*, 8142–8156.
135. Gupta, M.N.; Roy, I. How Corona Formation Impacts Nanomaterials as Drug Carriers. *Mol. Pharm.* 2020, *17*, 725–737.
136. Arrighetti, N.; Corbo, C.; Evangelopoulos, M.; Pastò, A.; Zuco, V.; Tasciotti, E. Exosome-like Nanovectors for Drug Delivery in Cancer. *Curr. Med. Chem.* **2018**, *26*, 6132–6148.
137. Geeurickx, E.; Tulkens, J.; Dhondt, B.; Van Deun, J.; Lippens, L.; Vergauwen, G.; Heyrman, E.; De Sutter, D.; Gevaert, K.; Impens, F.; et al. The generation and use of recombinant extracellular vesicles as biological reference material. *Nat. Commun.* **2019**, *10*, 1–12.
138. Morelli, A.E.; Larregina, A.T.; Shufesky, W.J.; Sullivan, M.L.G.; Stolz, D.B.; Papworth, G.D.; Zahorchak, A.F.; Logar, A.J.; Wang, Z.; Watkins, S.C.; et al. Endocytosis, intracellular sorting, and processing of exosomes by dendritic cells. *Blood* **2004**, *104*, 3257–3266.
139. Tosar, J.P.; Cayota, A.; Eitan, E.; Halushka, M.K.; Witwer, K.W. Ribonucleic artefacts: are some extracellular RNA discoveries driven by cell culture medium components? *J. Extracell. Vesicles* 2017, *6*.
140. Auber, M.; Fröhlich, D.; Drechsel, O.; Karaulanov, E.; Krämer-Albers, E.M. Serum-free media supplements carry miRNAs that co-purify with extracellular vesicles. *J. Extracell. Vesicles* **2019**, *8*, 1656042.
141. Varga, Z.; Fehér, B.; Kitka, D.; Wacha, A.; Bóta, A.; Berényi, S.; Pipich, V.; Fraikin, J.L. Size Measurement of Extracellular Vesicles and Synthetic Liposomes: The Impact of the Hydration Shell and the Protein Corona. *Colloids Surfaces B Biointerfaces* **2020**, *192*, 111053.
142. Hyland, M.; Mennan, C.; Wilson, E.; Clayton, A.; Kehoe, O. Pro-Inflammatory Priming of Umbilical Cord Mesenchymal Stromal Cells Alters the Protein Cargo of Their Extracellular Vesicles. *Cells* **2020**, *9*, 726.
143. Bobrie, A.; Colombo, M.; Krumeich, S.; Raposo, G.; Théry, C. Diverse subpopulations of vesicles secreted by different intracellular mechanisms are present in exosome preparations obtained by differential ultracentrifugation. *J. Extracell. Vesicles* **2012**, *1*.
144. Willms, E.; Johansson, H.J.; Mäger, I.; Lee, Y.; Blomberg, K.E.M.; Sadik, M.; Alaarg, A.; Smith, C.I.E.; Lehtiö, J.; El Andaloussi, S.; et al. Cells release subpopulations of exosomes with distinct molecular and biological properties. *Sci. Rep.* **2016**, *6*, 1–12.
145. Esfandiarei, M.; McManus, B.M. Molecular Biology and Pathogenesis of Viral Myocarditis. *Annu. Rev. Pathol. Mech. Dis.* **2008**, *3*, 127–155.
146. Ikwegbue, P.C.; Masamba, P.; Oyinloye, B.E.; Kappo, A.P. Roles of heat shock proteins in apoptosis, oxidative stress, human inflammatory diseases, and cancer. *Pharmaceuticals* 2018, *11*.
147. Liu, L.; Zhang, H.; Mao, H.; Li, X.; Hu, Y. Exosomal miR-320d derived from adipose tissue-derived MSCs inhibits apoptosis in cardiomyocytes with atrial fibrillation (AF). *Artif. Cells, Nanomedicine, Biotechnol.* **2019**, *47*, 3976–3984.
148. Pužar Dominkuš, P.; Stenovec, M.; Sitar, S.; Lasič, E.; Zorec, R.; Plemenitaš, A.; Žagar, E.; Kreft, M.; Lenassi, M. PKH26 labeling of extracellular vesicles: Characterization and cellular internalization of contaminating PKH26 nanoparticles. *Biochim. Biophys. Acta - Biomembr.* **2018**, *1860*, 1350–1361.

149. Matula, Z.; Németh, A.; Lőrincz, P.; Szepesi, Á.; Brózik, A.; Buzás, E.I.; Lőw, P.; Német, K.; Uher, F.; Urbán, V.S. The Role of Extracellular Vesicle and Tunneling Nanotube-Mediated Intercellular Cross-Talk Between Mesenchymal Stem Cells and Human Peripheral T Cells. *Stem Cells Dev.* **2016**, *25*, 1818–1832.
150. Jiang, C.; Xie, P.; Sun, R.; Sun, X.; Liu, G.; Ding, S.; Zhu, M.; Yan, B.; Liu, Q.; Chen, X.; et al. c-Jun-mediated microRNA-302d-3p induces RPE dedifferentiation by targeting p21Waf1/Cip1. *Cell Death Dis.* **2018**, *9*, 451.
151. Li, A.; Dubey, S.; Varney, M.L.; Dave, B.J.; Singh, R.K. IL-8 directly enhanced endothelial cell survival, proliferation, and matrix metalloproteinases production and regulated angiogenesis. *J. Immunol.* **2003**, *170*, 3369–76.
152. Cohen, T.; Nahari, D.; Cerem, L.W.; Neufeld, G.; Levin, B.Z. Interleukin 6 induces the expression of vascular endothelial growth factor. *J. Biol. Chem.* **1996**, *271*, 736–741.
153. Anderson, J.D.; Johansson, H.J.; Graham, C.S.; Vesterlund, M.; Pham, M.T.; Bramlett, C.S.; Montgomery, E.N.; Mellema, M.S.; Bardini, R.L.; Contreras, Z.; et al. Comprehensive proteomic analysis of mesenchymal stem cell exosomes reveals modulation of angiogenesis via nuclear factor-kappaB signaling. *Stem Cells* **2016**, *34*, 601–613.
154. Zhu, K.; Pan, Q.; Zhang, X.; Kong, L.-Q.; Fan, J.; Dai, Z.; Wang, L.; Yang, X.-R.; Hu, J.; Wan, J.-L.; et al. MiR-146a enhances angiogenic activity of endothelial cells in hepatocellular carcinoma by promoting PDGFRA expression. *Carcinogenesis* **2013**, *34*, 2071–2079.
155. Lei, Z.; van Mil, A.; Brandt, M.M.; Grundmann, S.; Hoefer, I.; Smits, M.; el Azzouzi, H.; Fukao, T.; Cheng, C.; Doevendans, P.A.; et al. MicroRNA-132/212 family enhances arteriogenesis after hindlimb ischaemia through modulation of the Ras-MAPK pathway. *J. Cell. Mol. Med.* **2015**, *19*, 1994–2005.
156. Seo, H.-H.; Lee, S.-Y.; Lee, C.Y.; Kim, R.; Kim, P.; Oh, S.; Lee, H.; Lee, M.Y.; Kim, J.; Kim, L.K.; et al. Exogenous miRNA-146a Enhances the Therapeutic Efficacy of Human Mesenchymal Stem Cells by Increasing Vascular Endothelial Growth Factor Secretion in the Ischemia/Reperfusion-Injured Heart. *J. Vasc. Res.* **2017**, *54*, 100–108.
157. Mao, G.; Liu, Y.; Fang, X.; Liu, Y.; Fang, L.; Lin, L.; Liu, X.; Wang, N. Tumor-derived microRNA-494 promotes angiogenesis in non-small cell lung cancer. *Angiogenesis* **2015**, *18*, 373–382.
158. Chen, S.; Zhao, G.; Miao, H.; Tang, R.; Song, Y.; Hu, Y.; Wang, Z.; Hou, Y. MicroRNA-494 inhibits the growth and angiogenesis-regulating potential of mesenchymal stem cells. *FEBS Lett.* **2015**, *589*, 710–717.
159. Tugues, S.; Honjo, S.; König, C.; Padhan, N.; Kroon, J.; Gualandi, L.; Li, X.; Barkefors, I.; Thijssen, V.L.; Griffioen, A.W.; et al. Tetraspanin CD63 promotes vascular endothelial growth factor receptor 2-β1 integrin complex formation, thereby regulating activation and downstream signaling in endothelial cells in Vitro and in Vivo. *J. Biol. Chem.* **2013**, *288*, 19060–19071.
160. Thijssen, V.L.; Griffioen, A.W. Galectin-1 and -9 in angiogenesis: A sweet couple. *Glycobiology* **2014**, *24*, 915–920.
161. Thijssen, V.L.J.L.; Postel, R.; Brandwijk, R.J.M.G.E.; Dings, R.P.M.; Nesmelova, I.; Satijn, S.; Verhofstad, N.; Nakabeppu, Y.; Baum, L.G.; Bakkers, J.; et al. Galectin-1 is essential in tumor angiogenesis and is a target for antiangiogenesis therapy. *Proc. Natl. Acad. Sci.* **2006**, *103*, 15975–15980.
162. Tang, D.; Gao, J.; Wang, S.; Ye, N.; Chong, Y.; Huang, Y.; Wang, J.; Li, B.; Yin, W.; Wang, D. Cancer-associated fibroblasts promote angiogenesis in gastric cancer through galectin-1 expression. *Tumor Biol.* **2016**, *37*, 1889–1899.
163. Mokarizadeh, A.; Delirezh, N.; Morshedi, A.; Mosayebi, G.; Farshid, A.A.; Mardani, K. Microvesicles derived from mesenchymal stem cells: Potent organelles for induction of tolerogenic signaling. *Immunol. Lett.* **2012**, *147*, 47–54.
164. Gieseke, F.; Böhringer, J.; Bussolari, R.; Dominici, M.; Handgretinger, R.; Müller, I. Human multipotent mesenchymal stromal cells use galectin-1 to inhibit immune effector cells. *Blood* **2010**, *116*, 3770–3779.
165. Seropian, I.M.; González, G.E.; Maller, S.M.; Berrocal, D.H.; Abbate, A.; Rabinovich, G.A. Galectin-1 as an Emerging Mediator of Cardiovascular Inflammation: Mechanisms and

Therapeutic Opportunities. *Mediators Inflamm.* 2018, *2018*.
166. Domenis, R.; Cesselli, D.; Toffoletto, B.; Bourkoula, E.; Caponnetto, F.; Manini, I.; Beltrami, A.P.; Ius, T.; Skrap, M.; Di Loreto, C.; et al. Systemic T Cells Immunosuppression of Glioma Stem Cell-Derived Exosomes Is Mediated by Monocytic Myeloid-Derived Suppressor Cells. *PLoS One* **2017**, *12*, e0169932.
167. Zhang, B.; Yin, Y.; Lai, R.C.; Tan, S.S.; Choo, A.B.H.; Lim, S.K. Mesenchymal Stem Cells Secrete Immunologically Active Exosomes. *Stem Cells Dev.* **2014**, *23*, 1233–1244.
168. Cibrián, D.; Sánchez-Madrid, F. CD69: from activation marker to metabolic gatekeeper. *Eur. J. Immunol.* **2017**, *47*, 946–953.
169. Groux, H.; O'Garra, A.; Bigler, M.; Rouleau, M.; Antonenko, S.; De Vries, J.E.; Roncarolo, M.G. A CD4+ T-cell subset inhibits antigen-specific T-cell responses and prevents colitis. *Nature* **1997**, *389*, 737–742.
170. Jutel, M.; Akdis, M.; Budak, F.; Aebischer-Casaulta, C.; Wrzyszcz, M.; Blaser, K.; Akdis, C.A. IL-10 and TGF-β cooperate in the regulatory T cell response to mucosal allergens in normal immunity and specific immunotherapy. *Eur. J. Immunol.* **2003**, *33*, 1205–1214.
171. Franzin, C.; Ulivi, V.; Pascucci, L.; Bosco, M.C.; Pozzobon, M.; Principi, E.; Varesio, L.; Becherini, P.; Reverberi, D.; Balbi, C.; et al. Mesenchymal Stem Cell-Derived Extracellular Vesicles as Mediators of Anti-Inflammatory Effects: Endorsement of Macrophage Polarization. *Stem Cells Transl. Med.* **2017**, *6*, 1018–1028.
172. de Witte, S.F.H.; Luk, F.; Sierra Parraga, J.M.; Gargesha, M.; Merino, A.; Korevaar, S.S.; Shankar, A.S.; O'Flynn, L.; Elliman, S.J.; Roy, D.; et al. Immunomodulation By Therapeutic Mesenchymal Stromal Cells (MSC) Is Triggered Through Phagocytosis of MSC By Monocytic Cells. *Stem Cells* **2018**, *36*, 602–615.
173. Martinez, F.O.; Gordon, S.; Locati, M.; Mantovani, A. Transcriptional Profiling of the Human Monocyte-to-Macrophage Differentiation and Polarization: New Molecules and Patterns of Gene Expression. *J. Immunol.* **2006**, *177*, 7303–7311.
174. Gabrusiewicz, K.; Li, X.; Wei, J.; Hashimoto, Y.; Marisetty, A.L.; Ott, M.; Wang, F.; Hawke, D.; Yu, J.; Healy, L.M.; et al. Glioblastoma stem cell-derived exosomes induce M2 macrophages and PD-L1 expression on human monocytes. *Oncoimmunology* **2018**, *7*, e1412909.
175. Barros, M.H.M.; Hauck, F.; Dreyer, J.H.; Kempkes, B.; Niedobitek, G. Macrophage polarisation: An immunohistochemical approach for identifying M1 and M2 macrophages. *PLoS One* **2013**, *8*.
176. Luz-Crawford, P.; Djouad, F.; Toupet, K.; Bony, C.; Franquesa, M.; Hoogduijn, M.J.; Jorgensen, C.; Noël, D. Mesenchymal Stem Cell-Derived Interleukin 1 Receptor Antagonist Promotes Macrophage Polarization and Inhibits B Cell Differentiation. *Stem Cells* **2016**, *34*, 483–492.
177. Vannella, K.M.; Wynn, T.A. Mechanisms of Organ Injury and Repair by Macrophages. *Annu. Rev. Physiol.* **2016**, *79*, 593–617.
178. Courties, G.; Heidt, T.; Sebas, M.; Iwamoto, Y.; Jeon, D.; Truelove, J.; Tricot, B.; Wojtkiewicz, G.; Dutta, P.; Sager, H.B.; et al. In vivo silencing of the transcription factor IRF5 reprograms the macrophage phenotype and improves infarct healing. *J. Am. Coll. Cardiol.* **2014**, *63*, 1556–1566.
179. Kambara, K.; Ohashi, W.; Tomita, K.; Takashina, M.; Fujisaka, S.; Hayashi, R.; Mori, H.; Tobe, K.; Hattori, Y. In vivo depletion of CD206+ M2 macrophages exaggerates lung injury in endotoxemic mice. *Am. J. Pathol.* **2015**, *185*, 162–171.
180. Bellón, T.; Martínez, V.; Lucendo, B.; del Peso, G.; Castro, M.J.; Aroeira, L.S.; Rodríguez-Sanz, A.; Ossorio, M.; Sánchez-Villanueva, R.; Selgas, R.; et al. Alternative activation of macrophages in human peritoneum: implications for peritoneal fibrosis. *Nephrol. Dial. Transplant.* **2011**, *26*, 2995–3005.
181. Abebayehu, D.; Spence, A.; Boyan, B.D.; Schwartz, Z.; Ryan, J.J.; McClure, M.J. Galectin-1 promotes an M2 macrophage response to polydioxanone scaffolds. *J. Biomed. Mater. Res. - Part A* **2017**, *105*, 2562–2571.
182. Barrionuevo, P.; Beigier-Bompadre, M.; Ilarregui, J.M.; Toscano, M.A.; Bianco, G.A.; Isturiz, M.A.; Rabinovich, G.A. A Novel Function for Galectin-1 at the Crossroad of Innate and Adaptive Immunity: Galectin-1 Regulates Monocyte/Macrophage Physiology through a Nonapoptotic ERK-Dependent Pathway. *J. Immunol.* **2007**, *178*, 436–445.
183. Ito, K.; Scott, S.A.; Cutler, S.; Dong, L.-F.; Neuzil, J.; Blanchard, H.; Ralph, S.J. Thiodigalactoside

inhibits murine cancers by concurrently blocking effects of galectin-1 on immune dysregulation, angiogenesis and protection against oxidative stress. *Angiogenesis* **2011**, *14*, 293–307.
184. Mukherjee, R.; Kim, S.W.; Park, T.; Choi, M.S.; Yun, J.W. Targeted inhibition of galectin 1 by thiodigalactoside dramatically reduces body weight gain in diet-induced obese rats. *Int. J. Obes.* **2015**, *39*, 1349–1358.
185. Tsai, Y.T.; Liang, C.H.; Yu, J.H.; Huang, K.C.; Tung, C.H.; Wu, J.E.; Wu, Y.Y.; Chang, C.H.; Hong, T.M.; Chen, Y.L. A DNA Aptamer Targeting Galectin-1 as a Novel Immunotherapeutic Strategy for Lung Cancer. *Mol. Ther. - Nucleic Acids* **2019**, *18*, 991–998.
186. Sheikh, M.H.; Solito, E. Annexin A1: Uncovering the many talents of an old protein. *Int. J. Mol. Sci.* 2018, *19*.
187. Li, Y.; Cai, L.; Wang, H.; Wu, P.; Gu, W.; Chen, Y.; Hao, H.; Tang, K.; Yi, P.; Liu, M.; et al. Pleiotropic regulation of macrophage polarization and tumorigenesis by formyl peptide receptor-2. *Oncogene* **2011**, *30*, 3887–3899.
188. Saiz, M.L.; Rocha-Perugini, V.; Sánchez-Madrid, F. Tetraspanins as Organizers of Antigen-Presenting Cell Function. *Front. Immunol.* **2018**, *9*, 1074.
189. Zhang, S.; He, K.; Zhou, W.; Cao, J.; Jin, Z. MiR-494-3p regulates lipopolysaccharide-induced inflammatory responses in RAW264.7 cells by targeting PTEN. *Mol. Med. Rep.* **2019**, *49*, 4288–4296.
190. Dang, T.M.; Wong, W.C.; Ong, S.M.; Li, P.; Lum, J.; Chen, J.; Poidinger, M.; Zolezzi, F.; Wong, S.C. MicroRNA expression profiling of human blood monocyte subsets highlights functional differences. *Immunology* **2015**, *145*, 404–416.
191. Liu, F.; Li, Y.; Jiang, R.; Nie, C.; Zeng, Z.; Zhao, N.; Huang, C.; Shao, Q.; Ding, C.; Qing, C.; et al. MiR-132 inhibits lipopolysaccharide-induced inflammation in alveolar macrophages by the cholinergic anti-inflammatory pathway. *Exp. Lung Res.* **2015**, *41*, 261–269.
192. Lindoso, R.S.; Collino, F.; Bruno, S.; Araujo, D.S.; Sant'Anna, J.F.; Tetta, C.; Provero, P.; Quesenberry, P.J.; Vieyra, A.; Einicker-Lamas, M.; et al. Extracellular Vesicles Released from Mesenchymal Stromal Cells Modulate miRNA in Renal Tubular Cells and Inhibit ATP Depletion Injury. *Stem Cells Dev.* **2014**, *23*, 1809–1819.
193. Steiner, D.F.; Thomas, M.F.; Hu, J.K.; Yang, Z.; Babiarz, J.E.; Allen, C.D.C.; Matloubian, M.; Blelloch, R.; Ansel, K.M. MicroRNA-29 Regulates T-Box Transcription Factors and Interferon-γ Production in Helper T Cells. *Immunity* **2011**, *35*, 169–181.
194. Fleming, V.; Hu, X.; Eline Weller, C.; Weber, R.; Groth, C.; Riester, Z.; H€ User, L.; Sun, Q.; Nagibin, V.; Kirschning, C.; et al. Tumor Biology and Immunology Melanoma Extracellular Vesicles Generate Immunosuppressive Myeloid Cells by Upregulating PD-L1 via TLR4 Signaling. **2019**.
195. Boussiotis, V.A.; Chatterjee, P.; Li, L. Biochemical Signaling of PD-1 on T Cells and Its Functional Implications. *Cancer J.* **2014**, *20*, 265–271.
196. Cunningham, E.K.; Jackson, M. V; McAuley, D.F.; O'Kane, C.M.; Krasnodembskaya, A.D.; Morrison, T.J.; Kissenpfennig, A. Mesenchymal Stromal Cells Modulate Macrophages in Clinically Relevant Lung Injury Models by Extracellular Vesicle Mitochondrial Transfer. *Am. J. Respir. Crit. Care Med.* **2017**, *196*, 1275–1286.
197. Balbi, C.; Piccoli, M.; Barile, L.; Papait, A.; Armirotti, A.; Principi, E.; Reverberi, D.; Pascucci, L.; Becherini, P.; Varesio, L.; et al. First Characterization of Human Amniotic Fluid Stem Cell Extracellular Vesicles as a Powerful Paracrine Tool Endowed with Regenerative Potential. *Stem Cells Transl. Med.* **2017**, *6*, 1340–1355.
198. Florek, M.; Schneidawind, D.; Pierini, A.; Baker, J.; Armstrong, R.; Pan, Y.; Leveson-Gower, D.; Negrin, R.; Meyer, E. Freeze and thaw of CD4+CD25+Foxp3+ regulatory T cells results in loss of CD62L expression and a reduced capacity to protect against graft-versus-host disease. *PLoS One* **2015**, *10*.
199. Fu, S.; Yopp, A.C.; Mao, X.; Chen, D.; Zhang, N.; Chen, D.; Mao, M.; Ding, Y.; Bromberg, J.S. CD4+ CD25+ CD62+ T-Regulatory Cell Subset Has Optimal Suppressive and Proliferative Potential. *Am. J. Transplant.* **2004**, *4*, 65–78.
200. Ermann, J.; Hoffmann, P.; Edinger, M.; Dutt, S.; Blankenberg, F.G.; Higgins, J.P.; Negrin, R.S.; Fathman, C.G.; Strober, S. Only the CD62L + subpopulation of CD4 +CD25 + regulatory T

cells protects from lethal acute GVHD. *Blood* **2005**, *105*, 2220–2226.
201. Bzowska, M.; Guzik, K.; Barczyk, K.; Ernst, M.; Flad, H.D.; Pryjma, J. Increased IL-10 production during spontaneous apoptosis of monocytes. *Eur. J. Immunol.* **2002**, *32*, 2011–2020.
202. Cheng, D.E.; Chang, W.A.; Hung, J.Y.; Huang, M.S.; Kuo, P.L. Involvement of IL10 and granulocyte colonystimulating factor in the fate of monocytes controlled by galectin1. *Mol. Med. Rep.* **2014**, *10*, 2389–2394.
203. Monguió-Tortajada, M.; Roura, S.; Gálvez-Montón, C.; Pujal, J.M.; Aran, G.; Sanjurjo, L.; Franquesa, M.; Sarrias, M.R.; Bayes-Genis, A.; Borràs, F.E. Nanosized UCMSC-derived extracellular vesicles but not conditioned medium exclusively inhibit the inflammatory response of stimulated T cells: Implications for nanomedicine. *Theranostics* **2017**, *7*, 270–284.

7. List of publications

Articles:

Maring JA, **Beez CM**, FalkV, Seifert M, Stamm C. Myocardial Regeneration via Progenitor Cell-Derived Exosomes. *Stem Cells Int.* **2017**;2017:7849851. doi:10.1155/2017/7849851. Epub 2017 Nov 23. PMID: 29333167 (Review article)

Detert S, Stamm C, **Beez C**, Diedrichs F, Ringe J, Van Linthout S, Seifert M, Tschöpe C, Sittinger M, Haag M. The Atrial Appendage as a Suitable Source to Generate Cardiac-derived Adherent Proliferating Cells for Regenerative Cell-based Therapies. *J Tissue Eng Regen Med.* **2018** Mar;12(3):e1404-e1417. doi:10.1002/term.2528. Epub 2017 Nov 21. PMID: 28752609 (Original Research)

Beez CM, Haag M, Klein O, Van Linthout S, Sittinger M, Seifert M. Extracellular Vesicles from Regenerative Human Cardiac Cells Act as Potent Immune Modulators by Priming Monocytes. *J Nanobiotechnology*. **2019** May 27;17(1):72. doi: 10.1186/s12951-019-0504-0. PMID: 31133024 (Original Research)

Wolf M, Vári B, Blöchl C, Raninger AM, Poupardin R, **Beez CM**, Hoog A, Brachtl G, Eminger E, Binder H-M, Oeller M, Spittler A, Heuser T, Obermayer A, Seifert M, Huber CG, Schallmoser K, Volk H-D, Strunk D. Extracellular Vesicles from Therapeutic Grade Allogenic Human Placental Stromal Cells Induce Angiogenesis and Modulate Immunity. PREPRINT **2019** Oct. doi: 10.1101/808808 (Original Research)

Andrzejewska A, Catar R, Schoon J, Qazi TH, Sass FA, Jacobi D, Blankenstein A, Reinke S, Krüger D, Streitz M, Schlickeiser S, Richter S, Souidi N, **Beez C**, Kamhieh-Milz J, Krüger U, Zemojtel T, Jürchott K, Strunk D, Reinke P, Duda G, Moll G, Geissler S. Multi-parameter Analysis of Biobanked Human Bone Marrow Stromal Cells Shows Little Influence for Donor Age and Mild Comorbidities on Phenotypic and Functional Properties. *Front Immunol.* **2019** Nov 8;10:2474. doi: 10.3389/fimmu.2019.02474.eCollection 2019. PMID: 31781089 (Original Research)

Beez CM, Schneider M, Haag M, Pappritz K, Van Linthout S, Sittinger M, Seifert M. Cardiac Extracellular Vesicles (EVs) Released in the Presence or Absence of Inflammatory Cues Support Angiogenesis in Different Manners. *Int J Mol Sci.* **2019** Dec 17;20(24):636. doi: 10.3390/ijms20246363. PMID: 31861211 (Original Research)

Nazari-Shafti TZ, Neuber S, Duran AG, Exarchos V, **Beez CM**, Meyborg H, Krüger K, Wolint P, Buschmann J, Böni R, Seifert M, Falk V, Emmert MY. MiRNA Profiles of Extracellular Vesicles Secreted by Mesenchymal Stromal Cells – Can They Predict Potential Off-target Effects?. *Biomolecules*. **2020** *(accepted;* Original Research)

Presentations:

- Oral presentations:
  - Lecture series of the Institute of medical Immunology (2015, 2016, and 2019 in Berlin, Germany)
  - Springmeeting(s) of the working group immunology of transplantation funded by DGFI (2017 in Berlin and 2019 in Mainz, both in Germany)
  - World conference of the International Society of Tissue Engineering and Regenerative Medicine (2018 in Kyoto, Japan)
  - Meeting of the German and Austrian Society of Extracellular Vesicles (2019 in Freising, Germany)

- Poster presentations:
  - BSRT Symposium (2015 and 2016 in Berlin, Germany)
  - Meeting of the International Society of Extracellular Vesicles (2016 in Rotterdam, Netherlands)
  - European conference of the International Society of Tissue Engineering and Regenerative Medicine (2017 in Davos, Switzerland)
  - EMBL course on extracellular vesicles (2016 in Heidelberg, Germany)

8. Statutory declaration

I declare that I have authored this thesis independently, that I have not used other than the declared sources/recources, and that I have explicity marked all materials which have been quoted either literally or by content from the used sources.

In addition, I declare that all texts, figures, and tables included in the following manuscripts:

- **Beez CM**, Haag M, Klein O, Van Linthout S, Sittinger M, Seifert M. Extracellular Vesicles from Regenerative Human Cardiac Cells Act as Potent Immune Modulators by Priming Monocytes. *J Nanobiotechnology*. **2019** May 27;17(1):72. doi: 10.1186/s12951-019-0504-0. PMID: 31133024 (Original Research)
- **Beez CM**, Schneider M, Haag M, Pappritz K, Van Linthout S, Sittinger M, Seifert M. Cardiac Extracellular Vesicles (EVs) Released in the Presence or Absence of Inflammatory Cues Support Angiogenesis in Different Manners. *Int J Mol Sci*. **2019** Dec 17;20(24):636. doi: 10.3390/ijms20246363. PMID: 31861211 (Original Research)

Were generated by myself. Prof. Dr. Martina Seifert primarily supervised the PhD project work. Listed co-authors were involved in experimental support or proofreading of the manuscripts. On this account, excerpts and text passages, figures and figure legends as well as tables from both manuscripts were used partly or modified in the present thesis work. Permissions to use the manuscript material was further asked and obtained from Nanobiotechnology and the International Journal of Molecular Sciences.

…….. ……..

Place & date Christien M. Beez

9. Acknowledgement

First, I would like to thank my supervisors, reviewers and mentors of this PhD thesis: Prof. Dr. Martina Sefert, Prof. Dr. Hans-Dieter Volk, PD Dr. Irina Nazarenko, Prof. Dr. York Winter, Prof. Dr. Enrico Klotzsch, Prof. Dr. Michael Sittinger and PD Dr. Sophie Van Linthout.

Thank you Martina for giving me the opportunity to work on this really interesting and challenging project – about the world of extracellular vesicles and not electric cars – in your research group, for your guidance during my doctoral thesis, for the intellectual support, and continual encouragement through the project. Moreover, thank you for being a superior dedicated to a professional and pleasant working atmosphere but also a person always honestly interested in staff beyond the work, which created a familiar basis in the group.

I also want to thank Prof. Hans-Dieter Volk and PD Dr. Irina Nazarenko for reviewing my thesis, and Prof. Dr. York Winter and Prof. Dr. Enrico Klotzsch for immediately agreeing to be part of the evaluation board. As a member of the BSRT graduate school, I also would like to thank Sabine Bartosch for her continuous help and interesting tasks like interview the new ones of the BSRT, as well as my supervisor and mentor throughout this project, Prof. Dr. Michael Sittinger and PD Dr. Sophie Van Linthout. I highly appreciate that both of you always made time available when there was need to critically discuss results, plans, pleasant annually progress report meetings, or that papers about CardAP EVs needed to be reviewed. A special thanks also goes to Dr. Sven Geißler, whom made it possible that I could work on project´s of his group together and that he funded me the last months in 2019

All my present and former colleagues from the Transplantation Immunology lab of Prof. Dr. Martina Seifert, namely Dr. Maria Schneider, Dr. Naima Souidi, Falk Diedrichs, Meaghan Stolk, all our former Master and Bachelor students, especially Niklas Fellmer, whom performed his Bachelor thesis under the supervision of Martina and me: THANKS A LOT for the nice time in the lab, lab meetings, and outside of the lab, suggestions what to read, where to eat, and in general it was a great time.

Also a big thank you to Dr. Marion Haag, Anja Fleischmann, Dr. Oliver Klein, Petra Schrade, Dr. Maria Schneider, Satpal Nijjar, Dr. Kathleen Pappritz, Kerstin Puhl for superb technical support, Q&A sessions, or performance of experimental parts as outlined in the Material & Method section. Also a big thank you to AG Tschöpe, whom I somehow became an inofficial member.

Mille grazie/Arigato goza machta/Muchas Gracias/Vielen lieben Dank/Thanks a lot to all my friends whom accompanied me not only through the years of the PhD but also every other condition of life. And a special thanks to Eileenchen, Schwesterherz, and Marion for proofreading the thesis, stating from an artistic point of view whether the figures are acceptable. Dicken Knutscha.

MY very special gratitude goes to my Mom and my Inselaffe. Thank you both so much for all the moral and emotional support, four your patience and love. Even though we had to incour many backstrokes and had some painful losses, we always stuck together.

10. Appendix

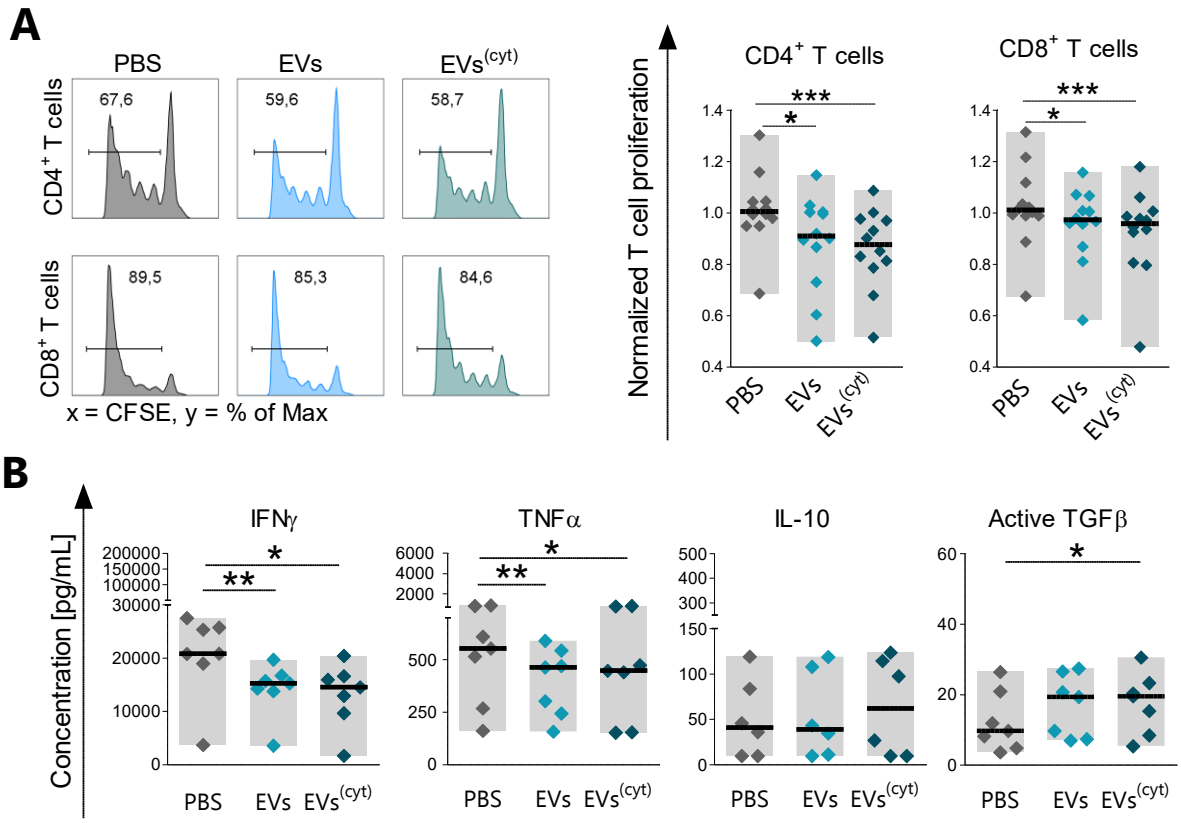

Appendix Figure 1: **Unstimulated and cytokine stimulated EVs diminished PHA induced immune responses in PBMC cultures.**
CFSE labelled PBMCs ($3x10^5$ cells/well) were stimulated with 0.5 µg/mL PHA (Sigma Aldrich, St. Louis, MO, USA) and treated with 6 µg/mL unstimulated (EVs), cytokine-stimulated ($EVs^{(cut)}$) EVs, PBS in equal volume of the EVs (PBS), or cells were left untreated. After three days, cells were investigated by flow cytometry, whereas the supernatant was colleted to be analysed by ELISA or bead-based Multiplex assay for cytokine concentrations. **(A):** Representative flow cytometry plots display the frequencies of proliferated $CD4^+$ and $CD8^+$ T cells in PHA stimulated PBMCs. T cell proliferation frequencies were normalized to the untreated control and the calculated normalized proliferation of $CD4^+$ (left) and $CD8^+$ (right) T cells in PHA stimulated PBMCs is presented as median with data range (PHA: n = 11; four different CardAP donors; five different PBMC donors). **(B):** The individual determined cytokine concentrations of IFNγ, TNFα, IL-10, and active TGFβ are displayed as median with data range for PHA stimulated PBMC cultures (n = 6 – 7; four different CardAP donors; five different PBMC donors). Statistical analysis was performed by Friedman´s test with Dunn´s multiple comparison *post hoc* test (*** $p < 0.001$, ** $p < 0.01$; * $p < 0.05$). Unstimulated as well as cytokine stimulated EVs were capable to reduce T cell proliferation and lower the inflammatory cytokine milieu in PHA stimulated PBMC cultures.

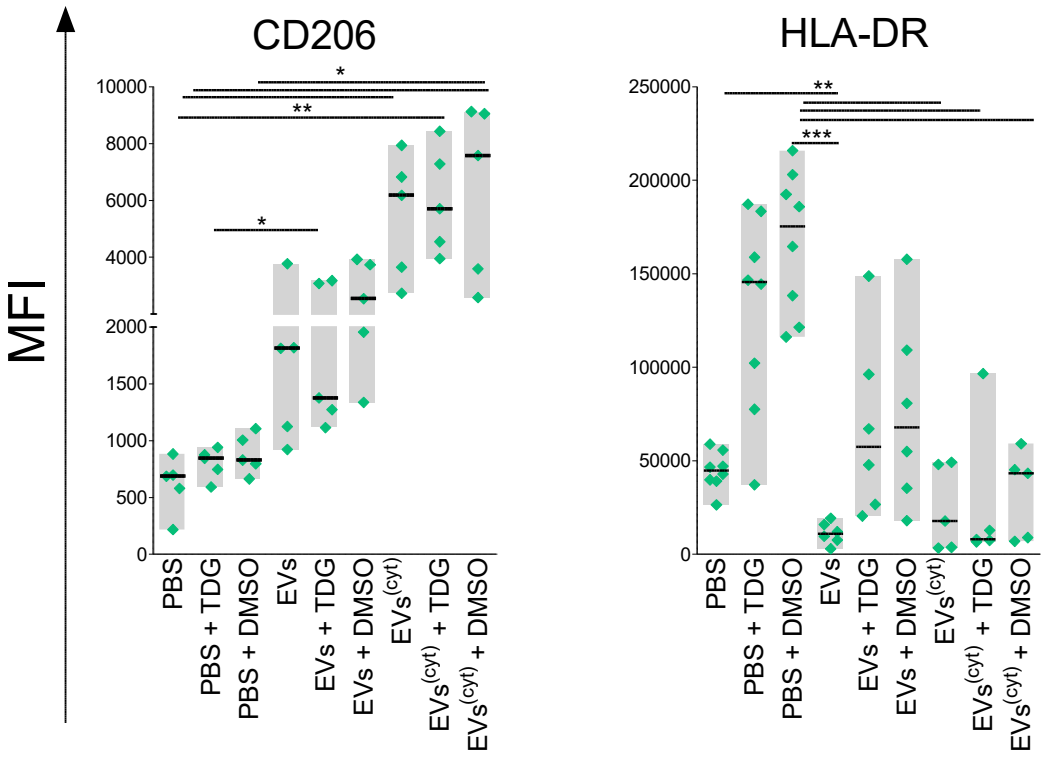

Appendix Figure 2: **Competitive binding of galectin-1 by Thiodiolgalectoside (TDG) could not be explicity shown to influence the impact of EVs on the phenotype of isolated CD14⁺ cells.**
By MACS purified CD14⁺ cells from isolated PBMCs were cultured in 6-well plates (1x10⁶ cells/well) and treated with 12 µg/mL unstimulated (EVs) or cytokine stimulated (EVs$^{(cyt)}$), and PBS in equal volume of the EVs (PBS). Additionally, each of these groups were supplemented with TDG (Cayman Chemical, Ann Arbor, MG, USA) solved in DMSO as a competitive binding molecule and with DMSO alone. After two days, cells were harvested, stained with human specific fluorescence labelled antibodies, and analysed by flow cytometry. The expression of the surface proteins CD206 and HLA-DR are shown as the geometrical mean fluorescence intensity (MFI) for the respective treatments as median with data range (CD206: n = 5 - 8; three different CardAP donors, four different PBMC donors). Statistical analysis was performed by Friedman´s test with Dunn´s multiple comparison *post hoc* test (* $p < 0.05$; ** $p < 0.01$; *** $p < 0.001$). Unstimulated and cytokine stimulated EVs induced an altered expression of CD206 and HLA-DR on CD14⁺ cells, but the influence of transported galectin1 by EVs could not yet be sufficiently clarified via a competitive binding assay with TDG.

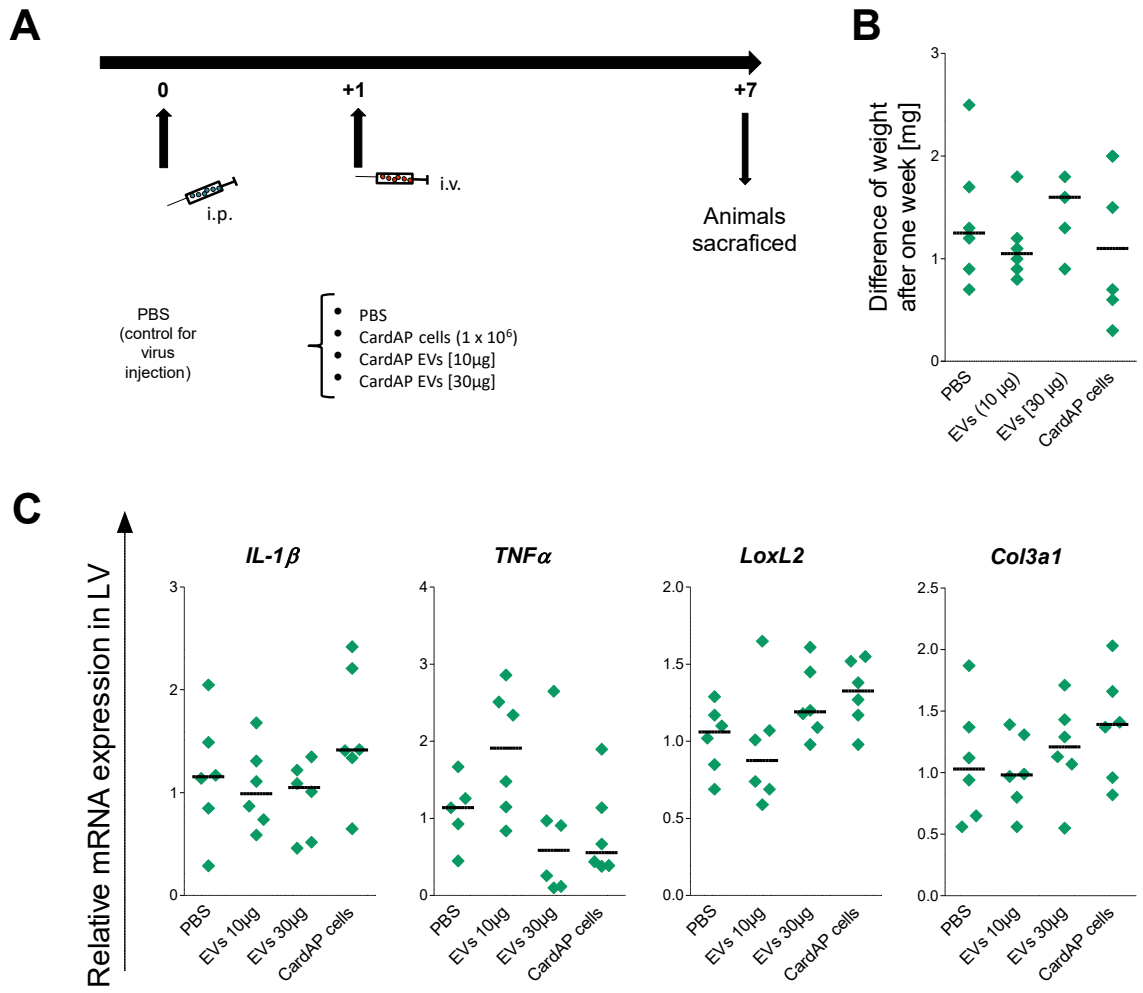

Appendix Figure 3: **The administration of isolated EVs to mice did not show signs of adverse effects.** The *in vivo* compatibility of isolated EVs was investigated by administrating intravenous 10 µg or 30 µg of unstimulated EVs (EV batch of three CardAP donors) to six 8-week old C57BL6/j mice (Charles Rivers), while one day prior, mice received an intraperitoneal injection with PBS (day 0) as a control for the virus application group. The weight of animals was checked daily and after one week, mice were sacrificed and the left ventricle (LV) examined for the expression of mRNA, by homogenizing LV material, isolating RNA, performing a reverse transcription and performing real time qRT-PCRs with murine RNA specific primers, respectively. **(A):** Design of the animal experiment with indicated time line. PBS at day 0 was injected as a control for the virus application group throughout the entire animal study. **(B):** The difference of weights during the animal experiment as calculated by subtracting the starting weight from the weight after one week is displayed as individual data for all six animals per group as median with data range (n = 6, EVs were a batch of three different CardAP donors). **(C):** The relative expression is shown for mRNA of *IL-1ß*, *TNFa*, *LoxL2* (lysyl oxidase homolog 2), and col3a1 (collagen alpha-1(III) for the individual data as median with data range (n =5 – 6; EVs were a batch of three different CardAP donors). Statistical analysis was performed by Friedman´s test with Dunn´s multiple comparison *post hoc* test. Unstimulated EVs did not cause severe side effects in mice that received two different concentrations of EVs. Application of two concentrations of unstimulated EVs into mice did not significantly changed the animal weight nor the expression of pro-inflammatory cytokines or important extracellular matrix proteins.

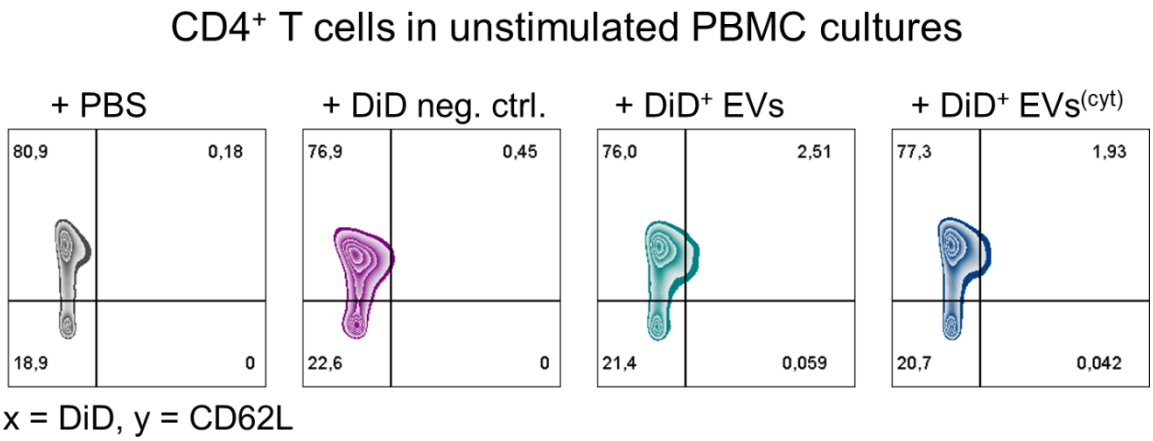

Appendix Figure 4: **Fluorescence labelled EVs interacted with CD62L$^+$CD4$^+$ T cells in unstimulated PBMC cultures.**
Unlabelled PBMCs (3x10^5 cells/well) were treated with 6 µg/mL DiD labelled EVs, either unstimulated (EVs) or cytokine stimulated (EVs$^{(cut)}$), PBS in equal volumes as EVs (PBS), or with a DiD negative control in equal volume as EVs (DiD neg. ctrl.). After two days, cells were measured at a flow cytometer (CantoII) and analysed for the occurrence of DiD signal of isolated EVs in PBMC cultures by flow cytometry. Representative flow cytometry plots display the frequencies of DiD + cells in the compartment of CD4$^+$ CD62L$^+$ T cells in otherwise unstimulated PBMC cultures (n= 2, two different CardAP donors, two different PBMC donors). Unstimulated as well as cytokine stimulated EVs were capable to interact to minor extent with CD4$^+$ CD62L$^+$ T cells in unstimulated PBMC cultures.

***Appendix Table 1*: Isolated EVs were enriched with proteins of the extracellular compartment.**
Peptides were derived from unstimulated EVs and cytokine stimulated EVs of three different CardAP donors by an overnight digestion with trypsin. Mass spectra obtained by liquid chromatography/electron spray ionization mass spectrometry (LC/ES MS) were evaluated by MASCOT software searching for protein matches in the SwissProt 51.9 database. In total 186 proteins were identified, which were further analysed with the help of String database to acquire information of their localisation and their involvement in biological processes. Successful assignment to wound healing, positive regulation of biological processes, angiogenesis, regulation of immune system processes and extracellular exosome compartment is indicated by a blue cross (**x**).

UniProt Identifier	Assignment by String analysis:					Complete name of the identified protein
	Wound healing	Pos. regulation of biological processes	Angio-genesis	Regulation of immune system processes	Extra-cellular exosome	
1433B		x		x	x	14-3-3 protein beta
1433E		x			x	14-3-3 protein epsilon
1433G		x			x	14-3-3 protein gamma
1433T		x			x	14-3-3 protein theta
1433Z	x	x			x	14-3-3 protein zeta/delta
2ABA		x	x			Serine/threonine-protein phosphatase 2A 55 kDa regulatory subunit B alpha isoform
4F2	x				x	4F2 cell-surface antigen heavy chain
5NTD		x			x	5'-nucleotidase
AAAT					x	Neutral amino acid transporter B(0)
ABCE1						ATP-binding cassette sub-family E member
ACLY		x			x	ATP-citrate synthase
ACTB	x	x		x	x	Actin; cytoplasmic 1
ACTN1	x				x	Alpha-actinin-1
ACTZ						Alpha-centractin

ALDOA	x				x	Fructose-bisphosphate aldolase A
AMPN			x		x	Aminopeptidase N
ANXA1	x			x	x	Annexin A1
ANXA2			x		x	Annexin A2
ANXA4					x	Annexin A4
ANXA5	x			x	x	Annexin A5
ANXA6					x	Annexin A6
AP2A1				x		AP-2 complex subunit alpha-1
APOA1	x	x		x	x	Apolipoprotein A-I
ARF1		x		x	x	ADP-ribosylation factor 1
ARP3		x		x	x	Actin-related protein 3
ARPC2				x	x	Actin-related protein 2/3 complex subunit 2
ARPC3		x		x	x	Actin-related protein 2/3 complex subunit 3
AT1A1		x			x	Sodium/potassium-transporting ATPase subunit alpha-1
AT2B1	x				x	Plasma membrane calcium-transporting ATPase 1
BGH3			x		x	Transforming growth factor-beta-induced protein ig-h3
CAB39					x	Calcium-binding protein 39
CALX					x	Calnexin
CAP1	x	x			x	Adenylyl cyclase-associated protein 1
CATB		x		x	x	Cathepsin B
CD276					x	CD276 antigen
CDC42	x	x	x	x	x	Cell division control protein 42 homolog
CDCP1						CUB domain-containing protein 1
CLH1					x	Clathrin heavy chain 1
CN37					x	2';3'-cyclic-nucleotide 3'-phosphodiesterase
CO3	x	x		x	x	Complement C3
CO6A1					x	Collagen alpha-1(VI) chain
CO6A3					x	Collagen alpha-3(VI) chain
COF1	x			x	x	Cofilin-1
CPNE1		x			x	Copine-1
CPNS1		x			x	Calpain small subunit 1
CTL2		x			x	Choline transporter-like protein 2
CTNA1						Catenin alpha-1
CTNB1		x	x	x	x	Catenin beta-1
DEST		x				Destrin
DPP4		x		x	x	Dipeptidyl peptidase 4
DSA2D						Putative dispanin subfamily A member 2d
DYHC1					x	Cytoplasmic dynein 1 heavy chain 1
DYSF	x				x	Dysferlin
EF1A1						Elongation factor 1-alpha 1
EF2		x			x	Elongation factor 2
EGLN	x	x	x			Endoglin
EHD2	x	x			x	EH domain-containing protein 2
ENOA		x			x	Alpha-enolase
EVA1B						Protein eva-1 homolog B
FAS		x			x	Fatty acid synthase
FLNA	x	x			x	Filamin-A
FSCN1					x	Fascin
G3P					x	Glyceraldehyde-3-phosphate dehydrogenase
G6PD					x	Glucose-6-phosphate 1-dehydrogenase
GBG12					x	Guanine nucleotide-binding protein G(I)/G(S)/G(O)
GDIB		x			x	Rab GDP dissociation inhibitor beta
GELS	x			x	x	Gelsolin
GNA11	x				x	Guanine nucleotide-binding protein subunit alpha-11
GNA13	x	x	x		x	Guanine nucleotide-binding protein subunit alpha-13
GNAI2	x	x			x	Guanine nucleotide-binding protein G(i) subunit alpha-2
GNAI3	x				x	Guanine nucleotide-binding protein G(k) subunit alpha
GSTP1		x			x	Glutathione S-transferase P
GTR1					x	Solute carrier family 2; facilitated glucose transporter member 1
H90B2						Putative heat shock protein HSP 90-beta 2
HS71A		x			x	Heat shock 70 kDa protein 1A
HSP7C						Heat shock cognate 71 kDa protein

IQGA1		x			x	Ras GTPase-activating-like protein IQGAP1
IST1				x	x	IST1 homolog
ITA5	x	x	x		x	Integrin alpha-5
ITAV	x	x	x		x	Integrin alpha-V
ITB1	x		x	x	x	Integrin beta-1
ITM2B					x	Integral membrane protein 2B
K1C9					x	Keratin; type I cytoskeletal 9
K22E					x	Keratin; type II cytoskeletal 2 epidermal
K2C1		x		x	x	Keratin; type II cytoskeletal 1
K2C5					x	Keratin; type II cytoskeletal 5
KAP0	x	x				cAMP-dependent protein kinase type I-alpha regulatory subunit
KPYM	x				x	Pyruvate kinase PKM
LAMA4						Laminin subunit alpha-4
LAMB1		x			x	Laminin subunit beta-1
LAMC1		x			x	Laminin subunit gamma-1
LAMP1		x		x	x	Lysosome-associated membrane glycoprotein 1
LAMP2	x				x	Lysosome-associated membrane glycoprotein 2
LDHA		x			x	L-lactate dehydrogenase A chain
LDHB					x	L-lactate dehydrogenase B chain
LEG1				x	x	Galectin-1
LG3BP					x	Galectin-3-binding protein
LOXL2		x	x			Lysyl oxidase homolog 2
LRC4C						Leucine-rich repeat-containing protein 4C
MAP1B		x				Microtubule-associated protein 1B
MMP14			x			Matrix metalloproteinase-14
MOES		x		x	x	Moesin
MVP					x	Major vault protein
MYH9	x	x	x		x	Myosin-9
MYL6					x	Myosin light polypeptide 6
MYL9	x					Myosin regulatory light polypeptide 9
MYO1B					x	Unconventional myosin-Ib
MYO1C		x		x	x	Unconventional myosin-Ic
NDKB					x	Nucleoside diphosphate kinase B
NIBL1					x	Niban-like protein 1
NID1		x			x	Nidogen-1
NID2					x	Nidogen-2
NRP1		x	x			Neuropilin-1
PA1B2		x			x	Platelet-activating factor acetylhydrolase IB subunit beta
PAI1						Plasminogen activator inhibitor 1
PCBP1					x	Poly(rC)-binding protein 1
PCBP2				x	x	Poly(rC)-binding protein 2
PDC6I		x			x	Programmed cell death 6-interacting protein
PDIA1					x	Protein disulfide-isomerase
PDIA3					x	Protein disulfide-isomerase A3
PGBM			x		x	Basement membrane-specific heparan sulfate proteoglycan core protein
PGK1		x			x	Phosphoglycerate kinase 1
PLAK		x			x	Junction plakoglobin
PLS1	x	x		x	x	Phospholipid scramblase 1
PLST						Plastin-3
PLXB2		x			x	Plexin-B2
PPIA	x	x			x	Peptidyl-prolyl cis-trans isomerase A
PRDX5		x			x	Peroxiredoxin-5; mitochondrial
PROF1	x	x			x	Profilin-1
PSME1				x	x	Proteasome activator complex subunit 1
PXDN					x	Peroxidasin homolog
RAB10					x	Ras-related protein Rab-10
RAB13					x	Ras-related protein Rab-13
RAB14					x	Ras-related protein Rab-14
RAB1A		x			x	Ras-related protein Rab-1A
RAB34					x	Ras-related protein Rab-34
RAB35					x	Ras-related protein Rab-35

RAB3B		x			x	Ras-related protein Rab-3B
RADI		x			x	Radixin
RALA		x			x	Ras-related protein Ral-A
RAP1A	x	x				Ras-related protein Rap-1A
RB22A					x	Ras-related protein Rab-22A
RFTN1		x		x	x	Raftlin
RHOA	x	x			x	Transforming protein RhoA
RHOC	x	x			x	Rho-related GTP-binding protein RhoC
RRAS		x			x	Ras-related protein R-Ras
RRAS2					x	Ras-related protein R-Ras2
S10AB					x	Protein S100-A11
S10AG					x	Protein S100-A16
S12A2					x	Solute carrier family 12 member 2
S38A2						Sodium-coupled neutral amino acid transporter 2
SCRB2					x	Lysosome membrane protein 2
SDCB1		x			x	Syntenin-1
SEPR	x	x	x		x	Prolyl endopeptidase FAP
SEPT2					x	Septin-2
SERPH				x	x	Serpin H1
STOM				x	x	Erythrocyte band 7 integral membrane protein
SYG					x	Glycine--tRNA ligase
SYWC			x		x	Tryptophan--tRNA ligase; cytoplasmic
TAGL2					x	Transgelin-2
TBA1A					x	Tubulin alpha-1A chain
TBB2A					x	Tubulin beta-2A chain
TBB5					x	Tubulin beta chain
TBB6						Tubulin beta-6 chain
TCPB					x	T-complex protein 1 subunit beta
TCPE					x	T-complex protein 1 subunit epsilon
TCPZ					x	T-complex protein 1 subunit zeta
TENA		x				Tenascin
TERA		x			x	Transitional endoplasmic reticulum ATPase
TGM2		x			x	Protein-glutamine gamma-glutamyltransferase 2
TLN1	x				x	Talin-1
TNAP3		x		x	x	Tumor necrosis factor alpha-induced protein 3
TNFA						Tumor necrosis factor
TPIS						Triosephosphate isomerase
TSN14		x				Tetraspanin-14
TSN3					x	Tetraspanin-3
TSP1	x	x	x	x	x	Thrombospondin-1
TTYH3					x	Protein tweety homolog 3
UBA1					x	Ubiquitin-like modifier-activating enzyme 1
VAT1					x	Synaptic vesicle membrane protein VAT-1 homolog
VATB2					x	V-type proton ATPase subunit B; brain isoform
VIME		x			x	Vimentin
VINC	x				x	Vinculin
VP37B		x			x	Vacuolar protein sorting-associated protein 37B
WDR1	x	x			x	WD repeat-containing protein 1
YES	x			x	x	Tyrosine-protein kinase Yes

***Appendix Table 2*: More miRNAs were detected in cytokine than in unstimulated EVs.**
Unstimulated EVs (EVs) and cytokine stimulated EVs ($EVs^{(cyt)}$) from three CardAP donors (D1, D2, and D3) were analysed for their miRNA content by nCounter® Human miRNA expression assay according to the manual. The obtained data of miRNA copies was analysed with the help of nSolver software (version 4.0, NanoString Technologies) by firstly normalizing it to the top 100 most abundant miRNAs in all samples as well as the positive controls, followed by a background correction via subtracting the mean plus two standard derivations of the negative control from each sample. These normalized and background corrected data are shown in the table as copy number for identified miRNAs

	EVs			$EVs^{(cyt)}$		
	D1	D2	D3	D1	D2	D3
hsa-miR-4454+hsa-miR-7975	4224	7429	2848	10484	6965	3454
hsa-miR-125b-5p	2213	4998	2380	8714	4588	1437
hsa-miR-100-5p	871	6140	1185	4617	3645	1134
hsa-miR-29b-3p	443	7199	272	5626	3129	739
hsa-miR-199a-3p+hsa-miR-199b-3p	387	5046	255	3134	1936	361
hsa-let-7b-5p	1029	3801	738	6321	2915	1143
hsa-miR-222-3p	35	2962	62	868	1173	146
hsa-let-7a-5p	222	2561	166	3925	1819	421
hsa-miR-23a-3p	447	1934	261	2172	1082	427
hsa-miR-29a-3p	173	1842	134	2637	1223	193
hsa-let-7i-5p	46	1772	122	1418	1252	394
hsa-miR-146a-5p	268	1491	107	3277	1283	210
hsa-miR-181a-5p	108	1280	156	1222	906	327
hsa-miR-127-3p	132	1171	102	555	591	107
hsa-miR-25-3p	134	871	146	1217	582	253
hsa-miR-191-5p	247	671	155	723	425	164
hsa-miR-16-5p	58	799	138	1207	742	303
hsa-miR-22-3p	48	826	102	1010	641	193
hsa-miR-150-5p	0	546	94	0	545	164
hsa-miR-376a-3p	87	433	0	135	175	14
hsa-miR-221-3p	304	379	42	1517	332	60
hsa-miR-302d-3p	196	232	238	0	85	134
hsa-miR-24-3p	99	318	0	454	300	41
hsa-miR-93-5p	176	220	0	442	209	11
hsa-miR-15b-5p	0	325	52	591	168	83
hsa-miR-574-5p	0	327	45	188	139	114
hsa-let-7d-5p	166	340	28	627	279	65
hsa-miR-612	218	166	130	103	156	115
hsa-miR-145-5p	223	111	0	578	240	0
hsa-let-7g-5p	0	291	18	183	190	84
hsa-miR-630	0	227	58	0	274	100
hsa-miR-34a-5p	0	173	63	136	122	89
hsa-miR-99b-5p	55	203	79	410	190	44
hsa-miR-890	187	32	0	108	141	0
hsa-miR-23b-3p	0	186	31	167	121	51
hsa-miR-19b-3p	58	138	0	157	73	0
hsa-miR-323b-3p	161	17	0	91	98	0
hsa-let-7e-5p	0	148	13	273	159	33
hsa-miR-551a	128	31	0	85	114	0
hsa-miR-98-5p	67	92	0	150	126	11
hsa-miR-532-5p	142	15	0	88	113	0
hsa-miR-548q	0	40	111	0	50	80
hsa-miR-151a-3p	97	53	0	152	94	0
hsa-miR-363-5p	133	17	0	53	106	0
hsa-miR-543	0	124	22	0	51	19
hsa-miR-944	121	23	0	59	136	0
hsa-miR-20a-5p+hsa-miR-20b-5p	74	70	0	120	89	0
hsa-miR-892a	126	16	0	68	91	0
hsa-miR-4286	70	99	42	253	74	28
hsa-miR-606	124	13	0	37	89	0
hsa-miR-186-5p	0	80	56	0	33	88
hsa-miR-451a	37	98	0	0	95	0
hsa-miR-548a-3p	89	44	0	41	85	0
hsa-miR-98-3p	111	21	0	68	108	0
hsa-miR-1290	0	49	83	0	48	100
hsa-miR-3164	117	13	0	37	97	0
hsa-miR-1910-3p	110	18	0	61	116	0
hsa-miR-548l	95	30	0	48	95	0

hsa-miR-548n	82	44	0	44	97	0
hsa-miR-875-3p	103	22	0	69	133	0
hsa-miR-3180-5p	94	26	0	41	72	0
hsa-miR-499a-5p	121	42	18	78	150	0
hsa-miR-1180-3p	83	37	0	56	89	0
hsa-miR-152-3p	82	37	0	43	79	0
hsa-miR-708-5p	104	13	0	75	102	0
hsa-miR-3690	103	14	0	46	117	0
hsa-miR-1255a	0	29	88	0	30	102
hsa-miR-193a-5p+hsa-miR-193b-5p	66	50	0	148	112	0
hsa-miR-1244	101	12	0	54	101	0
hsa-miR-342-3p	55	58	0	49	101	0
hsa-miR-99a-5p	0	95	15	136	37	66
hsa-miR-28-5p	0	70	39	0	35	39
hsa-miR-1247-5p	95	11	0	29	56	0
hsa-miR-548y	0	29	78	0	23	107
hsa-miR-654-3p	90	16	0	39	74	0
hsa-miR-31-5p	36	70	0	25	79	0
hsa-miR-523-3p	92	12	0	74	58	0
hsa-miR-548ah-5p	0	40	64	0	32	98
hsa-miR-132-3p	0	75	26	27	97	42
hsa-miR-520d-5p+hsa-miR-527+hsa-miR-518a-5p	88	13	0	44	61	0
hsa-miR-374b-5p	70	29	0	43	48	0
hsa-miR-105-5p	83	16	0	29	68	0
hsa-miR-610	85	11	0	37	91	0
hsa-miR-2117	76	19	0	100	90	0
hsa-let-7f-5p	0	75	19	72	58	41
hsa-miR-4521	76	18	0	44	73	0
hsa-miR-1-3p	77	15	0	0	36	0
hsa-miR-1183	72	18	0	0	56	0
hsa-miR-299-5p	0	51	39	0	13	64
hsa-miR-548d-5p	75	13	0	27	59	0
hsa-miR-450a-1-3p	63	22	0	47	29	0
hsa-miR-125a-5p	0	48	33	154	76	0
hsa-miR-431-5p	63	17	0	56	52	0
hsa-miR-3136-5p	68	11	0	20	90	0
hsa-miR-548j-3p	57	22	0	37	50	0
hsa-miR-1197	0	20	56	0	24	74
hsa-miR-1260a	0	61	14	0	48	15
hsa-miR-548e-5p	0	17	55	0	0	68
hsa-miR-450a-2-3p	0	21	46	0	19	78
hsa-miR-30e-5p	0	40	26	0	19	38
hsa-miR-4458	54	10	0	0	35	0
hsa-miR-1305	0	10	52	0	0	74
hsa-miR-183-5p	0	22	37	0	27	91
hsa-miR-328-5p	0	21	37	0	0	82
hsa-miR-1228-3p	0	10	47	0	0	29
hsa-miR-887-5p	0	16	40	0	40	105
hsa-miR-939-5p	0	16	37	0	11	56
hsa-miR-301a-5p	0	22	28	0	0	52
hsa-miR-26b-5p	0	30	18	0	10	64
hsa-miR-32-5p	29	16	0	0	53	0
hsa-miR-873-3p	0	15	30	0	0	0
hsa-miR-615-3p	0	16	29	0	15	69
hsa-miR-1285-5p	0	12	31	0	0	52
hsa-miR-155-5p	0	23	17	122	0	33
hsa-miR-411-5p	0	16	14	0	0	23
hsa-miR-148b-3p	0	12	13	0	0	0
hsa-miR-494-3p	0	0	0	457	834	0
hsa-miR-21-5p	0	1079	0	557	449	64
hsa-miR-130a-3p	0	303	0	180	147	68
hsa-let-7c-5p	0	125	0	189	76	37
hsa-miR-382-5p	0	258	0	88	108	0
hsa-miR-3614-3p	126	0	0	78	97	0
hsa-miR-365a-3p+hsa-miR-365b-3p	0	60	0	174	39	34
hsa-miR-15a-5p	0	94	0	80	76	0
hsa-miR-524-3p	131	0	0	56	95	0
hsa-miR-545-3p	95	0	0	55	96	0
hsa-miR-92a-3p	86	0	0	87	62	0
hsa-miR-1248	96	0	0	60	84	0
hsa-miR-1910-5p	99	0	0	53	90	0
hsa-miR-3192-5p	136	0	0	56	87	0
hsa-miR-553	105	0	0	47	94	0
hsa-miR-671-3p	83	0	0	69	70	0
hsa-miR-520f-3p	72	0	0	44	95	0

hsa-miR-887-3p	112	0	0	37	102	0
hsa-miR-1233-3p	97	0	0	39	98	0
hsa-miR-5010-5p	88	0	0	55	80	0
hsa-miR-617	76	0	0	17	116	0
hsa-miR-601	86	0	0	49	82	0
hsa-miR-874-5p	77	0	0	46	82	0
hsa-miR-942-3p	104	0	0	52	76	0
hsa-miR-548o-3p+hsa-miR-548ah-3p+hsa-miR-548av-3p	93	0	0	56	72	0
hsa-miR-409-3p	0	63	0	60	64	0
hsa-miR-619-3p	71	0	0	37	87	0
hsa-miR-940	89	0	0	27	91	0
hsa-miR-152-5p	97	0	0	50	67	0
hsa-miR-596	100	0	0	36	81	0
hsa-miR-1908-5p	74	0	0	30	85	0
hsa-miR-1469	68	0	0	38	76	0
hsa-miR-153-3p	70	0	0	31	82	0
hsa-miR-767-3p	91	0	0	38	75	0
hsa-miR-3918	92	0	0	56	54	0
hsa-miR-561-3p	106	0	0	29	79	0
hsa-miR-1291	97	0	0	32	76	0
hsa-miR-580-3p	83	0	0	37	70	0
hsa-miR-491-5p	90	0	0	18	89	0
hsa-miR-3161	58	0	0	36	70	0
hsa-miR-556-3p	108	0	0	26	79	0
hsa-miR-130b-3p	73	0	0	39	66	0
hsa-miR-513b-5p	70	0	0	41	64	0
hsa-miR-4421	96	0	0	53	47	0
hsa-miR-3202	81	0	0	20	80	0
hsa-miR-199a-5p	0	88	0	79	46	24
hsa-miR-490-5p	66	0	0	19	78	0
hsa-miR-576-5p	94	0	0	18	77	0
hsa-miR-4435	64	0	0	22	73	0
hsa-miR-567	51	0	0	30	64	0
hsa-miR-574-3p	0	11	0	60	0	33
hsa-miR-374a-5p	0	216	0	34	66	34
hsa-miR-539-5p	60	0	0	33	54	0
hsa-miR-133b	66	0	0	13	73	0
hsa-miR-1245b-3p	77	0	0	26	60	0
hsa-miR-1288-3p	78	0	0	29	56	0
hsa-miR-320d	79	0	0	32	52	0
hsa-miR-1204	76	0	0	21	62	0
hsa-miR-578	73	0	0	27	55	0
hsa-miR-367-3p	39	0	0	21	61	0
hsa-miR-1271-3p	61	0	0	21	60	0
hsa-miR-3150b-3p	42	0	0	13	66	0
hsa-miR-3140-3p	61	0	0	17	62	0
hsa-miR-548ar-3p	0	0	35	0	10	66
hsa-miR-6503-3p	47	0	0	13	62	0
hsa-miR-615-5p	87	0	0	24	50	0
hsa-miR-519e-3p	31	0	0	23	50	0
hsa-miR-514a-5p	29	0	0	17	55	0
hsa-miR-381-5p	49	0	0	14	58	0
hsa-miR-196a-5p	60	0	0	15	55	0
hsa-miR-1306-5p	62	0	0	19	50	0
hsa-miR-124-3p	58	0	0	21	48	0
hsa-miR-320b	57	0	0	17	51	0
hsa-miR-3074-3p	0	0	0	33	35	0
hsa-miR-4787-3p	73	0	0	25	42	0
hsa-miR-1276	44	0	0	21	45	0
hsa-miR-128-1-5p	50	0	0	10	53	0
hsa-miR-525-5p	0	0	33	0	10	51
hsa-miR-29c-3p	12	0	0	12	49	0
hsa-miR-519b-5p+hsa-miR-519c-5p+hsa-miR-523-5p+hsa-miR-518e-5p+hsa-miR-522-5p+hsa-miR-519a-5p	61	0	0	15	44	0
hsa-miR-1299	11	0	0	10	48	0
hsa-miR-208b-5p	80	0	0	17	39	0
hsa-miR-3196	65	0	0	12	44	0
hsa-miR-525-3p	75	0	0	25	31	0
hsa-miR-1306-3p	0	0	41	0	10	43
hsa-miR-337-5p	0	140	0	0	24	21
hsa-miR-26a-5p	0	39	0	0	16	21
hsa-miR-331-3p	0	51	0	10	15	26
hsa-miR-320e	0	0	15	0	12	14